IMPERIAL COLLEGE OF SCIENCE, TECHNOLOGY AND MEDICINE
University of London

PLATE WAVES FOR THE NDT OF DIFFUSION BONDED TITANIUM

by

Michael John Stuart Lowe

A thesis submitted to the University of London
for the degree of Doctor of Philosophy

Department of Mechanical Engineering
Imperial College of Science, Technology and Medicine
London SW7

December 1992

Abstract

Diffusion bonding, the joining of two surfaces by the diffusion of material across the interface, has the attractions of very high strength and minimal distortion of the components. Recent developments of the diffusion bonding process in the aircraft industry has further exploited the process by the diffusion bonding and superplastic forming of sheets of titanium to create cellular structural components. Along with these developments has been the necessary research into inspection methods for quality control during production. An important inspection problem is the detection of a brittle layer of a phase of the titanium alloy which can occur at the bondline if air is present during bonding.

This thesis presents an evaluation of the potential of using ultrasonic plate waves for the detection of the presence of such a layer. The principle is that differences in the acoustic properties of the layer with respect to the adherends will affect the modal properties of wave propagation along the joint. Thus the presence of the layer could be detected by the measurement of a selected propagating mode.

A theoretical model is developed for the prediction of the modal properties of wave propagation along a layered plate. The model is applicable to plate systems of any numbers of layers of isotropic viscoelastic materials and can describe either free wave propagation or leaky wave propagation, when the plate is assumed to be immersed in a fluid or solid. The model predicts the velocities, frequencies and attenuations of the propagating modes as well as the distributions of displacements and stresses.

The acoustic properties of the brittle phase are measured and the model is used to predict the plate wave properties in good and defective joints. Two approaches are considered, one involving Lamb waves which occupy the full thickness of the joint and the other involving interface waves which travel along the brittle layer. The optimum modes and conditions for testing are identified and their sensitivities are compared with conventional normal incidence testing. It is found that both approaches show some sensitivity in principle to the presence of the layer but it is concluded that in practice it is not likely that either will offer advantages over normal incidence testing.

Acknowledgements

I would like to thank Dr Peter Cawley for his excellent guidance and support throughout this research project. I would also like to thank my colleagues in the Nondestructive Testing Laboratory - Tom Piałucha, David Alleyne, Paul Dewen, Ningqun Guo and Bruce Drinkwater - for many useful discussions and technical contributions.

I would like to thank British Aerospace for their financial support of the project, for their provision and analysis of materials and for useful discussions. In particular, I would like to thank Kevin Taylor, Dan Kells, Ainsley Killey and Jeff Sargent.

I would like to thank SERC for their financial support.

Contents

Chapter 3

Attenuating wave propagation along a multilayered plate

Chapter 4

Development of numerical model

Chapter 5

Validation of model

Chapter 6

Characterisation of defective joints

Chapter 7
Normal incidence inspection

Chapter 8
Lamb wave technique

Chapter 9
Interface wave technique

Chapter 10
Conclusions

List of Tables

List of Figures

Nomenclature

a_0, a_1, a_2,...	Antisymmetric Lamb modes, subscript refers to mode number
$A_{(L)}$,$A_{(S)}$	Amplitudes of longitudinal and shear waves
{A}	vector of wave amplitudes in a layer
b	Subscript, denotes bottom of layer
c	Wave speed
c_{ph}	Phase velocity
c_{gr}	Group velocity
C? ??C? ??	
C_2? ??C_i	Abbreviation constants (Equation 2.43)
d	Layer thickness
[D]	Field matrix within a layer (Equation 2.48)
E	Young's modulus
f	Characteristic function
g? , g?	Abbreviation constants (Equation 2.43)
HV	Vickers hardness
i	?(-1)
i	Interface label in layer model
k	Wavenumber
K	Effective material stiffness (= E in plane stress case)
L	Wavelength
L	Subscript, denotes longitudinal wave
L	Longitudinal wave displacement field
[L]	Layer matrix (Equation 2.52)
l	Layer label in layer model
n	Number of layers in multilayered plate
N	Unit length propagation vector
s	Snell constant
S	Subscript, denotes shear wave
S	Shear wave displacement field
s_0, s_1, s_2,...	Symmetric Lamb modes, subscript refers to mode number
[S]	System matrix (Equations 2.54, 2.87)
[S]'	System matrix for guided waves using transfer matrix method (Equations 2.60, 2.63, 2.65)
SED	Strain energy density
t	Time

t	Subscript, denotes top of layer
u	Displacements
x	Cartesian coordinate system
1,2,3	Subscripts, denote direction (Figure 2.2)
?	Bulk longitudinal wave speed
?	Bulk shear wave speed
?	Volumetric strain
?	Strain
?	Helmholtz scalar function
?	Wave phase
?	Attenuation of plate wave, Nepers per wavelength
? ???	Lamé's elastic stiffness constants
? '??'	Viscoelastic material constants
?	Poisson's ratio
?	Angle of incidence, measured from the normal to the plate
?	Density
?	Stress
?	Frequency (radians/sec)
?	Helmholtz vector function
+	Subscript, denotes wave propagating with positive component in x_2 direction
+	Superscript, denotes part of matrix or vector corresponding to + wave
-	Subscript, denotes wave propagating with negative component in x_2 direction
-	Superscript, denotes part of matrix or vector corresponding to - wave

Bold typeface denotes a vector.

Square brackets [] denote a matrix.

CHAPTER 1

Background

1.1 Introduction

Diffusion bonding of metals is the joining of two surfaces by the diffusion of material across the interface. This is achieved by careful preparation of the surfaces followed by the application of pressure for a period of time at elevated temperature. It is a relatively new joining method, depending heavily on modern production equipment, high quality materials and extensive research in the development of the process parameters.

A good diffusion bond offers many attractions to the engineer as a joining process. It can have the microstructure and mechanical properties of the parent material so that there is no loss of strength or toughness at the joint. It involves minimal distortion of the components so that close tolerances can be ensured. Loads can be spread evenly over the joint without stress concentration and there are no significant residual stresses. Extremely stiff joints can be made with minimal additional weight. Large areas of material may be joined in a single process, reducing the required number of components and manufacturing operations. Finally, maintenance costs in many applications can be much lower than for alternative methods because of reduced needs for routine maintenance inspection.

The attractions of diffusion bonding have not been missed by the industries which are concerned with high performance safety-critical mechanical components. In particular, in the aerospace industry major progress has been made in the diffusion bonding of titanium alloys, as reported by Stephen (1986), Broomfield (1986) and Partridge (1987). The technology has been developed in two categories, 'Massive DB' and 'Thin sheet DB'. Massive DB involves the joining of thick section machined parts and is performed under relatively high pressures. It has been used for airframe components, including the joining of hollow section components on the Space Shuttle, and for engine components, including blades for the Rolls Royce RB211-535 engine for the Boeing 757 aircraft. Thin sheet DB involves the joining of larger areas and has been used for panels, for example underwing access panels on the British Aerospace Airbus A310 aircraft. A particularly exciting development of thin sheet DB is the combination of diffusion bonding and superplastic forming which will be discussed further in the next section

of this chapter. Current developments in the Aerospace industry include the diffusion bonding of aluminium alloys and the diffusion bonding of dissimilar metals such as titanium to stainless steel.

As with the introduction of any new material or manufacturing method, appropriate quality control and inspection techniques must be developed for diffusion bonds before they can be used with confidence for safety-critical components. The requirements for inspection are strongly dependent on the applications and on the quality control but in general it is necessary to detect defects of known types above a threshold of size or distribution. The types of defect which could occur with a given bonding process have to be characterised and the threshold size determined from destructive mechanical testing. Currently the favoured techniques for nondestructive inspection are ultrasonics and radiography.

Outline of this chapter

A description of the diffusion bonding process is given in Section 1.2, introducing the particular titanium alloy which was studied in the research programme, the form of diffusion bond of interest here, and the defects which may potentially occur during bonding.

The conventional method of ultrasonic inspection, normal incidence reflectivity, is introduced in Section 1.3. This is the reference technique with which any new method of inspection must be compared.

The alternative inspection techniques which will be investigated in the thesis rely on waves which travel along the diffusion bonded joint or along the bondline of the joint. Much of the thesis will be concerned with the development of a model which can calculate the properties of such plate waves and the application of the model to make predictions about the waves in defective joints. A general introduction to plate waves is therefore given in Section 1.4 followed by a summary of the proposed plate wave inspection methods, in Section 1.5, and an introduction to the development of the model, in Section 1.6.

Much literature has been published both on plate waves and on nondestructive testing and, in order to keep the introductions in Sections 1.2 to 1.6 as readable as possible, a review of the literature is presented in its own section, Section 1.7, references being kept to a minimum elsewhere in this chapter.

The chapter is completed with an outline of the thesis, in Section 1.8, including a statement of the objectives.

1.2 The diffusion bonding process and potential defects

Good descriptions of the diffusion bonding process for titanium may be found in Partridge (1987) and Stephen (1986).

Thin sheet diffusion bonding is normally achieved by applying a fairly low pressure to the components, of just a few MPa, but at a high temperature. For titanium alloys the bonding temperature is typically about 950º C, higher than half of their absolute melting point temperature. The time necessary to achieve the bond depends strongly on the composition of the alloy and in particular on the grain size but is typically of the order of one or two hours.

The diffusion bonding process can be described in two stages. In the first stage, which takes a relatively short time, the contacting surface asperities undergo plastic and creep deformations so that the contact area increases. The interface then consists of regions of intimate contact separated by small voids. This process is sensitive to stress, the creep strain rate for titanium being described typically by a power law in stress of order 3-4, so that as the contact area increases the deformation rate diminishes rapidly. In the second stage, volume diffusion and grain boundary migration mechanisms take place so that at the end of the process there is ideally no evidence of the interface. The grain boundaries at the bondline are no longer planar and the small voids have been eliminated.

It is sometimes advantageous to use an interlayer of another material between the two adherends of a joint. Thin layers of a metal with a relatively low melting point, such as copper-nickel, may be electroplated or sputtered onto the surfaces of the adherends prior to bonding. During the bonding the interlayer melts, forming a liquid at the interface and subsequently diffusing into the adherends. The principal advantage with this method is that the bond may be made with much lower pressures and temperatures. It can also be beneficial for the bonding of dissimilar metals. Bonding using an interlayer is usually referred to as 'diffusion brazing', as distinct from 'diffusion welding' when no interlayer is used.

The research which is reported here addressed the inspection of diffusion bonds of thin sheets of a particular titanium alloy, joined without an interlayer. The alloy is the 6 % aluminium 4 % vanadium (Ti-6Al-4V) which is in widespread use in the aerospace industry. As produced, it

is a two-phase alloy consisting of 'alpha' and 'beta' grains, of which the alpha grains are relatively soft. The structure has been likened to grains of sand (beta) in a matrix of plasticene (alpha). It has been found to be particularly amenable to both diffusion bonding and superplastic forming.

At temperatures in excess of 800º C the alloy is highly reactive, strongly absorbing both oxygen and nitrogen. This is convenient to a certain extent because the thin oxide layer which is naturally present on the surfaces of the adherends is absorbed and the material is said to be self-cleaning. However it is very important that the material does not absorb larger quantities of oxygen or nitrogen because this can cause embrittlement. There are two aspects to this mechanism. First, the presence of these gases raises the beta transus temperature so that at the high bonding temperature the beta grains tend to transform to alpha. This is a softening process because the alpha is softer than the beta. Second, the gases cause interstitial locking of the alpha grains. Concentrations of locked alpha grains, called 'oxygen/nitrogen stabilised alpha', 'hard alpha' or 'alpha case' are considerably harder than the parent alloy and are rather brittle. Consequently the diffusion bonding of titanium is carried out with as little air present as possible. This is achieved by evacuation of the bonding press followed by purging with an inert gas such as argon.

An exciting development of the use of titanium has been to combine diffusion bonding with superplastic forming ('SPFDB'), to form a highly structured material, as discussed by Stephen (1986). An illustration of the formation of one such structure, an X-braced panel, is shown in Figure 1.1. In the example, the process starts with four flat sheets of titanium. A stop-off agent which prohibits bonding is printed onto the surfaces of the sheets in a predefined pattern and the sheets are put together and bonded, as illustrated in Figure 1.1(a). While maintaining a high temperature, an inert gas is then injected into the unbonded regions so that the pack of sheets expands, as illustrated in Figure 1.1(b). The final shape of the exterior of the structure is controlled by carrying out the process in a shaped mould. SPFDB structures can have a considerable weight advantage over other forms of construction. Manufacturing and assembly may also be simplified because of large reductions in the numbers of components.

Clearly the successful production of bonds depends on the careful control of a large number of parameters, including pressure, temperature, time, quality of material, surface preparation and cleanliness. Gross deviations may lead to total failure of the bond or perhaps to localised 'unbonded' regions. Other consequences may be the embedding of particles of contaminants or voids at the bondline. A particularly dangerous possibility however is the formation of a

brittle layer of alpha case, illustrated in Figure 1.1(c). This can happen if significant quantities of air are present during the bonding process. The surfaces of the sheets absorb the oxygen and nitrogen strongly as the material is heated, forming a continuous layer of alpha case at the bondline. The toughness of the whole joint is therefore reduced. This thesis is concerned with the nondestructive detection of the presence of this form of defect.

Figure 1.2 shows a micrograph of a section through a poor diffusion bonded joint where air has been introduced during the bonding process. The etching solution which was used for the section shows the presence of alpha case as a lighter colour than the parent titanium alloy. Here the alpha case appears to extend approximately 40 microns on each side of the bondline. A distribution of very small voids with dimensions of the order of a few microns can also be seen on the bondline.

1.3 Conventional ultrasonic inspection

The conventional ultrasonic technique for the detection of defects in plates is to send an ultrasonic pulse into the material and then to look for changes either in the transmitted signal on the other side of the plate ('through-transmission') or in reflections from the plate on the same side as the transmitter ('pulse-echo'). The transducers are set up so that the path of the signal is normal to the surfaces of the plate and in pulse-echo mode a single transducer is then used for both transmission and reception. Typically a broadband piezo-electric transducer with a focused beam and a short duration pulse excitation is used for this form of inspection.

Pulse-echo inspection is usually preferred when the aim is to detect planar defects or planar arrays of defects from which the direction of any reflected energy is predominantly towards the single receiver. The detection of an embedded layer of alpha case clearly falls into this category. Also, pulse-echo inspection requires access to only one side of the component. Through-transmission inspection is attractive when random scattering mechanisms are involved, for example due to grain boundaries. In such cases little energy is reflected back to the transmitting transducer but the transmitted signal may be affected significantly.

Figure 1.3 illustrates the pulse-echo inspection of a plate in which there is an embedded 'defect'. Part (a) of the figure shows the defective joint and identifies schematically the reflections from each of the interfaces of the joint. Part (b) shows the time trace which may be seen on an oscilloscope when the joint is inspected. The data has been simulated for the illustration. In this example the defect could be a continuous layer of alpha case embedded at

the bondline of a diffusion bonded joint, the thickness being exaggerated somewhat for the illustration. In general the defect may be any continuous or localised material with surfaces parallel to the plane of the plate. The key feature is that it must have different acoustic properties from the remainder of the plate. The system is immersed in water in order to provide good acoustic coupling between the transducer and the plate.

Each time the pulse is incident on an interface at which there is a change in acoustic impedance, a partial reflection takes place and returns to the transducer. The first three reflections, labelled R1, R2 and R3 in Figure 1.3(a), can be seen in the typical time trace in Figure 1.3(b). Subsequently an infinite series of diminishing reflections will be received as the pulse reverberates in the plate. The presence or absence of the defect can be determined simply by using an electronic gate, portrayed as a dashed line in the figure, to limit the monitoring of reflections to the time period when the first reflection would return from the bondline. If any reflection can be detected within the gate then some change of acoustic impedance is inferred at the bondline.

The normal incidence pulse-echo technique is very effective for detecting large changes in acoustic impedance such as voids or inclusions and it has the strong attraction of ease of application. The results of one such case are shown in a C-scan image in Figure 1.4. This shows the amplitude of the reflected pulse from the bondline, plotted over the area of a very poor diffusion bonded plate. Large regions of the plate were not bonded in this case and they can be identified by the strong reflections (black in the image). The plate consisted of two sheets of titanium, each 4 mm in thickness. The scan was performed using a broadband transducer with a 10 MHz centre frequency, focused on the bondline.

Unfortunately the effectiveness of normal incidence inspection is limited when the defects are small or their properties are similar to those of the plate, in which cases the amplitudes of the reflections are small. Embedded layers of alpha case fall into both categories. It is desirable to be able to detect alpha case with thickness down to some tens of microns yet its acoustic impedance does not differ significantly from that of titanium.

1.4 Introduction to plate waves

An alternative approach to normal incidence inspection is to consider some form of ultrasonic wave which propagates along the plate. This is very attractive in principle because the energy in certain waves travelling along a plate may be concentrated at the bondline so that the wave propagation properties may be sensitive to the properties at the bondline. An inspection method based on plate waves may therefore offer greater sensitivity to defects than normal incidence testing in some circumstances. However the drawback in devising such an inspection method is that the waves propagating along a plate are very much more complicated than the bulk waves which are utilised in normal incidence testing.

Two waves may travel in an infinite elastic solid medium, a compression wave and a shear wave (the 'bulk waves'). Each may travel in any direction but at a fixed speed which is independent of frequency and is given by the physical properties of the medium. These wave properties are analogous to the natural frequencies of a vibrating structure and are the modal properties of the system. In practice the modal properties are exploited in all types of ultrasonic testing because they describe the transfer of energy by 'longitudinal' or 'shear' wave from one location to another when a signal is transmitted. The fact that they are properly only modal solutions for an infinite space is not a problem. The received signal is usually gated so that unwanted reflections from boundaries are neglected, thus simulating an infinite space.

If an interface is introduced into the medium then the modal properties are changed dramatically. The simplest case is that of a free surface when the elastic medium extends to infinity from one side of the interface and the other side is vacuum. Now only one wave, the Rayleigh wave, exists as a modal property and it can only travel along the surface at a constant speed, independent of frequency. If the second side is not vacuum but another medium then it may still be possible for a wave to travel along the interface. The nature of this interface wave depends on the acoustic properties of the two media; it may carry all its energy along the interface (the Stoneley wave) or it may leak energy into the half-spaces as it travels.

As a third step another, parallel, interface can be introduced. This provides the physical description for a plate with a top and bottom surface which extends infinitely in width. If the two half-spaces are vacuum then the modal properties of the plate are the Lamb waves.

Figure 1.5 shows a plot of the velocities of the first two Lamb wave modes for a 1 mm thick titanium plate. These waves are clearly dispersive, that is to say their velocities vary with

frequency, and the plots are usually referred to as dispersion curves. Inset on the figure are illustrations showing the deformation shapes of the waves. At low frequency the two waves can easily be understood as extensional and bending waves travelling along the plate. The deformation of the plate is symmetric about the centre line of the plate for the extensional wave and antisymmetric for the bending wave. Accordingly the labels s_0 and a_0 denote them as the zero order symmetric and antisymmetric waves. As the frequency is increased the wavelength of the waves reduces in comparison to the thickness of the plate and the energy is concentrated increasingly near the surfaces of the plate. At very high frequency the two curves converge towards the Rayleigh wave speed, the limiting solution at infinite frequency being two independent Rayleigh waves, one travelling on each surface of the plate.

In fact there is an infinite number of Lamb wave modes in a plate. There are also families of modal solutions for other plate systems, including for multilayered plates in vacuum and for plates which are immersed in a fluid or embedded in a solid. Further discussion and a variety of examples will be given in Chapter 5. In the meantime it will be useful to introduce some of the terms which are used to classify plate waves:

Free waves. This description covers all solutions in which the wave propagates indefinitely without loss of energy. A Rayleigh wave, which travels along the surface of a semi-infinite elastic half-space adjacent to a half-space of vacuum is a free wave. Lamb waves, which are the whole family of modal solutions for a single layer of elastic material in a vacuum, are also free waves. In practice the modal solutions for the velocities of free waves are usually very reasonable approximations when the surrounding medium is not a vacuum but has a relatively low acoustic impedance. This is the case for example when a metal plate is immersed in water. Note however that the influence of water can be significant when the acoustic impedance of the plate is low, as is the case with carbon reinforced composites.

Leaky waves. Waves which leak energy from the plate into the adjoining media are termed leaky waves. Plate waves can only leak energy if at least one of the half-spaces is a solid or liquid and the velocity of the wave is higher than a certain threshold. For example a leaky Rayleigh wave can travel along the surface of a semi-infinite elastic half-space which is adjacent to a half-space of water. Similarly a leaky Lamb wave can propagate in a plate which is immersed in water. In both cases the wave leaks energy into the water. In practice any form of testing with fluid or solid coupling relies on the waves being leaky. Strict (free) Rayleigh or Lamb modes could only be excited or detected by non-contact methods such as electro-magnetic systems.

Guided waves. The term guided waves describes free waves which travel along plates or layers of plates without leakage of energy into adjacent non-vacuum layers. For example a guided wave may travel along a soft layer (low values of longitudinal and shear bulk velocities) which is sandwiched between two hard layers, such as in an adhesive joint, without leaking energy into the hard layers.

Surface waves. Surface waves travel along the surface of a plate and may be free or leaky. The best known surface wave is the Rayleigh wave. The majority of the energy of the wave is confined to a depth of approximately two wavelengths in the solid medium and there is no energy leakage away from the surface into the solid half-space. The wave is also non-dispersive; its velocity is constant for all frequencies. Surface waves can exist with other geometries. For a soft layer on top of a hard half-space a dispersive surface wave can exist, its velocity decreasing with frequency. Again, no energy is lost through leakage as the wave propagates. If the surface layer is harder than the half-space then a dispersive wave can exist for which the velocity increases with frequency and, at its higher velocities, energy can leak into the half-space.

Interface waves. Interface waves can exist at the boundary between two different media. The best known example of an interface wave is the Stoneley wave which can be considered as a generalisation of the Rayleigh wave, where both half-spaces are solids rather than one being solid and the other vacuum. The Stoneley wave is a free wave, the energy being retained at the interface without leakage into either half-space. The Stoneley wave can only exist for certain combinations of properties of the two media. For other combinations a leaky Stoneley wave may propagate, in which energy leaks into one or both of the half-spaces. Waves which travel along very thin interface layers may also be termed interface waves.

1.5 Approaches for inspection using plate waves

Two plate wave approaches have been identified as possible techniques for inspecting diffusion bonded joints for embedded layers of alpha case. The feasibility of each approach will be examined separately in the thesis. They will be referred to respectively as the Lamb wave technique and the interface wave technique.

The first idea is to exploit any changes which the layer may make to the properties of the Lamb waves. For example if the velocity of a particular Lamb wave is altered by the presence of the layer then a testing system could be based on detecting a change in the velocity of this wave.

Figure 1.6(a) shows one experimental arrangement which is used for the excitation and reception of Lamb waves. Water is used in this arrangement for acoustic coupling between the transducers and the plate. The transmitted signal may be used to excite waves in the plate with a particular velocity by the choice of the angle of incidence of the transducer. The frequency of excitation may also be chosen to preferentially excite waves at particular frequencies. Thus by choosing the angle of incidence and the frequency it is possible to target the energy on a particular location on the Lamb wave dispersion diagram.

Precise measurements of the velocity of a Lamb wave may be made either by receiving the wave at some distance from the transmitter or by detecting the fact that a wave has been excited, by employing a point measurement technique at the excitation location (Mal, Xu and Bar-Cohen (1989)). In either case the measurement relies on the detection of leaking or reflected energy returning from the plate to the receiving transducer.

The second plate wave idea is to consider an interface wave which travels within the embedded layer. This idea is illustrated in Figure 1.6(b). The transmitting transducer is angled such that the refracted wave within the top adherend arrives at the layer at the appropriate angle to excite a particular wave in the layer. The wave propagates along the layer, leaking energy back into the adherends as it travels. A receiving transducer is used to detect the wave, again either by detecting some of the leaking energy at an appropriate location downstream or by detecting the fact that a wave has been excited at the excitation point. The presence of an embedded layer is demonstrated if the interface wave can be excited and it may be possible to characterise the layer from the properties of the wave.

1.6 Development of model

Both of the methods discussed above require careful examination of the modal properties of good and bad bonds in order to select the best testing conditions. Some modes will inevitably be much more sensitive to the presence of an embedded layer than others and it is essential that such characteristics are investigated carefully if the methods are to be assessed favourably.

The Lamb waves for a single layer of material in vacuum are well known but general solutions are not available for a three layer system in vacuum, which would be required for the first method, or for a layer surrounded by another material, which would be required for the second method. A major part of the research programme has therefore been to develop a comprehensive modelling tool for calculating the modal properties of these systems.

The model is general in its capabilities. It can be used on plate systems of any numbers of layers of different materials and thicknesses, the only limitation being that the interfaces must all be parallel so that each layer is of uniform thickness throughout its width. The layers may be solid or liquid and their properties may be elastic or visco-elastic, so that material damping may be taken into account if required. The plate system may be in vacuum so that propagating waves in elastic materials travel indefinitely without leaking any energy. Alternatively the system may be 'immersed' in a liquid or in a solid so that energy may leak into the half-spaces causing the wave to decay as it travels. In all cases plane strain is assumed, being the best two dimensional representation of a wide wavefront.

The model calculates the dispersion curves for the layer system and displays them in a number of ways. Primarily the phase velocity curves can be plotted. Alternatively plots may be made of group velocity, coincidence angle, real wavenumber or attenuation versus frequency. The group velocity differs from the phase velocity in that it describes the velocity at which energy is transported rather than the velocity of wave crests - there is a difference between these velocities when the wave is dispersive, which will be discussed in Chapter 5. The coincidence angle is the angle of incidence of a bulk wave in a coupling medium being used to excite the wave, as introduced in the previous section. The real wavenumber is simply the reciprocal of the wavelength. The attenuation is the decay of the wave due either to leakage of energy into the half-spaces or to damping losses in viscoelastic materials. It is expressed as an exponential decay per unit distance or per wavelength along the plate.

The model also calculates the field distributions through the thickness of the layers, the mode shapes. Plots may be made of the distributions of all of the displacement and stress components and of the strain energy density which gives an indication of the distribution of the energy of the wave.

The model was implemented on a microcomputer and was validated against a number of cases of published solutions and experimental measurements.

1.7 Historical background

Materials and diffusion bonding

The diffusion bonding of titanium alloys is a relatively new joining process, having been under development for the last twenty years or so and in use for some components for around ten years. In the UK. the major progress has been made by British Aerospace plc and by Rolls Royce plc. Discussions about their bonding methods and applications have been published by Stephen (1986) and Broomfield (1986). An excellent review of the bonding process has also been presented by Partridge (1987), including a wide survey of the literature. All three of these authors include some discussion about the metallurgy of the material. Good background information can also be found in the metallographic summary published by the RMI Company (1981).

The mechanisms for the development of alpha case, when the material is exposed to oxygen or nitrogen at high temperature, are well known by the metallurgists. It is also understood from the microscopic point of view that saturated alpha case is likely to be somewhat stiffer than the raw alloy. Relatively little has been published however on the actual measurement of the acoustic properties of realistic concentrations of alpha case or on the nature of its distribution near an exposed surface. The major evidence comes from the researchers at Iowa State University who have measured some acoustic velocities (Thompson, Margetan, Rose and Batra (1992), Brasche, Margetan and Thompson (1992)) with an interest in developing inspection methods for the detection of discrete inclusions of alpha case embedded in titanium. They have also investigated the changes to the attenuation and backscattering of bulk waves due to the microstructural changes which occur when titanium is converted to alpha case, publishing a number of papers. See Thompson *et al*. (1992) and Margetan and Thompson (1992) for example.

NDT of diffusion bonds

The vast majority of research on the NDT of diffusion bonds has addressed the detection of voids or inclusions at the bondlines of joints. Fundamental work was reported by Baik and Thompson (1984) and Angel and Achenbach (1985) who developed equivalent static spring models for the interfaces of joints in which there is assumed to be an array of penny-shaped cracks. Their models were developed to determine the reflection of ultrasound at normal incidence from the bondline when the wavelength is large in comparison with the crack size.

Further developments have included the consideration of the resonant phenomena which can occur when the wavelength of the ultrasonic signal is similar to the dimensions of the crack (Rose (1990) for example), thus extending the applicability of the model to higher frequencies. The aim in these developments was to be able to determine crack sizes and distributions from measurements of reflection and transmission. A number of successful applications of these models have been reported, for example by Palmer, Rehbein, Smith and Buck (1988) and Margetan, Thompson, Gray and Rose (1990).

Two other approaches for the NDT of diffusion bonds should be mentioned. The first is the idea that it may be possible to correlate the quality of diffusion bonds with the attenuation of ultrasonic signals, attenuation at high frequencies being affected by grain structure. This approach was proposed by Rose (1989) who demonstrated that it has some potential in general (using IN-100 material). The second approach is the investigation of diffusion bonds using acoustic microscopes, reported for example by Weglein (1988) and Bond, Som, Shiloh and Taylor (1990). At present this work is limited to the examination of sections which have been cut through diffusion bonds, using surface waves.

Theory of plate waves

The earliest theory for the modal properties of multilayered media was Lord Rayleigh's derivation (1887) for waves travelling along the free surface of a semi-infinite elastic half-space. The derivation yields a third order expression whose roots determine the velocity of the propagating surface wave. A generalisation of the single interface problem was developed by Stoneley (1924) to describe waves travelling along the interface between two different elastic solids without leakage into the half-spaces. An examination of the ranges of existence of free wave solutions for these two wave equations has been conducted by Scholte (1947). An examination of leaky wave solutions was published by Pilant (1972).

Lamb (1917) added another interface to introduce the notion of a flat layer of finite thickness. His derivation was for plates in vacuum and the roots of his two equations (one for symmetric modes and one for antisymmetric modes) yield the well known Lamb wave dispersion curves. Love (1911) showed that transverse modes were also possible in layers of finite thickness. His modes involve shearing motion in the plane of the layer. Note that this mode of deformation is outside the scope of the model which is developed here.

The derivation of equations for wave propagation in media consisting of arbitrary numbers of flat layers was started by Thomson (1950). He introduced a transfer matrix which described the displacements and stresses at the bottom of a layer with respect to those at the top of the layer. The matrices for any number of layers could be multiplied and modal or response solutions could then be found by application of the appropriate boundary conditions. A small error in his derivation was corrected by Haskell (1953). The theory was developed specifically for seismological applications where interest was in surface waves on media consisting of multiple different rock layers.

Following Thomson's work, and aided by the availability of digital computers, there was an increase in investigations into the modelling of wave propagation in multilayered media, almost entirely for seismological applications. A number of papers over a long period of time have addressed the practicalities of solving the response equations or modal equations by computer with minimum loss of precision and maximum efficiency, for example Press, Harkrider and Seafeldt (1961), Knopoff (1964), Dunkin (1965), Randall (1967), Schwab and Knopoff (1972), Abo-Zena (1979). The most important problem is the loss of precision in the solution when layers of large thickness are present and high frequencies are being considered. Of particular note in this context is the introduction in Knopoff's paper (1964) of a global matrix for the full system instead of transfer matrices. A further improvement to the stability of the global matrix method was subsequently made by Schmidt and Jensen (1985) and Pialucha (1992), with which the problem of loss of precision has effectively been eradicated.

The majority of developments have been confined to systems of equations whose modal solutions describe free wave propagation only. However Gilbert (1964) considered the problem of modelling leaky waves and developed a theory based on complex frequency and real wavenumber which could describe the decay of propagating waves along the layer system. Alsop (1970) and Watson (1972) considered alternatively the possibility of assuming real frequency and complex wavenumber and concluded that either approach could be adopted, the more appropriate choice being based on the application in mind.

Furthermore the majority of applications of the multilayered plate theory have been to response models, in which case the solution of the equations is straightforward. Modal solution is more difficult, and is particularly challenging for attenuating waves. Very little has been published on methods of modal solution of attenuating waves, although clearly a number of researchers have developed modelling tools which are capable of predicting at least some cases of dispersion curves for attenuating waves. One approach utilised in the NDT community has been to

calculate dispersion curves by identifying minima in the reflection coefficient response. For example Mal, Xu and Bar-Cohen (1989) and (1990) used this approach to calculate the dispersion curves for leaky Lamb waves in plates in water. Whereas this is a reasonable approximation for mildly leaking waves, Chimenti and Rokhlin (1990) and Nagy and Adler (1989) have pointed out that the minima of the reflection coefficient do not correspond to the modal solution for leaky waves, and that the differences may be large when the leakage is strong. Nagy and Adler (1989) provided solutions for leaky waves for a layer of adhesive embedded in aluminium half-spaces, commenting on the difficulty of the solution. A number of authors have also published solutions for other specific cases of layered media. For example Chimenti, Nayfeh and Butler (1982) presented a modal analysis for leaky surface waves on a thin layer on a half-space and Kushibiki, Ishikawa and Chubachi (1990) presented solutions of the equations for leaky Sezawa waves.

Application of plate waves to NDT

In recent years considerable work has been done on the application of plate waves outside the field of seismology, principally for non-destructive testing.

A popular topic has been the application of Lamb waves for the inspection and characterisation of single layers of material. Worlton (1957) proposed the use of Lamb waves for the detection of defects in metal plates, identifying in particular the detection of internal laminar flaws lying parallel to the surface of a plate. Subsequently Frederick and Worlton (1962) proposed the use of Lamb waves for the measurement of the thickness of plates. Since then a wide range of applications has been reported, covering many industries, including such diverse applications as the on-line monitoring of the quality of paper in paper mills (Habeger, Mann and Baum (1979)) and the sizing of spot welds (Bendec, Peretz and Rokhlin (1984)). A review of Lamb wave applications may be found in Alleyne's thesis (1991) which is on the use of Lamb waves for the long range detection of flaws in plates.

Lamb waves have also been proposed for the inspection of multilayered media, in particular adhesive joints and composite materials. For example Bar-Cohen and Mal (1990) and Mal, Xu and Bar-Cohen (1989 and 1990) suggested using Lamb waves for the measurement of the cohesive properties of adhesively bonded aluminium. Dewen, Lowe and Cawley (1992) subsequently investigated the sensitivity of Lamb waves to the properties of the adhesive and to other parameters of the joints. The delamination of layered media may also be detected using

Lamb waves. An investigation of the inspection of composite plates for delamination has been reported by Guo and Cawley (1992).

A number of investigators have studied surface waves in thin surface layers on half-spaces, with a view to developing systems for measuring the layer thickness and its material properties. Some examples of generic studies may be found in Adler & Sun (1971), Nayfeh, Chimenti, Adler and Crane (1981), and Rose, Nayfeh, and Pilarski (1990). In practice the measurement could be achieved on a small scale by measuring the surface wave velocity with a line-focus acoustic microscope, as suggested for example by Kushibiki, Ishikawa, and Chubachi (1990). The use of surface waves for the detection of delamination of the thin layer from the half-space has been addressed by Mal and Kundu (1987) and Adler, de Billy and Quentin (1990).

Investigations have also been undertaken on utilising leaky, interface and guided wave propagation in internal layers in a solid for nondestructive testing. Rokhlin, Hefets and Rosen (1980,1981) and Rokhlin (1986) demonstrated that a guided wave travelling along a layer of adhesive between two half-space adherends may be used to determine the material properties of the adhesive (the cohesion properties). Lee and Corbly (1977), Claus and Kline (1979), Kumar (1983) and Pilarski (1985) investigated the use of an interface wave travelling along the boundary between two materials for the determination of the properties of the boundary. In the case of an adhesive joint this approach would address the very difficult problem of determining the quality of the interface between the adhesive and the adherend (the adhesion properties). Nagy and Adler (1989) and Nagy, Rypien and Adler (1990) proposed the use of a leaky wave in the adhesive to detect both poor cohesion and poor adhesion.

1.8 Outline of thesis

This thesis presents an investigation into the potential of using ultrasonic plate waves for the inspection of diffusion bonded titanium joints. The aim of the inspection is to detect the presence of a layer of the oxygen-rich brittle phase of titanium, alpha case, at the bondline of the joint. The principle is that differences in the acoustic properties of the layer with respect to the adherends will affect the modal properties of wave propagation along the joint. Thus the presence of the layer could be detected by the measurement of a selected propagating mode. The objective of the thesis is to assess the feasibility of using plate waves for the detection and characterisation of the layer and to determine whether they can offer any advantages over the conventional ultrasonic technique, the measurement of normal incidence reflectivity.

The development of the modal theory for free wave propagation is presented in Chapter 2. The chapter starts with the derivation of the equation of motion for isotropic materials and concludes with the description of a solution which satisfies both the equation of motion and the boundary conditions imposed by the interfaces between the layers. The solution is in the form of a characteristic function which must yield zero for a modal solution.

In Chapter 3 the modal theory is extended to include the possibility of the propagation of attenuating waves along the layer system. This enables the model to include material damping and the leakage of energy from the plate into the half-spaces. This chapter is written as a generalisation of the free wave theory of Chapter 2.

Chapter 4 covers the implementation of the theory into a computer model for the calculation of dispersion curves and mode shapes. Some of the difficulties of solving the characteristic function are discussed and systematic numerical procedures are developed. Algorithms for the generation of the dispersion curves and for the calculation of mode shapes are described.

The validation of the model is described in Chapter 5. Examples of the application of the model are presented and the modal solutions for a number of layered systems are discussed. Comparisons are also made with known analytical solutions, with solutions predicted by other models and with experimental measurements.

The properties of the materials are investigated in Chapter 6. An experimental study is reported in which alpha case was grown on sheets of titanium by exposing them in air at high temperature and the acoustic properties of both treated and untreated materials were measured. The variation of the alpha case contamination with depth from the exposed surfaces was also investigated by measuring hardness profiles.

Chapter 7 summarises a model study which was made in order to determine the limits of the detectability of defects using conventional normal incidence inspection. Normal incidence reflection measurements were simulated, assuming a variety of alpha case properties and property profiles. The study also includes a brief examination of the reflectivity from arrays of voids at the bondline, voids frequently accompanying alpha case in poor bonds.

The first plate wave approach for inspection, the Lamb wave technique, is assessed in Chapter 8. Model studies are used to determine the sensitivity of the Lamb waves to defects and to other parameters associated with the joints. The excitation and measurement of Lamb waves

is discussed and the method is assessed in the light of the detectability which can be achieved currently using the conventional ultrasonic inspection method.

The interface wave technique is assessed in Chapter 9. Two types of interface wave are considered: waves which travel along a single interface between two materials and waves which travel along an embedded layer. Dispersion curves are calculated and the nature of the waves is analysed. Methods are assessed for the excitation and measurement of interface waves and their potential for inspection is discussed.

The main conclusions of the thesis are presented in Chapter 10.

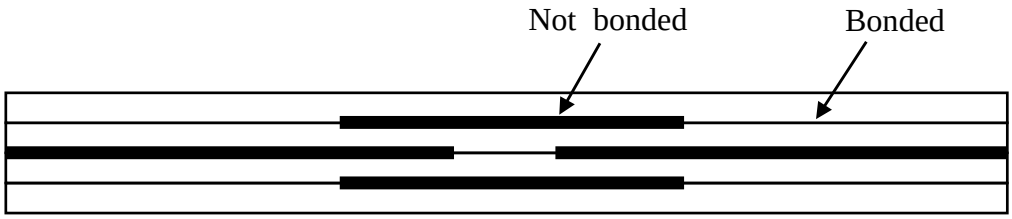

(a) Flat sheets diffusion bonded in predefined pattern

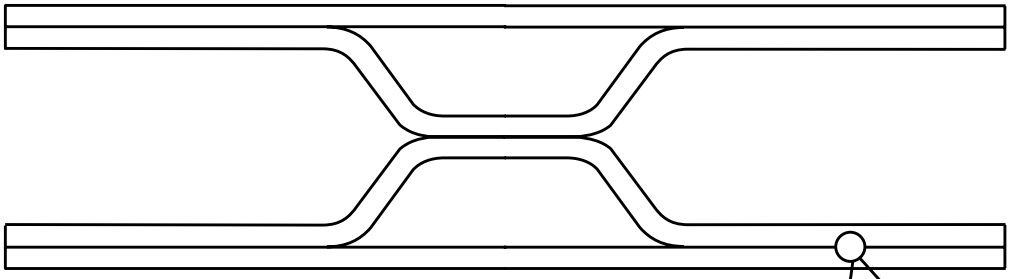

(b) Bonded pack expanded by gas pressure

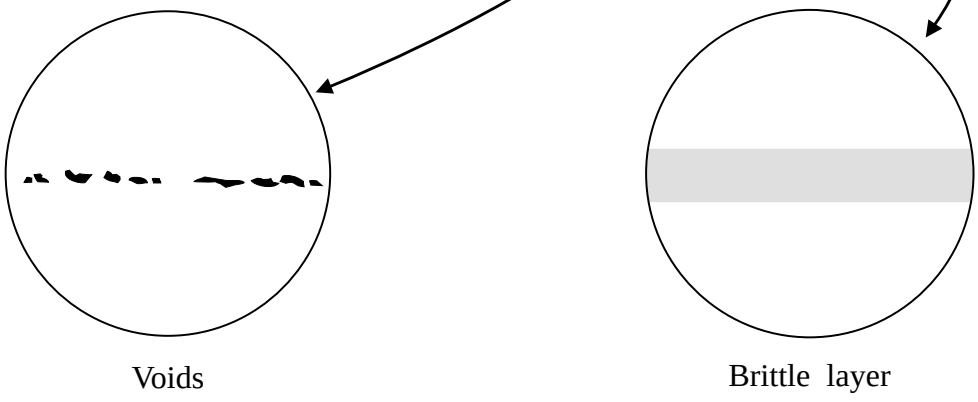

(c) Potential bond defects

Figure 1.1 X-braced structure formed by diffusion bonding and superplastic forming

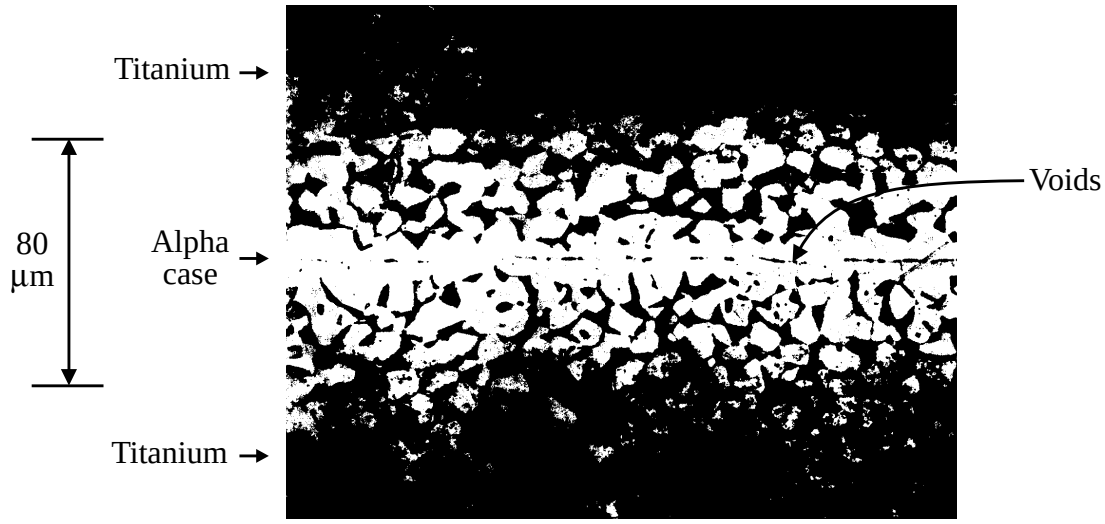

Figure 1.2 Micrograph of poor diffusion bonded joint

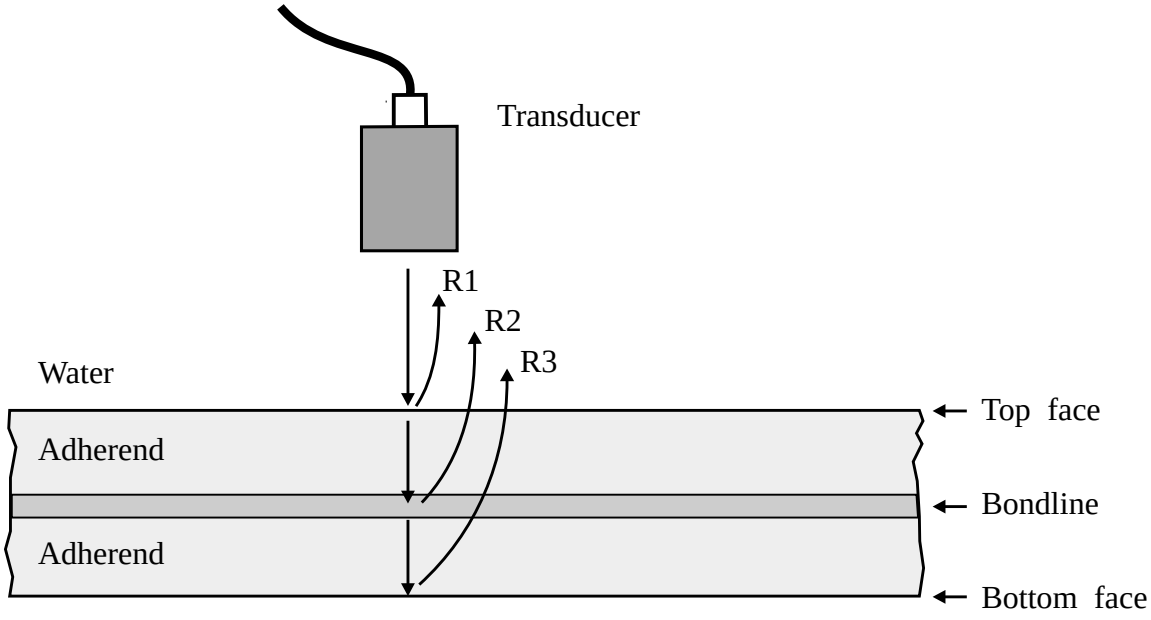

(a) Pulse-echo inspection of joint

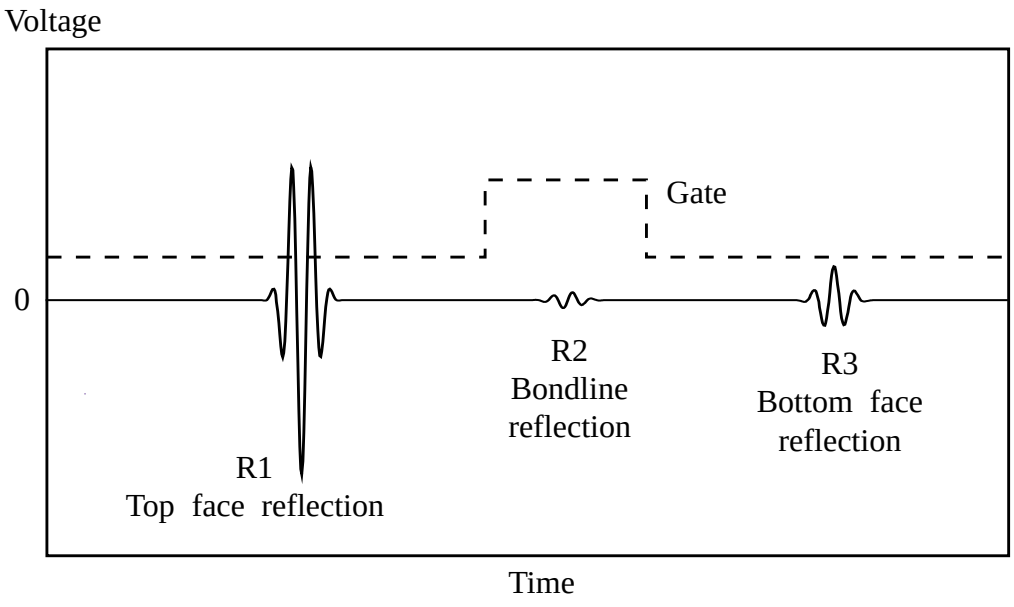

(b) Time trace on oscilloscope

Figure 1.3 Conventional ultrasonic pulse-echo inspection

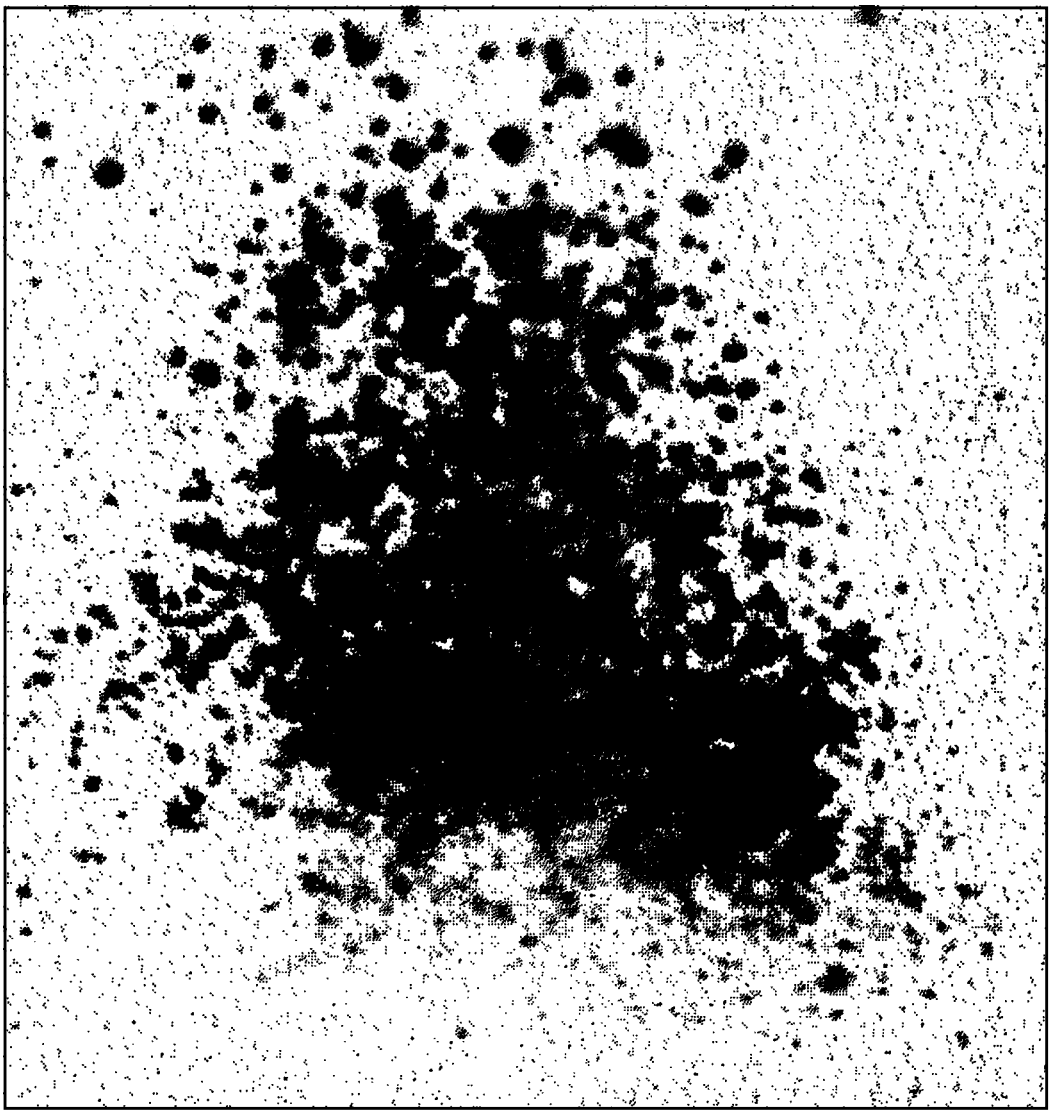

Black = strong reflection from bondline
White = no reflection from bondline

10 μm

Figure 1.4 C-scan of unbonded regions in very poor diffusion bonded joint

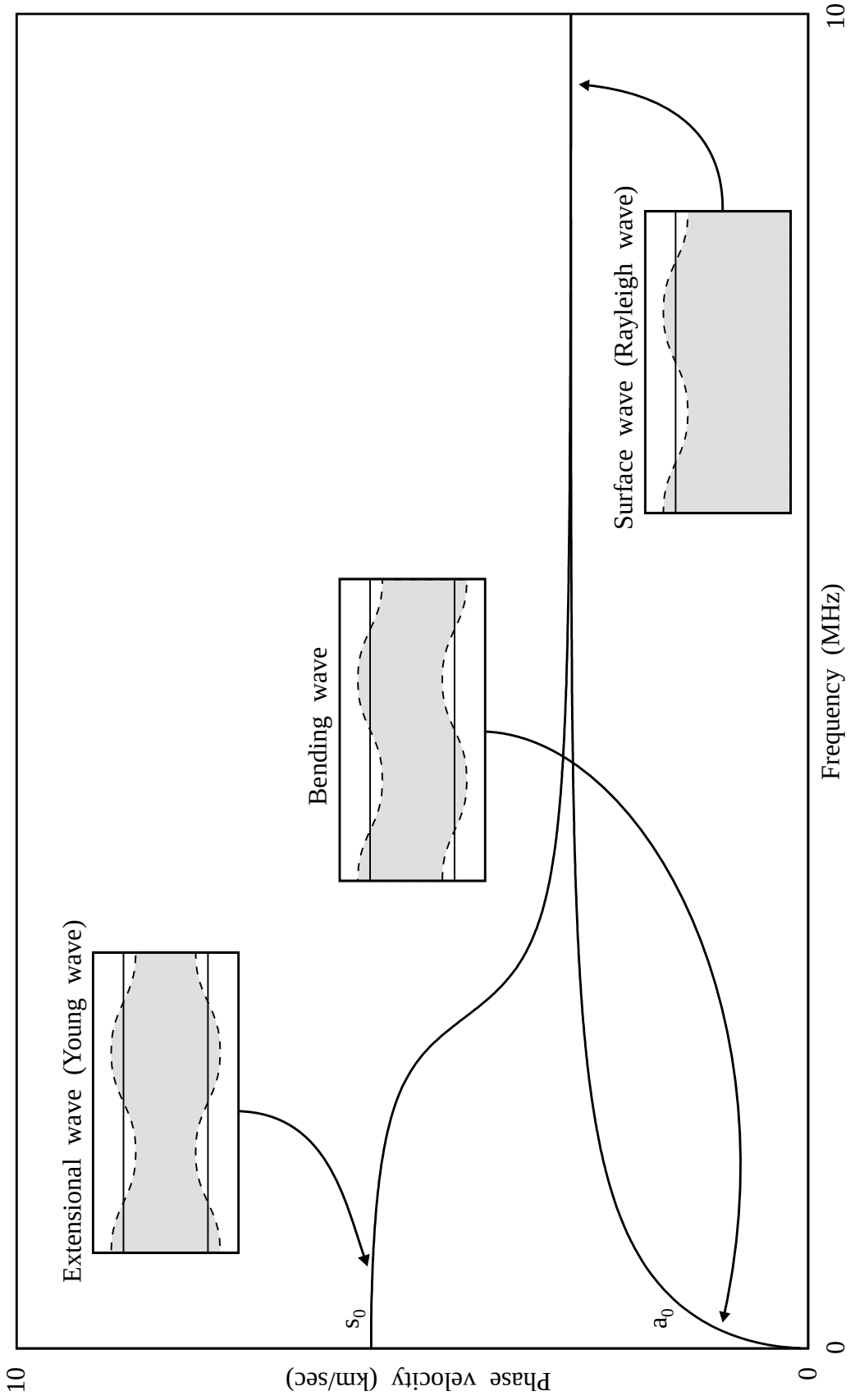

Figure 1.5 Dispersion curves for first two Lamb modes in 1.0 mm thick titanium sheet

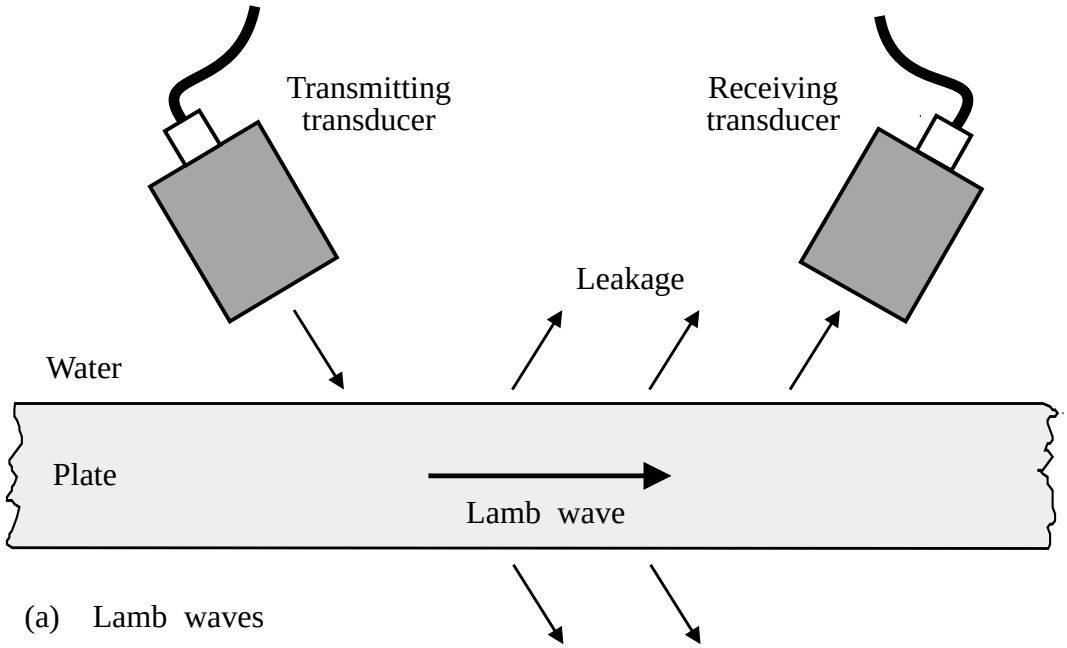

(a) Lamb waves

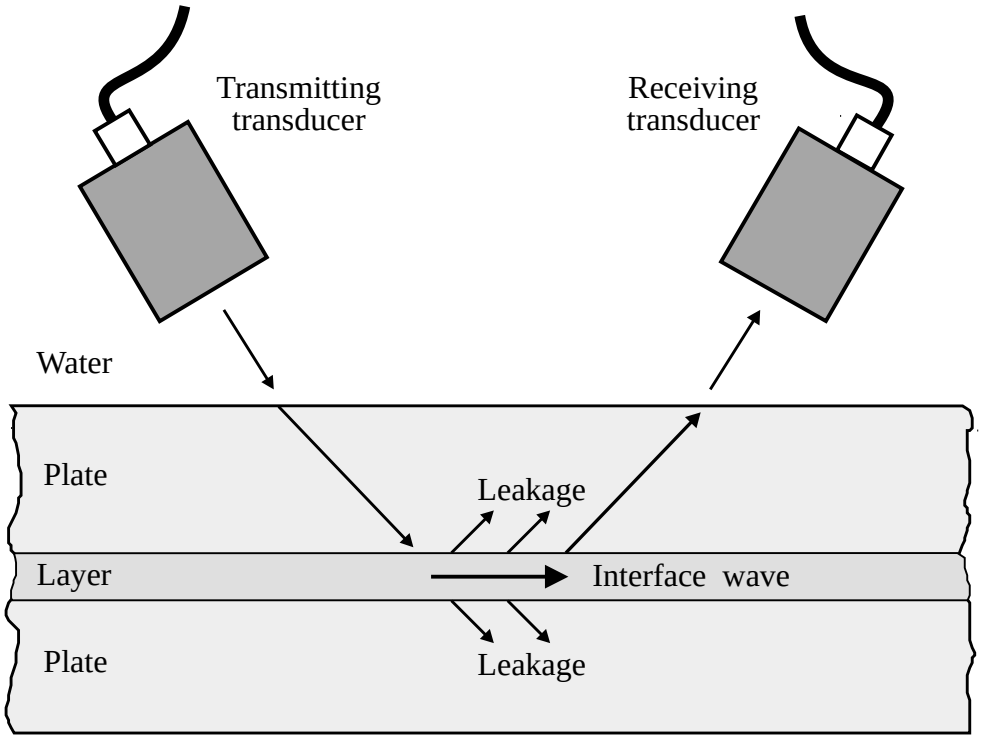

(b) Interface waves

Figure 1.6 Excitation and detection of plate waves

CHAPTER 2

Free wave propagation along a multilayered plate

2.1 Introduction

A modal theory for free wave propagation in a multilayered medium is described in this chapter. This theory, together with the theory for attenuating wave propagation in Chapter 3, forms the basis for the predictive model which was used for the feasibility studies. The implementation of the theories into the computer model will be described in Chapter 4.

A free propagating wave is defined as one which travels indefinitely without change of amplitude, without input of energy and without loss of energy. Free wave propagation in multilayered plates is therefore necessarily limited to elastic materials without material damping which would attenuate the waves. It is also limited to waves which do not leak energy into the surrounding media.

The multilayered medium considered here is a plate system consisting of an arbitrary number of perfectly flat layers, stacked together. Each layer is an isotropic material, with a given uniform finite thickness and each is connected rigidly to the layer below and the layer above, as illustrated in Figure 2.1. Above and below the plate system are semi-infinite half-spaces of elastic material or vacuum. The system is assumed to be infinite in all horizontal directions.

A modal solution for wave propagation in multilayered plates is a frequency domain solution for conditions under which waves may propagate along the plate. Just as bulk waves can only propagate in an infinite medium at two velocities, either longitudinal or shear, waves can only propagate along a multilayered plate under certain conditions. These conditions are in general frequency dependent so that solutions are described, not just by velocity, but by combinations of frequency and velocity. A modal solution for wave propagation states that a wave may travel with a particular frequency and velocity. The solution is a two-dimensional eigensolution for the system, where the frequency and velocity are an eigenvalue pair.

Overview

The approach which is taken here is to build a modal description of free wave propagation in a multilayered plate by the superposition of modal solutions for bulk wave propagation in each layer and the application of suitable boundary conditions at the interfaces between the layers. If all possible modal solutions are known for infinite media then it is possible to construct all possible solutions in the multilayered plate by their superposition in appropriate proportions.

The first task is to obtain solutions for bulk wave propagation in infinite media. It is shown that exactly two such waves can exist in an elastic isotropic medium, a 'longitudinal' wave in which motion consists of change of volume of the material and a 'shear' wave in which motion consists of distortion of the material by displacement normal to the direction of motion of the wave without change of volume. These two types of wave are the eigensolutions for an infinite medium and each has its characteristic propagation speed governed by the two elastic material constants and the density. In an infinite medium only these two types of 'bulk' wave can propagate in any direction.

Next, the general examination of wave propagation in an infinite medium is reduced to the special case of a two-dimensional infinite space in which plane strain and in-plane motion only are considered. The bulk waves are therefore restricted to those which propagate in directions lying in the plane and whose particle motion is also entirely in the plane. For these waves there is no variation of any field variables in the direction normal to the plane and so any plate wave which is described by their superposition will also have these properties. Particle displacements and stresses are derived for these waves.

The interaction of bulk waves with an interface is then examined. The theory is developed for the case of two semi-infinite media which meet at an infinitely long straight interface. In general four bulk waves can exist on each side of the interface, a longitudinal and a shear wave arriving and a longitudinal and a shear wave leaving. However there are four boundary conditions of displacements and stresses which must be satisfied at the interface in order that combinations of these bulk waves can exist as eigensolutions of the two-media system. This places the restrictions on the bulk waves that they must have the same frequency and the same wavenumber in the direction parallel to the interface. They therefore have the same velocity component in this direction, as will any wave which is described by the superposition of these waves. It is

also shown that, in order to satisfy these conditions in some circumstances, inhomogeneous longitudinal and shear waves can exist, propagating without diminishing along the interface but decaying in the direction normal to the interface.

Finally the analysis is extended to a multilayered plate by the consideration of a sequence of these interfaces, parallel to each other and spaced apart according to the layer thicknesses. An eigensolution will exist for wave propagation along this system when the interface boundary conditions are satisfied simultaneously at all of the interfaces. This means that for given geometry and material properties, suitable values of frequency and wavenumber (or wavelength or velocity) have to be found. Two different strategies are developed for the solution, each concluding with the definition of a characteristic function whose result must be zero for a modal solution to exist.

2.2 Plane waves in an infinite elastic medium

The development of the equations of motion for an infinite elastic solid has been covered in many texts (see Brekhovskikh and Goncharov, 1985, for example). The usual approach, presented here, is to start with an infinitesimal cubic element in an infinite elastic isotropic medium of density ρ. A Cartesian system is adopted, here with displacements u_1,u_2 and u_3 in directions x_1,x_2 and x_3 respectively. By application of Newton's second law, equilibrium requires that:

Equilibrium:

$$\rho \frac{\partial^2 u_1}{\partial t^2} = \frac{\partial \sigma_{11}}{\partial x_1} + \frac{\partial \sigma_{12}}{\partial x_2} + \frac{\partial \sigma_{13}}{\partial x_3}$$

$$\rho \frac{\partial^2 u_2}{\partial t^2} = \frac{\partial \sigma_{21}}{\partial x_1} + \frac{\partial \sigma_{22}}{\partial x_2} + \frac{\partial \sigma_{23}}{\partial x_3}$$

$$\rho \frac{\partial^2 u_3}{\partial t^2} = \frac{\partial \sigma_{31}}{\partial x_1} + \frac{\partial \sigma_{32}}{\partial x_2} + \frac{\partial \sigma_{33}}{\partial x_3} \qquad (2.1)$$

where $\sigma_{11,12}$ etc. are the stress components acting on the faces of the cube and t is time.

These are the fundamental stress equations of motion for the medium. It will be more convenient if they are expressed in terms of displacements, by substituting the stress-strain and the strain-displacement equations:

Stress-strain:

$$\sigma_{11} = \lambda\Delta+2\mu\varepsilon_{11} \quad , \quad \sigma_{22} = \lambda\Delta+2\mu\varepsilon_{22} \quad , \quad \sigma_{33} = \lambda\Delta+2\mu\varepsilon_{33}$$

$$\sigma_{12} = \mu\varepsilon_{12} \quad , \quad \sigma_{23}= \mu\varepsilon_{23}, \quad \sigma_{13} = \mu\varepsilon_{13} \tag{2.2}$$

where λ and μ are Lamé's elastic stiffness constants and $\Delta = \varepsilon_{11} + \varepsilon_{22} + \varepsilon_{33}$ is the change in volume (dilatation) of the element. λ and μ are related to Young's modulus (E) and Poisson's ratio (ν) by the expressions:

$$\lambda = \frac{E\nu}{(1+\nu)(1-2\nu)}$$

$$\mu = \frac{E}{2(1+\nu)}$$

$$E = \frac{\mu}{(\lambda+\mu)}(3\lambda+2\mu)$$

$$\nu = \frac{\lambda}{2(\lambda+\mu)} \tag{2.3}$$

Strain-displacement:

$$\varepsilon_{11} = \frac{\partial u_1}{\partial x_1} \quad , \quad \varepsilon_{22} = \frac{\partial u_2}{\partial x_2} \quad , \quad \varepsilon_{33} = \frac{\partial u_3}{\partial x_3}$$

$$\varepsilon_{12} = \frac{\partial u_1}{\partial x_2} + \frac{\partial u_2}{\partial x_1} \quad , \quad \varepsilon_{23} = \frac{\partial u_2}{\partial x_3} + \frac{\partial u_3}{\partial x_2} \quad , \quad \varepsilon_{13} = \frac{\partial u_1}{\partial x_3} + \frac{\partial u_3}{\partial x_1} \tag{2.4}$$

Substitution yields the displacement equations of motion:

$$\rho \frac{\partial^2 u_1}{\partial t^2} = (\lambda + \mu) \frac{\partial}{\partial x_1} \left(\frac{\partial u_1}{\partial x_1} + \frac{\partial u_2}{\partial x_2} + \frac{\partial u_3}{\partial x_3}\right) + \mu\nabla^2 u_1$$

$$\rho \frac{\partial^2 u_2}{\partial t^2} = (\lambda + \mu) \frac{\partial}{\partial x_2} \left(\frac{\partial u_1}{\partial x_1} + \frac{\partial u_2}{\partial x_2} + \frac{\partial u_3}{\partial x_3}\right) + \mu\nabla^2 u_2$$

$$\rho \frac{\partial^2 u_3}{\partial t^2} = (\lambda + \mu) \frac{\partial}{\partial x_3} \left(\frac{\partial u_1}{\partial x_1} + \frac{\partial u_2}{\partial x_2} + \frac{\partial u_3}{\partial x_3}\right) + \mu\nabla^2 u_3 \tag{2.5}$$

where ∇^2 is the operator $\left(\frac{\partial^2}{\partial x_1^2} + \frac{\partial^2}{\partial x_2^2} + \frac{\partial^2}{\partial x_3^2}\right)$.

These equations cannot be integrated directly. Therefore for any application, a form of solution must be assumed and checked for suitability by differentiation and substitution. Here it is assumed that the wavefront is an infinite plane which is normal to the direction of propagation, as illustrated in Figure 2.2. It is also assumed that, at any position in the propagation direction and at any instant in time, all displacements are uniform over the plane of the wavefront (this defines a homogeneous wave). Since the medium is isotropic it is only necessary to consider a wave travelling parallel to the x_1 axis without loss of generality. Thus the wave is infinite and unchanging in the x_2 and x_3 directions and all variations are in the x_1 direction only. In this case a solution of the following form may be assumed:

$$u_1,u_2,u_3 = A\, e^{i(2\pi x_1/L - \omega t)} + B\, e^{i(2\pi x_1/L + \omega t)} \tag{2.6}$$

where A and B are constants, L is the wavelength and ω is the frequency in radians per second. By recognising that velocity, c, is the product of frequency (in Hz) and wavelength, the solution can also be expressed in the form:

$$u_1,u_2,u_3 = A\, e^{i\omega(x_1/c - t)} + B\, e^{i\omega(x_1/c + t)} \tag{2.7}$$

or in terms of the wavenumber, $k = \omega/c$, in the form:

$$u_1,u_2,u_3 = A\, e^{i(kx_1 - \omega t)} + B\, e^{i(kx_1 + \omega t)} \tag{2.8}$$

In each case the first term represents a harmonic wave travelling with amplitude A in the positive x_1 direction and the second term represents a wave of amplitude B travelling in the opposite direction. The particle motion of the wave need not necessarily be parallel to the direction of propagation and is in general some combination of u_1,u_2,u_3.

Differentiation of (2.6), (2.7) or (2.8) and substitution into (2.5) yields two possible expressions for the speed c,

$$c = \frac{\omega L}{2\pi} = \frac{\omega}{k} = \left(\frac{\lambda+2\mu}{\rho}\right)^{1/2} = \left(\frac{E(1-\nu)}{\rho(1+\nu)(1-2\nu)}\right)^{1/2} = \alpha \text{ , say}$$

$$c = \frac{\omega L}{2\pi} = \frac{\omega}{k} = \left(\frac{\mu}{\rho}\right)^{1/2} = \left(\frac{E}{2\rho(1+\nu)}\right)^{1/2} = \beta \text{ , say} \qquad (2.9)$$

The first solution requires that the particle motion is entirely in the direction of propagation. In this case the wave motion consists of change of volume of the medium only (dilatation). The second solution requires that the motion is normal to the direction of propagation and the motion consists of rotation of the medium without change of volume.

Thus two types of homogeneous plane wave may travel through the medium in any direction, dilatational waves with speed α and rotational waves with speed β. These (bulk waves) are the eigensolutions for the equation of motion in an infinite elastic isotropic medium. Waves will propagate infinitely with these velocities, without changing direction or amplitude.

Dilatational waves are often referred to as 'longitudinal' waves and rotational waves as 'shear' waves. These terms can be a little misleading because 'longitudinal' and 'shear' deformations are not uncoupled - 'longitudinal' deformation involves both extensional and shear behaviour as can be seen from the presence of the Lamé constant μ for longitudinal waves in equation (2.9). However these terms are in very common use and for simplicity they will be adopted from now on.

Before proceeding with the analysis a great deal of simplification will be achieved by taking advantage of the principle of superposition and separating equations (2.5) into these two displacement fields, one of 'longitudinal' waves and the other of 'shear' waves. At the same time the specific coordinates x_1, x_2 and x_3 and the displacements u_1, u_2 and u_3 will be replaced in the equations by their general vector forms $\mathbf{x}$ and $\mathbf{u}$.

A neat and general way to separate the fields is to use the Helmholtz method (Malvern, 1969, for example). This defines two wave potentials, a scalar function ϕ and a vector function $\boldsymbol{\psi}$, representing longitudinal (L) and shear waves (S) respectively and performs the separation by the operations:

$$\mathbf{L} = \nabla\phi$$
$$\mathbf{S} = \nabla \text{ X } \boldsymbol{\psi} \tag{2.10}$$

where ∇ is the vector operator $\left(\frac{\partial}{\partial x_1} , \frac{\partial}{\partial x_2} , \frac{\partial}{\partial x3} \right)$ and X denotes the vector cross product.

The total displacement field is then given by the superposition of these two fields:

$$\mathbf{u} = \mathbf{L} + \mathbf{S} \tag{2.11}$$

and equation (2.5) breaks down into the two parts:

$$\rho \frac{\partial^2\phi}{\partial t^2} = (\lambda + 2\mu) \nabla^2 \phi$$

and

$$\rho \frac{\partial^2\boldsymbol{\psi}}{\partial t^2} = \mu \nabla^2 \boldsymbol{\psi} \tag{2.12}$$

Now the solution equation (2.6) can be expressed as:

$$\phi = A_{(L)} e^{i\omega(\mathbf{N}\bullet\mathbf{x}/\alpha - t)}$$

and

$$\boldsymbol{\psi} = A_{(S)} e^{i\omega(\mathbf{N}\bullet\mathbf{x}/\beta - t)} \tag{2.13}$$

where **N** is a vector of unit length which defines the direction of propagation and $A_{(L)}$ and $A_{(S)}$ are the longitudinal and shear wave amplitudes. The propagation vector **N** is introduced for convenience, to simplify the derivation. It is illustrated in Figure 2.3 together with an expansion of equation (2.13) into its component parts. To generalise the expressions the amplitudes may be taken as complex quantities $A_{(L)}e^{i\varphi}$, $A_{(S)}e^{i\varphi}$, where φ is the phase of the wave at the spatial and temporal origin $\mathbf{x} = 0$, $t = 0$.

Wavenumber description:

These equations are often expressed in a more general form:

$$\phi = A_{(L)}\, e^{i(\mathbf{k}\bullet\mathbf{x} - \omega t)}$$

$$\boldsymbol{\psi} = A_{(S)}\, e^{i(\mathbf{k}\bullet\mathbf{x} - \omega t)} \qquad (2.14)$$

where **k** is the wavenumber vector, describing the spatial distribution of the wave. **k** is real and parallel to **N** for an elastic homogeneous plane wave and is given by:

$$\mathbf{k} = \frac{\mathbf{N}\omega}{\alpha} \qquad \text{for longitudinal waves}$$

$$\mathbf{k} = \frac{\mathbf{N}\omega}{\beta} \qquad \text{for shear waves} \qquad (2.15)$$

The wave propagates with wavelength (L) and speed (c) in the **k** direction of :

$$L = \frac{2\pi}{|\mathbf{k}|}$$

$$c = \frac{\omega}{|\mathbf{k}|} \qquad (2.16)$$

2.3 Plane waves in a two-dimensional space

The analysis will now be restricted to the two-dimensional case of plane strain and the displacements and stresses associated with the plane waves will be derived.

The application of the model is to the propagation of waves along plates of significant width compared to the wavelengths. It is therefore appropriate to simplify the model to two-dimensional plane strain such that all behaviour in the plane is assumed to be identical in any other parallel plane. Thus the plate is assumed to be infinitely wide.

The analysis so far has been independent of the orientation of the Cartesian coordinate system. Any orientation of the coordinate system may therefore be chosen without influence on the model. An attractive one is that in which x_3 is the direction normal to the plane, as shown in Figure 2.4. For plane strain there is no variation of any quantity in the x_3 direction:

$$\frac{\partial}{\partial x_3} = 0 \qquad (2.17)$$

With this limitation, all solutions will describe waves propagating in the plane, i.e. in a direction consisting of components of x_1 and x_2 only. The direction x_1 will be associated later with the direction of propagation of the modal solutions along the plate and x_2 with the direction through the thickness of the plate. However for the moment the x_1 and x_2 dimensions are still considered to be infinite so that the two-dimensional bulk plane waves can be defined.

At this stage one further restriction is voluntarily placed on the model by stating that there is to be no displacement in the x_3 direction:

$$u_3 = 0 \tag{2.18}$$

This latter restriction limits solutions such that, in addition to the waves propagating only in the plane, the particle motion is also only in the plane. In particular it requires that shear waves (rotational motion) involve rotation about the x_3 axis only. This excludes 'in-plane' shear modes (Love waves for example) from the model.

Displacements of longitudinal waves:

From equation (2.10) and (2.13) the displacement vector of a longitudinal wave of potential ϕ is:

$$\mathbf{u} = \nabla\phi = \nabla(A_{(L)}\, e^{i\omega(\mathbf{N}\bullet\mathbf{x}/\alpha - t)}) \tag{2.19}$$

Expressing this in its component parts and re-scaling the (arbitrary) amplitude A_L:

$$u_1 = N_1\, A_{(L)}\, e^{i\omega(N_1x_1/\alpha + N_2x_2/\alpha - t)}$$

$$u_2 = N_2\, A_{(L)}\, e^{i\omega(N_1x_1/\alpha + N_2x_2/\alpha - t)} \tag{2.20}$$

Displacements of shear waves:

Similarly the displacement vector of a shear wave of potential $\boldsymbol{\psi}$ is

$$\mathbf{S} = \nabla \times \boldsymbol{\psi} = \nabla \times (A_{(S)}\, e^{i\omega(\mathbf{N}\bullet\mathbf{x}/\beta - t)}) \tag{2.21}$$

Here the potential $\boldsymbol{\psi}$ is the vector of rotation about the x_3 direction (note that equation (2.18) limits rotation to this axis). The cross product is therefore given by

$$\nabla \text{ X } \boldsymbol{\psi} = \begin{Bmatrix} \frac{\partial}{\partial x_1} \\ \frac{\partial}{\partial x_2} \\ \frac{\partial}{\partial x_3} \end{Bmatrix} \text{ X } \begin{Bmatrix} 0 \\ 0 \\ \psi_3 \end{Bmatrix} \tag{2.22}$$

and the component displacement parts are

$$u_1 = N_2 \, A_{(S)} \, e^{i\omega(N_1 x_1/\beta + N_2 x_2/\beta - t)}$$

$$u_2 = - N_1 \, A_{(S)} \, e^{i\omega(N_1 x_1/\beta + N_2 x_2/\beta - t)} \tag{2.23}$$

Stresses of plane waves:

Substituting equation (2.4) into (2.2), the stresses can be expressed in terms of the displacements as:

$$\sigma_{11} = \lambda \left(\frac{\partial u_1}{\partial x_1} + \frac{\partial u_2}{\partial x_2} + \frac{\partial u_3}{\partial x_3} \right) + 2\mu \frac{\partial u_1}{\partial x_1}$$

$$\sigma_{22} = \lambda \left(\frac{\partial u_1}{\partial x_1} + \frac{\partial u_2}{\partial x_2} + \frac{\partial u_3}{\partial x_3} \right) + 2\mu \frac{\partial u_2}{\partial x_2}$$

$$\sigma_{33} = \lambda \left(\frac{\partial u_1}{\partial x_1} + \frac{\partial u_2}{\partial x_2} + \frac{\partial u_3}{\partial x_3} \right) + 2\mu \frac{\partial u_3}{\partial x_3}$$

$$\sigma_{12} = \mu \left(\frac{\partial u_1}{\partial x_2} + \frac{\partial u_2}{\partial x_1} \right)$$

$$\sigma_{23} = \mu \left(\frac{\partial u_2}{\partial x_3} + \frac{\partial u_3}{\partial x_2} \right)$$

$$\sigma_{13} = \mu \left(\frac{\partial u_1}{\partial x_3} + \frac{\partial u_3}{\partial x_1} \right) \tag{2.24}$$

According to the plane strain condition of equation (2.17) these equations reduce to

$$\sigma_{11} = \lambda \left(\frac{\partial u_1}{\partial x_1} + \frac{\partial u_2}{\partial x_2} \right) + 2\mu \frac{\partial u_1}{\partial x_1}$$

$$\sigma_{22} = \lambda \left(\frac{\partial u_1}{\partial x_1} + \frac{\partial u_2}{\partial x_2} \right) + 2\mu \frac{\partial u_2}{\partial x_2}$$

$$\sigma_{33} = \lambda \left(\frac{\partial u_1}{\partial x_1} + \frac{\partial u_2}{\partial x_2} \right)$$

$$\sigma_{12} = \mu \left(\frac{\partial u_1}{\partial x_2} + \frac{\partial u_2}{\partial x_1} \right)$$

$$\sigma_{23} = \sigma_{13} = 0 \qquad (2.25)$$

Stresses of longitudinal waves:

The stresses associated with longitudinal waves are found by differentiating equation (2.19) with respect to x_1 and x_2 and substituting into equation (2.25):

$$\sigma_{11} = \left(\lambda N_1^2 + \lambda N_2^2 + 2\mu N_1^2 \right) \frac{i \omega A(L)}{\alpha} e^{i\omega(\mathbf{N}\bullet\mathbf{x}/\alpha - t)}$$

$$\sigma_{22} = \left(\lambda N_1^2 + \lambda N_2^2 + 2\mu N_2^2 \right) \frac{i \omega A(L)}{\alpha} e^{i\omega(\mathbf{N}\bullet\mathbf{x}/\alpha - t)}$$

$$\sigma_{33} = \left(\lambda N_1^2 + \lambda N_2^2 \right) \frac{i \omega A(L)}{\alpha} e^{i\omega(\mathbf{N}\bullet\mathbf{x}/\alpha - t)}$$

$$\sigma_{12} = \left(2\mu N_1 N_2 \right) \frac{i \omega A(L)}{\alpha} e^{i\omega(\mathbf{N}\bullet\mathbf{x}/\alpha - t)} \qquad (2.26)$$

Taking advantage of the unit length of vector **N** and substituting equations (2.9), these stress equations can be expressed in terms of the velocities α and β of the bulk waves:

$$\sigma_{11} = \left(\alpha - \frac{2\beta^2}{\alpha} N_2^2 \right) i \omega \rho A_{(L)} e^{i\omega(\mathbf{N}\bullet\mathbf{x}/\alpha - t)}$$

$$\sigma_{22} = \left(\alpha - \frac{2\beta^2}{\alpha} N_1^2 \right) i \omega \rho A_{(L)} e^{i\omega(\mathbf{N}\bullet\mathbf{x}/\alpha - t)}$$

$$\sigma_{33} = \left(\alpha - \frac{2\beta^2}{\alpha} \right) i \omega \rho A_{(L)} e^{i\omega(\mathbf{N}\bullet\mathbf{x}/\alpha - t)}$$

$$\sigma_{12} = \left(\frac{2\beta^2}{\alpha} N_1 N_2 \right) i \omega \rho A_{(L)} e^{i\omega(\mathbf{N}\bullet\mathbf{x}/\alpha - t)} \qquad (2.27)$$

Stresses of shear waves:

The stresses associated with shear waves are found similarly by differentiating equations (2.23) with respect to x_1 and x_2 and substituting into equation (2.25):

$$\sigma_{11} = \left(2\mu N_1 N_2 \right) \frac{i \omega A_{(S)}}{\beta} e^{i\omega(\mathbf{N}\bullet\mathbf{x}/\beta - t)}$$

$$\sigma_{22} = \left(-2\mu N_1 N_2 \right) \frac{i \omega A_{(S)}}{\beta} e^{i\omega(\mathbf{N}\bullet\mathbf{x}/\beta - t)} = - \sigma_{11}$$

$$\sigma_{33} = 0$$

$$\sigma_{12} = \left(N_2^2 - N_1^2 \right) \frac{i \omega A_{(S)}}{\beta} e^{i\omega(\mathbf{N}\bullet\mathbf{x}/\beta - t)} \qquad (2.28)$$

Again these stress equations can be expressed in terms of the velocities α and β of the bulk waves:

$$\sigma_{11} = \left(2 \beta N_1 N_2 \right) i \omega \rho A_{(S)} e^{i\omega(\mathbf{N}\bullet\mathbf{x}/\beta - t)}$$

$$\sigma_{22} = - \sigma_{11}$$

$$\sigma_{33} = 0$$

$$\sigma_{12} = \left(N_2^2 - N_1^2 \right) \beta \, i \omega \rho A_{(S)} e^{i\omega(\mathbf{N}\bullet\mathbf{x}/\beta - t)} \qquad (2.29)$$

2.4 Plane waves at the boundary between two media

The equations so far are sufficient to describe the behaviour and quantities of interest of bulk plane longitudinal and bulk plane shear waves in an infinite elastic medium. Now the derivation will be continued by examining the interaction of these waves with a plane boundary. An analysis of the interaction of plane waves with a boundary may also be found in Kolsky (1963) or Brekhovskikh and Goncharov (1985). This analysis will form the basis of the assembly of propagating waves in a layered system by the superposition of bulk wave components.

It is assumed now that there are two semi-infinite half-spaces in plane strain. The interface between the half-spaces is an infinite flat plane defined by the origin of the coordinate x_2. Thus all points on the interface have $x_2 = 0$ and waves propagate in the x_1 and x_2 plane, as shown in Figure 2.5.

Consider a longitudinal elastic bulk wave travelling in medium 1 and arriving at the interface (Figure 2.5). The wave is infinitely wide, extending from $-\infty$ to $+\infty$ in the x_1 direction, and is continuous in time. Its displacement in the x_1 direction is described for all positions in the half-space of medium 1 by equation (2.20):

$$u_1 = N_1 A_{(L)} e^{i\omega(N_1 x_1/\alpha + N_2 x_2/\alpha - t)} \qquad ((2.20))$$

The intersection of this wave with the interface is described by this equation when the coordinate x_2 is zero. This can be viewed as the projection of the wave onto the interface or as the x_1 component of the wave at the interface. Now the equation reduces to:

$$u_1 = N_1 A_{(L)} e^{i\omega(N_1 x_1/\alpha - t)} \qquad (2.30)$$

or, in terms of the wavenumber along the interface:

$$u_1 = N_1 A_{(L)} e^{i(k_1 x_1 - \omega t)} \qquad (2.31)$$

Similarly the u_2 displacement and all of the stress components for this wave will have the same harmonic exponent and therefore the same wavenumber k_1 along the interface.

Next two different cases are considered. First, the simple case when medium 2 is vacuum and, second, the general case when medium 2 is a different solid.

Case 1: Medium 2 is vacuum:

If medium 2 is vacuum then the displacements at the interface need not be constrained to any particular value but the stress normal to the boundary (σ_{22}) and the shear traction on the boundary (σ_{12}) must be zero in order to satisfy equilibrium. Therefore if this wave is to exist without violating the conditions for propagation in an infinite medium then at least one other wave must also be present, with equal and opposite stress components at all times and positions along the boundary such that these stresses are always cancelled at the boundary.

There are three other bulk waves which can exist in medium 1: a shear wave arriving at the interface, a longitudinal wave leaving the interface, and a shear wave leaving the interface. Their properties are constrained by Fourier's theorem which requires them to have the same frequency in order to contribute to this harmonic process and Snell's law which requires them to have the same spatial properties at the interface (i.e. the same k_1 wavenumber). Thus a longitudinal wave leaving the interface ('reflected') will have the same frequency as the longitudinal wave arriving at the interface ('incident') and the angle of incidence will be the same as the angle of reflection. Similarly an incident shear wave will have the same frequency and k_1 wavenumber (thus defining its angle of incidence) as the longitudinal waves and a reflected shear wave will leave at the same angle as the incident shear wave. In summary these constraints can be expressed for the incident (I) and reflected (R) longitudinal (L) and shear (S) waves as:

$$\omega_{(RL)} = \omega_{(RS)} = \omega_{(IL)} = \omega_{(IS)}$$

$$k_{1(RL)} = k_{1(RS)} = k_{1(IL)} = k_{1(IS)} \tag{2.32}$$

It follows that all of the waves have the same component of velocity along the x_1 direction (the x_1 phase velocity), given by

$$c_{ph} = \frac{\omega}{k_1} \tag{2.33}$$

The unknowns in this system are now only the amplitudes of three of the waves and to find them there are two stress equations to be satisfied ($\sigma_{22} = \sigma_{12} = 0$ at $x_2 = 0$). The

system cannot therefore be solved unless one of the three waves is known. In a practical analysis of reflections at such a boundary (a response analysis) it is probable that both incident waves will be known, in which case the solution is evidently possible. Note that the equations are all complex, as are the wave amplitudes, so that the solution must take account of the phases φ of the waves (as defined in equation (2.13)).

Case 2: Medium 2 is solid:

The second case is the general case when medium 2 is not vacuum and has different properties from medium 1. In the illustration in Figure 2.5, for example, the bulk velocities in medium 2 are faster than those in medium 1.

As with the analysis of the first medium there are four possible bulk waves in the second medium. Again these can combine harmonically and they are subject to the conditions discussed above.

There are also four boundary conditions which may be used to link the two half-spaces: normal stress (σ_{22}), shear stress (σ_{12}), normal displacement (u_2) and tangential displacement (u_1). In a 'welded' interface all of these components must be continuous across the interface, in a sliding interface only σ_{22} and u_2 are continuous, and so on.

In this analysis welded interfaces are assumed and equations (2.32) apply to all eight of the waves at the interface; the four in medium 1 and the four in medium 2. However it should be noted that the continuity of only one of these boundary conditions across the interface would be sufficient to apply this constraint. Thus equations (2.32) are extended to link medium 1 (1) and medium 2 (2):

$$\omega_{(2)} = \omega_{(1)}$$

$$k_{1(2)} = k_{1(1)} \qquad (2.34)$$

With eight waves at an interface and four equations of boundary conditions at the interface, a solution for the wave amplitudes is possible if any four of the waves are known. This could be the case if the two incident waves on each side of the interface were known and the amplitudes of the reflected and transmitted waves were required.

Wave propagation in the x_1 direction

The eight waves at the interface each propagate at some angle to the x_1 direction but it has been shown that the conditions of equations (2.32) and (2.34) force them to combine such that they all have the same velocity and wave number component in the x_1 direction at the interface. In fact inspection of equation (2.20) shows that this will be the case not only at the interface where x_2 is zero but on any line where x_2 is constant, so that equations (2.32) and (2.34) apply to the whole system. It should therefore be possible to express the wave equations for all waves and for all x_1,x_2 space in terms of their x_1 components. This will be a useful progression towards the description of plate waves where the interest is in the propagation in the x_1 direction.

From equations (2.32), (2.20) and (2.23) the relationship between longitudinal (L) and shear (S) waves is given by

$$\frac{N_{1(L)}}{\alpha} = \frac{N_{1(S)}}{\beta} \tag{2.35}$$

This equality is a constant for the whole system and, following the notation of Pialucha (1992), will be called s, the Snell constant. The wavenumber in the x_1 direction (k_1) and the phase velocity in the x_1 direction (c_{ph}), which are also constant for the system, can be related to s and to the angles of incidence and reflection as follows:

$$s = \frac{N_{1(L)}}{\alpha} = \frac{N_{1(S)}}{\beta} = \frac{k_1}{\omega} = \frac{1}{c_{ph}} = \frac{\sin(\theta_L)}{\alpha} = \frac{\sin(\theta_S)}{\beta} \tag{2.36}$$

where θ_L is the angle of incidence and reflection for longitudinal waves and θ_S for shear waves, as illustrated for two of the waves in Figure 2.5. The term 'angle of incidence' is generally used for all waves, whether incident, reflected or transmitted, and is the absolute value of the acute angle between the propagation axis of the wave and the normal to the interface.

So, from (2.35)

$$N_{1(L)} = \alpha s$$

$$N_{1(S)} = \beta s \tag{2.37}$$

Here it can be seen that a wave whose direction of propagation has a positive x_1 component has a positive value of s, and a wave with a negative x_1 component has a negative s.

Since the vectors $N_{(L)}$ and $N_{(S)}$ are of unit length their components in the x_2 direction can now be found:

$$N_{2(L\pm)} = \pm (1 - \alpha^2 s^2)^{1/2}$$

$$N_{2(S\pm)} = \pm (1 - \beta^2 s^2)^{1/2} \qquad (2.38)$$

Here (and from now on) a positive subscript denotes a wave whose direction of propagation has some component in the positive x_2 direction and a negative subscript denotes a wave whose direction of propagation has some component in the negative x_2 direction. Thus the upward travelling waves in Figure 2.5 are + waves and the downward travelling waves are - waves.

Now the displacement and stress equations (2.20), (2.23), (2.27) and (2.29), can be expressed in terms of s as:

For longitudinal waves:

$$u_1 = \alpha s A_{(L\pm)} e^{i\omega(sx_1 \pm (1 - \alpha^2 s^2)^{1/2} x_2/\alpha - t)}$$

$$u_2 = \pm (1 - \alpha^2 s^2)^{1/2} A_{(L\pm)} e^{i\omega(sx_1 \pm (1 - \alpha^2 s^2)^{1/2} x_2/\alpha - t)}$$

$$\sigma_{11} = (\alpha - \frac{2\beta^2}{\alpha} + 2 \alpha \beta^2 s^2) i \omega \rho A_{(L\pm)} e^{i\omega(sx_1 \pm (1 - \alpha^2 s^2)^{1/2} x_2/\alpha - t)}$$

$$\sigma_{22} = \alpha (1 - 2\beta^2 s^2) i \omega \rho A_{(L\pm)} e^{i\omega(sx_1 \pm (1 - \alpha^2 s^2)^{1/2} x_2/\alpha - t)}$$

$$\sigma_{33} = (\alpha - \frac{2\beta^2}{\alpha}) i \omega \rho A_{(L\pm)} e^{i\omega(sx_1 \pm (1 - \alpha^2 s^2)^{1/2} x_2/\alpha - t)}$$

$$\sigma_{12} = \pm 2 \beta^2 s (1 - \alpha^2 s^2)^{1/2} i \omega \rho A_{(L\pm)} e^{i\omega(sx_1 \pm (1 - \alpha^2 s^2)^{1/2} x_2/\alpha - t)}$$

(2.39)

and for shear waves:

$$u_1 = \pm \left(1 - \beta^2 s^2 \right)^{1/2} A_{(S\pm)} \, e^{i\omega(sx_1 \pm \left(1 - \beta^2 s^2 \right)^{1/2} x_2/\beta - t)}$$

$$u_2 = - \beta \, s \, A_{(S\pm)} \, e^{i\omega(sx_1 \pm \left(1 - \beta^2 s^2 \right)^{1/2} x_2/\beta - t)}$$

$$\sigma_{11} = \pm 2 \beta^2 s \left(1 - \beta^2 s^2 \right)^{1/2} i \, \omega \, \rho \, A_{(S\pm)} \, e^{i\omega(sx_1 \pm \left(1 - \beta^2 s^2 \right)^{1/2} x_2/\beta - t)}$$

$$\sigma_{22} = - \sigma_{11}$$

$$\sigma_{12} = \beta \left(1 - 2 \beta^2 s^2 \right) i \, \omega \, \rho \, A_{(S\pm)} \, e^{i\omega(sx_1 \pm \left(1 - \beta^2 s^2 \right)^{1/2} x_2/\beta - t)} \qquad (2.40)$$

2.5 Inhomogeneous waves

Consider a plane longitudinal wave incident at a free surface at an arbitrary angle θ_L between 0 and 90 degrees, as illustrated in Figure 2.6(a). Its velocity in its own direction of propagation is α (bulk velocity) and its frequency is ω. From equation (2.36) the Snell constant s can be calculated and, since $\sin(\theta)$ is less than unity, the product αs is less than unity. The phase velocity c_{ph} is also greater than the wave velocity α. In general a plane longitudinal wave is reflected at the same angle and a plane shear wave, having a lower bulk velocity, is reflected at a smaller angle. No other waves are present.

Now consider a shear wave incident at the free surface instead of the longitudinal wave, as shown in Figure 2.6(b). For small angles of incidence, θ_S the same behaviour should be expected, with the reflection of shear and longitudinal plane waves. The reflected shear wave leaves at the same angle of incidence as the incident wave and the reflected longitudinal wave leaves at a larger angle. However as the angle of incidence of the incoming shear wave is increased, a critical point is reached when the shear angle is still less than 90 degrees but the reflected longitudinal angle is equal to 90 degrees. At this point a longitudinal plane wave propagates exactly parallel to the free surface, its product αs is unity and its phase velocity c_{ph} is equal to its bulk velocity α.

At shear angles of incidence larger than this critical value, the shear wave behaviour is unchanged but the longitudinal wave is inhomogeneous. Its product αs is greater than unity and its phase velocity c_{ph} is less than its bulk velocity α. Now equation (2.38)

yields an imaginary value for $N_{2(L)}$ rather than a real value and equations (2.39) for the displacements become:

$$u_1 = \alpha\, s\, A_{(L+)}\, e^{i\omega(sx_1 + i(\,\alpha^2 s^2 - 1\,)^{1/2}\, x_2/\alpha - t\,)}$$

$$u_2 = i\,(\,\alpha^2 s^2 - 1\,)^{1/2}\; A_{(L+)}\, e^{i\omega(sx_1 + i(\,\alpha^2 s^2 - 1\,)^{1/2}\, x_2/\alpha - t\,)} \qquad (2.41)$$

Separating the real parts of the exponents from the imaginary parts gives

$$u_1 = \alpha\, s\, A_{(L+)}\, e^{i\omega\,(sx_1 - t\,)}\; e^{-\omega\,(\,\alpha^2 s^2 - 1\,)^{1/2}\, x_2/\alpha}$$

$$u_2 = i\,(\,\alpha^2 s^2 - 1\,)^{1/2}\; A_{(L+)}\, e^{i\omega\,(sx_1 - t\,)}\; e^{-\omega\,(\,\alpha^2 s^2 - 1\,)^{1/2}\, x_2/\alpha} \qquad (2.42)$$

Both of these equations show, by their first exponents, propagation of a wave along the x_1 direction which satisfies the frequency and spatial requirements of the boundary (equation 2.32), and by their second exponents, an exponential decay in the x_2 direction. Thus the inhomogeneous (or 'evanescent') wave is characterised by propagation along the interface to satisfy the boundary conditions with the other wave(s) and by decay away from the boundary. It can be seen also from equation (2.42) that this 'longitudinal' inhomogeneous wave has a displacement component u_2 normal to its direction of propagation and out of phase with its u_1 displacement.

In general, inhomogeneous waves, either longitudinal or shear, will exist under any circumstances of reflection or transmission across interfaces where the phase velocity at the interface is less than the bulk velocity in one of the adjoining media. They are incapable of taking energy away from the interface because of their decay in the x_2 direction but are valid propagating waves, carrying energy parallel to the interface.

The term 'critical angle' is often used to describe the conditions for the propagation of inhomogeneous waves in a solid when excited by incident waves in a coupling liquid. The longitudinal critical angle is the angle of incidence when the transmitted longitudinal wave is (just) homogeneous and travels exactly parallel to the interface (the transmission angle is 90 degrees); a smaller angle of incidence would result in a homogeneous longitudinal wave with a transmission angle of less than ninety degrees and a larger angle of incidence would result in an inhomogeneous longitudinal wave travelling parallel to the interface. The shear critical angle is the (larger) angle of incidence when the same conditions exist for the shear wave component in the solid.

Rayleigh wave

The Rayleigh wave is a special and well known case of the combination of inhomogeneous waves. It propagates along a free surface and consists of a combination solely of an inhomogeneous longitudinal wave and an inhomogeneous shear wave. The proportions, phases and wavelengths of these two wave components are such that their normal and shear stresses σ_{22} and σ_{12} both cancel at the free surface, thus satisfying the equilibrium requirement there.

The phase velocity of the Rayleigh wave depends on the material properties but for all elastic bodies the range of possible values of Poisson's ratio limits the Rayleigh velocity to the range 0.8741 β to 0.9554 β. The velocity is therefore only just lower than the bulk shear velocity for the medium. It is also independent of frequency. Because both wave components are inhomogeneous, all displacement and stress quantities for the Rayleigh wave decay with distance from the free surface.

2.6 Assembly of layered system

The theory developed so far is sufficient to describe the characteristics of individual infinite homogeneous bulk waves in an infinite elastic medium and the combination of a set of these waves which is necessary for their existence when the medium is divided into two half-spaces with different material properties. With this development from individual waves to a set of waves, the emphasis was changed from waves travelling in their own individual directions to the idea of a compound wave, consisting of the linear superposition of the individual waves, travelling in the direction parallel to the interface. In addition the possibility was discussed of an inhomogeneous wave which may be present along the boundary as a valid part of this compound wave.

The next stage will be to consider the addition of further parallel interfaces such that layers of finite thickness are described. The addition of a second interface will describe a single infinitely long plate in plane strain with a semi-infinite half-space on each side of it. The addition of a third interface will extend this to a two-layer plate, and so on.

The description of wave propagation along the multi-layered system in terms of infinite bulk waves relies on the satisfactory coupling of the wave components in each layer at all of the interfaces. A valid solution for a propagating plate wave therefore consists of a

frequency (ω), a wavenumber in the direction along the plate (k_1) and a set of wave amplitudes, $A_{(L+)}$, $A_{(L-)}$, $A_{(S+)}$ and $A_{(S-)}$ for each layer, such that all of the interface boundary conditions are satisfied. Valid solutions cannot be found for all values of ω and k_1. The approach will therefore be to build a description of the full layered system in terms of the wave amplitudes and then to find valid pairs of ω and k_1 such that all of the interface conditions are satisfied.

The quantities necessary for the coupling of the waves at the interfaces are the two displacements u_1 and u_2, the stress normal to the interface σ_{22} and the shear stress σ_{12}. The other stress components need not be continuous across a 'welded' interface nor need they be any particular value at a free or fixed boundary. They therefore do not play a part in the solution. The four necessary quantities come from equations(2.39) and (2.40). They can be simplified by making the following substitutions:

$$C_\alpha = (1 - \alpha^2 s^2)^{1/2} \quad , \qquad C_\beta = (1 - \beta^2 s^2)^{1/2} \quad ,$$

$$C_{2\beta} = 1 - 2 \beta^2 s^2 \quad , \qquad g_\alpha = e^{i\omega(1 - \alpha^2 s^2)^{1/2} x_2/\alpha} \quad ,$$

$$g_\beta = e^{i\omega(1 - \beta^2 s^2)^{1/2} x_2/\beta} \quad , \qquad C_i = i \omega \rho \qquad (2.43)$$

Thus for longitudinal waves travelling with increasing x_2, the displacements at any location can be expressed as:

$$u_1 = \alpha s g_\alpha e^{i\omega(sx_1 - t)} A_{(L+)}$$

$$u_2 = C_\alpha g_\alpha e^{i\omega(sx_1 - t)} A_{(L+)}$$

$$\sigma_{22} = \alpha C_i C_{2\beta} g_\alpha e^{i\omega(sx_1 - t)} A_{(L+)}$$

$$\sigma_{12} = 2 s \beta^2 C_i C_\alpha g_\alpha e^{i\omega(sx_1 - t)} A_{(L+)} \qquad (2.44)$$

For longitudinal waves travelling with decreasing x_2:

$$u_1 = \frac{\alpha s}{g_\alpha} e^{i\omega(sx_1 - t)} A_{(L-)}$$

$$u_2 = \frac{- C_\alpha}{g_\alpha} e^{i\omega(sx_1 - t)} A_{(L-)}$$

$$\sigma_{22} = \frac{\alpha\, C_i\, C_{2\beta}}{g_\alpha}\, e^{i\omega(sx_1 - t)}\, A_{(L-)}$$

$$\sigma_{12} = \frac{-2\, s\, \beta^2\, C_i\, C_\alpha}{g_\alpha}\, e^{i\omega(sx_1 - t)}\, A_{(L-)} \qquad (2.45)$$

For shear waves travelling with increasing x_2:

$$u_1 = C_\beta\, g_\beta\, e^{i\omega(sx_1 - t)}\, A_{(S+)}$$

$$u_2 = -\beta\, s\, g_\beta\, e^{i\omega(sx_1 - t)}\, A_{(S+)}$$

$$\sigma_{22} = -2\, s\, \beta^2\, C_i\, C_\beta\, g_\beta\, e^{i\omega(sx_1 - t)}\, A_{(S+)}$$

$$\sigma_{12} = \beta\, C_i\, C_{2\beta}\, g_\beta\, e^{i\omega(sx_1 - t)}\, A_{(S+)} \qquad (2.46)$$

and for shear waves travelling with decreasing x_2:

$$u_1 = \frac{-C_\beta}{g_\beta}\, e^{i\omega(sx_1 - t)}\, A_{(S-)}$$

$$u_2 = \frac{-\beta\, s}{g_\beta}\, e^{i\omega(sx_1 - t)}\, A_{(S-)}$$

$$\sigma_{22} = \frac{2\, s\, \beta^2\, C_i\, C_\beta}{g_\beta}\, e^{i\omega(sx_1 - t)}\, A_{(S-)}$$

$$\sigma_{12} = \frac{\beta\, C_i\, C_{2\beta}}{g_\beta}\, e^{i\omega(sx_1 - t)}\, A_{(S-)} \qquad (2.47)$$

Note that the term $e^{i\omega(sx_1 - t)}$ is common for all of the equations. This is the description for the harmonic propagation in the x_1 direction. Since it applies equally to all of the individual waves it is of no use in determining their contributions to the compound plate wave. Therefore for convenience from now on it will be omitted from the equations. However it should be assumed to be implicit in all expressions of displacement or stress. Thus the solution will depend spatially only on variations in the x_2 direction and temporally only on any phase difference between components.

In general it is useful to describe the superpositions of the displacements and stresses for the four waves at any x_2 position. This is easily done by summing equations (2.44) to (2.47) in matrix form:

$$\begin{Bmatrix} u_1 \\ u_2 \\ \sigma_{22} \\ \sigma_{12} \end{Bmatrix} = \begin{bmatrix} \alpha s g_\alpha & \frac{\alpha s}{g_\alpha} & C_\beta g_\beta & \frac{-C_\beta}{g_\beta} \\ C_\alpha g_\alpha & \frac{-C_\alpha}{g_\alpha} & -\beta s g_\beta & \frac{-\beta s}{g_\beta} \\ \alpha C_i C_{2\beta} g_\alpha & \frac{\alpha C_i C_{2\beta}}{g_\alpha} & -2s\beta^2 C_i C_\beta g_\beta & \frac{2s\beta^2 C_i C_\beta}{g_\beta} \\ 2s\beta^2 C_i C_\alpha g_\alpha & \frac{-2s\beta^2 C_i C_\alpha}{g_\alpha} & \beta C_i C_{2\beta} g_\beta & \frac{\beta C_i C_{2\beta}}{g_\beta} \end{bmatrix} \begin{Bmatrix} A_{(L+)} \\ A_{(L-)} \\ A_{(S+)} \\ A_{(S-)} \end{Bmatrix} \qquad (2.48)$$

The matrix in equation (2.48) is the field matrix, describing the relationship between the wave amplitudes and the displacements and stresses at any location in any layer. Its coefficients depend on the through-thickness position in the plate (x_2), the material properties of the layer at this position (ρ, α and β), the frequency (ω), and the Snell constant (s). The Snell constant is determined from the wavenumber along the plate (k_1) and the frequency, according to equation (2.36). The field matrix will be abbreviated in the analysis to [D].

Figure 2.7 shows the labelling system which will be used in the analysis of multilayered plates. A five layer system is illustrated as an example, consisting of a three layer plate with two semi-infinite half-spaces. The half-spaces are always included as layers in the description of the model, even if they are vacuum. The layers of the system are labelled ℓ 1 to ℓ 5, and the interfaces, $\imath$ 1 to $\imath$ 4. Although the orientation of the plate in space is arbitrary, it is convenient to refer to the layers and interfaces in terms of their vertical positions in a stack and to the top and bottom surfaces, as in the orientation in the figure. Accordingly the x_2 direction is defined as downwards, from the top to the bottom of the plate. Each layer has its own x_2 origin, defined as the location of its top interface, except for the first layer (ℓ 1) which has its origin at its interface with ℓ 2 in order to avoid having an origin at - ∞. A single origin for the whole system is not necessary because phase differences from interface to interface can be accounted for by the complex wave amplitudes. A reference phase is also not necessary for the modal solution but it will be required for the calculation of mode shapes in Chapter 4. The reference phase is defined by the positive longitudinal wave L+ in the first finite layer ℓ 1 which is given zero phase φ so that its amplitude is real. The directions of positive longitudinal and shear waves, L+ and S+, and of negative waves L- and S- are also shown in the figure.

Thus, for example, the displacements and stresses in layer ℓ 3 at its interface with layer ℓ 2 (interface i 2) are expressed as:

$$\begin{Bmatrix} u_1 \\ u_2 \\ \sigma_{22} \\ \sigma_{12} \end{Bmatrix}_{\ell\,3,\,\mathrm{top}} = [D]_{\ell\,3,\,\mathrm{top}} \begin{Bmatrix} A_{(L+)} \\ A_{(L-)} \\ A_{(S+)} \\ A_{(S-)} \end{Bmatrix}_{\ell\,3} \tag{2.49}$$

2.7 Solution: transfer matrices method

Two different approaches for the solution of the multilayered system for free propagating waves have been considered, a 'transfer matrices' method and a 'global matrix' method. The transfer matrices method will be described in this subsection and the global matrix method in the next subsection. The transfer matrices method was the original of the two ideas but it was found to be numerically unstable under certain conditions, as will be discussed in Chapter 4. The global matrix method was developed to avoid the numerical instability and it is the method which was employed in the modal model which is developed in this thesis. The transfer method is presented here because it is intuitive and is amenable to the examination of the modal properties.

The 'Transfer matrices' method works by condensing the multilayered system into a set of four equations relating the boundary conditions at the first interface (i 1) to the boundary conditions at the last interface (i 4 in the illustration). In the process, the equations for the intermediate interfaces are eliminated so that if the four final equations are satisfied then all equations are satisfied.

The basic principle of a transfer matrix description for layered media should be attributed to Thomson (1950). Haskell (1953) subsequently corrected an error in Thomson's formulation and went on to demonstrate that the method could be used to find the modal solutions for surface waves. The derivation of the theory for the solution of other classes of free waves is a straightforward extension of Haskell's idea. Formulations which use transfer matrix equations for multilayered media are frequently referred to in the literature as 'Thomson-Haskell' formulations.

Assume that the displacements and stresses are known at the first interface, i 1. The amplitudes of the four waves at the top of layer ℓ 2 can now be found by inverting the matrix [D]:

$$\begin{Bmatrix} A_{(L^+)} \\ A_{(L^-)} \\ A_{(S^+)} \\ A_{(S^-)} \end{Bmatrix}_{\ell\,2} = [D]^{-1}_{\ell\,2,\,\text{top}} \begin{Bmatrix} u_1 \\ u_2 \\ \sigma_{22} \\ \sigma_{12} \end{Bmatrix}_{\ell\,2,\,\text{top}} \tag{2.50}$$

Now move to the next interface, i 2. Knowing the wave amplitudes in layer ℓ 2, the displacements and stresses at the bottom of the layer can be expressed:

$$\begin{Bmatrix} u_1 \\ u_2 \\ \sigma_{22} \\ \sigma_{12} \end{Bmatrix}_{\ell\,2,\,\text{bottom}} = [D]_{\ell\,2,\,\text{bottom}} [D]^{-1}_{\ell\,2,\,\text{top}} \begin{Bmatrix} u_1 \\ u_2 \\ \sigma_{22} \\ \sigma_{12} \end{Bmatrix}_{\ell\,2,\,\text{top}} \tag{2.51}$$

The matrix product in this equation now relates the displacements and stresses between the top and bottom surfaces of a single layer. This matrix will be referred to as the layer matrix, abbreviation [L], which for layer ℓ 2 is:

$$[L]_{\ell\,2} = [D]_{\ell\,2,\,\text{bottom}} [D]^{-1}_{\ell\,2,\,\text{top}} \tag{2.52}$$

The displacements and stresses must be continuous across a 'welded' interface. Therefore:

$$\begin{Bmatrix} u_1 \\ u_2 \\ \sigma_{22} \\ \sigma_{12} \end{Bmatrix}_{\ell\,3,\,\text{top}} = \begin{Bmatrix} u_1 \\ u_2 \\ \sigma_{22} \\ \sigma_{12} \end{Bmatrix}_{\ell\,2,\,\text{bottom}} = [L]_{\ell\,2} \begin{Bmatrix} u_1 \\ u_2 \\ \sigma_{22} \\ \sigma_{12} \end{Bmatrix}_{\ell\,2,\,\text{top}} \tag{2.53}$$

Equation (2.53) now gives the displacements and stresses at the top of layer ℓ 3 in terms of those at the top of layer ℓ 2. Clearly this process can be continued layer by layer for all subsequent layers, resulting in the equation:

$$\begin{Bmatrix} u_1 \\ u_2 \\ \sigma_{22} \\ \sigma_{12} \end{Bmatrix}_{\ell\,n,\,\text{top}} = [S] \begin{Bmatrix} u_1 \\ u_2 \\ \sigma_{22} \\ \sigma_{12} \end{Bmatrix}_{\ell\,2,\,\text{top}} \tag{2.54}$$

where n is the last layer (ℓ 5 in the example illustrated in Figure 2.7) and [S] is the system matrix consisting of the matrix product of the layer matrices:

$$[S] = [L]_{\ell 2} [L]_{\ell 3} \ldots . [L]_{\ell (n-1)} \tag{2.55}$$

A free wave travels along the plate without attenuation and without input of energy from outside the system. There are two ways, illustrated in Figure 2.8, in which these conditions can be met:

Solution for plate in vacuum

If the plate is in vacuum then the stresses must be zero at the extreme interfaces ℓ 1 and ℓ (n-1), where n is the total number of layers in the system, as illustrated in Figure 2.8(a). Now equation (2.54) reduces to:

$$\begin{Bmatrix} u_1 \\ u_2 \\ 0 \\ 0 \end{Bmatrix}_{\ell \text{ n, top}} = [S] \begin{Bmatrix} u_1 \\ u_2 \\ 0 \\ 0 \end{Bmatrix}_{\ell \text{ 2, top}} \tag{2.56}$$

Expanding this equation for the two (zero) stress terms on the left hand side gives:

$$\begin{Bmatrix} 0 \\ 0 \end{Bmatrix} = \begin{bmatrix} S_{31} & S_{32} \\ S_{41} & S_{42} \end{bmatrix} \begin{Bmatrix} u_1 \\ u_2 \end{Bmatrix}_{\ell \text{ 2, top}} \tag{2.57}$$

where the two-by-two matrix is the bottom left sub-matrix of [S] (rows 3 and 4 and columns 1 and 2). For this equation to be satisfied, the submatrix must be singular. Thus, defining the determinant as the characteristic function (f) for the system:

$$f = S_{31} * S_{42} - S_{41} * S_{32} = 0 \tag{2.58}$$

If a pair of values of frequency and k_1 wavenumber corresponding to a free wave are used in the assembly of the system matrix then this equation will be satisfied.

Solution for guided waves

Free waves may also travel in systems in which one or both of the half-spaces are not vacuum, but only under the condition that no energy leaks from the plate into the half-

spaces. For this condition to be satisfied, any wave components in the half-spaces ℓ 1 and ℓ n must be inhomogeneous so that they may carry energy along the plate but are unable to carry energy away from the extreme interfaces i 1 and i (n-1). Waves which meet this condition are known as guided waves.

If a half-space is not vacuum then the stresses at the extreme interface are not necessarily zero. The formulation based on stresses is therefore not applicable and is replaced by a formulation based on wave amplitudes.

Taking first of all the case in which neither half-space is vacuum, equation (2.54) can be expanded, using equations (2.49) and 2.50) to describe the system in terms of the wave amplitudes in both half-spaces:

$$\begin{Bmatrix} A_{(L+)} \\ A_{(L-)} \\ A_{(S+)} \\ A_{(S-)} \end{Bmatrix}_{\ell\, n} = [D]^{-1}_{\ell\, n,\, top}\, [S]\, [D]_{\ell\, 1,(x_2=0)} \begin{Bmatrix} A_{(L+)} \\ A_{(L-)} \\ A_{(S+)} \\ A_{(S-)} \end{Bmatrix}_{\ell\, 1} \tag{2.59}$$

The condition for free wave propagation is that there should be no energy coming into the system. Therefore the incoming waves in the two half-spaces must be zero (Figure 2.8(b)) and equation (2.59) reduces to

$$\begin{Bmatrix} A_{(L+)} \\ 0 \\ A_{(S+)} \\ 0 \end{Bmatrix}_{\ell\, n} = [D]^{-1}_{\ell\, n,\, top}\, [S]\, [D]_{\ell\, 1,(x_2=0)} \begin{Bmatrix} 0 \\ A_{(L-)} \\ 0 \\ A_{(S-)} \end{Bmatrix}_{\ell\, 1} \tag{2.60}$$

Denoting the matrix product in equation (2.60) as [S]' and expanding this equation for the two (zero) wave amplitude terms on its left hand side gives:

$$\begin{Bmatrix} 0 \\ 0 \end{Bmatrix} = \begin{bmatrix} S'_{22} & S'_{24} \\ S'_{42} & S'_{44} \end{bmatrix} \begin{Bmatrix} A_{(L-)} \\ A_{(S-)} \end{Bmatrix}_{\ell\, 1} \tag{2.61}$$

where the two-by-two matrix is the appropriate sub-matrix of [S]' (rows 2 and 4 and columns 2 and 4). For this equation to be satisfied, the determinant of the submatrix must be zero. Thus the characteristic function (f) for this system is:

$$f = S'_{22} * S'_{44} - S'_{42} * S'_{24} = 0 \tag{2.62}$$

Similarly, characteristic functions can be expressed for the two hybrid cases where one half-space is vacuum and the other supports an inhomogeneous wave. In summary, for vacuum as the top half-space the equations are:

$$[S]' = [D]^{-1}_{\ell\, n,\, top}\ [S] \tag{2.63}$$

$$f = S'_{21} * S'_{42} - S'_{22} * S'_{41} = 0 \tag{2.64}$$

and for vacuum as the bottom half-space:

$$[S]' = [S]\ [D]_{\ell\, 1,(x2=0)} \tag{2.65}$$

$$f = S'_{32} * S'_{44} - S'_{42} * S'_{34} = 0 \tag{2.66}$$

Nature of the characteristic functions

Solutions of the characteristic functions can only be found for cases of free wave propagation. Zeroes of the functions cannot be found for cases where one of the half-spaces is not vacuum and homogeneous waves leave the layered system (leaky waves). Furthermore, the solution of a characteristic function does not strictly prove the existence of a modal solution, only that a sub-matrix of the transfer matrix is singular. However examination of the coefficients of the sub-matrix show that singularity can only occur in unrealistic cases, for example if the material has zero density or zero bulk wave velocities.

The characteristic functions consist of complex quantities and in general they should be expected to yield complex results. However it can be shown, as follows, that for all cases of free wave propagation the characteristic function is always real. This general proof has not been found elsewhere, the only other proof known to the author is for the specific case of free surface waves by Haskell (1953).

Consider the layer matrix [L] introduced in equations (2.51) and (2.52) and consisting of a [D] matrix at the bottom of the layer postmultiplied by an inverted [D] matrix at the top of the layer. It would be useful, both from the analytical point of view and to reduce computational effort when calculating solutions, to find an explicit expression for the inverted matrix and then to perform the multiplication to give an explicit expression for the layer matrix.

An explicit expression for an inverted matrix at the top of the layer (coordinate $x_2 = 0$) was presented by Haskell (1953). However the Thomson-Haskell matrix formulation was slightly different from that presented here because Thomson chose to derive the field equations in terms of sums and differences of wave amplitudes rather than simply the four wave amplitudes. An explicit expression for the inversion of the matrix [D] discussed here was found by the author and his colleague T. Pialucha. The inverted matrix is:

$$[D]^{-1} = \begin{bmatrix} \frac{\beta^2 s}{\alpha} & \frac{C_{2\beta}}{2C_\alpha} & \frac{1}{2\alpha C_i} & \frac{s}{2C_\alpha C_i} \\ \frac{\beta^2 s}{\alpha} & \frac{-C_{2\beta}}{2C_\alpha} & \frac{1}{2\alpha C_i} & \frac{-s}{2C_\alpha C_i} \\ \frac{C_{2\beta}}{2C_\beta} & -\beta s & \frac{-s}{2C_\beta C_i} & \frac{1}{2\beta C_i} \\ \frac{-C_{2\beta}}{2C_\beta} & -\beta s & \frac{s}{2C_\beta C_i} & \frac{1}{2\beta C_i} \end{bmatrix}_{top} \tag{2.67}$$

Premultiplying this matrix by the [D] matrix gives the layer matrix [L] explicitly. Its coefficients are:

$$L_{11} = \beta^2 s^2 \left(g_\alpha + \frac{1}{g_\alpha}\right) + \frac{C_{2\beta}}{2}\left(g_\beta + \frac{1}{g_\beta}\right)$$

$$L_{12} = \frac{\alpha s C_{2\beta}}{2C_\alpha}\left(g_\alpha - \frac{1}{g_\alpha}\right) + C_\beta\, \beta\, s \left(-g_\beta + \frac{1}{g_\beta}\right)$$

$$L_{13} = \frac{s}{2C_i}\left(g_\alpha + \frac{1}{g_\alpha} - g_\beta - \frac{1}{g_\beta}\right)$$

$$L_{14} = \frac{\alpha s^2}{2C_\alpha C_i}\left(g_\alpha - \frac{1}{g_\alpha}\right) + \frac{C_\beta}{2\beta C_i}\left(g_\beta - \frac{1}{g_\beta}\right)$$

$$L_{21} = \frac{C_\alpha b^2 s}{\alpha}\left(g_\alpha - \frac{1}{g_\alpha}\right) + \frac{C_{2\beta}\beta s}{2C_\beta}\left(-g_\beta + \frac{1}{g_\beta}\right)$$

$$L_{22} = \frac{C_{2\beta}}{2}\left(g_\alpha + \frac{1}{g_\alpha}\right) + \beta^2 s^2 \left(g_\beta + \frac{1}{g_\beta}\right)$$

$$L_{23} = \frac{C_\alpha}{2\alpha C_i}\left(g_\alpha - \frac{1}{g_\alpha}\right) + \frac{\beta s^2}{2C_\beta C_i}\left(g_\beta - \frac{1}{g_\beta}\right)$$

$$L_{24} = L_{13}$$

$$L_{31} = C_i C_{2\beta} \beta^2 s \left(g_\alpha + \frac{1}{g_\alpha} - g_\beta - \frac{1}{g_\beta}\right)$$

$$L_{32} = \frac{C_i C_{2\beta} \beta^2 \alpha}{2C_\alpha} \left(g_\alpha - \frac{1}{g_\alpha}\right) + 2C_i C_\beta \beta^3 s^2 \left(g_\beta - \frac{1}{g_\beta}\right)$$

$$L_{33} = L_{22}$$

$$L_{34} = L_{12}$$

$$L_{41} = \frac{2C_\alpha C_i s^2 \beta^4}{\alpha} \left(g_\alpha - \frac{1}{g_\alpha}\right) + \frac{C_i C_{2\beta} \beta^2}{2C_\beta} \left(g_\beta - \frac{1}{g_\beta}\right)$$

$$L_{42} = L_{31}$$

$$L_{43} = L_{21}$$

$$L_{44} = L_{11} \qquad (2.68)$$

Since the layer matrix is independent of the wave amplitudes, relating only displacements and stresses, it could also be found in this form from Haskell's matrices. Haskell did not go so far as to perform the multiplication but it has been reported, subsequent to the derivation discussed here, by Hosten (1991).

Examination of the term L_{11} shows that it is real for all input values, including inhomogeneous cases where g_α and/or g_β are imaginary. Similarly the term L_{22} is always imaginary. In fact all terms in the layer matrix [L] are either real or imaginary, in the following pattern, where 'R' denotes a real value and 'I' denotes an imaginary value:

$$[L] = \begin{bmatrix} R & I & I & R \\ I & R & R & I \\ I & R & R & I \\ R & I & I & R \end{bmatrix} \qquad (2.69)$$

It can readily be seen that multiplication of two matrices of this form results in a matrix also of this form. Thus the system matrix for any number of layers, [S], always has this pattern of real and imaginary coefficients. The characteristic function for a plate in vacuum, equation (2.58), is therefore of the form:

$$f = I * I - R * R \tag{2.70}$$

from which it can be seen that it must always yield a real value.

If one or both of the semi-infinite half-spaces is not vacuum, then the system matrix is further modified for guided waves according to equations (2.59), (2.63) or (2.65). The modifications involve the [D] matrix evaluated at $x_2=0$ and the $[D]^{-1}$ matrix evaluated at $x_2=0$. In general these two matrices have the patterns respectively:

$$[D] = \begin{bmatrix} R & R & R_\beta & R_\beta \\ R_\alpha & R_\alpha & R & R \\ I & I & I_\beta & I_\beta \\ I_\alpha & I_\alpha & I & I \end{bmatrix} \tag{2.71}$$

$$[D]^{-1} = \begin{bmatrix} R & R_\alpha & I & I_\alpha \\ R & R_\alpha & I & I_\alpha \\ R_\beta & R & I_\beta & I \\ R_\beta & R & I_\beta & I \end{bmatrix} \tag{2.72}$$

where R_α means that the term is real if C_α is real (else imaginary), R_β means that the term is real if C_β is real (else imaginary), and so on. However for guided waves in either or both half-spaces C_α and C_β must both be imaginary so that the wave components are inhomogeneous and no energy leaks from the plate. The patterns of (2.71) and (2.72) are therefore simplified to:

$$[D] = \begin{bmatrix} R & R & I & I \\ I & I & R & R \\ I & I & R & R \\ R & R & I & I \end{bmatrix} \tag{2.73}$$

$$[D]^{-1} = \begin{bmatrix} R & I & I & R \\ R & I & I & R \\ I & R & R & I \\ I & R & R & I \end{bmatrix} \tag{2.74}$$

Construction of the system matrices [S]' for guided waves results in the following patterns and characteristic functions:

For solid or liquid in both half-spaces:

$$[S]' = \begin{bmatrix} R & R & I & I \\ R & R & I & I \\ I & I & R & R \\ I & I & R & R \end{bmatrix} \tag{2.75}$$

$$f = R * R - I * I = 0 \tag{2.76}$$

and for solid or liquid in the bottom half-space and vacuum in the top half-space:

$$[S]' = \begin{bmatrix} R & I & I & R \\ R & I & I & R \\ I & R & R & I \\ I & R & R & I \end{bmatrix} \tag{2.77}$$

$$f = R * R - I * I = 0 \tag{2.78}$$

In both cases it can be seen that the characteristic function must always yield a real value. Due to symmetry it is not necessary to consider the third case, where the top half-space is solid or liquid and the bottom half-space is vacuum.

2.8 Solution: global matrix method

The approach with the global matrix method is to assemble directly a single matrix which represents the complete system. The system matrix consists of 4(n-1) equations, where n is the total number of layers. The equations are based, in sets of four, on satisfying the boundary conditions at each interface. Thus no assumption is made a priori about any interdependence between the sets of equations for each interface. The solution is carried out on the full matrix.

The originator of the global matrix description for layered media was Knopoff (1964) who wished to avoid the problem of numerical instability which can occur with the Thomson-Haskell method. This problem will be examined further in Chapter 4. He also showed that the method could be used to solve some cases of free waves. Subsequently an important improvement was made independently by Schmidt and Jensen (1985) and Pialucha (1992), in both cases with an interest in developing robust response models.

The general method for the modal solution using the global matrix method was developed by the present author.

Consider a single interface, for example the second interface (i 2) in Figure 2.7. The displacements and stresses at the interface can be expressed as a function of the amplitudes of the waves at the top of the third layer (ℓ 3). This was shown in equation (2.49). They may also be expressed as a function of the amplitudes of the waves at the bottom of the second layer (ℓ 2):

$$\begin{Bmatrix} u_1 \\ u_2 \\ \sigma_{22} \\ \sigma_{12} \end{Bmatrix}_{\ell\ 2,\ \text{bottom}} = [D]_{\ell\ 2,\ \text{bottom}} \begin{Bmatrix} A_{(L+)} \\ A_{(L-)} \\ A_{(S+)} \\ A_{(S-)} \end{Bmatrix}_{\ell\ 2} \tag{2.79}$$

For continuity of displacements and stresses at the interface, these two equations should give equal results. Therefore

$$[D]_{\ell\ 2,\ \text{bottom}} \begin{Bmatrix} A_{(L+)} \\ A_{(L-)} \\ A_{(S+)} \\ A_{(S-)} \end{Bmatrix}_{\ell\ 2} = [D]_{\ell\ 3,\ \text{top}} \begin{Bmatrix} A_{(L+)} \\ A_{(L-)} \\ A_{(S+)} \\ A_{(S-)} \end{Bmatrix}_{\ell\ 3} \tag{2.80}$$

This equation can be expressed in a single matrix as:

$$\Big[[D_{2b}][-D_{3t}] \Big] \begin{Bmatrix} A_{(L+)2} \\ A_{(L-)2} \\ A_{(S+)2} \\ A_{(S-)2} \\ A_{(L+)3} \\ A_{(L-)3} \\ A_{(S+)3} \\ A_{(S-)3} \end{Bmatrix} = \{0\} \tag{2.81}$$

where the subscripts 2 and 3 refer to layers ℓ 2 and ℓ 3 and t and b to the top and bottom of each layer. This equation describes the interaction at interface i 2 of the waves in the adjoining layers ℓ 2 and ℓ 3.

Before proceeding, a modification can be introduced here to improve the numerical performance of the method. This is the modification which was proposed independently

by Schmidt and Jensen (1985) and Pialucha (1992). Instead of defining the origin for all of the waves in a layer to be the top of the layer, the origin of all waves is defined to be at their entry to the layer. Thus downward travelling waves (L+, S+) have their origin at the top of the layer and upward travelling waves (L-, S-) have their origin at the bottom of the layer. No change is made for the semi-infinite half-spaces. With this modification, and referring to equation (2.48), the [D] matrices for the top and bottom of a layer can be expressed, respectively as:

$$[D_t] = \begin{bmatrix} \alpha s & \alpha s g_\alpha & C_\beta & -C_\beta g_\beta \\ C_\alpha & -C_\alpha g_\alpha & -\beta s & -\beta s g_\beta \\ \alpha C_i C_{2\beta} & \alpha C_i C_{2\beta} g_\alpha & -2s\beta^2 C_i C_\beta & 2s\beta^2 C_i C_\beta g_\beta \\ 2s\beta^2 C_i C_\alpha & -2s\beta^2 C_i C_\alpha g_\alpha & \beta C_i C_{2\beta} & \beta C_i C_{2\beta} g_\beta \end{bmatrix}$$

$$[D_b] = \begin{bmatrix} \alpha s g_\alpha & \alpha s & C_\beta g_\beta & -C_\beta \\ C_\alpha g_\alpha & -C_\alpha & -\beta s g_\beta & -\beta s \\ \alpha C_i C_{2\beta} g_\alpha & \alpha C_i C_{2\beta} & -2s\beta^2 C_i C_\beta g_\beta & 2s\beta^2 C_i C_\beta \\ 2s\beta^2 C_i C_\alpha g_\alpha & -2s\beta^2 C_i C_\alpha & \beta C_i C_{2\beta} g_\beta & \beta C_i C_{2\beta} \end{bmatrix} \qquad (2.82)$$

A similar equation to (2.81) can now be written for the interface i 3 and simply added to the global matrix so that interfaces i 2 and i 3 and layers ℓ 2, ℓ 3 and ℓ 4 are described:

$$\begin{bmatrix} [D_{2b}] & [-D_{3t}] & \\ & [D_{3b}] & [-D_{4t}] \end{bmatrix} \begin{Bmatrix} \{A_2\} \\ \{A_3\} \\ \{A_4\} \end{Bmatrix} = \{0\} \qquad (2.83)$$

where the wave amplitudes in each layer, $A_{(L+)}$,$A_{(L-)}$,$A_{(S+)}$,$A_{(S-)}$, have been abbreviated simply to a layer wave vector {A}. The process is continued for all interfaces, resulting in a matrix of 4(n-1) equations and 4n unknowns. In the case of the example in Figure 2.7 the matrix equation is:

$$\begin{bmatrix} [D_{1b}] & [-D_{2t}] & & \\ & [D_{2b}] & [-D_{3t}] & \\ & & [D_{3b}] & [-D_{4t}] \\ & & & [D_{4b}] & [-D_{5t}] \end{bmatrix} \begin{Bmatrix} \{A_1\} \\ \{A_2\} \\ \{A_3\} \\ \{A_4\} \\ \{A_5\} \end{Bmatrix} = \{0\} \qquad (2.84)$$

As it stands this system cannot be solved for the 20 wave amplitudes because in this case there are only sixteen equations, and in general for any system there will always be four

more unknowns than there are equations. In order to progress further, either for response or modal solution, four of the wave amplitudes must be known and removed from the system.

For the modal solution of plate waves it is convenient to select as the four known waves the incoming waves in the two half-spaces, that is to say $A_{(L+)1}$, $A_{(S+)1}$, $A_{(L-)n}$ and $A_{(S-)5}$. These can be moved to the right hand side of equation (2.84) to give:

$$\begin{bmatrix} [D^-_{1b}] & [-D_{2t}] & & & \\ & [D_{2b}] & [-D_{3t}] & & \\ & & [D_{3b}] & [-D_{4t}] & \\ & & & [D_{4b}] & [-D^+_{5t}] \end{bmatrix} \begin{Bmatrix} \{A^-_1\} \\ \{A_2\} \\ \{A_3\} \\ \{A_4\} \\ \{A^+_5\} \end{Bmatrix} = \begin{bmatrix} [-D^+_{1b}] & & \\ & & \\ & & \\ & & [D^-_{5t}] \end{bmatrix} \begin{Bmatrix} \{A^+_1\} \\ \{0\} \\ \{0\} \\ \{0\} \\ \{A^-_5\} \end{Bmatrix} \tag{2.85}$$

where the superscripts + and - denote those parts of the matrices or vectors corresponding to + and - waves respectively. Thus the vectors $\{A^+\}$ and $\{A^-\}$ each consist of half of the vector $\{A\}$ and the matrices $[D^+]$ and $[D^-]$ are four-by-two partitions of the matrix $[D]$. The partitioning is as follows:

$$\{A^+\} = \begin{Bmatrix} A_{(L+)} \\ A_{(S+)} \end{Bmatrix}$$

$$\{A^-\} = \begin{Bmatrix} A_{(L-)} \\ A_{(S-)} \end{Bmatrix}$$

$$[D^+] = \begin{bmatrix} D_{11} & D_{13} \\ D_{21} & D_{23} \\ D_{31} & D_{33} \\ D_{41} & D_{43} \end{bmatrix}$$

$$[D^-] = \begin{bmatrix} D_{12} & D_{14} \\ D_{22} & D_{24} \\ D_{32} & D_{34} \\ D_{42} & D_{44} \end{bmatrix} \tag{2.86}$$

The matrices on both sides of equation (2.85) are square and of dimension 4(n-1). A solution for any set of waves on the left hand side can now be calculated for known right hand sides.

Solution for guided waves

The modal solution for guided waves is straightforward because the system is already described in terms of the wave amplitudes. For a free wave travelling along the plate without input of energy from outside the system, there are no incoming waves, as discussed in Section 2.7 and illustrated in Figure 2.8(b), and so the right hand side of equation (2.85) must be zero. Thus, denoting the matrix on the left hand side as the system matrix [S]:

$$[S]\begin{Bmatrix} \{A^-_1\} \\ \{A_2\} \\ \{A_3\} \\ . \\ . \\ . \\ \{A^+_n\} \end{Bmatrix} = \{0\} \tag{2.87}$$

For this equation to be satisfied, the system matrix must be singular, so its determinant must be zero. This yields the characteristic function for the solution of guided wave propagation in multilayered plates using the global matrix method:

$$f = |S| = 0 \tag{2.88}$$

General solution

If the top and bottom half-spaces are vacuum then the $[D^+]$ and $[D^-]$ matrices cannot be evaluated. Modification is therefore required to the system matrix to account properly for the absence of waves in vacuum and for zero stresses on the free surfaces. This can be done by reformulating the problem, resulting in a smaller system matrix. The sub-matrices and wave amplitudes associated with the half-spaces are removed from equation (2.79) and the remaining top and bottom sub-matrices are partitioned into their stress and displacement rows. The stress partitions are then taken onto the right hand side as knowns, leaving a square system matrix again, and the solution is then possible. However a much simpler alternative, which leaves the solution completely general, is to retain the full system matrix and to modify the layer constants for the vacuum half-spaces in such a way that the $[D^+]$ and $[D^-]$ matrices can be evaluated, hence solution is possible and the resulting surface stresses are zero. This is achieved by setting the bulk

velocities α and β of the vacuum to arbitrary non-zero values and the density ρ to zero. With these modifications, the matrix assembly and solution is identical to that for guided waves.

Nature of the characteristic function

The characteristic function of the global matrix method yields a complex value, in general, for all inputs. Furthermore, as with the transfer matrices method, zeroes of the function can only be found when any waves in non-vacuum half-spaces are inhomogeneous (guided waves). Solutions cannot be found for cases where homogeneous waves leave the layered system (leaky waves).

It was explained in Section 2.7 that the solution of the characteristic function for the transfer matrices method does not automatically prove the existence of a modal solution, a further condition being that any other (trivial) causes of singularity of the sub-matrices are avoided. Similarly it is evident that the solution of the characteristic function for the global matrix method does not strictly prove the existence of a mode. However in this case there is one non-trivial circumstance in which the matrix is singular. This is when the wavenumber of the propagating wave is equal to the wavenumber of either of the bulk waves in any of the internal layers of the system. Here the system matrix has two or more identical columns and is singular. Physically the explanation for this is that the + and - waves in this layer both travel parallel to the layer and are therefore indistinguishable in their effect on stresses and displacements at the adjacent interfaces. Consequently a solution for these wave amplitudes is not possible and the matrix is singular.

2.9 Phase properties of free waves

Further analysis by the author of the modal equations for free wave propagation in multilayered plates has revealed that there are consistent phase relationships between the field quantities in free waves. Relationships can be identified between the displacement and stress components in a plate and it can be shown that the wavefront of a free wave is always normal to the propagation direction.

Plate in vacuum

The analysis is most easily performed using the theory of the transfer matrices method of section 2.7. It was shown in equation (2.57) that a two-by-two submatrix of the system

matrix [S] must be singular for a solution to exist in a plate in vacuum. The expansion of this sub-matrix into its two constituent equations gives:

$$S_{31} * u_1 + S_{32} * u_2 = 0$$
$$S_{41} * u_1 + S_{42} * u_2 = 0 \qquad (2.89)$$

where u_1 and u_2 are the displacements at the free surface at the top of the plate. It was also shown, in equations (2.69) and (2.70), that the coefficients S_{31} and S_{42} are always imaginary and the coefficients S_{32} and S_{41} are always real, regardless of the number of layers in the system. For non-trivial solutions, the system matrix is always fully populated and the displacements are not zero. It follows therefore from equation (2.89) that the displacement components u_1 and u_2 at the free surface at the top of the plate must have a phase difference of 90 degrees.

Suppose that the in-plane displacement at the top surface u_1 is real so that the normal displacement at the surface u_2 is imaginary. This assumption is permissible because the absolute phases of the displacements and stresses are arbitrary. Now the displacements and stresses may be calculated at any location (x2) in the top layer of the plate (ℓ 2) using the layer matrix [L] defined in equation (2.51):

$$\begin{Bmatrix} u_1 \\ u_2 \\ \sigma_{22} \\ \sigma_{12} \end{Bmatrix}_{\ell\, 2,\, x_2} = [L]_{\ell\, 2} \begin{Bmatrix} u_1 \\ u_2 \\ 0 \\ 0 \end{Bmatrix}_{\ell\, 2,\, \text{top}} \qquad (2.90)$$

It was shown in equation (2.69) that the layer matrix always has a fixed pattern of real and imaginary coefficients, denoted 'R' and 'I' respectively in the equation. Continuing with this description, the phase pattern of equation (2.90) can be written:

$$\begin{Bmatrix} u_1 \\ u_2 \\ \sigma_{22} \\ \sigma_{12} \end{Bmatrix}_{\ell\, 2,\, x_2} = \begin{bmatrix} R & I & I & R \\ I & R & R & I \\ I & R & R & I \\ R & I & I & R \end{bmatrix} \begin{Bmatrix} R \\ I \\ 0 \\ 0 \end{Bmatrix} \qquad (2.91)$$

Multiplication of the coefficients on the right hand side of this equation shows that the displacements and stresses are all either real or imaginary, and this holds for any depth in the layer:

$$\begin{Bmatrix} u_1 \\ u_2 \\ \sigma_{22} \\ \sigma_{12} \end{Bmatrix}_{\ell\ 2,\ x_2} = \begin{Bmatrix} R \\ I \\ I \\ R \end{Bmatrix} \tag{2.92}$$

The u_1 displacement and the σ_{12} stress are always real and the u_2 displacement and the σ_{22} stress are always imaginary. Thus in general the phase differences between the two displacement components and between the two stress components are always 90 degrees, and the normal stress σ_{22} is always in phase (0 degrees) or in opposite phase (180 degrees) with the in-plane displacement u_1. It follows also that the wavefront of the plate wave is parallel to the x_2 axis, normal to the plane of the layers and the propagation direction.

Continuing to a second finite layer (ℓ 3) in a multilayered plate, the displacements and stresses at any depth are given by the product of the layer matrix for this layer and the vector of displacements and stresses at the interface between the layers:

$$\begin{Bmatrix} u_1 \\ u_2 \\ \sigma_{22} \\ \sigma_{12} \end{Bmatrix}_{\ell\ 3,\ x_2} = [L]_{\ell\ 3} \begin{Bmatrix} u_1 \\ u_2 \\ \sigma_{22} \\ \sigma_{12} \end{Bmatrix}_{\ell\ 2,\ \text{bottom}} \tag{2.93}$$

The phase pattern of the displacements and stresses is known at the interface from the above analysis and it is not changed by the premultiplication by [L]. The phase pattern in the second layer (ℓ 3) is therefore the same as that in the first layer (ℓ 2). Clearly the same is true for any further layers in the system.

Plate with solid or liquid in both half-spaces

The two-by-two submatrix of the system matrix [S]' for a plate with two solid or liquid half-spaces was shown in equation (2.61). Expanding it into its two constituent equations gives:

$$\begin{aligned} S'_{22} * A_{(L-)} + S'_{24} * A_{(S-)} &= 0 \\ S'_{42} * A_{(L-)} + S'_{44} * A_{(S-)} &= 0 \end{aligned} \tag{2.94}$$

where $A_{(L-)}$ and $A_{(S-)}$ are the amplitudes of the longitudinal and shear waves 'leaving' the top interface of the system (Actually these waves must be inhomogeneous for a guided wave solution so they do not leave the interface but travel along it). It was shown

in equation (2.75) that the coefficients S'_{22} and S'_{44} are always real and the coefficients S'_{24} and S'_{42} are always imaginary so, again for non-trivial solutions, the wave amplitudes must have a phase difference of 90 degrees.

The stresses and displacements at any location (x_2) in the top finite layer of the multilayered plate (ℓ 2) are given by the equation:

$$\begin{Bmatrix} u_1 \\ u_2 \\ \sigma_{22} \\ \sigma_{12} \end{Bmatrix}_{\ell\ 2,\ x_2} = [L]_{\ell\ 2}\,[D]_{\ell\ 1,(x_2=0)} \begin{Bmatrix} 0 \\ A_{(L-)} \\ 0 \\ A_{(S-)} \end{Bmatrix}_{\ell\ 1} \tag{2.95}$$

The phase patterns for both of the matrices in this equation are fixed (equations (2.69) and (2.73)). Assuming a real longitudinal wave amplitude $A_{(L-)}$ and an imaginary shear wave amplitude $A_{(S-)}$, the phase pattern for equation (2.95) is found from:

$$\begin{Bmatrix} u_1 \\ u_2 \\ \sigma_{22} \\ \sigma_{12} \end{Bmatrix}_{\ell\ 2,\ x_2} = \begin{bmatrix} R & I & I & R \\ I & R & R & I \\ I & R & R & I \\ R & I & I & R \end{bmatrix} \begin{bmatrix} R & R & I & I \\ I & I & R & R \\ I & I & R & R \\ R & R & I & I \end{bmatrix} \begin{Bmatrix} 0 \\ R \\ 0 \\ I \end{Bmatrix} \tag{2.96}$$

This evaluates once again to a vector of displacements and stresses which are all either real or imaginary. With the assumption which was made here of real longitudinal wave amplitude and imaginary shear wave amplitude, the phase pattern of the displacements and stresses is identical to that for the plate in vacuum. The analysis for additional layers then follows that for the plate in vacuum.

Therefore the relationships between the phases of the displacements and stresses in guided waves where both half-spaces are solid or liquid are the same as in the case of the plate in vacuum, and the wavefront is again normal to the x_2 axis.

Plate with solid or liquid in one half-space and vacuum in the other

Due to symmetry it is only necessary to consider one of the two cases in which one half-space is solid or liquid and the other is vacuum. If the top half-space is chosen to be vacuum then the analysis of the system equation (2.63) and its phase pattern (2.77) reveals immediately that there is a phase difference of 90 degrees between the two displacement components u_1 and u_2 at the free surface at the top of the plate. The

remainder of the analysis and the conclusions are then identical to those for a plate in vacuum.

2.10 Conclusions

The modal theory has been developed for the propagation of free plate waves in multilayered systems. The theory is applicable to plates consisting of any number of flat, parallel layers of elastic material, rigidly connected together. The plates may be assumed to be in vacuum or to be embedded in semi-infinite elastic half-spaces. In the latter case the solution is restricted to guided waves in which no energy leaks from the plate into the half-spaces.

Two different methods of solution have been developed. In the first method, the transfer matrix method, the equations for the system are condensed to a matrix which simply relates the boundary conditions at the top of the plate to those at the bottom of the plate. In the second method, the global matrix method, a large matrix is assembled containing the equations for all of the layers of the plate. In both cases a characteristic function has been found which has to be solved to find the conditions for free wave propagation. The function takes as its input the material and geometric descriptions of the layers, a value of frequency and a value of the wavenumber in the plane of the plate. For free wave propagation the characteristic function must yield zero as its result. For the first method the function has been shown to be real in all ranges of solutions which are relevant for free waves. For the second method the function is complex.

It has been shown that the phases of the stresses and displacements of free plate waves bear the same relationship to each other for all solutions. The wavefront of free waves is also always normal to the plane of the plate.

The implementation of the characteristic function in the computer model will be described in chapter 4.

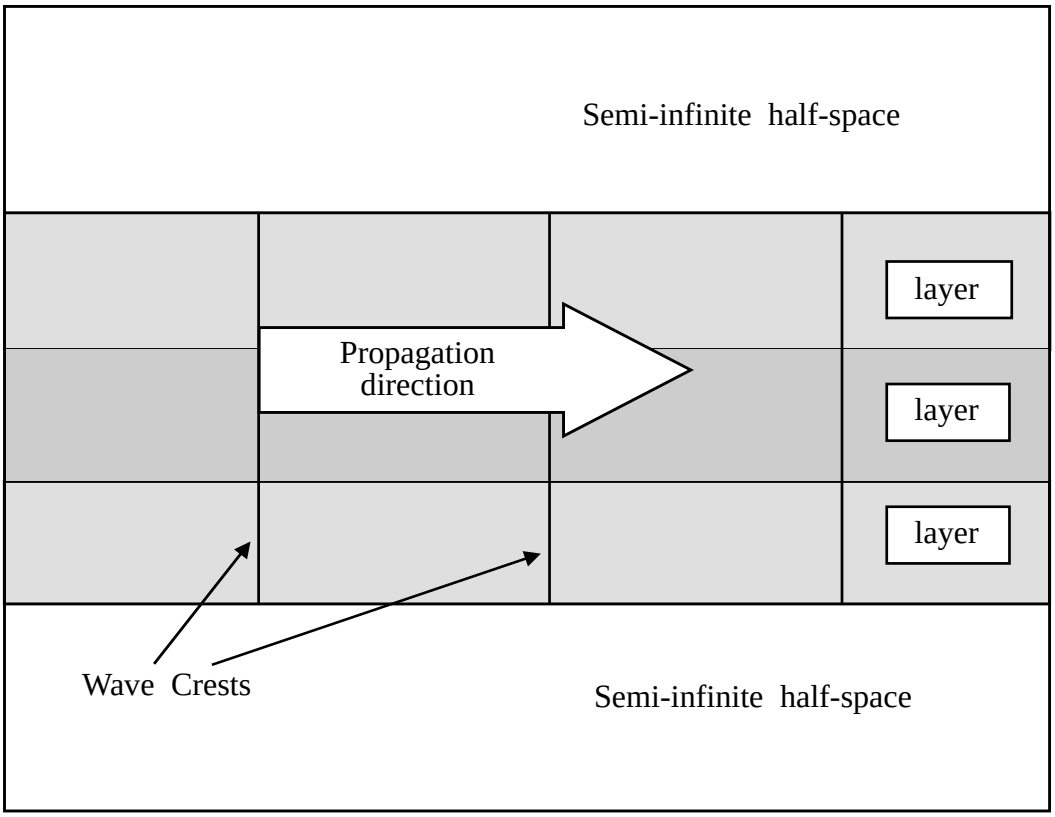

Figure 2.1 Wave propagation along multilayered plate

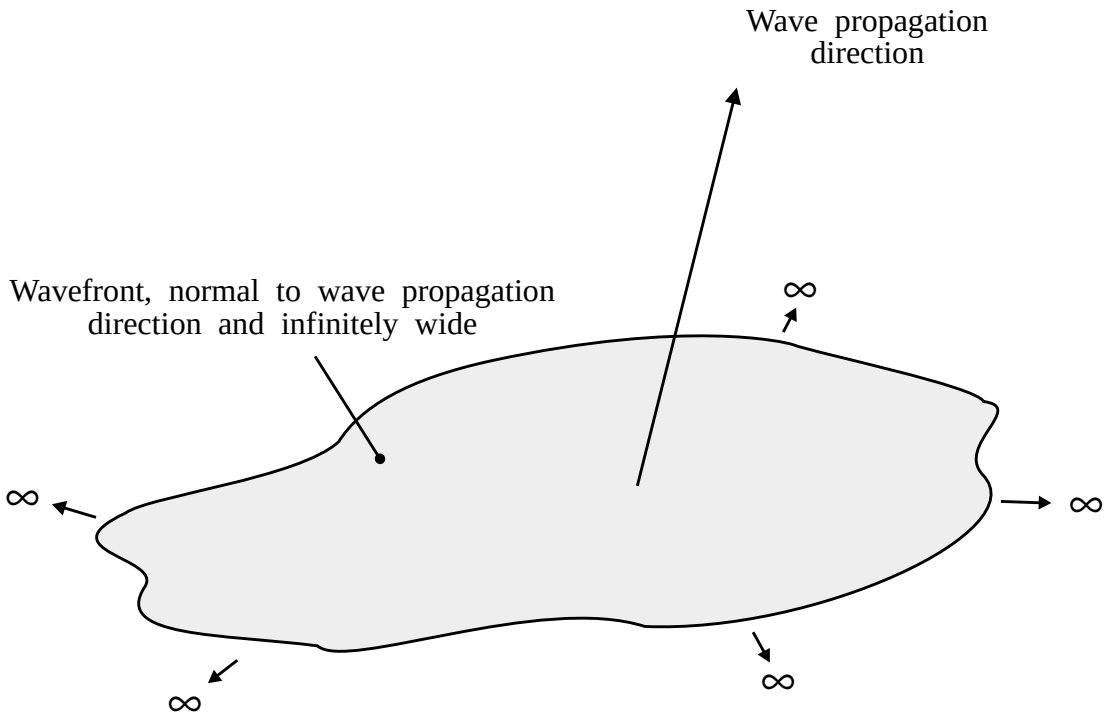

Figure 2.2 Propagation of a plane wave in an infinite elastic medium

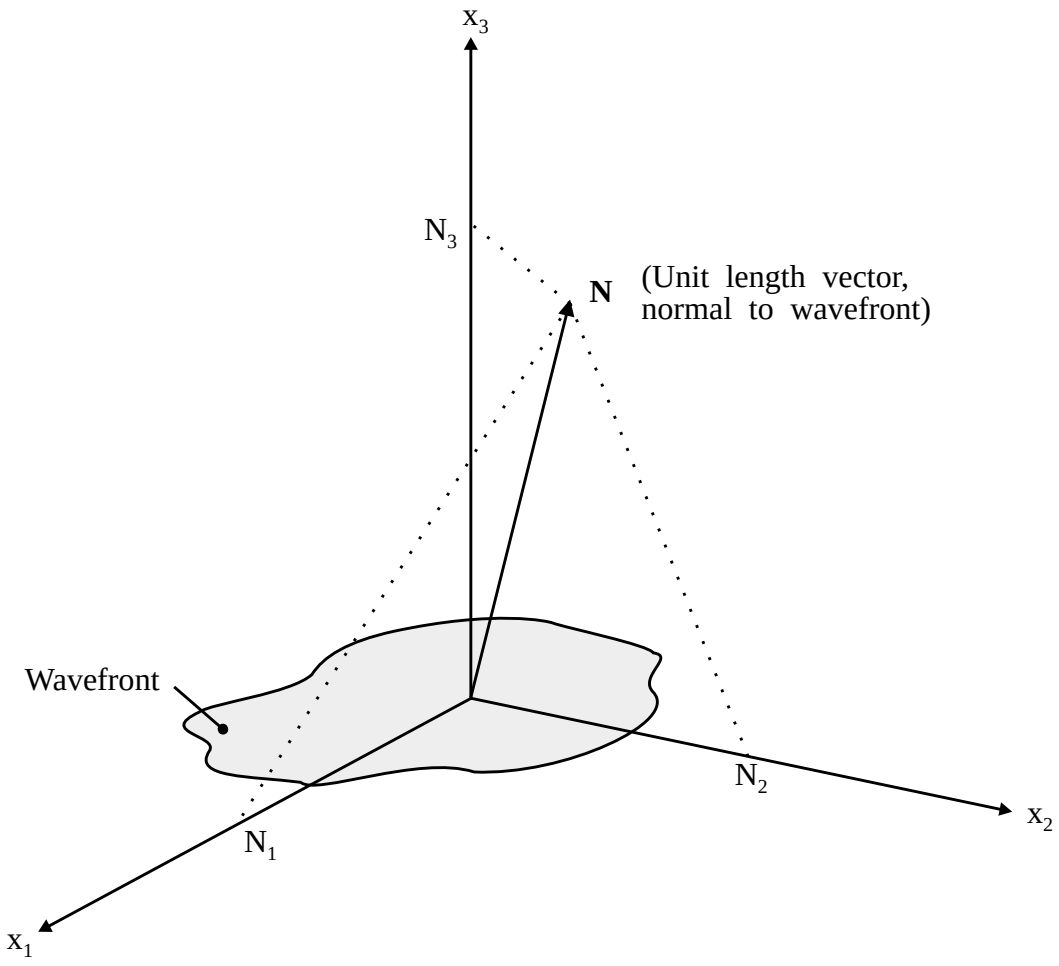

$$\phi = A\, e^{i\omega(\mathbf{N}\cdot\mathbf{x}/\alpha - t)} = A\, e^{i\omega(N_1x_1/\alpha + N_2x_2/\alpha + N_3x_3/\alpha - t)}$$

$$\psi = A\, e^{i\omega(\mathbf{N}\cdot\mathbf{x}/\beta - t)} = A\, e^{i\omega(N_1x_1/\beta + N_2x_2/\beta + N_3x_3/\beta - t)}$$

(Equation 2.13)

Figure 2.3 Unit length wave propagation vector, N, in 3-D space

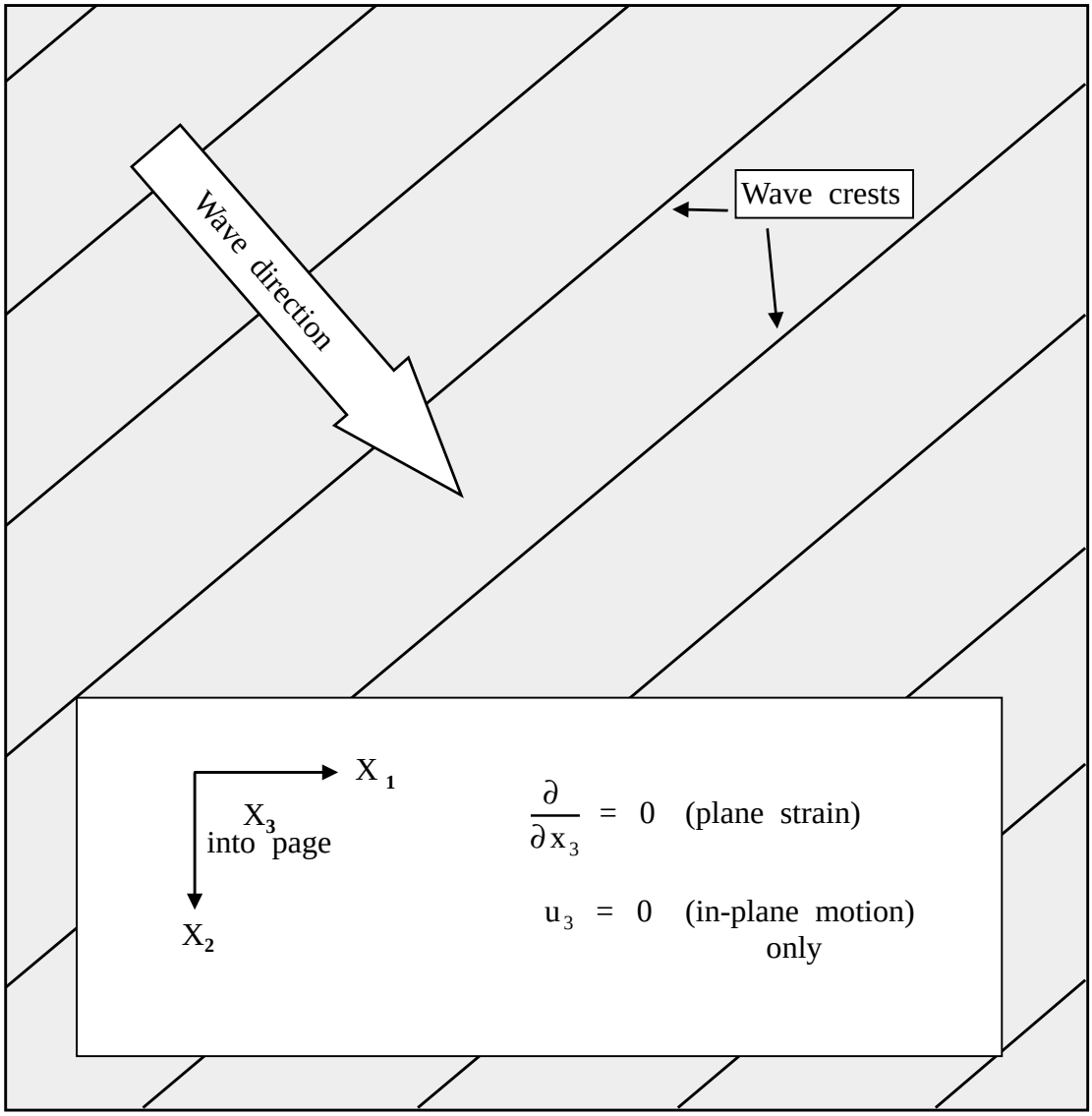

Figure 2.4 Coordinate system and constraints for in-plane wave propagation in a 2-D infinite medium

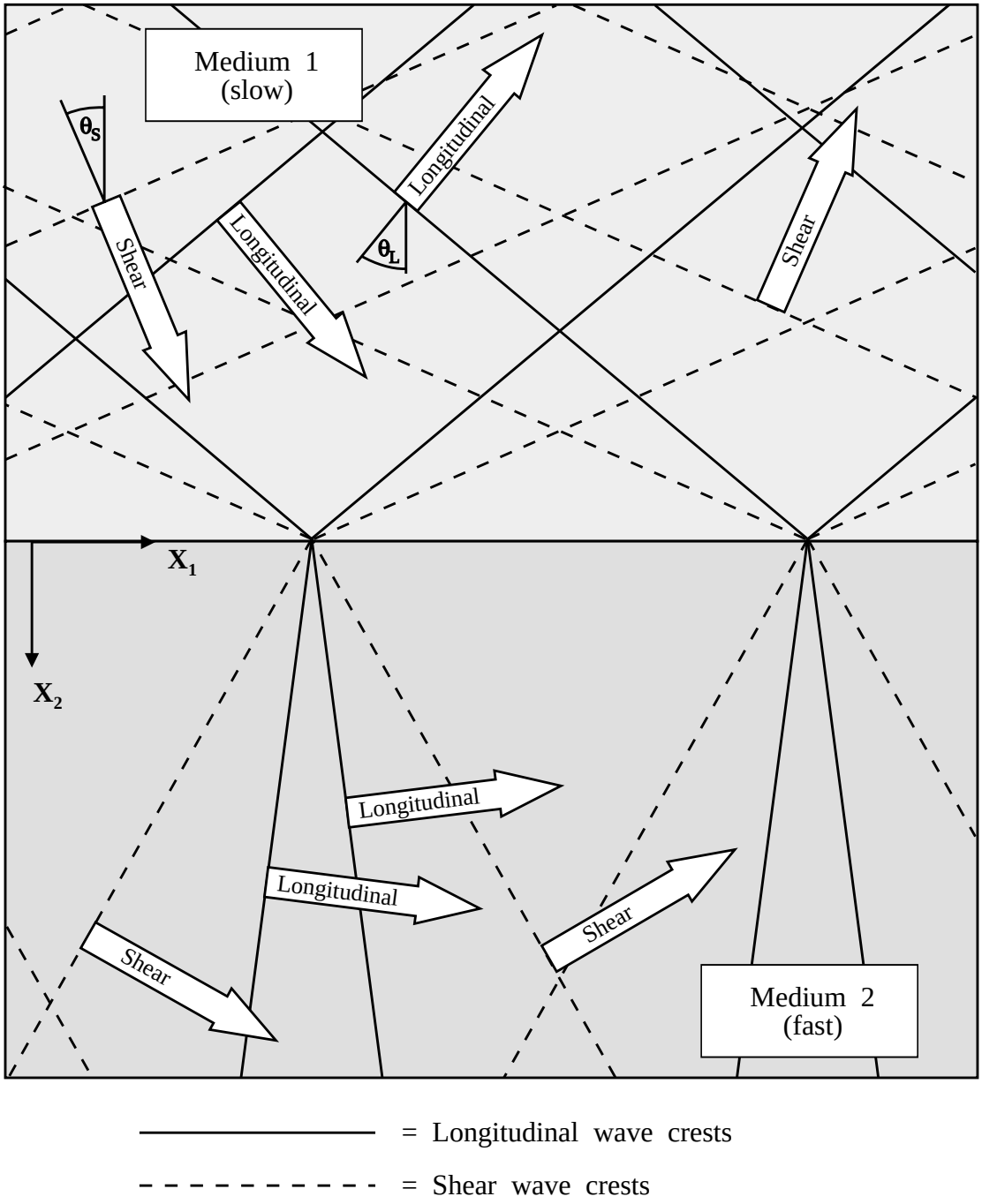

Figure 2.5 Plane waves at the boundary between two semi-infinite media

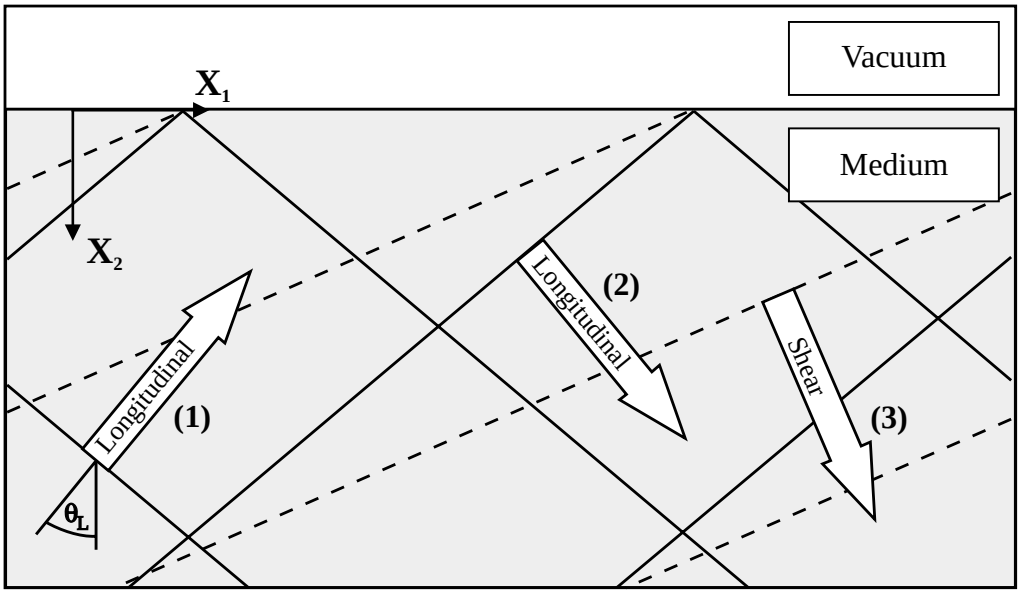

(a) Homogeneous waves: (1): Incident longitudinal, (2): Reflected longitudinal and (3): Reflected shear

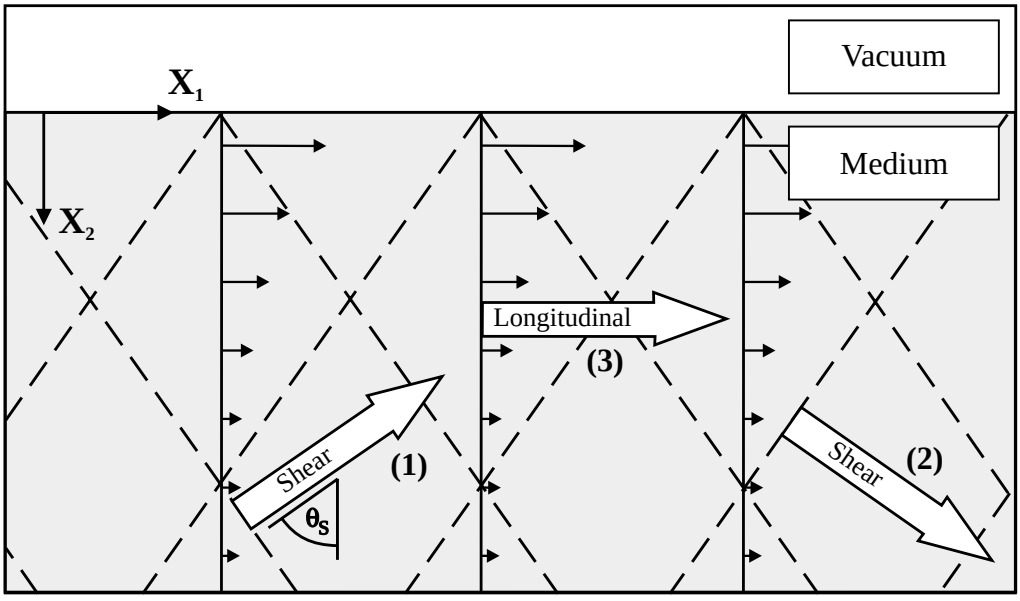

(b) Homogeneous and inhomogeneous waves: (1): Incident shear (homogeneous), (2): Reflected shear (homogeneous) and (3): Reflected longitudinal (inhomogeneous)

Figure 2.6 Homogeneous and inhomogeneous waves at a free surface

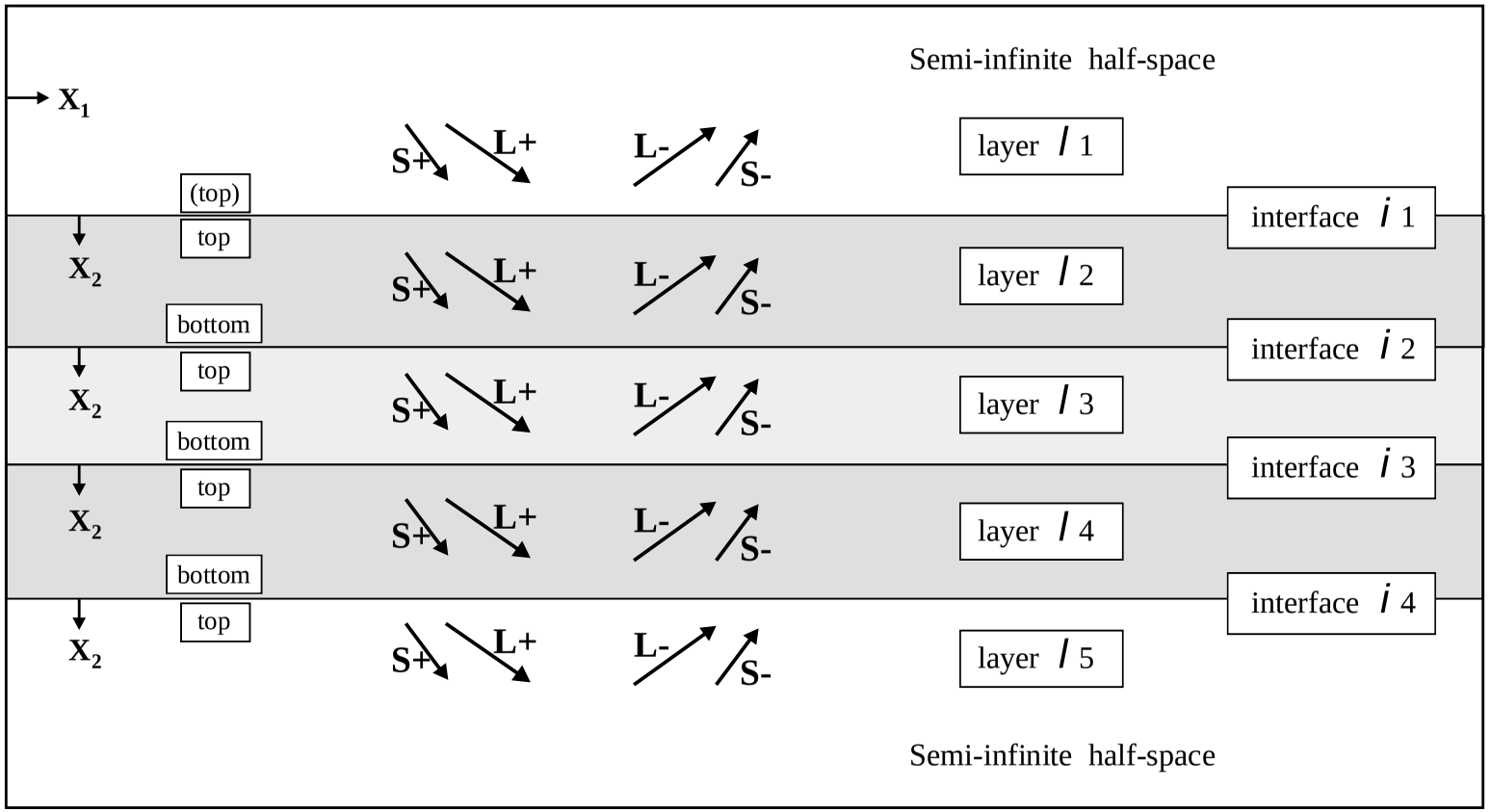

Example, using three-layer plate with semi-infinite half-spaces.

Figure 2.7 Labelling system for multilayered plate

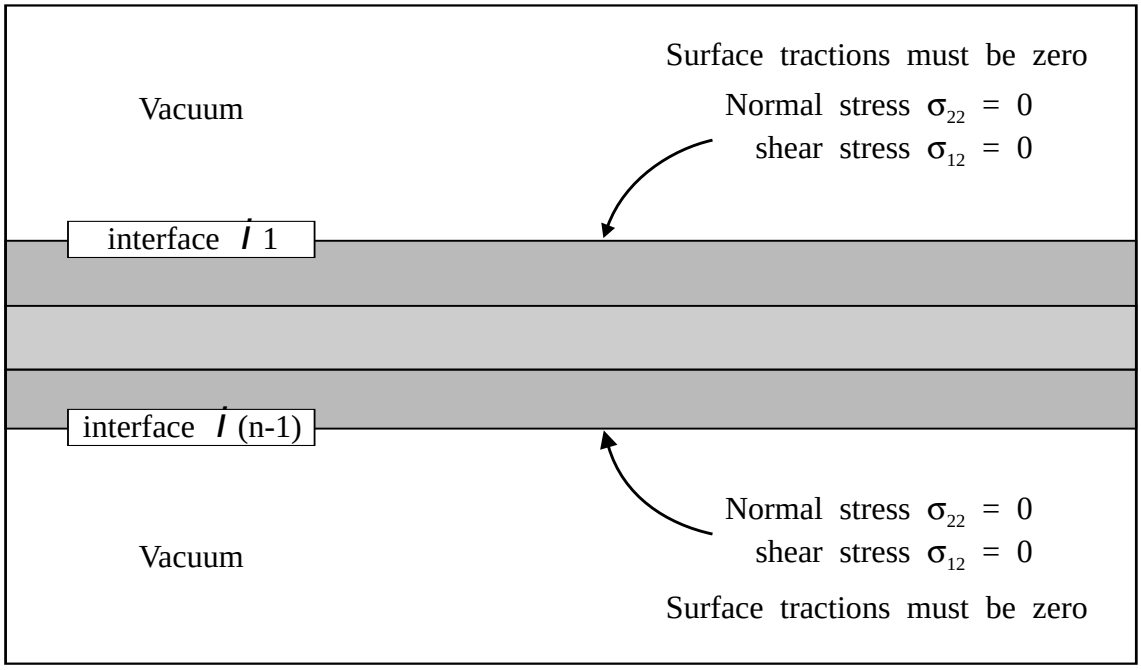

(a) Plate in vacuum

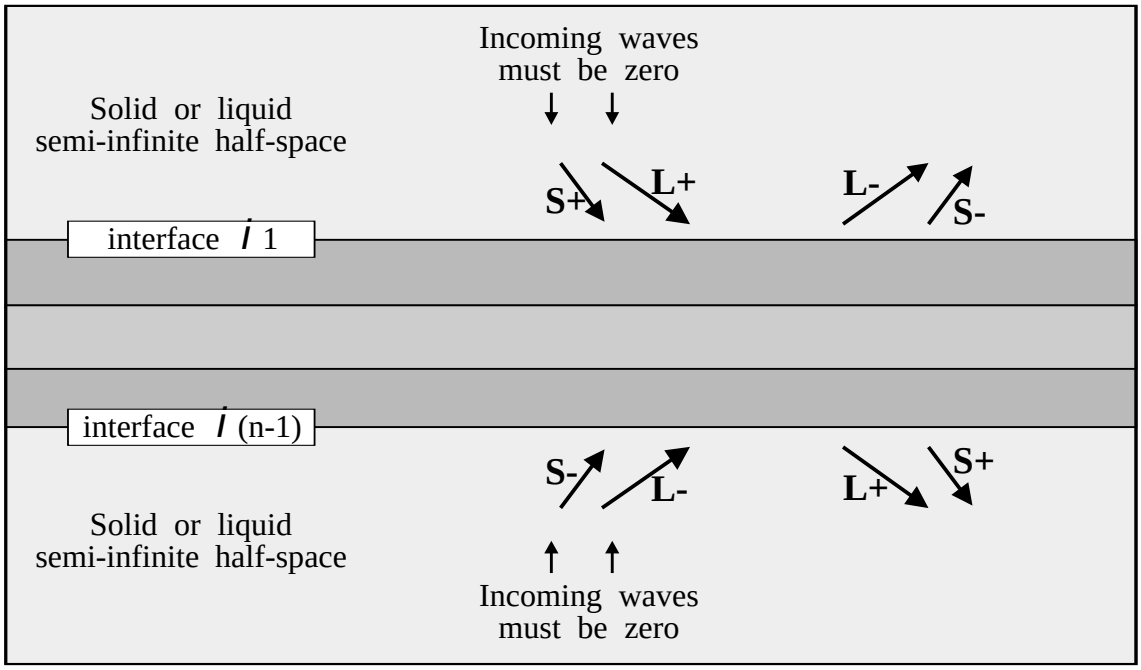

(b) Plate in solid or liquid semi-infinite half-spaces

Figure 2.8 Boundary conditions for free wave propagation in plates

CHAPTER 3

Attenuating wave propagation along a multilayered plate

3.1 Introduction

A modal theory for attenuating wave propagation in a multilayered medium is described in this chapter. The theory is developed as a generalisation of the theory for free wave propagation which was presented in Chapter 2. The implementation of the theory into the computer model will be described in Chapter 4.

Attenuation of a wave is simply loss of energy with distance travelled. Two causes of attenuation of waves in plates can be observed in practical applications. The first is material damping. Media in general are not perfectly elastic, but exhibit some form of damping which absorbs the energy of mechanical waves. This can be seen and measured directly with bulk waves and must be expected to occur too with plate waves. The second cause of attenuation of plate waves is known as leakage. If the plate is immersed in a liquid or solid then the plate wave may emit bulk waves into the surrounding medium, thus losing its own energy and decaying as it travels.

The idea with the development of a modal solution for attenuating wave propagation is to extend the formulation for free wave propagation such that each modal solution includes some description of the manner in which the wave decays. The basic philosophy is not changed, a solution still describes the modal properties of the system in terms of a frequency and a velocity at which a wave can travel indefinitely without further input of energy. However the amplitude of the wave may diminish with distance travelled and the rate at which the wave decays has to be found as part of the modal solution. The attenuation description is independent of the value of the amplitude of the wave, it simply describes a fixed rate of decay which is relevant for any wave amplitude at any location along the plate.

Since the theory for attenuating wave propagation is a generalisation of the theory for free wave propagation, it is not necessary to classify waves before attempting the solution of the equations. The general theory is equally applicable to all classes of plate wave propagation: free waves (including guided waves), damped waves and leaky

waves. In cases of attenuating waves the rate of decay is evaluated as part of the solution; in cases of free waves the rate of decay is found during the solution to be zero.

Overview

In order to extend the analysis to include the possibility of attenuating wave propagation, the key element is to generalise the equations at their basic levels. If this is done effectively then the development of the formulation for free waves which was presented in Chapter 2 remains relevant for all types of waves and a free wave becomes simply a special case of the general theory. Thus material damping is introduced by generalising the stress-strain relationship to include visco-elasticity and Snell's law is generalised to describe the attenuation of the waves along the plate.

The first task is to obtain solutions for bulk wave propagation in infinite visco-elastic media. It is shown that two bulk waves can exist in a viscoelastic medium, a 'longitudinal' wave and a 'shear' wave. Each has its propagation characteristics governed by the two elastic constants and two visco-elastic constants. The propagation of an attenuating wave is described by a complex vector, the real part representing the harmonic properties and the direction of propagation, and the imaginary part representing the rate of decay and the principal direction of decay. The descriptions reduce to those of the elastic theory of Chapter 2 when the visco-elastic constants are set to zero.

The analysis is reduced to a two-dimensional space and the interaction of bulk waves at the boundary between two semi-infinite media is examined. It is found that the rules for interaction still apply but that a complex form of Snell's law is required, the real part of the wavenumber along the plate describing the harmonic properties of the waves in this direction and the imaginary part describing the decay of the waves in this direction. All waves on both sides of the interface must have the same harmonic properties and the same rate of decay along the interface, whether elastic, viscoelastic, homogeneous or inhomogeneous.

The construction of a plate wave from the component waves in the layers, as developed in Chapter 2, is consistent with the generalised theory except that now the wavenumber for the plate wave is complex, the imaginary part adding the rate of decay to the spatial description. The characteristic functions for the modal solution are now complex for both solution techniques. Furthermore the zeroes of the characteristic functions can only be found when appropriate sets of frequency, real wavenumber and imaginary

wavenumber (attenuation) are input. Thus the modal solution is extended from a function taking two real variables, frequency and wavenumber, to a function taking one real variable and one complex variable.

3.2 Plane waves in an infinite viscoelastic medium

Material damping may be modelled in a number of ways. A convenient and valid constitutive model for small-displacement dynamic behaviour is the Kelvin-Voigt viscoelastic description in which a velocity-dependent damping force is added to the equation of motion for an infinitesimal element of the material. Symbolically the model consists of a dashpot representing the damping in parallel with the spring representing the elastic stiffness. A thorough discussion of several alternatives, including this model, may be found in Malvern (1969). He also presents a completely general derivation of the wave equations for infinite media. A specific analysis of viscoelastic wave propagation may also be found in Pialucha (1992).

To implement the model in a three-dimensional isotropic solid, the Lamé constants λ and μ are replaced by the operators:

$$\lambda \text{ becomes: } \lambda + \frac{\lambda'}{\omega}\frac{\partial}{\partial t}$$

$$\mu \text{ becomes: } \mu + \frac{\mu'}{\omega}\frac{\partial}{\partial t} \tag{3.1}$$

where the constants λ' and μ' are the viscoelastic material constants and ω is the frequency. The model clearly reduces to elasticity if the viscoelastic constants are zero.

Now the stress-strain relationship can be expressed:

Stress-strain:

$$\sigma_{11} = \left(\lambda + \frac{\lambda'}{\omega}\frac{\partial}{\partial t}\right)\Delta + 2\left(\mu + \frac{\mu'}{\omega}\frac{\partial}{\partial t}\right)\varepsilon_{11}$$

$$\sigma_{22} = \left(\lambda + \frac{\lambda'}{\omega}\frac{\partial}{\partial t}\right)\Delta + 2\left(\mu + \frac{\mu'}{\omega}\frac{\partial}{\partial t}\right)\varepsilon_{22}$$

$$\sigma_{33} = \left(\lambda + \frac{\lambda'}{\omega}\frac{\partial}{\partial t}\right)\Delta + 2\left(\mu + \frac{\mu'}{\omega}\frac{\partial}{\partial t}\right)\varepsilon_{33}$$

$$\sigma_{12} = \left(\mu + \frac{\mu'}{\omega}\frac{\partial}{\partial t}\right)\varepsilon_{12}$$

$$\sigma_{23} = \left(\mu + \frac{\mu'}{\omega}\frac{\partial}{\partial t}\right)\varepsilon_{23}$$

$$\sigma_{13} = \left(\mu + \frac{\mu'}{\omega}\frac{\partial}{\partial t}\right)\varepsilon_{13} \qquad (3.2)$$

Substitution of equation (3.2) and the strain-displacement relationship (equation (2.4)) into the equilibrium equation (equation (2.1)) gives the displacement equation of motion for viscoelastic materials, shown here in vector form:

$$\rho\frac{\partial^2\mathbf{u}}{\partial t^2} = (\lambda+\mu)\nabla(\nabla\bullet\mathbf{u}) + \mu\nabla^2\mathbf{u} + \left(\frac{\lambda'+\mu'}{\omega}\right)\nabla(\nabla\bullet\frac{\partial\mathbf{u}}{\partial t}) + \left(\frac{\mu'}{\omega}\right)\nabla^2\frac{\partial\mathbf{u}}{\partial t} \qquad (3.3)$$

This equation can be separated into the dilatational ('longitudinal') and rotational ('shear') fields by the Helmholtz method to give:

$$\rho\frac{\partial^2\phi}{\partial t^2} = \left(\lambda+2\mu+\frac{\lambda'+2\mu'}{\omega}\frac{\partial}{\partial t}\right)\nabla^2\phi$$

$$\rho\frac{\partial^2\boldsymbol{\psi}}{\partial t^2} = \left(\mu+\frac{\mu'}{\omega}\frac{\partial}{\partial t}\right)\nabla^2\boldsymbol{\psi} \qquad (3.4)$$

where ϕ and $\boldsymbol{\psi}$ are the scalar and vector wave potentials for the two fields respectively.

Now solutions are assumed for ϕ and $\boldsymbol{\psi}$ in the same form as in equations (2.13):

$$\phi = A_{(L)}\, e^{i\omega(N\bullet x/\alpha - t)}$$

$$\boldsymbol{\psi} = A_{(S)}\, e^{i\omega(N\bullet x/\beta - t)} \qquad (3.5)$$

Differentiating these and substituting into equations (3.4) shows that they are suitable assumptions when **N** is a complex vector of unit length and the constants α and β are:

$$\alpha = \left(\frac{\lambda+2\mu - i(\lambda'+2\mu')}{\rho} \right)^{1/2}$$

$$\beta = \left(\frac{\mu - i\mu'}{\rho} \right)^{1/2} \qquad (3.6)$$

Characteristics of the waves:

Equations (3.5) may also be expressed in terms of the wavenumber vector **k**:

$$\phi = A_{(L)}\, e^{i(\mathbf{k}\bullet\mathbf{x} - \omega t)}$$

$$\boldsymbol{\psi} = A_{(S)}\, e^{i(\mathbf{k}\bullet\mathbf{x} - \omega t)} \qquad (3.7)$$

k is now a complex vector given by:

$$\mathbf{k} = \frac{\mathbf{N}\omega}{\alpha} \qquad \text{for longitudinal waves}$$

$$\mathbf{k} = \frac{\mathbf{N}\omega}{\beta} \qquad \text{for shear waves}$$

$$= \mathbf{k}_{real} + i\mathbf{k}_{imag} \quad , \text{say} \qquad (3.8)$$

Separating the real and imaginary parts in equations (3.7) for ϕ or $\boldsymbol{\psi}$ gives:

$$\phi,\boldsymbol{\psi} = A_{(L,S)}\, e^{i(\mathbf{k}_{real}\bullet\mathbf{x} - \omega t)}\, e^{-\mathbf{k}_{imag}\bullet\mathbf{x}} \qquad (3.9)$$

Here the first exponential term, which is wholly imaginary, describes the harmonic propagation of the wave in the direction of the vector $\mathbf{k}_{real}$ and the second, real, term describes the exponential decay of the wave with distance in the direction of the vector $\mathbf{k}_{imag}$. The decay is therefore described in a spatial manner.

The harmonic term shows that the wave propagates in the $\mathbf{k}_{real}$ direction with wavelength (L) and speed (c) in this direction of :

$$L = \frac{2\pi}{|\mathbf{k}_{real}|}$$

$$c = \frac{\omega}{|\mathbf{k}_{real}|} \tag{3.10}$$

If a 'plane' wave is propagated into a viscoelastic medium from the face of an unfocused transducer then a reasonable assumption is that the attenuation vector is parallel to the propagation direction. For the strict analysis of plane waves discussed here we must assume that the transducer is infinitely wide and that the motion of the transducer is identical at all locations on its face. For such a wave with parallel $\mathbf{k}_{real}$ and $\mathbf{k}_{imag}$ vectors, the attenuation term $\mathbf{k}_{imag}$ describes the residual amplitude of the wave after each unit distance of propagation. Thus a wave of unit amplitude is reduced to an amplitude of $e^{-\mathbf{k}imag}$ after travelling one unit of distance. When attenuation is expressed in this form the units of the attenuation $\mathbf{k}_{imag}$ are said to be Nepers per unit distance.

The complex material constants α and β can be related to the (measurable) decay of plane bulk waves by equation (3.8). Since the propagation vector **N** has unit length, its square (**N•N)** is unity and the squares of equation (3.8) are:

$$\mathbf{k}^2 = \mathbf{k} \bullet \mathbf{k} = \frac{\omega^2}{\alpha^2} \quad \text{for longitudinal waves}$$

$$\mathbf{k}^2 = \mathbf{k} \bullet \mathbf{k} = \frac{\omega^2}{\beta^2} \quad \text{for shear waves} \tag{3.11}$$

Expanding the wavenumber vector into its real and imaginary parts:

$$\frac{\omega^2}{\alpha^2}, \frac{\omega^2}{\beta^2} = \mathbf{k}_{real} \bullet \mathbf{k}_{real} - \mathbf{k}_{imag} \bullet \mathbf{k}_{imag} + 2i\, \mathbf{k}_{real} \bullet \mathbf{k}_{imag} \tag{3.12}$$

If $\mathbf{k}_{real}$ and $\mathbf{k}_{imag}$ are parallel, as with the plane wave leaving the transducer in the discussion above, then this equation will be satisfied by the following expression for the material constants α and β:

$$\alpha, \beta = \frac{\omega}{|\mathbf{k}_{real}| + i|\mathbf{k}_{imag}|} \tag{3.13}$$

This can also be expressed in terms of the wave speed c by substituting equation (3.10):

$$\alpha , \beta = \frac{c}{1 + \frac{i|\mathbf{k}_{imag}|}{|\mathbf{k}_{real}|}} = \frac{c}{1 + i\kappa/(2\pi)} \tag{3.14}$$

where κ is the attenuation in Nepers per wavelength, so that a wave of unit amplitude is reduced to an amplitude of $e^{-\kappa}$ after travelling one wavelength. Note from the equation that for a given material the attenuation per unit distance increases linearly with frequency but the attenuation per wavelength is constant.

It has been shown therefore that there are two bulk waves which can exist in an infinite viscoelastic medium, a longitudinal wave and a shear wave, and that they can be described by a generalisation of the equations for the bulk waves in an elastic medium. The only modification to the input to the material description is the extension of the two constants α and β to include imaginary parts which describe the attenuation of the propagating waves. It has also been shown how the complex constants can be related to measurements of the speed and attenuation of bulk waves. The model reduces to elasticity when the imaginary parts of the material constants are zero.

Restriction of the model to a two-dimensional space follows exactly the theory for elastic waves which was presented in Section 2.3 of Chapter 2. Thus the displacement and stress fields are given by equations (2.19) to (2.29), in which the wave propagation vector **N** and the material constants α and β are now complex.

3.3 Plane waves at boundaries

The derivation for the interaction of viscoelastic waves at a boundary differs from that for elastic waves by the addition of further constraints which describe the relationships of the attenuations of all of the waves. Analyses of the interaction of viscoelastic waves at plane boundaries may also be found in Pialucha (1992) or Deschamps and Roux (1991).

Consider two semi-infinite half-spaces in plane strain, one on each side of an infinite flat plane. The half-spaces are joined at the interface and its location is defined by the origin of the coordinate x_2, as in the system of Section 2.4 and Figure 2.5 of Chapter 2.

Consider a longitudinal viscoelastic wave travelling in medium 1 and arriving at the interface. Its u_1 particle displacement at the interface was given in terms of its wavenumber by equation (2.31) as:

$$u_1 = N_1 A_{(L)} e^{i(k_1 x_1 - \omega t)} \qquad ((2.31))$$

Now the wavenumber **k** is complex and so, separating the real and imaginary parts:

$$u_1 = N_1 A_{(L)} e^{i(k_{1real} x_1 - \omega t)} e^{-k_{1imag} x_1} \qquad (3.15)$$

Here it can be seen that the component of the wave in the x_1 direction consists of a harmonic part and an exponential decay. This is to be expected because it simply represents the projection of the decaying bulk wave onto the interface.

Similarly it can be seen that the u_2 displacement and the stress components all share exactly the same harmonic and attenuation functions along the interface.

Now in order for the stress and displacement boundary conditions to be satisfied between this wave and any other waves at the interface, all waves will have to have the same attenuation in the x_1 direction in addition to having the same frequency and wavelength. Thus the conditions for elastic waves are extended by stating that the k_1 wavenumber, which must be the same for all waves, is now complex rather than real. Now the Snell constant s is complex, given by:

$$s = \frac{k_1}{\omega} = \frac{N_{1(L)}}{\alpha} = \frac{N_{1(S)}}{\beta} = \frac{\sin(\theta_L)}{\alpha} = \frac{\sin(\theta_S)}{\beta} \qquad (3.16)$$

The phase velocity (c_{ph}) is related to the real parts of s and k_1 by:

$$c_{ph} = \frac{1}{s_{real}} = \frac{\omega}{k_{1real}} \qquad (3.17)$$

and the attenuation of all of the waves along the interface is:

$$\text{Loss per unit length} = 1 - e^{-k_{1imag}} = 1 - e^{-\omega s_{imag}}$$

$$\text{Loss per wavelength} = 1 - e^{-\kappa} = 1 - e^{-2\pi k_{1imag}/k_{1real}} = 1 - e^{-2\pi s_{imag}/s_{real}} \qquad (3.18)$$

On first inspection this description of the interaction of viscoelastic waves at an interface appears to run into difficulty if the attenuation of the bulk waves is not the same on both

sides of the interface. This is not the case however because the reflected and transmitted waves at the interface need not necessarily have their attenuation vectors parallel to their propagation directions. The limitations are only that the boundary conditions be satisfied *along* the interface and that the attenuation normal to the interface be such that the equations of motion (3.4) are satisfied.

For the boundary conditions to be satisfied, the complex k_1 wavenumber for a reflected or transmitted wave is required by equation (3.16) to be governed by the value of the Snell constant:

$$k_1 = s\omega \tag{3.19}$$

For the equations of motion to be satisfied, the full wavenumber vector (**k**) must satisfy equations (3.8). Recalling the expansion of these equations in equation (3.12) and expanding the dot products fully gives:

$$\begin{aligned} \frac{\omega^2}{\alpha^2}, \frac{\omega^2}{\beta^2} &= \mathbf{k}^2 \\ &= k_{1real}^2 + k_{2real}^2 - k_{1imag}^2 - k_{2imag}^2 \\ &\quad + 2\,i\,(k_{1real}\,k_{1imag} + k_{2real}\,k_{2imag}) \end{aligned} \tag{3.20}$$

Thus from equations (3.19) and (3.20) the complex wavenumber for any participating wave in either of the media is defined.

The coupling conditions are illustrated in Figure 3.1. Part (a) of the figure shows the coupling of the harmonic terms. The real part of the wavenumber along the interface, k_{1real}, must be the same for all waves. Part (b) shows the coupling of the attenuations. The imaginary part of the wavenumber along the interface, k_{1imag}, must be the same for all waves, even if it means that the attenuation vector for a wave is not parallel to its propagation vector.

As examples consider three cases of wave interactions at an interface. For simplicity only longitudinal waves are considered although the principles apply to all waves at the interface. In all cases there is an incident wave arriving at the interface in medium 1, a reflected wave leaving the interface in medium 1 and a transmitted wave leaving the interface in medium 2. Cases 2 and 3 are illustrated in Figures 3.2(a) and 3.2(b) respectively.

Case 1: Both media are elastic

If both media are elastic then the incident wave is not attenuative, α is real and so s is real (equations 3.14 and 3.16). Now for the reflected wave and the transmitted wave, k_1 is real (equation 3.19) and, since these waves are also elastic, their **k** vectors are real. Their k_2 components are therefore real and all behaviour is elastic and non-attenuative. Thus the model reduces to the description of elastic wave interaction.

Case 2: First medium is elastic, second medium is viscoelastic

If the incident wave arrives in an elastic medium (Figure 3.2(a)) then s is real, even though the second medium is attenuative, because it is defined here by the incident wave. The reflected wave is therefore elastic according to the arguments of the first case. The transmitted wave is attenuative but has no component of attenuation in the x_1 direction, according to equation (3.19). Its attenuation vector is therefore parallel to the x_2 direction (normal to the interface) with magnitude given by equations (3.20). In other words the attenuating wave is constrained not to decay along the interface and has to have a sufficient decay component normal to the interface to satisfy the equations of motion in the medium.

Case 3: First medium is viscoelastic, second medium is elastic

Finally, consider the case where the incident wave arrives in a viscoelastic medium but the second medium is elastic, illustrated in Figure 3.2(b). Assuming that the attenuation vector for the incident wave is parallel to the propagation direction, s is complex and is evaluated from equation (3.19). The reflected wave is also longitudinal in this case and travels in the same medium so it shares the same α, $\mathbf{k}^2$, $\mathbf{k}_{real}$ and $\mathbf{k}_{imag}$. It follows from equation (3.20) that its attenuation vector is also parallel to its propagation direction. The transmitted wave now is constrained to attenuate in the x_1 direction even though it is travelling in an elastic medium. Thus its k_1 is complex but its **k** is real. If **k** is real then the right hand side of equation (3.20) must be real so that the imaginary part must be zero:

$$2\,i\,(\,k_{1real}\,k_{1imag} + k_{2real}\,k_{2imag}\,) = 0 \qquad (3.21)$$

The attenuation vector for the transmitted wave must therefore have the component normal to the interface of :

$$k_{2imag} = -k_{1imag}\left(\frac{k_{1real}}{k_{2real}}\right) \tag{3.22}$$

Thus the transmitted wave has negative attenuation in the direction normal to the interface.

The term in brackets in equation (3.21) is the dot product of the real and imaginary parts of the wavenumber. For this to be zero the attenuation vector must be normal to the direction of propagation of the wave. There is therefore no attenuation in the direction of propagation. In general for all elastic waves the attenuation vector is either zero or normal to the direction of propagation of the wave.

Concluding the analysis of the interaction of viscoelastic waves at an interface, it has been shown that the relationships between the waves can be described by a complex generalisation of Snell's law. The real part describes the harmonic coupling in the same manner as for elastic waves and the imaginary part is added to describe the coupling of the attenuations of the waves in the direction parallel to the interface.

The displacements and stresses in viscoelastic waves can be expressed in terms of the Snell constant in an identical fashion to the derivation for elastic waves, given in equations (2.39) and (2.40), utilising the complex values of the material constants α and β and the Snell constant s.

3.4 Assembly and solution

It has been shown that the descriptions of the displacements and stresses in viscoelastic waves and their relationships at an interface are identical to those for elastic waves, except that the material constants α and β and the vectors **N** and **k** are now complex. Consequently the development of the equations for the assembly of a layered system as discussed in section 2.6 of Chapter 2 apply equally here, with these same generalisations.

Continuing the development of the equations, the transfer matrices method or the global matrix method may be used for the modal solution of multilayered viscoelastic systems. Furthermore the introduction of the complex form of Snell's law also enables solutions to be found, in general, of attenuating wave propagation even when the materials are all elastic. This would be the case for example when an elastic wave propagates along an immersed plate, leaking bulk waves into the adjacent material. The model is therefore

not restricted to free and guided waves but may be used to solve any type of propagating plate wave provided that a zero value of the characteristic function can be found.

The characteristic function for either solution method now requires as input a complex value of the wavenumber and a (real) value of frequency and both methods yield, in general, a complex result. If a zero value of the characteristic function can be found then a modal solution has been found. In this case the imaginary part of the wavenumber describes the attenuation of the wave along the plate (equation 3.18). Physically it should be expected that systems involving material damping or leakage of energy from the plate into the half-spaces should require complex values of the wavenumber for their solution. Systems consisting of elastic materials without leakage reduce the model to the free wave descriptions of Chapter 2 when solutions are found with real values of the wavenumber.

Finally it should be noted that the analysis of the phase properties of free plate waves in Chapter 2 does not hold for attenuating waves. The coefficients of the matrices in the transfer matrix method are no longer wholly real or wholly imaginary and so the analysis of the phases is not valid.

3.5 Conclusions

The modal theory for free waves in multilayered plates which was developed in Chapter 2 has been extended to include attenuating wave propagation, either due to material damping or to leakage of energy from the plate into the half-spaces. The extension of the theory was achieved by generalising both the material model and the coupling constraints for the interaction of waves at an interface. The generalisation of the material model incorporates viscoelastic material constants which describe the attenuation of bulk waves in an infinite elastic solid. The generalisation of the coupling constraints allows for attenuation of waves in the direction along the plate and constrains all wave components in the plate to share the same attenuation in this direction.

The transfer matrices method and the global matrix method remain valid approaches for the solution of the equations. In either case the characteristic function now requires as input an imaginary part of the wavenumber, corresponding to the attenuation of the plate wave, in addition to the real wavenumber and the frequency. The functions both yield complex results.

The generalised theory may be used to solve all types of attenuating wave, whether due to material damping or leakage, in addition to free waves. It is not necessary to classify waves prior to the solution.

The implementation of the characteristic function in the computer model will be described in chapter 4.

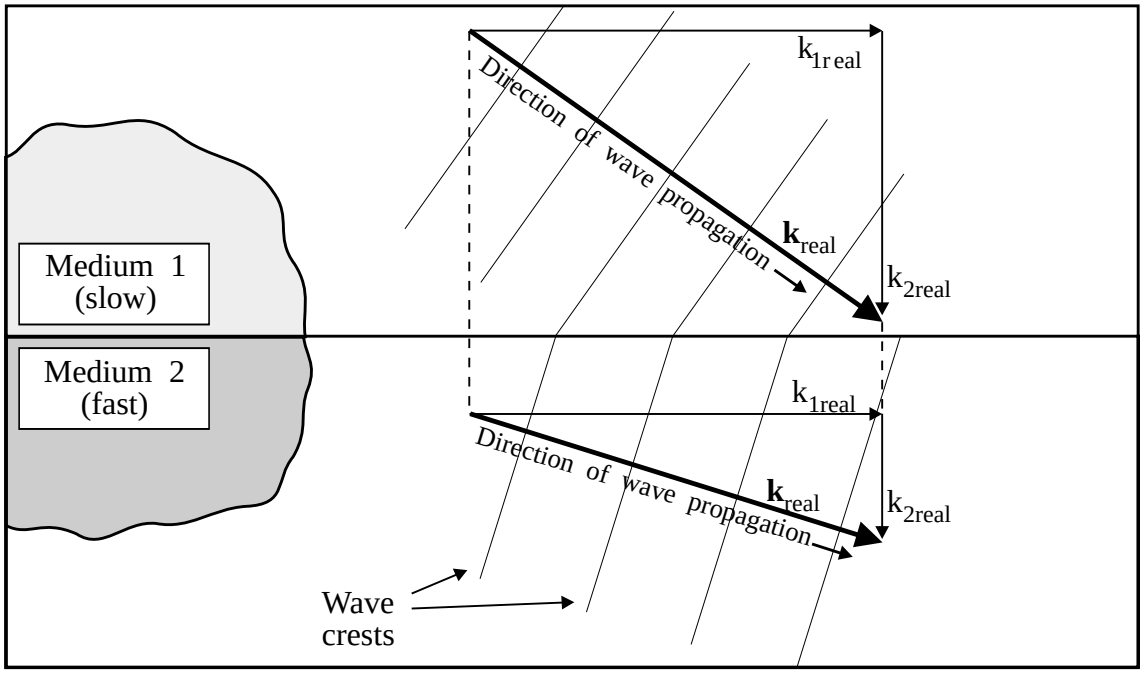

(a) Coupling of harmonic terms: k_{1real} must be the same length in both media

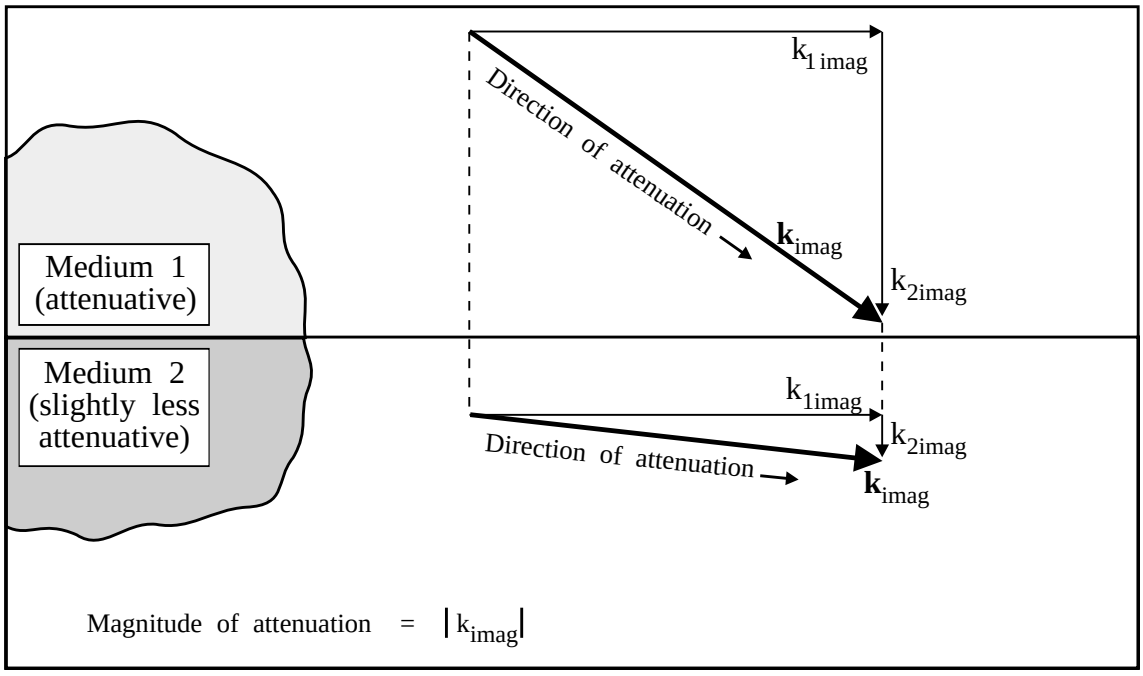

(a) Coupling of attenuation: k_{1imag} must be the same length in both media

Figure 3.1 Conditions for spatial coupling of viscoelastic waves at an interface

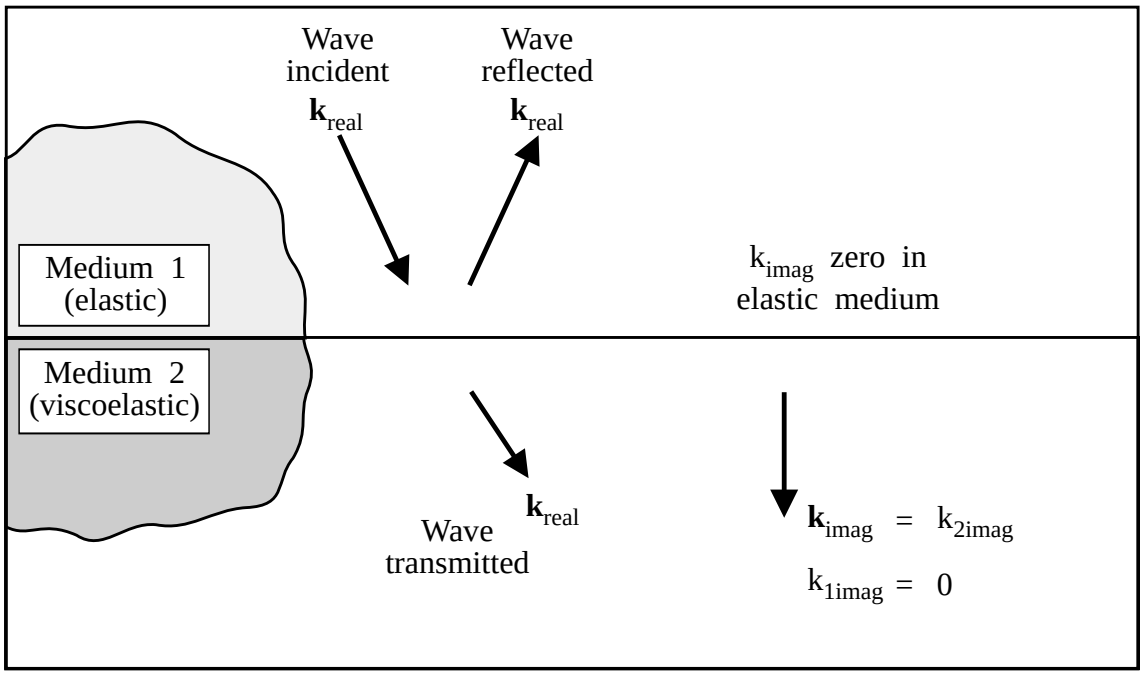

(a) Incident and reflected waves in elastic medium, transmitted wave in viscoelastic medium

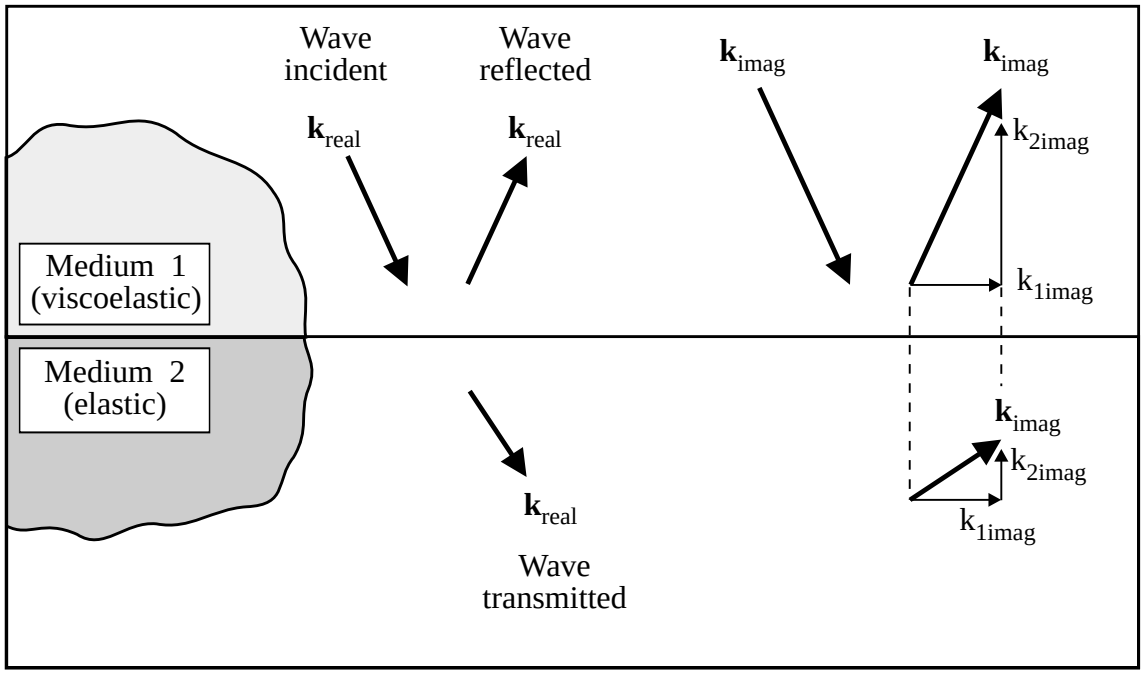

(b) Incident and reflected waves in viscoelastic medium, transmitted wave in elastic medium

Figure 3.2 Wavenumber and attenuation vectors at interfaces between elastic and viscoelastic media

CHAPTER 4

Development of numerical model

4.1 Introduction

This chapter covers the implementation of the theory of Chapters 2 and 3 into a general purpose computer model for the prediction of the modal properties of multilayered media. The model predicts the dispersion curves for plate waves and their mode shapes.

A dispersion curve is a plot describing the variation of velocity with frequency for a plate wave. From the theoretical point of view it is a plot of the locus of solutions of the characteristic function (equation 2.58, 2.62, 2.64, 2.66 or 2.88). Any point on a dispersion curve represents conditions of frequency and velocity (or wavenumber) for which the characteristic function yields a zero value. Under these conditions a propagating wave continues to travel without requiring any input of energy from outside the layered system. In the case of a free plate wave, the wavenumber is real and the wave continues indefinitely without diminishing and without leaking any energy from the layered system. In the case of an attenuating plate wave the wavenumber is complex and the wave continues indefinitely but with an exponential decay in its amplitude caused by damping losses in viscoelastic materials or leakage into the half-spaces.

A mode shape is the distribution of a displacement or stress component through the thickness of the plate. Mode shapes are calculated at a particular location on a dispersion curve and are used to reveal the physical nature of a mode. They are also used to determine the positions through the thickness of the plate where the energy of a wave is concentrated.

Overview

The core task of the dispersion curve model is to find the solutions (zeroes) of the characteristic function. Each point on a dispersion curve is found numerically by repeatedly evaluating the function whilst varying the input (frequency and wave number) according to a robust search algorithm. A dispersion curve is generated by finding a sequence of such solutions, using a trace algorithm to extrapolate from the end of the

curve to each new point. The global matrix method is selected for the definition of the characteristic function.

A coarse search is conducted first in order to locate approximately all modes of interest at a particular frequency or wave number. The coarse search steps with constant increments through a range of one of the input parameters, identifying minima in the function as approximate solutions. A fine search then starts from one of the approximate solutions and locates each of these modes accurately. It uses an unconditionally stable bisection algorithm. For attenuating modes, where the imaginary part of the wavenumber must be found in addition to the frequency and real wavenumber, the fine search also involves a sequence of alternate searches of the real variable (frequency or real wavenumber) and the imaginary variable (attenuation).

The curve tracing algorithm generates a dispersion curve for each mode by starting from each of these solution points and incrementing the wave number slowly. A further fine search is performed at each point on its path by varying the frequency. The first estimate of each new point is obtained by quadratic extrapolation from three of the preceding solution points. The process continues for each curve until the maximum frequency of interest is reached. Dispersion curves are plotted as phase velocity, group velocity, real wavenumber or incident angle in the coupling medium versus frequency. Attenuation is plotted in Nepers per wavelength or Nepers per unit distance along the plate versus frequency.

Mode shapes are calculated at any solution point which has been identified by the search algorithms. An arbitrary amplitude of one of the wave components is assumed and all of the other component wave amplitudes are evaluated with respect to this. The displacement and stress equations are then evaluated at a discrete number of locations through the thickness of the plate. Mode shapes are plotted for the displacement and stress components and for the strain energy density.

4.2 Selection of characteristic function

The theoretical development of Chapter 2 ended with two different procedures for the solution, both resulting in characteristic functions for which zero values must be found. Both of these methods are mathematically correct but in practical applications the transfer matrices method suffers from a fundamental numerical weakness under certain conditions. It has therefore been rejected in the implementation described here in favour of the global matrix method. This is unfortunate because the transfer matrices method is

the more intuitive idea, is more amenable to examination of the properties of the modal solution and has the convenience of always being real when calculating solutions for free waves. It is also computationally more efficient, particularly as the number of layers is increased.

The difficulty with the transfer matrices method comes from its requirement for the displacements and stresses at each interface to be expressed in terms of those at the next interface. It can be seen in the assembly of the layer matrix [L], given explicitly in equation (2.68). Look for example at term L_{11}. This value gives the relationship of the u_1 displacement at the bottom of the layer to that at the top of the layer. The terms g_α and g_β (defined in equation 2.43) are exponential expressions of imaginary quantities for homogeneous waves or real quantities for inhomogeneous waves. When the exponents are imaginary the evaluation of L_{11} is straightforward. However if either exponent is real then the expression contains, in brackets, the sum of a real positive exponential term and a real negative exponential term. There is no problem if the exponents are reasonably close to unity but if the exponents are very large or very small then each of the expressions in brackets consists of the sum of a very large number and a very small number. Similarly the other coefficients of the [L] matrix also consist of sums or differences of large and small numbers. Clearly therefore the matrix becomes ill-conditioned if the exponents are very large.

The condition for the exponent of g_α or g_β to be real is when $\alpha^2 s^2$ or $\beta^2 s^2$ in equation (2.43) is greater than unity, corresponding to the condition for an inhomogeneous wave. The exponent can also be seen in this equation to be linearly dependent on the product of the frequency and the distance x_2 from the top of the layer. Physically now it can be seen that the problem is associated with large exponential decays of inhomogeneous waves through the thickness of the layer. The small exponential terms relate the displacements and stresses at the bottom of the layer to those at the top, due to an inhomogeneous wave at the top of the layer. The large exponential terms relate the displacements and stresses due to an inhomogeneous wave at the bottom of the layer.

Practical implementation of the transfer matrices method has shown indeed that the solution becomes unstable for high values of the product of frequency and layer thickness when inhomogeneous waves are present. A study made by the author using the transfer matrices method and utilising 64 bit precision for real numbers and 128 bit precision for complex numbers has shown that the practical limit for the analysis of the first two modes in a titanium plate in vacuum is about 15 MHz-mm. At high frequencies these two modes consist of inhomogeneous longitudinal and shear waves and are both

asymptotic to the Rayleigh wave solution. The largest exponent is associated with the shear wave because the bulk shear velocity is lower than the bulk longitudinal velocity (see equation (2.43)). Assuming a typical value for the bulk shear velocity for titanium and that the product $\beta^2 s^2$ is just less than unity, the magnitude of the exponent at 15 MHz-mm is about 30 and so the large and small exponential terms are about 10^{13} and 10^{-13} respectively. The coefficients in the [L] matrix are therefore composed of the sums and differences of numbers which differ by 26 orders of magnitude.

Stable solutions for higher frequency-thickness products using transfer matrices have been achieved by other researchers, often for specific applications, by further manipulations of the formulation or in some circumstances by monitoring and re-scaling of variables. A number of papers have been published on this matter with specific regard to geophysical applications, for example Dunkin (1965), Abo-Zena (1979) and Evans (1985). However it was decided during the development reported here that the best way to avoid the risk of instability in the general purpose model is to adopt the global matrix formulation which is inherently stable so that the risk can be dismissed entirely.

The fundamental attraction of the global matrix method is that it does not involve the expression of displacements and stresses at one interface with respect to those at any other. Each equation in the matrix is formed at an interface and the solution of the characteristic function simply implies that all of the equations have been satisfied independently. This does not mean that the interfaces are completely independent, because the equations at an interface are influenced by the arrival of waves from the neighbouring interfaces. However, as the frequency-thickness product is increased, the influence of an inhomogeneous wave travelling along one interface on the displacements and stresses at the next interface simply reduces. The extent of the influence is determined by the exponential terms in the global matrix. These terms are always decaying functions for inhomogeneous waves if the modification of Schmidt and Jensen (1985) and Pialucha (1992) is made to the origins of the waves (see equations 2.82). Thus in the limit these terms vanish and an inhomogeneous wave travelling along one interface has no influence on the waves at the next interface. The method therefore remains perfectly stable for any frequency-thickness product because it does not rely on the coupling of waves from one interface to another.

4.3 Evaluation of characteristic function

Examination of the characteristic equations of Chapter 2 shows that they describe both the layered system and its boundary conditions. Specifically any evaluation of the

function yields a result which is determined by the material properties and thicknesses of all of the layers, and the frequency and wave number. Additionally if the evaluation of the function yields zero then the function represents a solution to the equation, implying that the desired boundary conditions have been satisfied.

The material properties and thicknesses are input to the model as constant descriptions. A sequence of layers is defined, each with a thickness, a density, a longitudinal bulk wave velocity and attenuation and a shear bulk wave velocity and attenuation. For ease of discussion these properties will be treated as constants in the evaluation of the characteristic functions because typically they do not vary significantly, if at all, over the frequency and wave number solution space. In general however any variation of these properties with frequency is permissible, provided that it is sufficiently slow not to upset the search algorithm, because each solution of the equation exists only at its single frequency and wavenumber. Any such variations are assumed to be accommodated by re-sampling the 'constant' data at each evaluation of the function.

The theory has now been condensed to a function which requires as input a value of frequency and a value of wave number and whose output indicates whether or not these inputs are appropriate for wave propagation. The frequency is real in all cases and the wave number is real for free waves and complex for attenuating waves (see section 3). Strictly speaking the wavenumber is a vector but the analyses of Chapters 2 and 3 showed that the characteristic function is expressed in terms only of its components (real and imaginary) in the direction parallel to the plane of the layers. All references to the wavenumber in this chapter therefore refer to this component (k_1) of the wavenumber. Referring to equations (2.36), (3.16) and (3.17), the input can be further generalised for practical applications by relating the real part of the wave number to the phase velocity of the plate wave or to the angle of incidence (θ) of a bulk wave with velocity c_i in one of the half-spaces, if present:

$$k_{real} = \frac{\omega}{c_{ph}} = \frac{\omega.\sin\theta}{c_i} \tag{4.1}$$

The significance of relating the wavenumber to the angle of incidence of bulk waves in a half-space is that the excitation and reception of plate waves is often achieved using the coincidence principle, which will be described in Chapters 5 and 8, in which the transducers must be oriented at this angle. The imaginary part of the wavenumber, if present, describes the attenuation of the wave along the plate:

$$\text{Loss of amplitude per unit length} = 1 - e^{-k_{imag}}$$

$$\text{Loss of amplitude per wavelength} = 1 - e^{-\kappa}$$

$$= 1 - e^{-2\pi k_{imag}/k_{real}} \qquad (4.2)$$

To evaluate the function, the global system matrix is assembled according to section 2.8 using the input values of frequency and wavenumber and its determinant is calculated (equation 2.88). Since the aim is to find zero values of the determinant, the matrix which is assembled is frequently close to being singular. Nevertheless for the search algorithms to converge successfully the determinant must be calculated accurately. Furthermore, the generation of a dispersion curve typically requires many thousands of evaluations of the function. A very important part of the development therefore was the implementation of a robust algorithm for the calculation of the determinant of the complex global matrices.

The ideal approach for the calculation of the determinant would be to use repeated Laplace expansions, because this would involve multiplications, additions and subtractions only and would be totally robust. However this method would be extremely inefficient for large matrices and it has been found that in practice it is not necessary to be so cautious. The fact that the determinant can be found by Laplace expansions has its use however because it demonstrates simply that the characteristic function is analytic within the desired solution space. The coefficients of the system matrix are analytic in all space with the exception of the square root expressions in the exponents of g_α and g_β in equation (2.43). Each square root expression has two possible evaluations in general, corresponding to a wave arriving at the interface and a wave leaving the interface. These possibilities are identified separately in the analysis and the signs of the roots are constrained so that there is no discontinuity in their evaluations. Therefore, with this constraint, the coefficients of the system matrix are analytic. The sums, differences and products of analytic functions are themselves analytic. Therefore the characteristic function is analytic. This property is useful because it means that it is valid to assume that the characteristic function is continuous and smooth.

There are many published algorithms for the calculation of the determinant of a matrix. An introductory discussion, an implementation and further references may be found in Press, Flannery, Teukolsky and Vetterling (1986). Commercial library program routines may also be utilised, for example the routines of the Numerical Algorithms Group (Ref. NAG Ltd.). However in order to address the specific demands of the application discussed here, with maximum efficiency, it was considered preferable not to rely on

such general purpose routines. An algorithm was therefore developed, based on a complex form of Gaussian reduction. It has been found to perform perfectly. The global system matrix is reduced systematically to upper diagonal form and the determinant is then evaluated as the product of all of the diagonal elements. Partial pivoting of rows is employed so that the best possible condition is achieved on each reduction. The banded nature of the global matrix is also exploited as far as is possible with the partial pivoting. Divisions are monitored when pivoting so that if the absolute value of the denominator drops below a small tolerance of 10^{-20} then a zero determinant can be declared rather than the solution fail due to zero division. In practice however the iteration of the solution has always been found to converge to an acceptable accuracy without a zero determinant being declared.

4.4 Searches

The task of the search algorithms is to find input values to the characteristic function which are acceptably close to yielding zero results. The searches are carried out in two stages, a coarse search is used to find the approximate locations of modes over a wide range of solution space and a fine search is used to improve the accuracy, as required, of any of these approximate solutions. The fine search algorithm is also used repeatedly for the generation of dispersion curves.

Coarse search

The coarse search involves sampling the function over a range of one parameter whilst holding the other independent parameters constant. Thus a frequency search consists of a sweep of frequency by constant increments over a selected range at a fixed phase velocity and attenuation, and a velocity search consists of a sweep of velocity at fixed frequency and attenuation. A frequency search and a velocity search are illustrated in Figure 4.1. Also shown as an example in the figure, in dotted lines, are the Lamb wave dispersion curves for a 1 mm thick sheet of titanium. The coarse searches should identify approximately the locations where these dispersion curves cross the sweep lines. This is achieved by examining the array of complex values (the results of the sweep) and identifying the minima of their amplitudes.

Typical results of a coarse search for a free wave problem are shown in Figures 4.2 and 4.3. The example is the 1 mm thick sheet of titanium, introduced above. The material is assumed to be perfectly elastic and the plate is in vacuum. The sweep line is shown in Figure 4.1. The sweep is of 101 samples at 20 kHz intervals over a range of frequency of

1.5 MHz to 3.5 MHz, at a constant velocity of 8 km/s and a constant attenuation of zero. Figure 4.2 shows the results of the sweep in complex space, revealing the existence of the two modes in this range. These can be seen where the path of the sweep passes through the origin of the plot. The frequencies of the modes can also be identified by the locations of the minima in the amplitudes of the function, shown in Figure 4.3. Since the solutions are for free waves the choice of attenuation of zero is correct. It can therefore be assumed that further refinement of the sampling interval would improve the accuracy with which the frequencies of the modes are known and that in the limit the minima would be zeroes of the function.

Figures 4.4 and 4.5 show the same plots for an attenuating wave propagation problem when the same plate is immersed in water. Here it can be seen that the path of the sweep does not pass through the origin. Therefore zeroes of the function can not be found by refining the sampling interval, only minima can be identified. For the path to pass through the origin for either of the modes it would be necessary for the sweep to be performed at the appropriate value of attenuation corresponding to the leaky solution for the mode.

The coarse search does not always reveal minima for attenuating waves. The minima are clearly identifiable in Figure 4.5 but they tend to be much blunter when the value of attenuation which is used in the sweep is very different from the value which is appropriate to the leaky solution. This is normally the case when zero attenuation is used in the sweep but the wave is very leaky. In fact in many cases of strongly attenuating waves it is necessary to perform the sweep a number of times with a range of different attenuations in order to detect the minima.

Fine search

Having identified the approximate input values for a modal solution, the fine search is used to improve the values to acceptable accuracy. This would be straightforward if only free modes were required but it is rather difficult when the possibility of attenuating modes is to be considered, for two reasons. The first difficulty is evident already: in general there are three values of input to be considered, real wavenumber, imaginary wavenumber and frequency, so that simple refinement of the sweep method is not sufficient. The second difficulty is that modes can exist at very close or even coincident locations (note the crossing of the dispersion curves at some locations in Chapter 5). This means that the fine search algorithm may be influenced by more than one mode. It is therefore extremely risky to employ any fast-converging methods based on slopes or

extrapolations, such as Newton's method. Such methods may be beneficial for specific problems where modes are well separated - Clayton and Derrick (1977) claim to have had success with a complex Regula Falsi method which resorts to a Monte Carlo technique for restarting when a wild extrapolation occurs. However, a study made by the author using complex Regula Falsi indicated that wild extrapolations are extremely frequent when modes are close. It was therefore decided to develop a robust algorithm which is not dependent on the evaluation of gradients and which does not involve any extrapolations.

The scheme works by performing an alternating sequence of searches of one of the real inputs to the function and the attenuation. First, a single-variable search of a real input (frequency, real wavenumber or velocity) is performed to find the minimum of the function to a high degree of accuracy. The other real input and the attenuation (in Nepers per wavelength, κ) are kept constant. A check is then made to determine whether the minimum is acceptably close to a zero of the function and, if so, the search is complete. If not, the single-variable search is repeated with the attenuation as the variable so that an accurate minimum of the attenuation is found. Again the check is made to determine whether the minimum is acceptably close to a zero. If not, the real input is varied again, and so on until convergence is achieved.

The single-variable search is itself carried out in two stages. The first stage is simply a refinement of the coarse search technique. The sign of the gradient of the amplitude of the function is found by taking a very small arbitrary step of the input variable. This determines whether the input variable should be increased or decreased to find a lower function amplitude. The input variable is then incremented (or decremented) in fixed small steps until a minimum is passed.

At this point the strategy is changed and a robust bisection method is employed, still retaining the same input parameter as the variable. This method is similar in approach to the 'Golden Section Search' discussed by Press *et al.* (1986). An iteration cycle of this method starts with three samples: a current minimum, a sample obtained with a lower value of the variable and a sample obtained with a higher value of the variable. These are the 'centre' sample, the 'left' sample and the 'right' sample respectively. The size of the sampling interval between left and centre is the same as between centre and right. The function is then sampled at the two mid-points of these intervals so that a total of five equi-spaced samples are known. For the next iteration cycle, the sample with the lowest absolute value out of these five becomes the new centre, and its neighbours become the new left and right. Examination of each of the possibilities during a cycle of

the algorithm shows that this process must converge unconditionally. Convergence on the minimum is deemed to have been achieved when the sampling interval has been reduced to an acceptable tolerance. Typically a tolerance of 10 Hz is used for frequency, the tolerance for the real wavenumber is such that a 0.01 m/sec tolerance is achieved for phase velocity and the tolerance for attenuation is 0.001 Nepers/wavelength. Convergence on the minimum is normally achieved in about 10-20 iterations when starting from an approximate value given by a coarse search.

After each iteration of the single-variable search the result is examined to see whether it is a valid solution. Since the gradient of the function varies significantly over the solution space it is not advisable to decide whether the minimum is a solution simply by comparing its magnitude with an arbitrary tolerance. This would result in large variations of the accuracy of the solution over the solution space and different levels of accuracy for different plate systems. Instead the angle is calculated between the vectors in complex space from the origin to the sampling points just before and just after the converged minimum, as shown in Figure 4.6. Since the function is smooth, an exact solution in the limit should have an angle of 180 degrees. A solution is considered to have been found if the angle is greater than 90 degrees.

An illustration of the application of the fine search algorithm is shown in Figure 4.7. The example is of the 1 mm titanium sheet in water whose coarse search was shown in Figures 4.4 and 4.5. In fact part of the coarse search plot of Figure 4.4 is included in the figure, from which it can be seen that the fine search in this example starts from the second minimum of the coarse search. The fine search starts with the variation of the frequency to find an accurate minimum, which in this case is very close to one of the sampling positions of the coarse search. The attenuation is then varied, then the frequency, then the attenuation and so on. Only three applications of the single-variable search are shown; a further five were required before the solution converged. The attenuation in this case was found to be fairly large, at 0.462 Nepers per wavelength. The frequency was calculated as 2.866 MHz, some 13 kHz lower than that for the plate in vacuum.

The speed of convergence of the fine search algorithm depends on the accuracy of the starting values, the proximity of modes and the degree of attenuation (large numbers of iterations are often necessary for very leaky solutions). When searching for free modes the solution is always rapid, provided that the coarse search has been performed with zero attenuation, because the algorithm detects each solution in one application of the single-variable search.

4.5 Curve tracing

The task of the curve tracing algorithm is to generate a dispersion curve by finding a smooth sequence of solutions for a given mode. The algorithm works on one mode at a time, starting from a user-selected position (found by a coarse search) and finishing at a selected upper limit of frequency. An illustration of the generation of a dispersion curve is shown in Figure 4.8(a).

The curves could be generated as either phase velocity dispersion curves or wavenumber dispersion curves. For convenience, wavenumber curves are generated because they are closer to straight lines and are therefore easier to predict with extrapolation algorithms. Any other dispersion curves (phase velocity, group velocity or angle of incidence) can be calculated from the wavenumber curves. A constant wavenumber increment, Δk, is chosen and solutions are found by performing a fine search for a sequence of wavenumbers with this spacing. Each fine search uses frequency as the real variable, keeping the real wavenumber constant.

The algorithm starts by performing a fine search to obtain an accurate first point in the frequency - wavenumber space. A very small increment (one thousandth of Δk) is then added to the wavenumber and a new solution is found by a fine search. This pair of solutions gives the gradients of frequency and of attenuation of the dispersion curve at this location and enables a linear extrapolation to be made to a position exactly Δk from the first point, where another fine search is performed. A second linear extrapolation yields the third point and so on.

After six points have been found the algorithm switches to a quadratic extrapolation scheme. For a polynomial where solutions y_0, y_1 and y_2 are known for equally spaced inputs x_0, x_1 and x_2, it can be shown that the extrapolation

$$y_3 = y_0 - 3y_1 + 3y_2 \tag{4.3}$$

for the next equally spaced input x_3, is exact for the constant, linear and quadratic terms. This extrapolation is employed with $2\Delta k$ as the equally spaced input and is used to extrapolate both frequency and attenuation, as illustrated in Figure 4.8(b). Thus, following the solution at point n, the predictions for frequency f_{n+1} and attenuation κ_{n+1} are:

$$f_{n+1} = f_{n-5} - 3f_{n-3} + 3f_{n-1}$$

$$\kappa_{n+1} = \kappa_{n-5} - 3\kappa_{n-3} + 3\kappa_{n-1} \qquad (4.4)$$

The use of a quadratic extrapolation scheme improves the estimate of the prediction enormously over a linear extrapolation. This reduces the number of iterations required by the fine search after each extrapolation but, more importantly, it minimises the risk of following the wrong curve when two dispersion curves cross (see examples of crossing curves in Chapter 5). In practice it is extremely rare for this error to occur with this scheme. The spacing for the input is chosen to be $2\Delta k$ rather than simply Δk in order to reduce the influence of errors in the individual solutions on the extrapolation. Two possibilities can occur. Firstly, if solution f_n is incorrect because it converges on the wrong mode (perhaps one which is about to cross the one of interest) then extrapolation to point n+1 using the solution at point n risks following the other mode. With the spacing increased to $2\Delta k$ the erroneous result at point n is not used until a step later when the danger is reduced. Secondly, the influence of any error at a point (some small error must always be expected even after convergence) on the extrapolation is dependent on the spacing, as with any numerical differentiation process. As the spacing is increased, the extrapolation error for any given set of three solution errors is reduced.

Having traced the wavenumber dispersion curve, the phase velocity and angle of incidence dispersion curves are easily calculated from equation (4.1). Additionally the group velocity (the velocity at which energy is carried along the plate) is calculated from the differential expression:

$$c_{gr} = \frac{d\omega}{dk} \qquad (4.5)$$

Any of these real quantities or the attenuation of the plate wave, in Nepers per wavelength or Nepers per unit distance, may be plotted using the model.

4.6 Mode shapes

A mode shape of a plate wave is the distribution of one of the field variables through the thickness (x_2 direction) of the multilayered system. Thus a u_1 displacement mode shape shows the variation of the u_1 displacement with depth through the plate, and similarly with the other displacement and stress components. The variation in the x_1 direction is not of interest because it is always sinusoidal for all components, with wavelength equal

to the wavelength of the plate wave. Mode shapes may be calculated at any location on a dispersion curve. Some examples of mode shapes will be shown in Chapter 5.

The calculation of mode shapes starts with the calculation of the amplitudes of the four component waves $A_{(L+)}$, $A_{(L-)}$, $A_{(S+)}$, $A_{(S-)}$ in each of the layers of the system at a chosen position on a dispersion curve. Ideally this would be done by inverting the system matrix [S] on the left hand side of equation (2.85) and using this to pre-multiply both sides of the equation to give:

$$\begin{Bmatrix} \{A^-_1\} \\ \{A_2\} \\ \{A_3\} \\ \{A_4\} \\ \{A^+_5\} \end{Bmatrix} = [S]^{-1} \begin{bmatrix} [-D^+_{1b}] & & \\ & & \\ & & [D^-_{5t}] \end{bmatrix} \begin{Bmatrix} \{A^+_1\} \\ \{0\} \\ \{0\} \\ \{0\} \\ \{A^-_5\} \end{Bmatrix} \tag{4.6}$$

However the inversion of [S] at a position on a dispersion curve is not possible because by definition it is singular for any modal solution. It is not surprising that this is the case because the modal solution describes the conditions for the existence of plate waves but it does not describe their amplitudes. Propagating waves of any amplitude are therefore permissible.

The problem is solved by assuming an amplitude of one of the wave components in one of the layers and scaling the others accordingly. Incidentally, by this assumption the amplitude of the plate wave is also assumed. The choice is arbitrary; in the implementation described here a unit real amplitude is assumed for the downward longitudinal wave (A(L+)) in the first finite layer of the plate (layer ℓ 2). The assembly of the system equation (2.85) is therefore modified slightly. Instead of moving the equations for all four of the incoming waves ($A_{(L+)1}$, $A_{(S+)1}$, $A_{(L-)5}$ and $A_{(S-)5}$) to the right hand side, as described in Chapter 2, only three of them are moved and the place of the fourth is taken by the assumed unit component $A_{(L+)2}$. The modified system matrix is still square and is in general non-singular and the right hand side of the system equation is non-zero. The equation can therefore be solved for the array of wave amplitudes. The solution yields the amplitudes of all of the layer wave components for unit real $A_{(L+)2}$.

The modified system matrix is in general non-singular but there is a condition when it becomes singular. As discussed in Chapter 2, Section 2.8, the system matrix is singular when the wavenumber of the plate wave is equal to the wavenumber of either of the component waves in one of the layers. However this singularity is not a problem.

Firstly, the existence of the singularity is due to the fact that the + waves and the - waves with this wavenumber are indistinguishable in their influence on the displacements and stresses. Any error in the evaluation of the relative amplitudes of these + and - waves will therefore have no effect on the calculated mode shapes. Secondly, failure of the solution algorithm due to zero division is unlikely because of numerical rounding. A practical investigation conducted by the author has shown that, even if the matching wave numbers are specified exactly to full precision, sufficient precision is lost in the calculation of the exponential functions to avoid the trap for zero division in the solution routine.

Having found the wave amplitudes, the stress and displacement components can be calculated at any position through the thickness from equations (2.39) and (2.40), remembering to adjust the x_2 values for upwards travelling waves in order to account for the location of their origins at the bottoms of the layers (Chapter 2, Section 2.8). Thus plots can be made of the through-thickness variations. In the implementation described here, plots may be made of any of the stress or displacement components, or of the strain energy density , given by half of the sum of the stress-strain products:

$$\text{SED} = \frac{1}{2}\left(\sigma_{11}\frac{\partial u_1}{\partial x_1} + \sigma_{22}\frac{\partial u_2}{\partial x_2} + \sigma_{12}\left(\frac{\partial u_1}{\partial x_2} + \frac{\partial u_2}{\partial x_1}\right)\right) \tag{4.7}$$

The displacements and stresses do not in general share the same phase in the x_1 direction (or time). For convenience when comparing plots, all of the mode shapes are therefore plotted with phases such that in each case the value at the top of the first finite layer of the plate is real and positive. Also, the displacement components are scaled such that the Euclidean norm of the two arrays of displacement values through the thickness of the plate is unity. The choice of scaling is arbitrary but it is useful to be able to compare different displacement components of a mode on the same scale and to maintain a reasonably consistent scale for all modes. Similarly the stress components are scaled to the Euclidean norm of the stresses.

4.7 Conclusions

The theory for free waves and attenuating waves of Chapters 2 and 3 has been implemented into a general purpose predictive tool for calculating the modal properties of multilayered plates.

The two possible solution methods which were introduced in Chapter 2 were examined and the global matrix method was chosen for the implementation. An algorithm based on complex Gaussian reduction with partial pivoting was developed for the evaluation of the characteristic function and a robust scheme was developed for searching for the complex roots. The generation of dispersion curves is achieved by repeated applications of the search scheme, employing quadratic extrapolation for the prediction of each new point. A procedure for calculating the mode shapes of propagating waves was developed by modification of the system matrix.

The model calculates dispersion curves as phase velocity, group velocity, real wavenumber or incident angle, versus frequency. The attenuation of the plate waves may also be plotted. Mode shapes are plotted for the displacement and stress components and for the strain energy density. They may be plotted at any location on a dispersion curve.

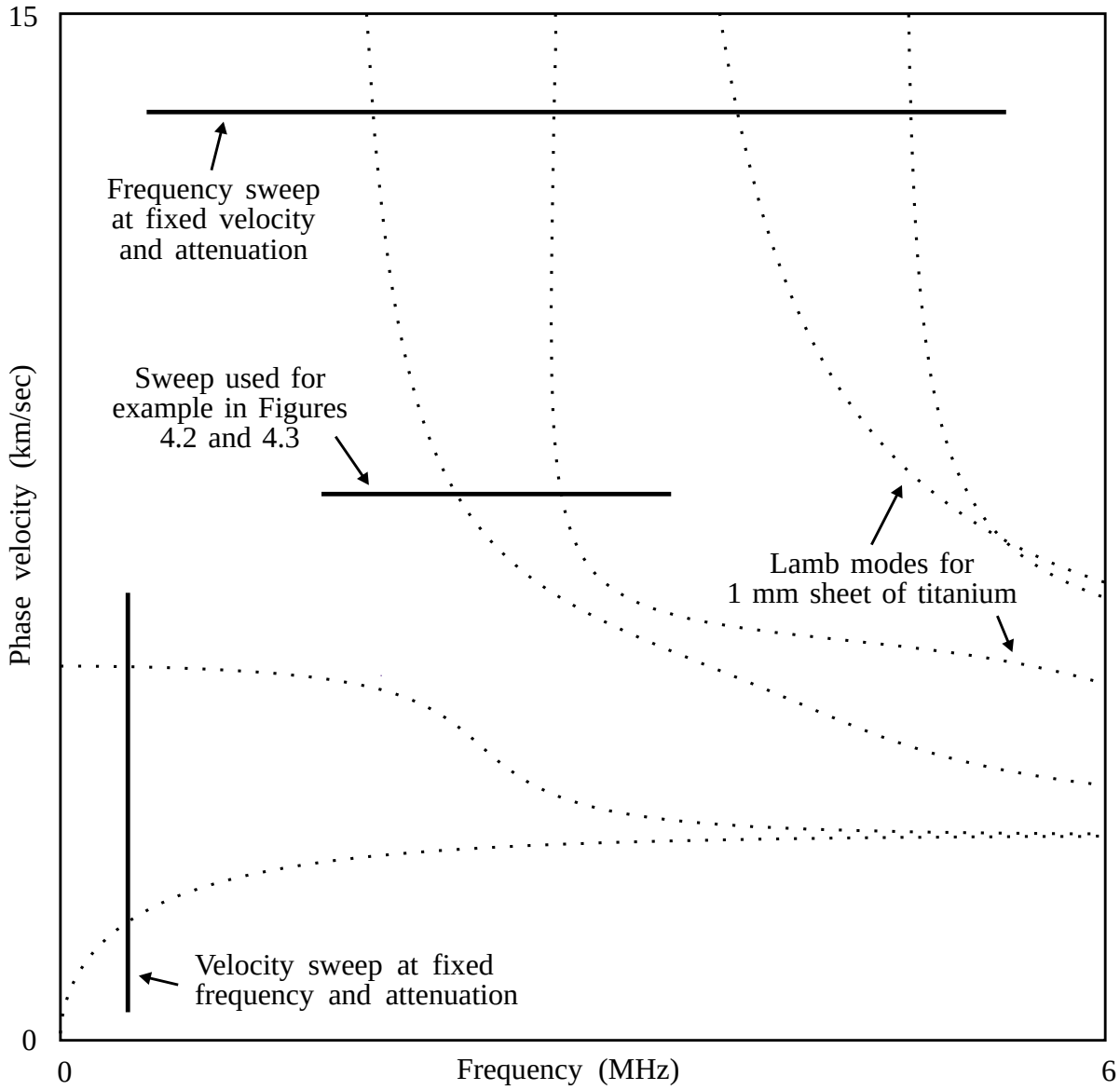

Figure 4.1 Coarse searches for location of modes

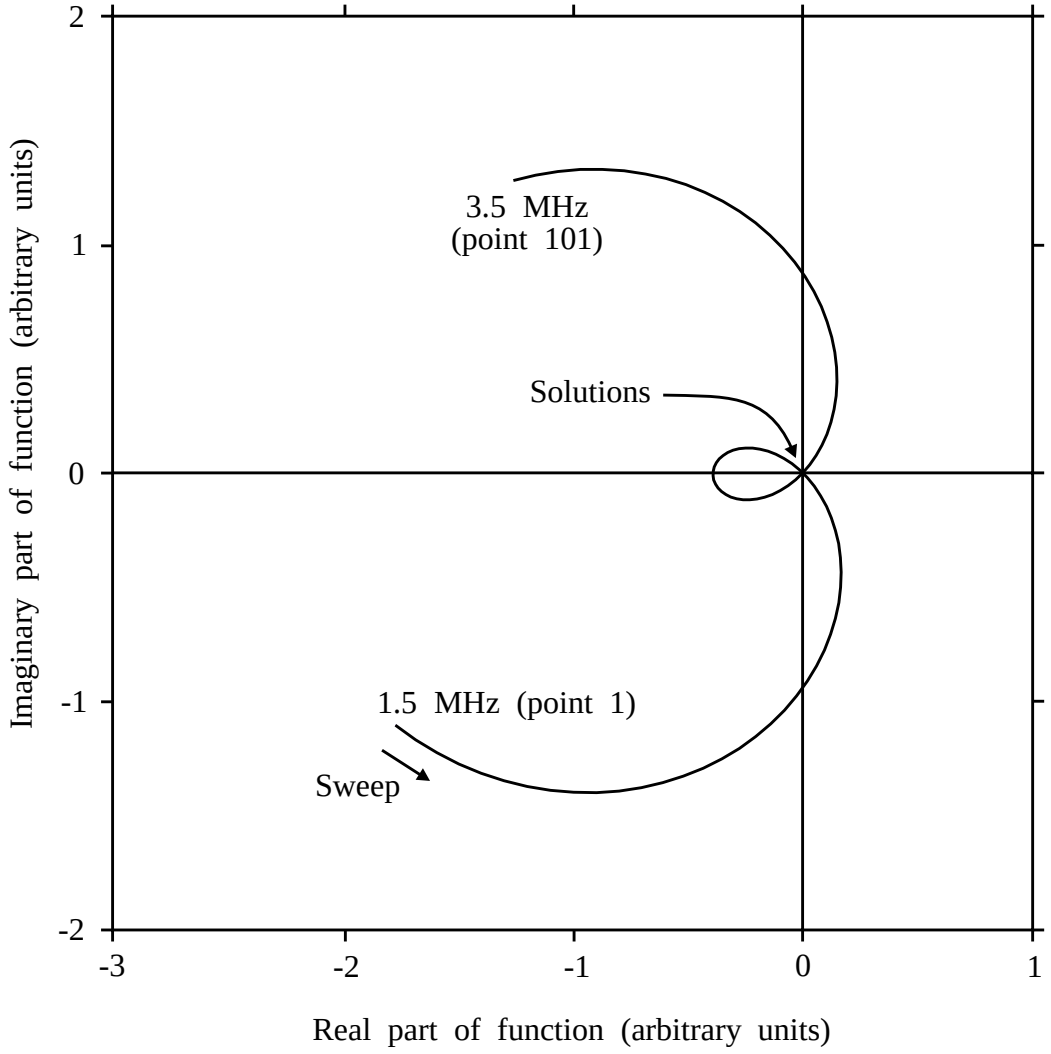

1 mm sheet of titanium in vacuum.
Frequency sweep from 1.5 MHz to 3.5 MHz in increments of 20 kHz.
Velocity 8 km/sec, attenuation 0.

Figure 4.2 Complex evaluations of characteristic function for free waves

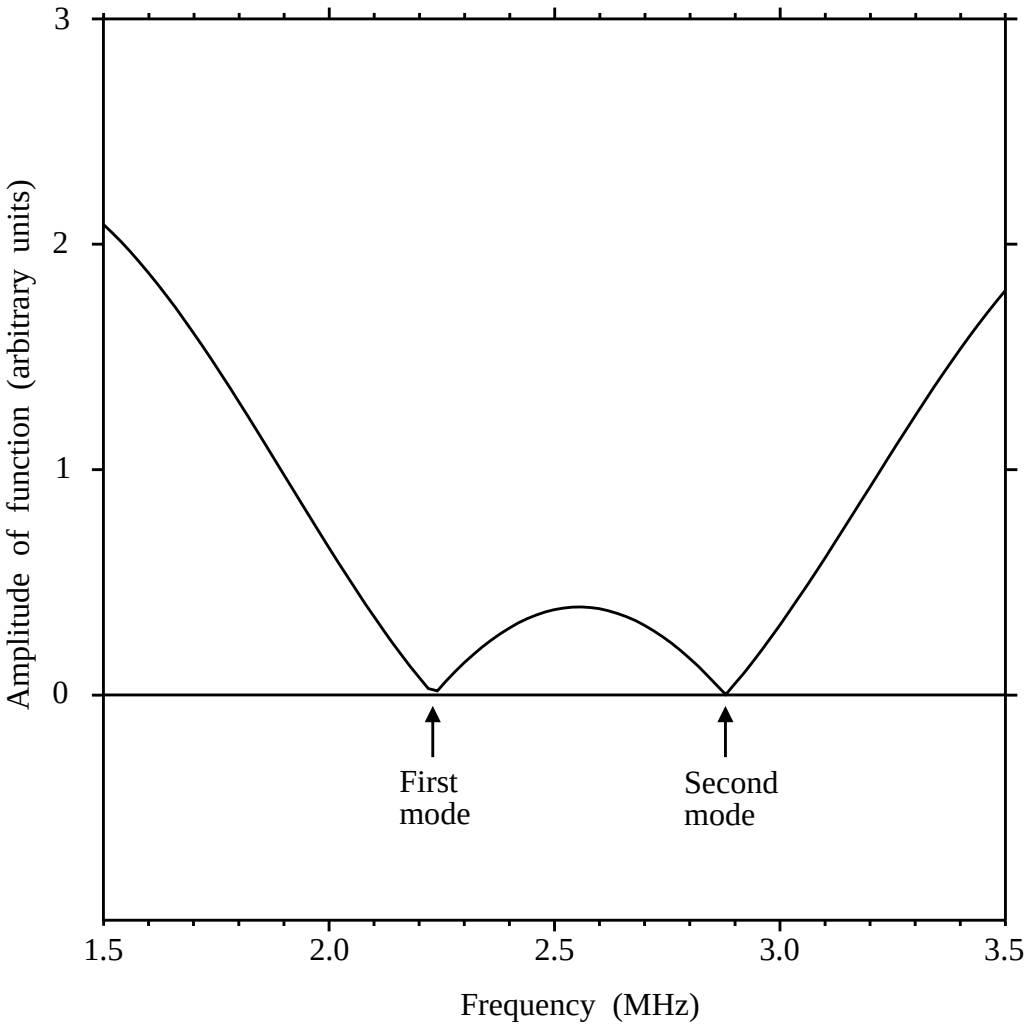

1 mm sheet of titanium in vacuum.
Frequency sweep from 1.5 MHz to 3.5 MHz in increments of 20 kHz.
Velocity 8 km/sec, attenuation 0.

Figure 4.3 Amplitude of evaluations of characteristic function for free waves

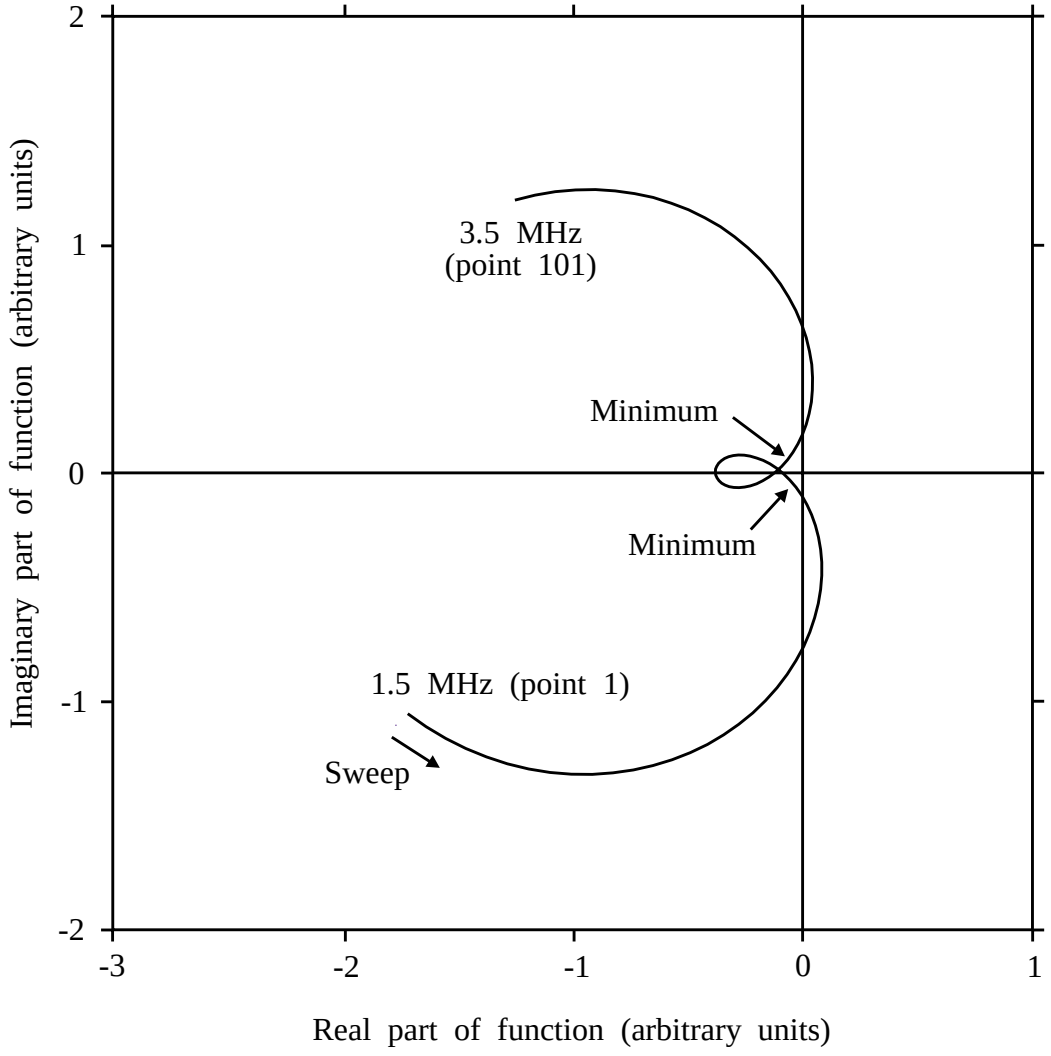

1 mm sheet of titanium in water.
Frequency sweep from 1.5 MHz to 3.5 MHz in increments of 20 kHz.
Velocity 8 km/sec, attenuation 0.

Figure 4.4 Complex evaluations of characteristic function for attenuating waves

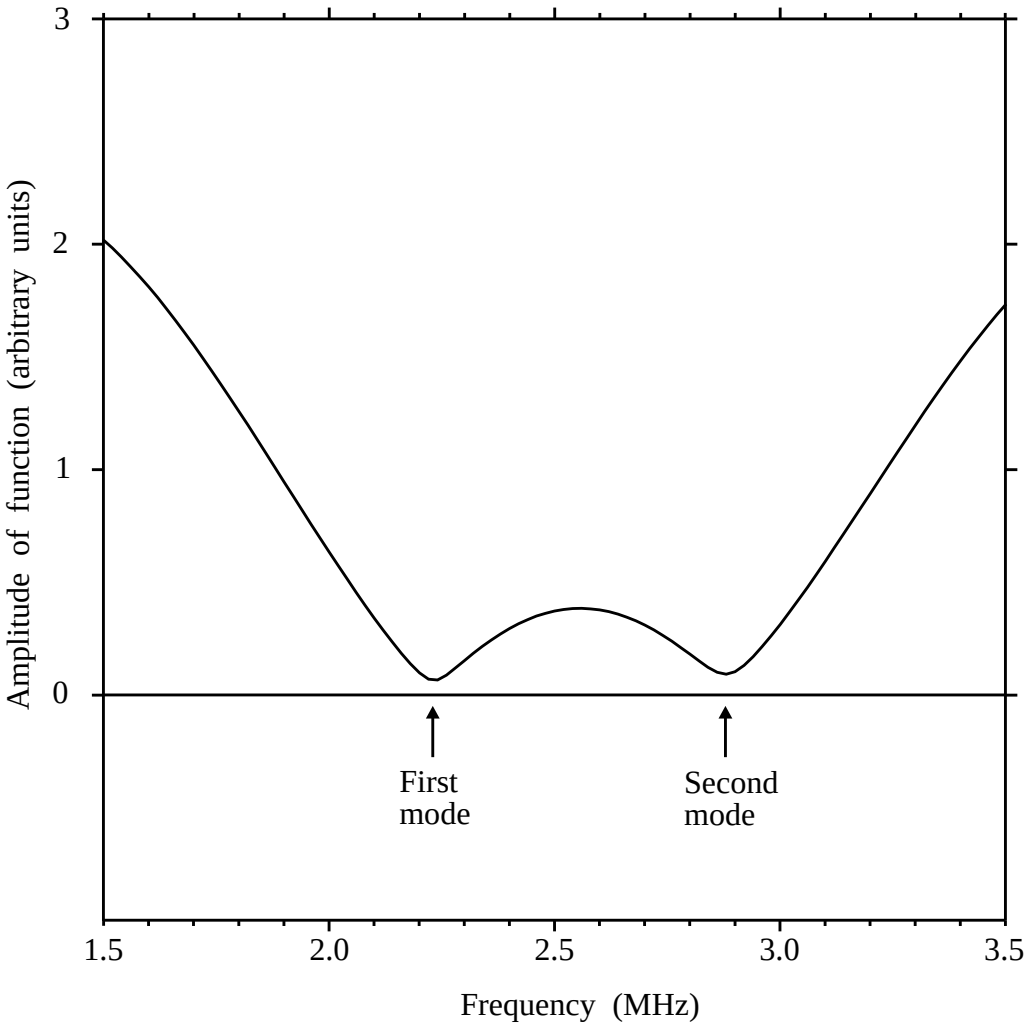

1 mm sheet of titanium in water.
Frequency sweep from 1.5 MHz to 3.5 MHz in increments of 20 kHz.
Velocity 8 km/sec, attenuation 0.

Figure 4.5 Amplitude of evaluations of characteristic function for attenuating waves

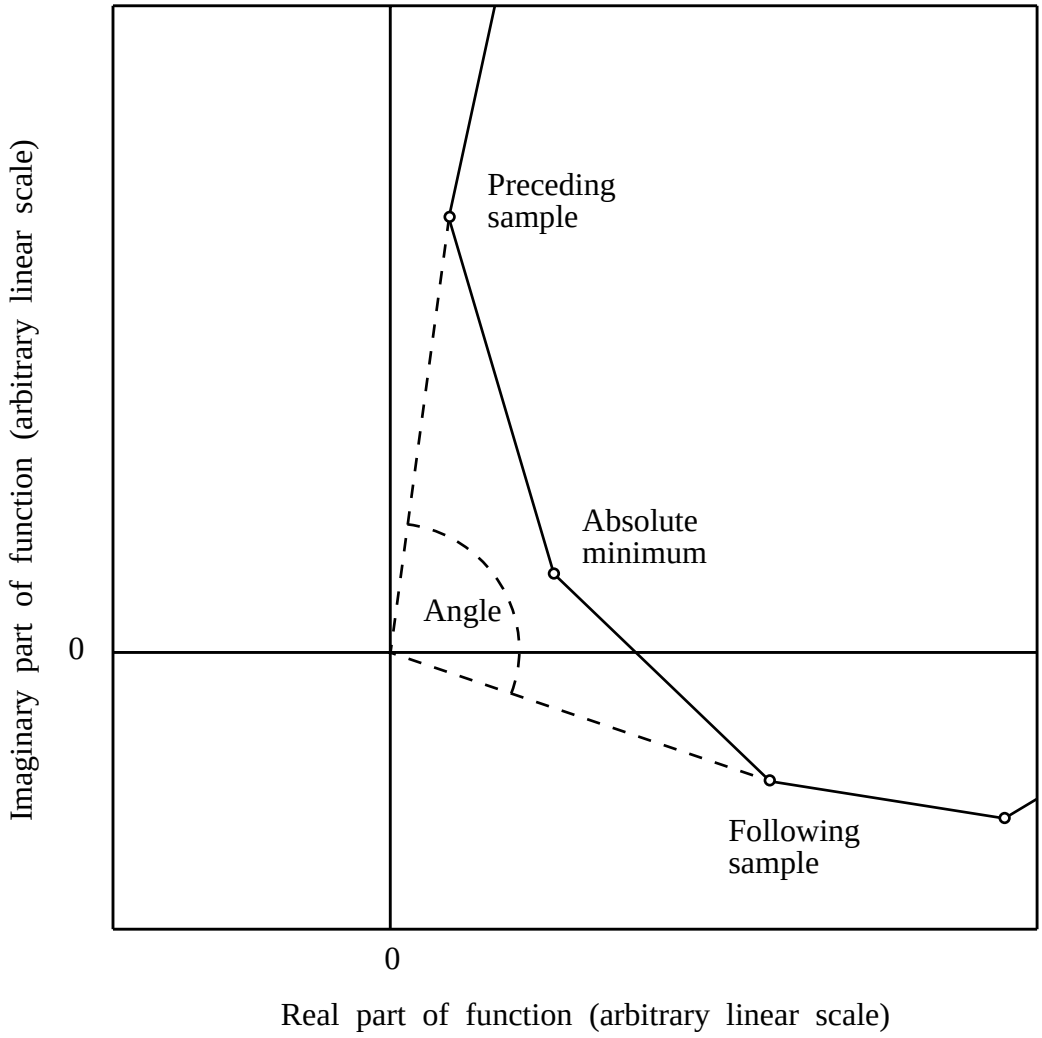

Figure 4.6 Angle used to check for convergence of fine search

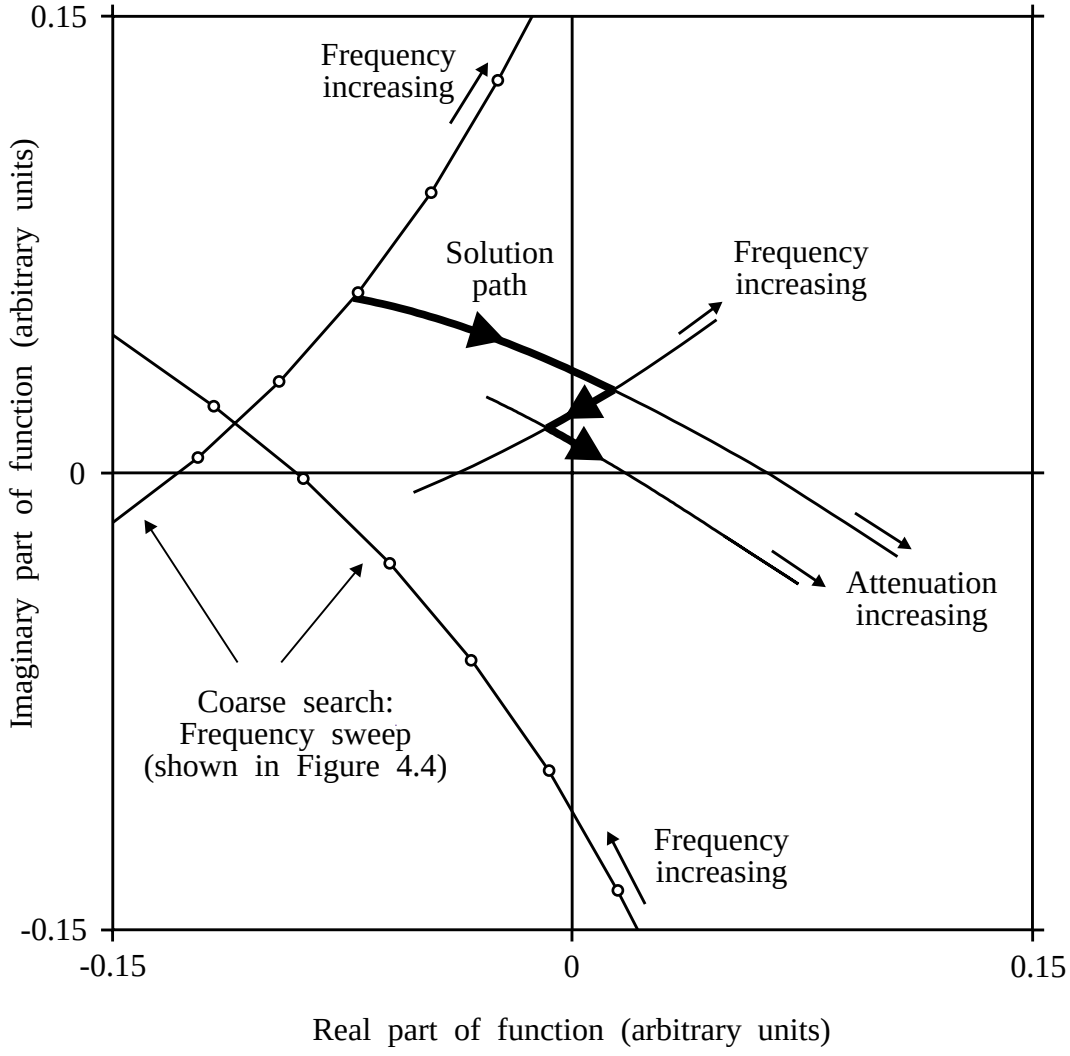

Figure 4.7 Progression of solution for attenuating wave

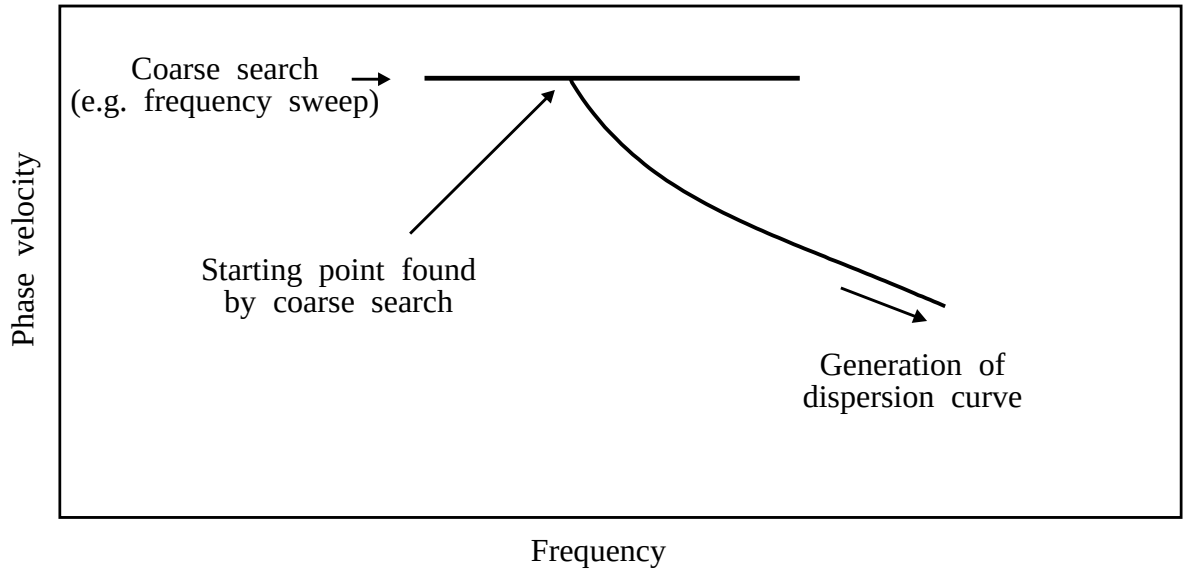

(a) Procedure for generation of curve

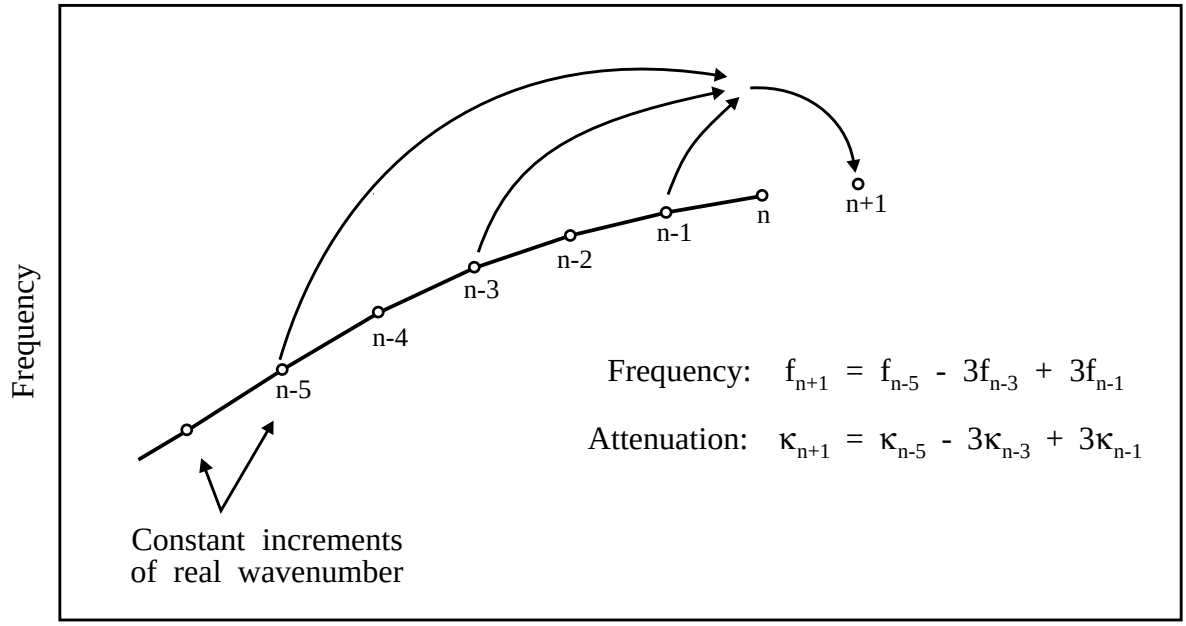

(b) Extrapolation scheme

Figure 4.8 Generation of dispersion curve

CHAPTER 5

Validation of model

5.1 Introduction

The purpose of this chapter is to demonstrate that the model which was developed in Chapters 2 to 4 is a suitable tool for the modal analysis of a wide range of plate systems and waves and that it is capable of making accurate predictions of dispersion curves and mode shapes.

Large numbers of modal solutions have been calculated with the dispersion curve model, initially to confirm its accuracy and subsequently in the course of research. A few examples of its application are described in Section 5.2. They have been selected to show the versatility of the model, covering a range of plate systems and wave types, including the well known cases of Rayleigh, Stoneley and Lamb waves, and both free and attenuating solutions. The different forms of plotting dispersion curves are demonstrated and illustrations are given of displacement and stress mode shapes.

Section 5.3 is devoted to the verification of the model by comparison with analytical solutions. There are known analytical solutions for particular cases of the simpler plate systems and these can be used to check the accuracy of the model to a high degree of precision at specific locations in the solution space.

In Section 5.4 some predictions which were made using the model are compared with measurements and with predictions made by other models. These include measurements of surface waves made by the author, published measurements and predictions of Sezawa waves and predictions of near-field reflections when waves are being excited, made using a response model.

The material properties for all of the examples are given in Table 5.1.

5.2 Examples of applications of the model

Rayleigh wave on titanium half-space

Figure 5.1(a) shows the mode shapes for a Rayleigh wave in titanium. The geometry required for a Rayleigh wave is a semi-infinite half-space of the solid, adjacent to vacuum, as illustrated in the inset diagram in the figure. The energy of the wave is retained close to the surface and in an elastic material it does not attenuate. The Rayleigh wave velocity was calculated by the model to be 2996.342 m/sec (independent of frequency). The modes were plotted for a frequency of 10 MHz and so the wavelength in this case was about 0.3 mm. Thus it can be seen that the depth in the plate in which the stresses and displacements are significant is approximately two wavelengths. This is the case for all frequencies because the wavelength and the depth axis of the mode shapes both scale inversely with frequency. It can also be seen that the stress normal to the surface and the shear stress are zero at the surface, as required by definition for a free surface, but that they build up sharply just below the surface. The third stress component, that parallel to the surface, is not constrained by the boundary conditions at the surface and indeed it peaks at this location.

If the half-space of vacuum next to the titanium is replaced by a half-space of water then the Rayleigh wave becomes a leaky Rayleigh wave. Its speed is faster than the speed of bulk longitudinal waves in water and so it leaks a homogeneous longitudinal wave into the water. It therefore attenuates as it travels. The velocity of the leaky Rayleigh wave in titanium was calculated by the model to be 3001.051 m/sec, some 5 m/sec faster than the free Rayleigh wave. Its attenuation is 0.114 Nepers/wavelength for all frequencies. Its attenuation per unit distance is therefore linearly proportional to the frequency, exactly as with viscoelastic bulk waves. In the example discussed here the frequency is 10 MHz and so the attenuation is 0.381 Nepers/mm and the wave loses 32 % of its energy per mm travelled.

The mode shapes for leaky Rayleigh waves are almost identical to those for free Rayleigh waves, with the exception of the normal stress close to the surface. Figure 5.1(b) shows a detailed plot of the stresses for both waves very close to the surface, the depth scale being magnified by 20 compared to the previous figure. The solid lines are for the free wave and the dashed lines for the leaky wave. It can be seen that the normal stress is not zero at the surface for the leaky wave; the small value of stress here is associated with the transfer of energy from the titanium into the water. There is no shear

stress at the surface because the water is assumed to have no shear stiffness. (Actually the water is given a very small shear stiffness, implied by the very small shear velocity in Table 5.1. This is a convenience to avoid a singularity in the solution; it has no significant effect on the results.)

If the half-space next to the titanium is vacuum but the material has viscoelastic damping properties then again the wave attenuates as it travels. If the attenuation per wavelength for bulk longitudinal waves is the same as that for bulk shear waves then it is evident from the formulation that the Rayleigh wave must also have this value of attenuation. Furthermore the velocity of the attenuating Rayleigh wave in this case is identical to that of the free wave. If the attenuations of the two bulk waves are different then the attenuation of the Rayleigh wave is dominated by the value of attenuation of the shear bulk wave because Rayleigh waves consist mainly of shear wave components. For example if the attenuations of the bulk longitudinal and bulk shear waves are 0.01 and 0.02 Nepers/wavelength respectively, then the attenuation of the Rayleigh wave in titanium is 0.019 Nepers/wavelength. In general the attenuation of any non-leaking plate wave in viscoelastic material lies somewhere between the maximum and minimum values of the attenuations of bulk waves in the layers.

Stoneley wave at the interface between titanium and steel

The second example is the next simplest case of plate wave propagation, the Stoneley wave. A Stoneley wave, by original definition (Stoneley (1924)), is a free wave which can propagate along the interface between two solids. The energy of the wave is retained close to the interface in both media and it does not attenuate as it travels. In fact Stoneley waves can only exist between certain pairs of materials, as observed by Stoneley (1924) and defined rigorously by Scholte (1946). A general condition for their existence is that the shear velocities of the two materials must be very similar and in some cases must be identical. The Stoneley wave travels at a velocity slightly lower than the bulk shear velocity(ies).

Figure 5.2 shows the mode shapes for a Stoneley wave at the interface between steel and titanium. These materials have similar bulk shear velocities; for convenience they were given identical shear velocities in the calculation (Table 5.1) so that it was possible to find a free solution. The wave was found to have a velocity of 3221.329 m/s, slightly lower than the bulk shear velocity, as expected. The displacements and stresses can be seen to decay as the distance from the interface is increased, as was observed with the Rayleigh wave. None of the components is zero at the interface but it can be seen that

the requirement for the two displacement components and the normal and shear stresses to be continuous across the interface has been satisfied. The third stress component, the stress parallel to the surface, is unconstrained at the interface and a step change can be observed here.

If the conditions for Stoneley waves are not satisfied then a free wave solution can not be found. However in many cases attenuating solutions can be found. These are for leaky Stoneley waves, in which the velocity of the interface wave is higher than one or both of the bulk shear velocities. In these cases energy leaks into the half-spaces and the waves attenuate as they travel. A theoretical examination of leaky Stoneley waves is given by Pilant (1972).

Lamb waves in titanium sheet

If a second interface is added to the system and the simplest case is taken, of vacuum half-spaces, then the geometry is appropriate for the propagation of Lamb waves. Lamb waves are free waves which travel indefinitely in elastic plates in vacuum. From a practical engineering point of view there is no difference between the solutions for Lamb waves for a metal plate in air and those for a plate in vacuum because the acoustic impedance of air is negligible in comparison with that of the plate. For the same reason the Lamb waves are also good approximations in most cases when the half-spaces are water. As an example of Lamb waves, the modes for a 1.0 mm thick titanium sheet have been calculated and are shown in Figures 5.3 to 5.5 and 5.7.

Figure 5.3 shows the phase velocity dispersion curves for the full set of Lamb modes for frequencies up to 10 MHz and phase velocities up to 10 km/sec.

The two modes which can exist at very low frequencies, labelled a_0 and s_0 as is the convention for Lamb waves, are those which were introduced in Chapter 1 and were illustrated in Figure 1.5. Figure 1.5 also showed the shapes of the waves at the low frequency limit from which it could be seen that s_0 is an 'extensional' mode and a_0 is a 'bending' mode. At the low frequency limit s_0 is often called the 'Young' wave, its velocity being determined simply from Young's modulus and the plane stress boundary conditions in the plane of the plate (plane strain still applies in the section through the plate, as discussed in Section 2.3 of Chapter 2). At all frequencies the deformations and stresses of s_0 are entirely symmetric with respect to the centre line of the plate and those of a_0 are entirely antisymmetric. Their respective labels 's' and 'a' refer to these properties and the subscript '0' indicates that they are the first modes in series of

symmetric and antisymmetric modes. In fact all Lamb modes are either perfectly symmetric or perfectly antisymmetric throughout their frequency ranges.

Both a_0 and s_0 can be seen to be dispersive, that is to say their velocities vary with frequency, and as the frequency is increased they converge on each other. At the high frequency end of the plot, a_0 and s_0 appear to have the same phase velocity but still exist as separate modes. They only converge to the same phase velocity at infinity, when they are both asymptotic to the Rayleigh wave solution. As the frequency is increased the ratio of the wavelength to the plate thickness decreases. The deformation is also increasingly confined to the material adjacent to the top and bottom surfaces of the plate. Thus at very high frequencies two identical Rayleigh-like waves travel along the top and bottom surfaces of the plate, as was shown for the top surface in the inset diagram in Figure 1.5. Both Rayleigh-like waves share the same phase for the s_0 solution (symmetric) and are in opposite phase for the a_0 solution (antisymmetric).

The other modes in Figure 5.3 are the higher order symmetric modes (s_1, s_2, s_3,....) and antisymmetric modes (a_1, a_2, a_3,....). These are the first few modes of two infinite sets of symmetric and antisymmetric modes. Modes continue to be introduced to the diagram as the frequency range is increased, to infinity. All of these modes extend upwards in the plot to infinite phase velocity. Note that this is physically possible because energy is not transported at the phase velocity but at the group velocity, as will be discussed shortly. At the high frequency limit all of these modes converge on the bulk shear velocity of the plate material.

Figure 5.4 shows the real wavenumber dispersion curves for the same modes. This plot describes the spatial distribution of the waves, the number of wavelengths per unit distance along the plate. In fact the imaginary part of the wavenumber is zero in all of these cases because there is no attenuation of the modes. Here it can be seen that for the most part the wavenumber varies very smoothly with the frequency and that any curve can be described over its full length by steadily increasing or steadily decreasing the wavenumber, without change of sign. It is for these reasons that it was decided in Chapter 4 to generate the dispersion curves by incrementing the real wavenumber.

Figure 5.5 shows the group velocity dispersion curves. When a narrow band signal is used to excite a dispersive plate wave then a 'packet' or 'envelope' of waves is observed to travel along the plate. Although the phase velocity measured at any frequency complies with the phase velocity dispersion curves, the wave packet itself may not travel along the plate at the same velocity. It can be shown (Brekhovskikh and Goncharov (1985) for

example) that the velocity of the packet is the velocity at which the energy is propagated along the plate. This velocity is called the group velocity and it may be calculated directly from the gradient of the wavenumber dispersion curves by equation (4.5). If the mode is not dispersive then the group velocity is equal to the phase velocity.

The group velocity dispersion curves provide useful information for understanding the long range propagation of waves. If a narrow band packet of waves is propagated under conditions where the group velocity varies with frequency then there is a tendency for the wave packet to spread as it travels along the plate. Much larger propagation distances can be achieved if the wave packet is chosen such that the group velocity is steady (i.e. a maximum or a minimum on the group velocity dispersion curve), when the packet retains its shape. The long range propagation of Lamb waves is discussed by Alleyne (1991).

It is interesting to note in Figure 5.5 that mode s_1 has negative group velocity at its lowest frequencies. This implies that the energy of a narrow band packet of s_1 waves travels in the opposite direction to the phase velocity. This strange behaviour of s_1 has received some attention from other researchers. For example, Wolf, Ngoc, Kille and Mayer (1988) predicted and measured negative group velocity for the s_1 mode in a brass plate over a short frequency range. Furthermore, close examination of the data of Figure 5.5 reveals that mode a_2 also has negative group velocity over a very small range of frequencies. In the plot this can only be seen as a slight extension of the end of the curve below the axis but when expanded this region of the curve has the same shape as that for mode s_1.

The excitation of Lamb waves is often achieved by using water as a coupling medium and positioning a transducer at an angle to the plate, according to the coincidence principle. The coincidence principle, illustrated in Figure 5.6, states that an incident wave in a coupling medium may be used to excite a plate wave if the component of its wavenumber in the direction along the plate matches the wavenumber of the plate wave. By the same analysis, a transducer positioned to receive a leaking signal from the plate would be set at the same angle from the normal. This means that waves with high phase velocities are excited and received using transducers at small angles of incidence and waves with low phase velocities, using transducers at large angles. Clearly it is not possible to excite waves with velocities lower than the bulk velocity in the coupling medium. The application of the coincidence principle to the measurement of Lamb waves will be discussed further in Chapter 8.

Figure 5.7 shows the dispersion curves for the titanium plate in terms of the angle of incidence of a longitudinal wave in water. The vertical axis therefore shows the angle at which the transducer should be set in order to excite the modes. Now the significance of infinite phase velocity can be seen. Infinite phase velocity corresponds to zero angle of incidence. In the infinite phase velocity limit, the Lamb modes cease to propagate and become through-thickness vibration modes in the plate (standing wave solutions). All of the vibration modes consist of multiple half-wavelengths of either longitudinal bulk waves or shear bulk waves. The shear modes (a_1, s_2, a_2, s_3 and a_4) and the longitudinal modes (s_1, a_3 and s_4) are each symmetric for even numbers of half-wavelengths through the thickness and antisymmetric for odd numbers of half-wavelengths. Thus the shear modes and the longitudinal modes are each spaced at constant intervals along the horizontal axis in the figure at zero angle of incidence.

Strictly speaking the angle of incidence dispersion curves in Figure 5.7 are incorrect because the solution was obtained for a plate in vacuum whereas the calculation of the angle of incidence required at least one of the half-spaces adjacent to the plate to be water. However in practice dispersion curves for plates in vacuum may usually be used for plates which are immersed in water because the presence of the water has only a small influence on the velocities and wavenumbers of the modes. Furthermore, Lamb waves are sometimes excited and received using only local immersion at the locations of the transducers while the majority of the plate is in air, in which case it is perfectly appropriate to use these angle of incidence dispersion curves.

The phase velocity dispersion curves for a plate in water are shown in Figure 5.8. These curves were calculated for the same 1 mm thick titanium plate but with both half-spaces consisting of water instead of vacuum. The plate waves are now in general attenuative and are classed as leaky Lamb waves. Within the solution space which is plotted, the velocities of the modes are almost identical to those of the free Lamb modes, with two exceptions. The first is the break in the a_0 mode at low velocity and the second is the discontinuity of the s_1 mode at high velocity.

The velocity of the break in a_0 is the bulk velocity of longitudinal waves in water. For the region of the curve below this critical velocity, any waves in the water must be inhomogeneous. The low-velocity plate wave is therefore a free wave, with zero attenuation, guided between the two half-spaces of water. As the velocity increases this part of the mode becomes asymptotic to the bulk velocity of the water. In calculating the curve, the solution was terminated arbitrarily at about 1.5 MHz, at which frequency the value of the velocity was indistinguishable from that of the water. Above the critical

velocity the wave leaks homogeneous waves into the water and attenuates. It is interesting to note that there is some frequency overlap of the two parts of the mode. This behaviour of a_0 has been studied both theoretically and experimentally for steel plates by Osborne and Hart (1946 and 1947). They made the same observation about the nature of the curve.

The discontinuity in the s_1 mode occurs because there is a singularity in the solution for the attenuation of the wave. As discussed previously, the s_1 mode has negative group velocity where the curve has high phase velocity, but positive group velocity elsewhere. When calculating the modal solutions for leaky modes with negative group velocity, the model predicts a negative value of the attenuation. This is a perfectly reasonable result because the energy of the wave travels in the opposite direction to the phase. The singularity exists at the point where the group velocity is zero, when the wave is non-propagating and the attenuation is infinite. In generating the curve, the attenuation of the s_1 mode increases rapidly as the velocity approaches the critical value. In this case the mode was generated by constant decrements of wavenumber (i.e. from right to left in the figure) and the solution was stopped when the attenuation started to rise sharply. Mode a_2 also has a discontinuity but it is at a much higher velocity. In general most modes have high values of attenuation at high phase velocities and their calculation can be difficult.

The attenuations of the leaky Lamb waves are plotted in Figure 5.9, in Nepers/mm, plotted for the ranges of the dispersion curves which are shown in Figure 5.8. Here it can be seen that all modes other than the low velocity part of a_0 (which has zero attenuation and is not shown in Figure 5.9) are attenuative to some extent and that most modes have regions which are quite strongly attenuative. At 0.1 Nepers/mm a wave loses 10 % of its amplitude per mm travel and at 0.2 Nepers/mm, 18 %. The other notable feature is that the s_0 and a_0 modes both have strongly increasing attenuation with frequency and that above about 5 MHz they and the Rayleigh wave are generally more attenuative than the other modes. In the high frequency limit the a_0 and s_0 modes converge on a steady gradient of attenuation per mm or constant attenuation per wavelength, given by the leaky Rayleigh wave solution. The sharp gradient of the attenuation of s_1 at its low frequency end can also be seen in the figure.

Finally, note that the horizontal axis of all of the Lamb wave and leaky Lamb wave plots may be scaled linearly by the thickness. Thus for example the plotted velocity of a mode at 1 MHz for the 1 mm thick plate would be appropriate for a 2 mm thick plate at 0.5 MHz. Lamb wave dispersion curves are often plotted with the horizontal axis as the frequency-thickness product (MHz-mm).

Surface wave on thin epoxy layer on aluminium half-space

Figure 5.10 shows the phase velocity dispersion curve for a surface wave on a system consisting of a thin layer of epoxy adhesive on a half-space of aluminium, as illustrated in the inset diagram. Four different thicknesses of epoxy were modelled, from 50 microns to 400 microns.

It can be seen that the phase velocity of the surface wave is dispersive and is also extremely sensitive to the layer thickness. At very low frequency the depth of influence of the wave is large compared to the layer thickness and so the wave solution is dominated by the aluminium half-space properties. The low frequency limit therefore corresponds to the Rayleigh wave velocity in aluminium, as indicated by a dashed line in the figure. At very high frequency the depth of influence of the wave is small compared to the layer thickness and so the wave solution is dominated by the epoxy properties. The solution is therefore asymptotic to the Rayleigh wave velocity in epoxy as the frequency is increased, again indicated by a dashed line in the figure. The solution is free for all frequencies and thicknesses because the velocity is always lower than the bulk velocities in the aluminium and so it is not possible for energy to leak into the half-space.

Surface wave on thin layer of alpha case on titanium half-space

Figure 5.11(a) shows the phase velocity dispersion curve for a surface wave on a system consisting of a thin layer of alpha case on a half-space of titanium, as illustrated in the inset diagram. For the purpose of this example the alpha case material was assumed to be 10 % faster in both its longitudinal and shear velocities but to have the same density as titanium. The actual properties of alpha case will be discussed further in Chapter 6. The system is therefore qualitatively different to that of the epoxy layer on aluminium, the layer material properties being faster than the half-space. Three different thicknesses of alpha case were modelled, from 25 microns to 100 microns.

Again it can be seen that the phase velocity of the surface wave is dispersive and is also extremely sensitive to the layer thickness. At low frequency the wave solution is dominated by the titanium half-space properties and at high frequency, by the alpha case layer properties. The trend therefore is for the velocity to increase with frequency. The low frequency limit corresponds to the Rayleigh wave velocity in titanium and the high frequency limit to the Rayleigh wave velocity in alpha case, as indicated by the top and bottom dashed lines in the figure. The third dashed line shows the velocity of bulk shear

waves in the titanium, at which each curve shows a change in slope. The reason for this is that the mode is in two parts. Below this velocity the wave is free because no energy can leak into the half-space and above this velocity a shear wave leaks into the half-space. This threshold can be seen clearly in the plots of attenuation in Figure 5.11(b) where non-zero attenuation only exists for the high velocity regions of the modes.

5.3 Comparisons with analytical solutions

Rayleigh wave velocity

Solutions for the Rayleigh wave velocity may be calculated from Rayleigh's third order equation (Rayleigh (1887)) and may also be found in Timoshenko and Goodier (1970), for example. For Poisson's ratio of 0.25 the Rayleigh wave velocity is given by the latter authors to four decimal places to be 0.9194 times the shear bulk wave velocity. Velocities calculated by the model agree exactly with this expected figure when the appropriate value of Poisson's ratio is used. As an example the velocity of the Rayleigh wave for steel was calculated, using steel properties of Young's modulus of 200 GPa, Poisson's ratio of 0.25 and density of 8000 kg/m^3. The Rayleigh wave velocity was calculated to be 2907.403 m/sec, a factor of 0.919402 times the shear bulk wave velocity.

Stoneley wave velocity

Solutions for the Stoneley wave velocity may be calculated from his paper of 1924. The formulation is presented as a real characteristic function whose result must be zero for the solution to exist. The example discussed in the previous section, of a Stoneley wave at the interface between steel and titanium half-spaces, was checked with this function. The prediction, of a velocity of 3221.329 m/sec, was found to be correct to all three decimal places.

Lamb waves

The low frequency cut-off value of the Young wave (s_0) can be found from simple stiffness calculations on a small element. For very low frequencies the wavelength is very long compared with the plate thickness and the plate behaves in plane stress in its own plane. Of course it is still in plane strain in the plane defined by the wave propagation direction and the through-thickness direction. The stiffness (K) in the direction of wave propagation (the x direction, say) can therefore be calculated as:

$$\sigma_{xx} = K\,\varepsilon_{xx} = \frac{4\mu(\lambda+\mu)}{\lambda+2\mu}\,\varepsilon_{xx} = \frac{E}{1-\nu^2}\,\varepsilon_{xx} \qquad (5.1)$$

and the velocity of propagation is then given by:

$$c = \left(\frac{K}{\rho}\right)^{1/2} \qquad (5.2)$$

Again, velocities calculated by the model agree with this expected figure to three decimal places in m/sec. For example, the Young wave velocity in titanium was calculated by equation (5.2) to be 5465.891 m/sec. The same value was predicted by the dispersion curve program for low frequencies, of less than 1 kHz.

The cut-off frequencies of the higher order Lamb modes at normal incidence can be compared with the solutions for through-thickness vibration of the plate. These modes consist of multiples of half-wavelengths of shear or longitudinal bulk waves and so their frequencies can be shown (for example, see Pialucha, Guyott and Cawley, 1989) to be given by

$$\text{Frequency (Hz)} = \frac{nc}{2d} \qquad (5.3)$$

where n is the mode number (1,2,3....), c is the shear or longitudinal bulk wave velocity and d is the plate thickness. The model can not be used for perfectly normal incidence because the phase velocity is infinite. However predictions at a phase velocity of 1,000,000 km/sec showed perfect agreement with the solutions obtained using this equation.

Surface wave on thin layer

The low frequency and high frequency limits of the examples of the surface waves on thin layers can be checked by comparison with the Rayleigh velocities in the layers and half-spaces. The curves are considerably more dispersive than the Young mode discussed above and so it is necessary to calculate the low frequency values at much lower frequencies. It was found that calculations at 10 Hz were sufficient to demonstrate agreement in both cases. At the high frequency limit agreement was obtained in both cases by calculations at 100 MHz. The Rayleigh velocities in the four materials were calculated to be:

	Rayleigh wave Velocity (m/sec)
Epoxy	1035.184
Aluminium	2957.100
Alpha case	3295.976
Titanium	2996.342

Multiple identical layers

Finally, a useful verification is to compare the dispersion curves for a single plate with those for the same thickness of plate divided into two or more layers with identical properties, and to make sure that there are no differences. Reference to the theory of Chapters 2 and 3 shows that this is not a trivial case. Tests have been performed on two, three and four layer systems for free and leaky solutions and have shown perfect agreement.

5.4 Comparisons with measurements and other predictions

Measurements of surface waves

The results of two experiments are shown in Figure 5.12. Both involved measurements of the phase velocity of surface waves. The waves were excited and received by a pair of broadband plane-wave piezo-electric transducers with a 4 MHz centre frequency. The plates were immersed in water and the transducers were set at the appropriate angle for the excitation of the waves according to the coincidence principle, as was illustrated in Figure 5.6. Pulse excitation was employed and two signals were captured by the receiver for each measurement, one a known distance downstream from the other. The phase velocities over the range of frequencies of the broadband received signal were calculated using the amplitude spectrum method (Pialucha, Guyott and Cawley (1989)).

In the first case a leaky Rayleigh wave was excited on the surface of a 13.0 mm thick aluminium plate. The measured velocities are shown as discrete points in Figure 5.12(a). The maximum frequency at which measurements were obtained was about 4 MHz because of attenuation of the wave at high frequencies. Also shown in the plot, as a continuous horizontal line, is the solution predicted by the model. The prediction was made using elastic properties of the aluminium which were determined by measuring the

through-thickness times-of-flight of ultrasonic pulses. A plane wave transducer was used to measure the bulk longitudinal velocity and a shear wave transducer to measure the bulk shear velocity. The measurements are consistently lower than the predicted velocity, perhaps due to an overestimate of the bulk velocities. The shear velocity in particular is rather difficult to measure accurately. However the difference is less than 10 m/sec so agreement has been achieved to an accuracy of better than 0.3 %.

Note that the measurements should be expected to differ from the Rayleigh wave calculations at very low frequencies because separate s_0 and a_0 Lamb waves should be excited rather than Rayleigh waves. Examination of Figure 5.3 indicates that the lowest frequency-thickness product at which these two waves are indistinguishable from each other and from the Rayleigh wave is about 8 MHz-mm for titanium. The same is found to be true for aluminium. Therefore any surface wave measurements made above about 0.6 MHz in the 13.0 mm plate should be representative of Rayleigh waves. The lowest frequency of measurement was 0.8 MHz.

In the second case a thin layer of epoxy adhesive was cast onto the surface of a 13.0 mm thick aluminium plate. Spacers were used to hold a glass sheet on top of the epoxy with a separation distance from the aluminium of 0.2 mm so that the epoxy cured as a consistent 0.2 mm thick layer. The glass sheet was coated with release agent so that it could be removed easily after the curing. A separate specimen of epoxy was cast at the same time so that its bulk wave velocities and density could be measured.

The measurements are shown in Figure 5.12(b) with the model prediction. Measurements were only taken up to 2.7 MHz because of the strong attenuation of the waves and the practical difficulty of making measurements when the transducers are at large angles of incidence. As the frequency is increased the phase velocity of the surface wave decreases and the transducer angle required to excite it increases. At angles greater than about 40 degrees it was found that the excitation and reception were weak and prone to cross-talk between the transducers. However the results show good agreement with the predictions, the accuracy achieved being similar to that obtained in the Rayleigh wave measurements.

Lamb waves

A number of careful comparisons was made between the predictions of the model and the predictions of Lamb wave solutions made by a model developed by Alleyne (1991). Alleyne's model has the advantage that its formulation is completely different from the

model presented here. This is because it is restricted in its applicability to single layer plates in vacuum and accordingly it calculates the Lamb wave solutions directly from Lamb's equations (see Lamb (1917) or Viktorov (1970)).

Comparisons were made between the phase velocities, group velocities and wavenumbers at arbitrary locations on the dispersion curves. Comparisons were also made between displacement mode shapes at a number of discrete locations. Perfect agreement was found in all cases.

Sezawa waves

Figure 5.13 shows predictions of dispersion curves for Sezawa and leaky Sezawa waves in a system consisting of a layer of gold on a half-space of fused quartz. The properties of the system were chosen to match a theoretical and experimental analysis which was performed by Kushibiki, Ishikawa and Chubachi (1990). Following the sources of their analysis, the acoustic properties of the gold were taken from Anderson (1965) and those of the fused quartz from Mason (1958). Two cases were considered, one in which the system was assumed to be in vacuum and the other in which it was immersed in water. The geometry of the systems is shown in inset diagrams in the figure.

The Sezawa wave is a free surface wave which can propagate in a system consisting of a solid elastic layer on a solid elastic half-space. A general theoretical analysis may be found in Tolstoy and Usdin (1953). In the case considered here the Sezawa wave strictly exists only in the system in vacuum and only at high frequencies. Under all other conditions the wave leaks energy from the layer and is a leaky or 'pseudo' Sezawa wave.

Consider first the system in vacuum. The phase velocity of the wave, shown as a solid line in Figure 5.13(a), decreases steadily with frequency throughout the range of the solution. At zero frequency it is equal to that of the bulk longitudinal wave in the quartz half-space and at the high frequency limit it tends to the bulk shear wave velocity in the layer. At low frequencies its velocity is higher than the bulk velocity in the quartz and it leaks a bulk shear wave into the half-space. This leaky region is characterised by non-zero attenuation, shown in Figure 5.13(b). In the higher frequency region the wave is non-attenuating.

The phase velocity curve for the system in water, shown as a dashed line in the figure, differs only slightly from that for the system in vacuum. However there is a marked increase in the attenuation because the wave additionally leaks a longitudinal bulk wave

into the water throughout the frequency range. The sharp drop in attenuation at about 120 MHz corresponds again to the threshold when the wave stops leaking energy into the half-space.

Kushibiki *et al.* (1990) performed measurements and predictions of the velocities and attenuations of the immersed system over a range of frequencies, including both regions of the solution. Their measurements agreed very closely with their predictions. The predictions presented in the figures here also matched their published graphs.

Incidentally, another mode was also found for this system during the calculations which is qualitatively similar to the surface wave which was predicted for the epoxy layer on aluminium. It lies below the Sezawa wave on the phase velocity dispersion curve diagram. Its phase velocity is equal to the Rayleigh velocity in quartz at zero frequency and drops to the Rayleigh velocity in gold at high frequency.

Near-field model predictions of Rayleigh and Lamb waves

The final comparison to be presented here is between some modal predictions of leaky waves made using the dispersion curve model and predictions of the near-field responses when the waves are excited by a plane wave transducer, made by a response model. Two cases are considered, one of a leaky Rayleigh wave and the other of a leaky s_0 Lamb wave. The cases are intended to demonstrate the accuracy of the calculation of attenuation of leaky modes.

The response predictions were made using a model which was developed by T. Pialucha (1992). The model calculates reflection and transmission from multilayered plates consisting of any number of layers of arbitrary thickness with arbitrary elastic or viscoelastic properties. The calculations are made in the frequency domain so that reflection and transmission coefficients can be studied as a function of frequency. Infinite plane waves are assumed and any angle of incidence is permitted. However the model can incorporate the spatial behaviour of a realistic finite sized transducer by performing a Fourier decomposition of the finite field in front of the transducer into infinite plane wave components, solving separately for each of the plane waves, and summing the results. Furthermore, an inverse Fourier transform may be applied to the frequency domain solutions, yielding predictions of the time domain signal which would be seen on an oscilloscope.

In the study which is presented here the model was used to predict the frequency domain solution for the reflected field when a plate is excited at a single frequency by a finite transducer. The solution for the reflected field is therefore the summation of a set of frequency domain solutions for plane waves. The simulation is illustrated in Figure 5.14(a).

A 5 mm diameter unfocused transducer was modelled for all of the predictions. A Gaussian variation was assumed for the amplitude of the field in front of the transducer, as illustrated in Figure 5.14(a) and plotted in Figure 5.14(b). The field was decomposed into 1024 infinite plane waves for the solution. Following the solution, the reflected plane waves were summed along a line normal to the reflected beam, as illustrated in Figure 5.14(a). Thus the predictions which were made were of the reflected field in the region of the point reflection from the surface of the plate.

In general a specular reflection may be expected from the plate. However, if the angle of incidence of the transducer and the frequency are appropriate for the excitation of a plate wave then the reflection changes. The point reflection along the axis of the beam is modified, and more significantly, a signal is received downstream of the beam due to leakage of energy from the plate wave. The leaking signal on the downstream side of the received field is illustrated in Figure 5.14(a).

In the first case a leaky Rayleigh wave was modelled on a half-space of titanium in water. A transducer frequency of 50 MHz was assumed and the transducer was simulated at the appropriate angle of incidence (29.6 degrees) for the excitation of the wave. The reflected field is shown (on a linear scale) in Figure 5.15(a) from which it can be seen that the reflection is not specular but is weighted on the downstream side of the centre line of the beam. The calculations were then repeated for three other cases with different values of the density of the water in order to observe different rates of leakage of the wave. The reflected fields are plotted in Figures 5.15(b) to 5.15(d) in decreasing order of water density. Now the leakage from the waves can be seen clearly on the downstream sides of the fields and it is evident that the rate of attenuation of the leaking waves decreases as the density is decreased.

The fields of Figure 5.15 have been re-plotted in Figure 5.16 using a natural logarithm scale for the amplitude. The variations of the amplitudes on the downstream sides of the fields are extremely linear on this scale, indicating that the amplitudes decay exponentially with distance. The average rate of decay of each field was calculated from the results and is shown in the Figure in Nepers/mm.

Modal solutions were calculated for these four leaky Rayleigh wave cases and the attenuations were compared with the decays of the leaking fields. In order to make the correct comparisons, the decays of the fields, which are normal to the reflected beam direction, were projected onto the plane of the plate by multiplication by the cosine of the angle of incidence. The comparisons showed excellent agreement, as follows:

	Normal water	Light water: 1/2 density	Light water: 1/10 density	Light water: 1/50 density
Rayleigh velocity (m/s)	3000.9	2997.5	2996.4	2996.3
Angle of incidence (deg)	29.616	29.653	29.665	29.666
Attenuation calculated by modal model (Nepers/mm)	1.907	0.955	0.191	0.0382
Attenuation calculated from field (Nepers/mm)	1.900	0.951	0.191	0.0382

Finally, a similar comparison was made between the predicted near-field response and the modal solution for a leaky s_0 Lamb wave in a 100 micron thick plate. A strongly dispersive location on the leaky Lamb wave dispersion curve was selected, where the attenuation is high, as shown in the two plots in Figure 5.17. The selected phase velocity was 4500 m/sec corresponding to an angle of incidence of 19.242 degrees. The modal model predicted a frequency of 23.172 MHz and attenuation of 0.170 Nepers/mm. The field predictions are shown on linear and log scales in Figure 5.18 from which the attenuation normal to the reflected beam was calculated to be 0.180 Nepers/mm. When projected onto the plane of the plate the attenuation was found to agree exactly with the modal solution.

5.5 Conclusions

A number of modal solutions has been presented in this Chapter in order to demonstrate the validity and accuracy of the dispersion curve model.

Predictions of Rayleigh waves, Stoneley waves and Lamb waves have shown that the model is capable of reproducing the familiar published solutions. The versatility of the program in its capabilities of plotting different forms of dispersion curves and mode shapes has also been demonstrated. Additionally, predictions for more advanced cases of leaky waves and multiple layers have demonstrated that the program has the capacity for the general purpose modelling of all classes of plane strain plate waves and is therefore a suitable tool for the research which is to be conducted on waves in interface layers.

A number of numerical comparisons with analytical solutions have been performed and have shown in all cases that the model predicts the modal solutions with an extremely high degree of accuracy. Predictions made using the model have also been shown to agree with measurements, with published solutions and with predictions made with two other models.

Material	Longitudinal velocity (m/s)	Shear velocity (m/s)	Density (kg/m^3)
Titanium	6060	3230	4460
Alpha case	6666	3553	4460
Steel	5960	3230	7930
Aluminium	6370	3170	2700
Epoxy	2610	1100	1170
Gold	3217	1195	19488
Fused quartz	5968	3764	2197
Water	1483	0.01	1000

All materials assumed to be perfectly elastic.

Table 5.1 Material properties used in the validation calculations

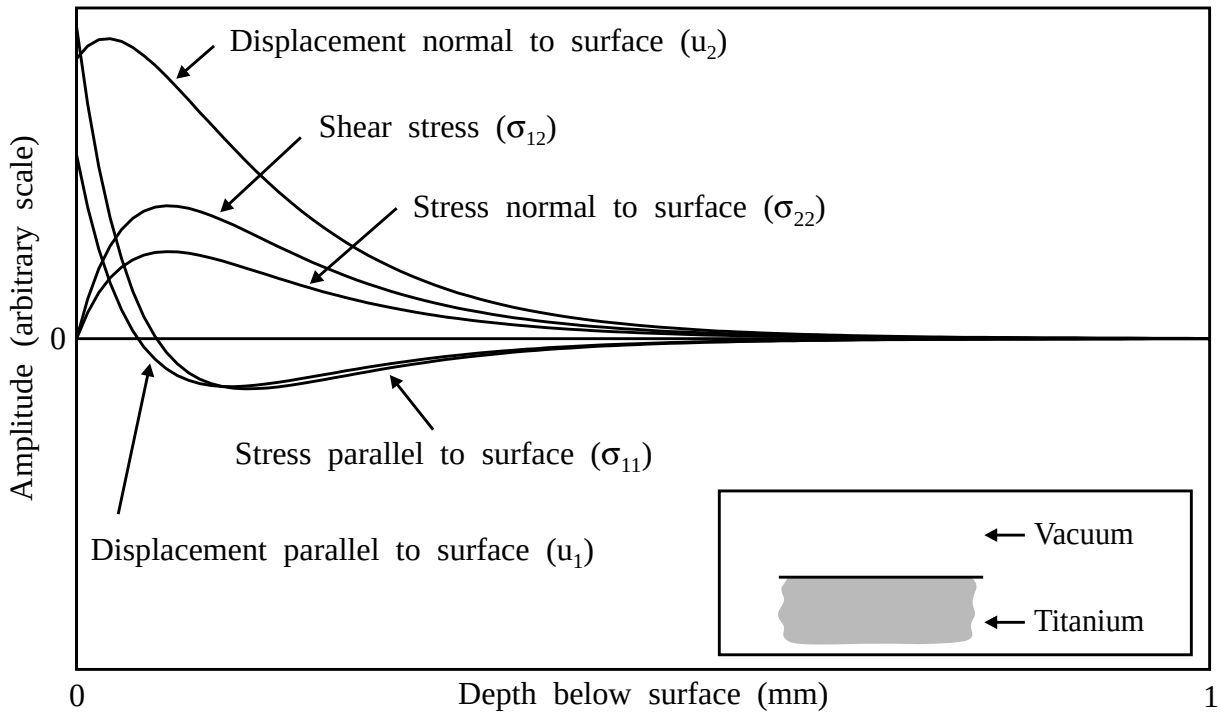

(a) Mode shapes for free Rayleigh wave

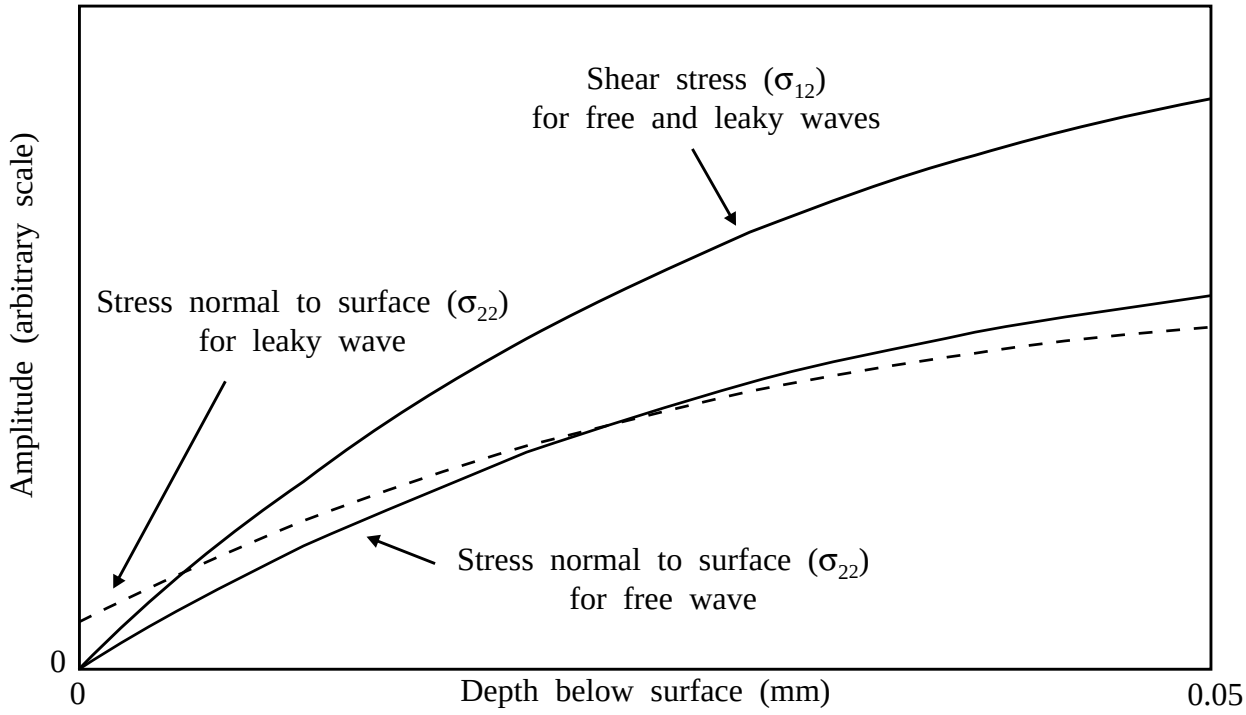

(b) Comparison of near-surface stresses for free and leaky Rayleigh waves

Figure 5.1 Mode shapes for Rayleigh waves in titanium at 10 MHz

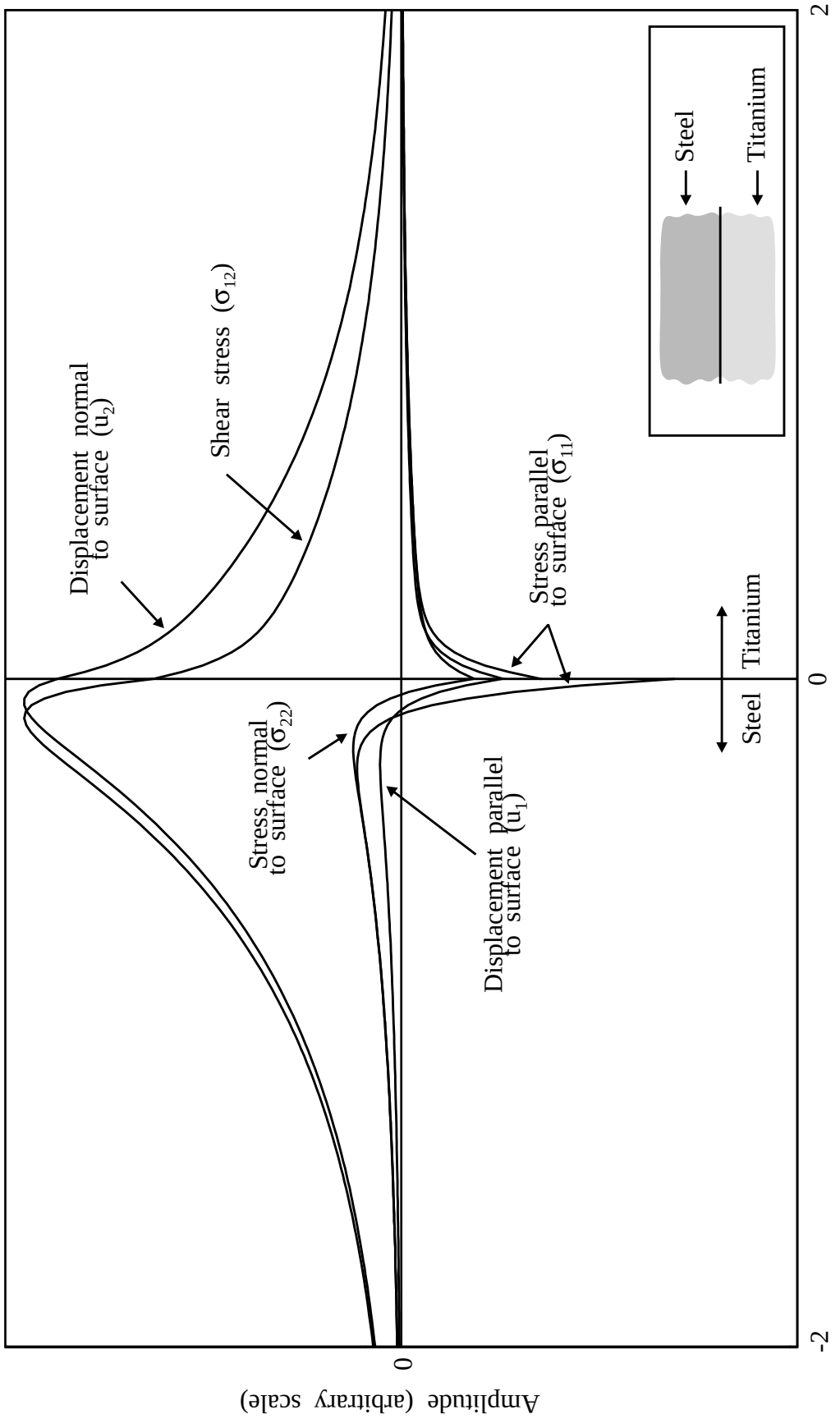

Figure 5.2 Mode shapes for Stoneley wave between titanium and steel at 10 MHz

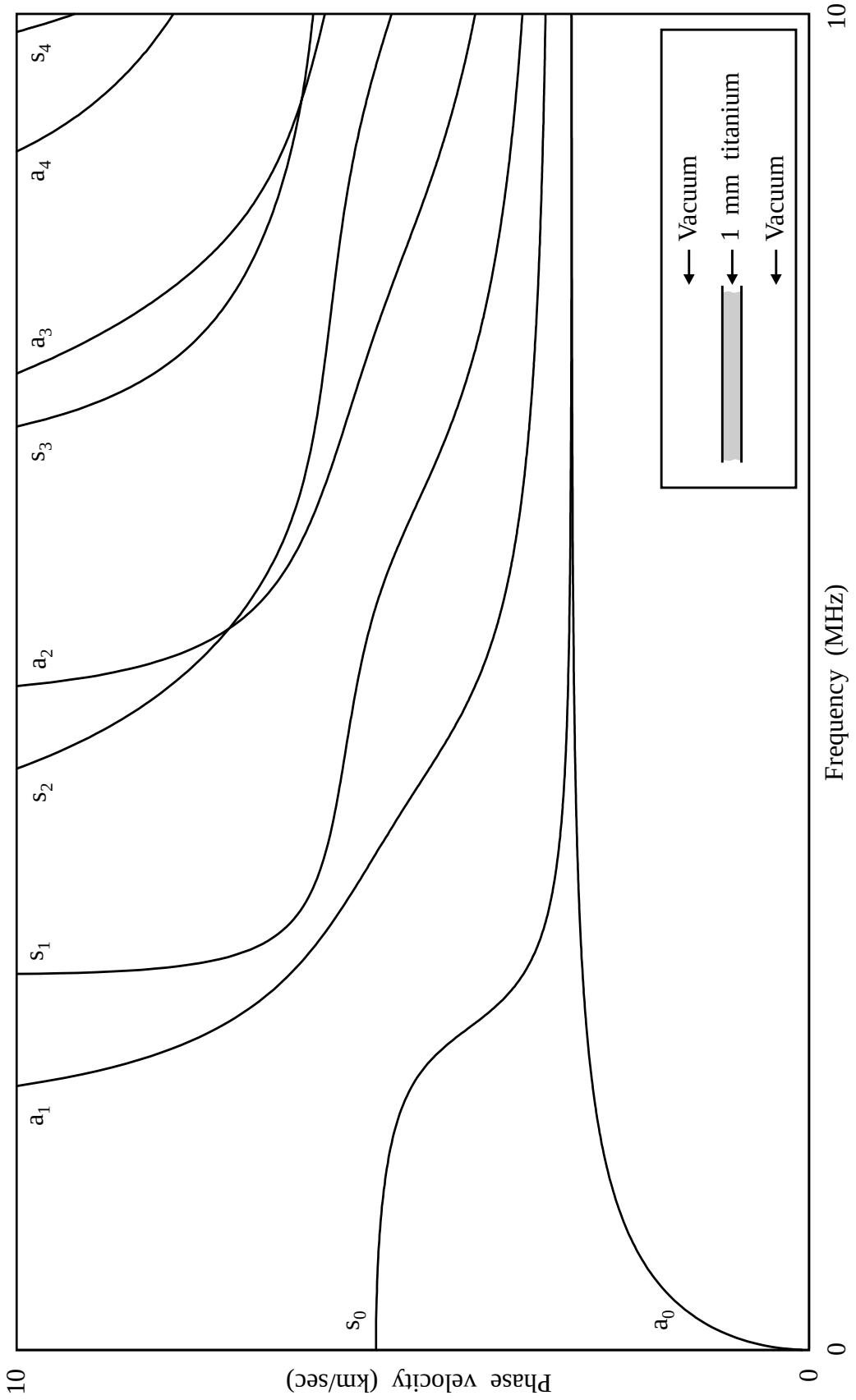

Figure 5.3 Dispersion curves for Lamb modes in 1.0 mm thick titanium sheet - Phase velocity

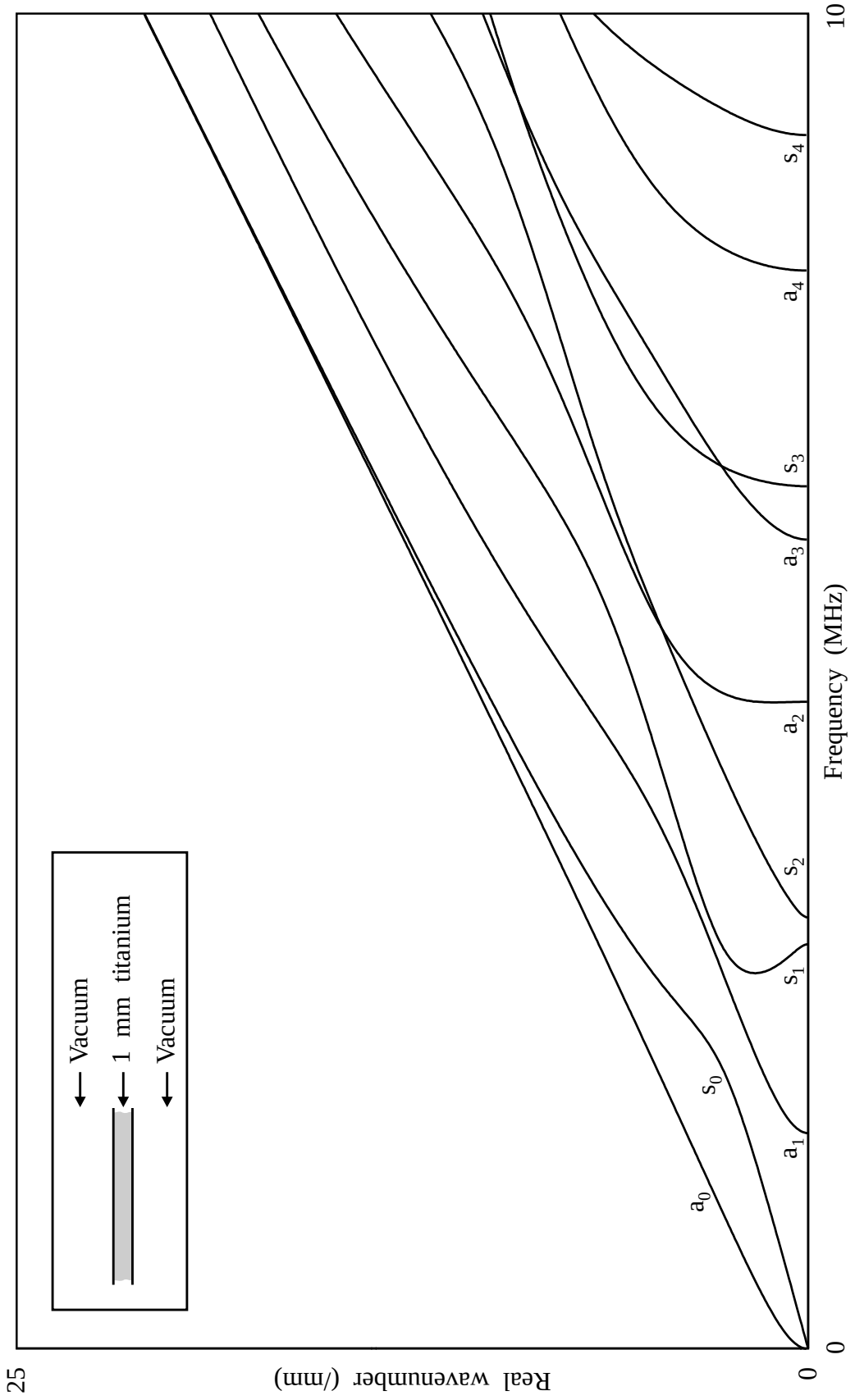

Figure 5.4 Dispersion curves for Lamb modes in 1.0 mm thick titanium sheet - Real wavenumber

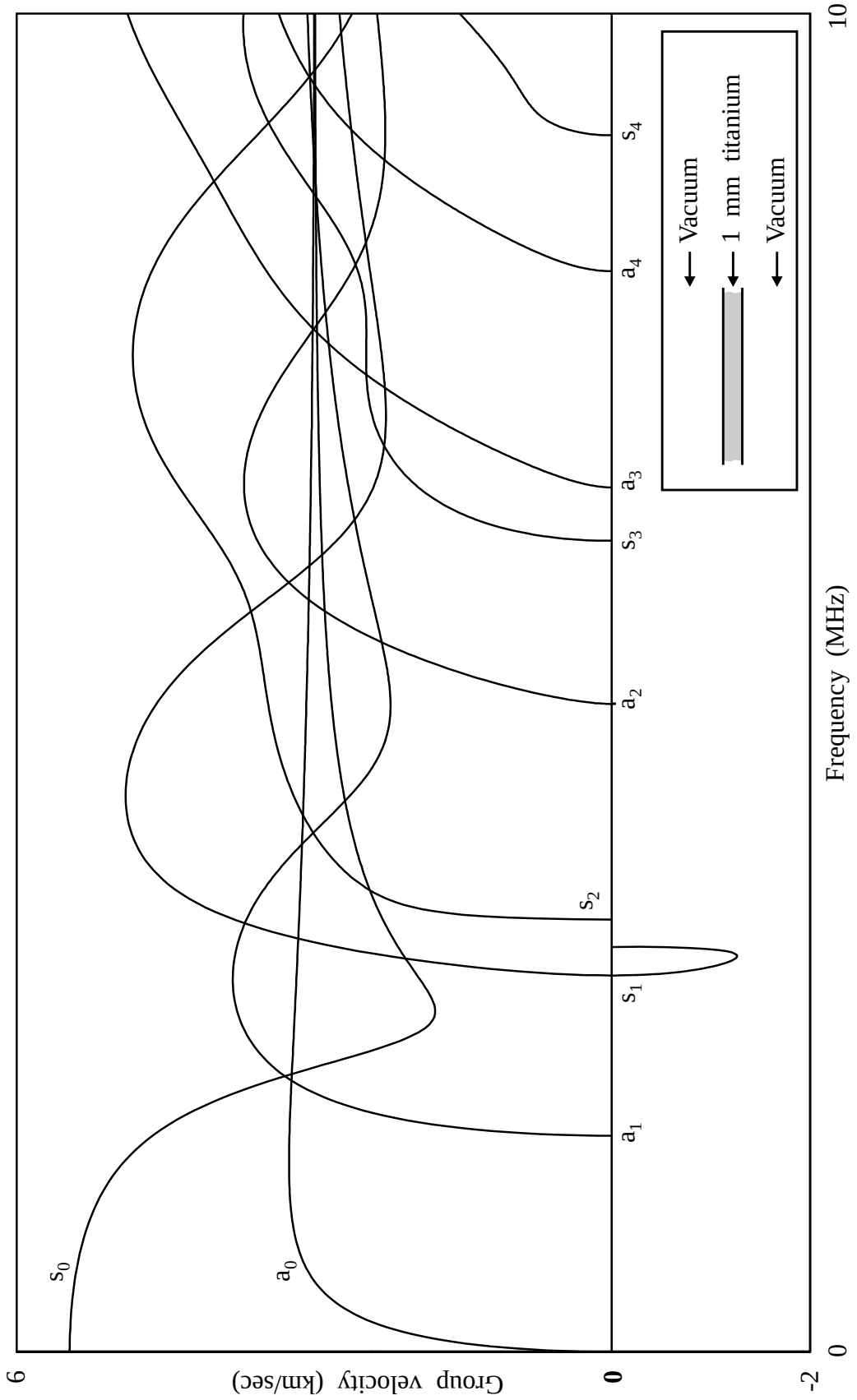

Figure 5.5 Dispersion curves for Lamb modes in 1.0 mm thick titanium sheet - Group velocity

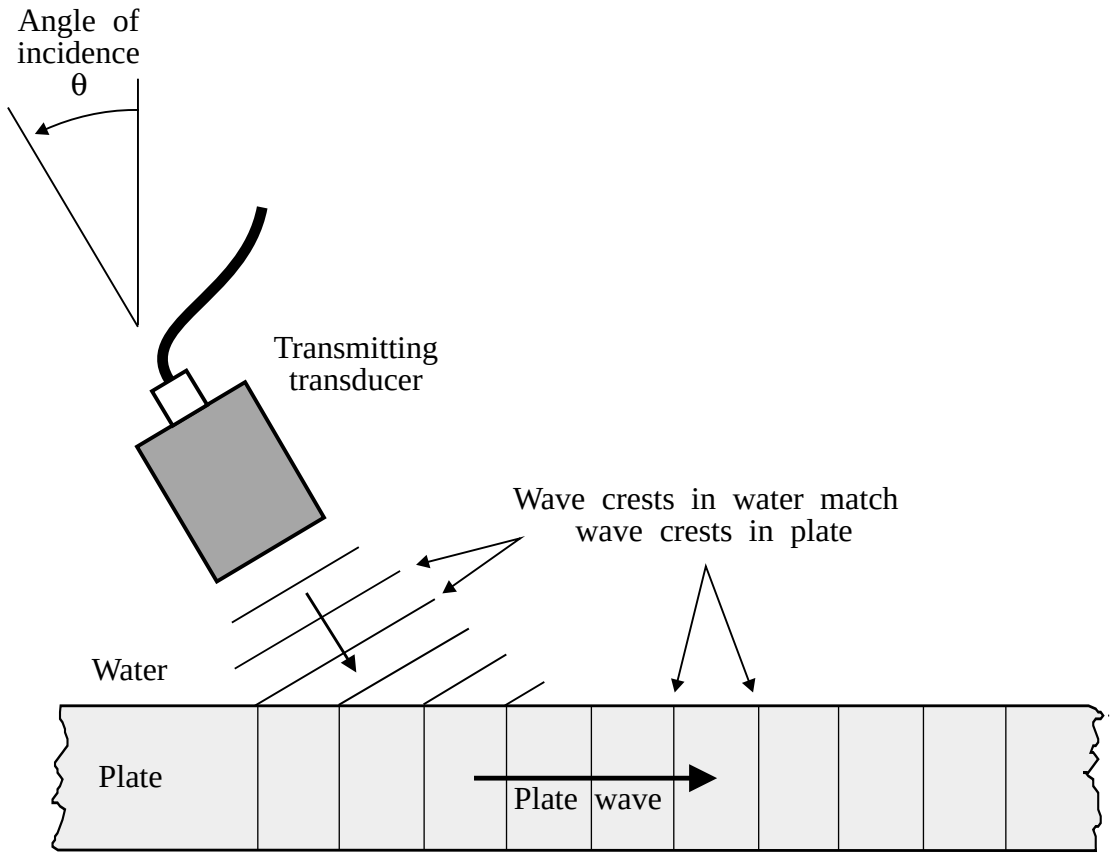

$$\text{Plate wave velocity} = \frac{\text{Velocity in water}}{\sin(\theta)} \qquad \text{(Equation 4.1)}$$

Figure 5.6 The coincidence principle for the excitation of plate waves

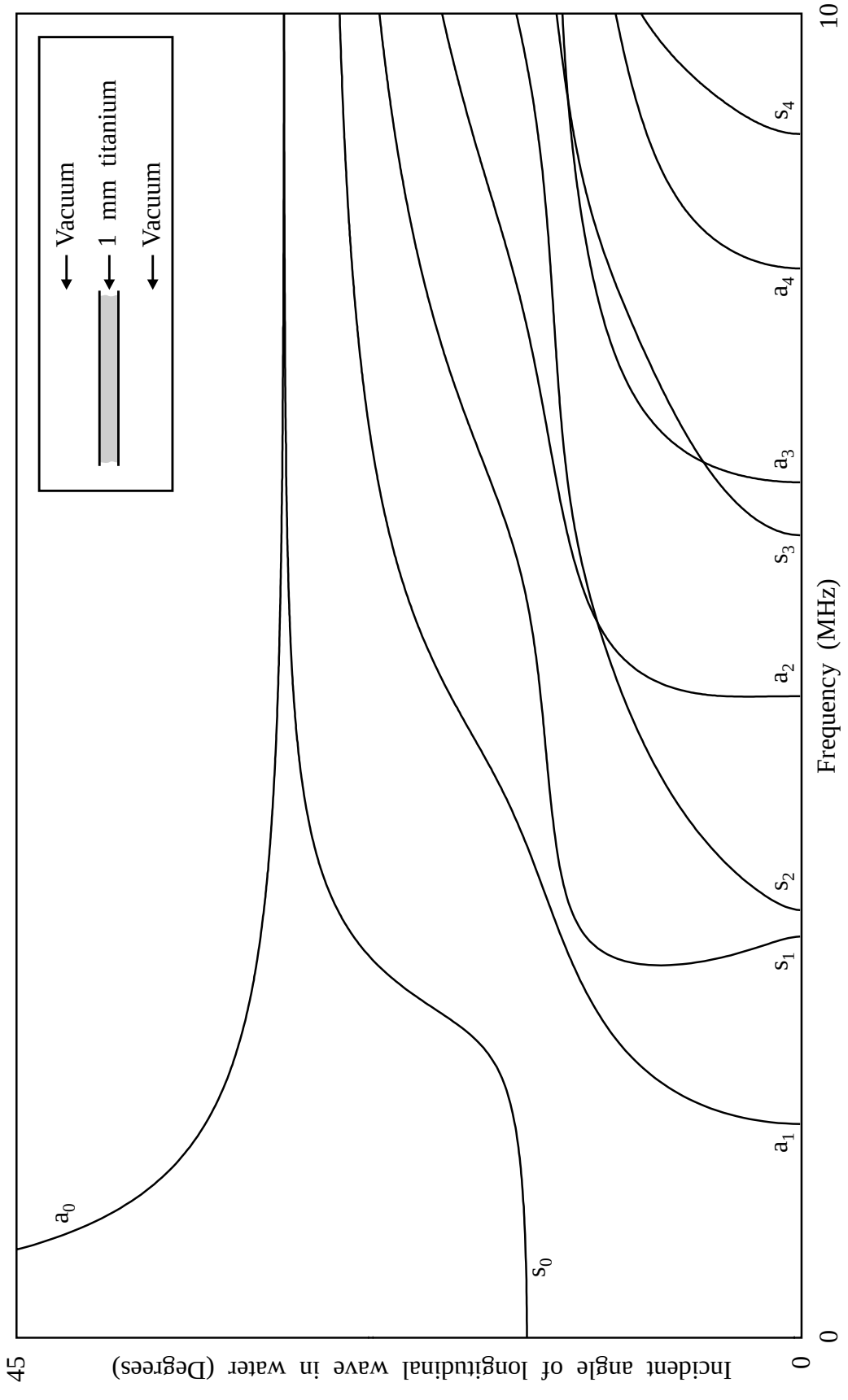

Figure 5.7 Dispersion curves for Lamb modes in 1.0 mm thick titanium sheet - Equivalent incident angle in water

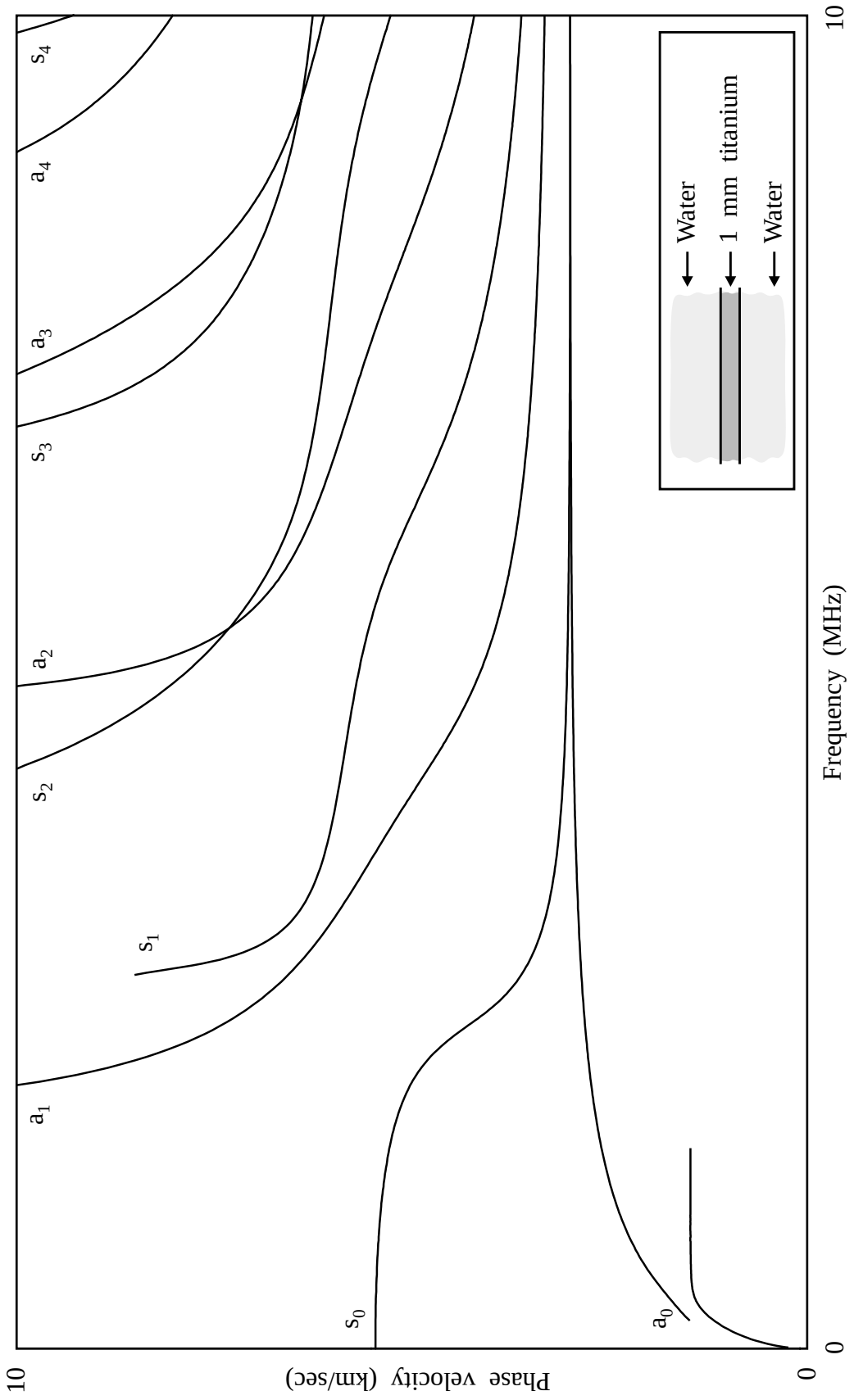

Figure 5.8 Dispersion curves for leaky Lamb modes in 1.0 mm thick titanium sheet in water - Phase velocity

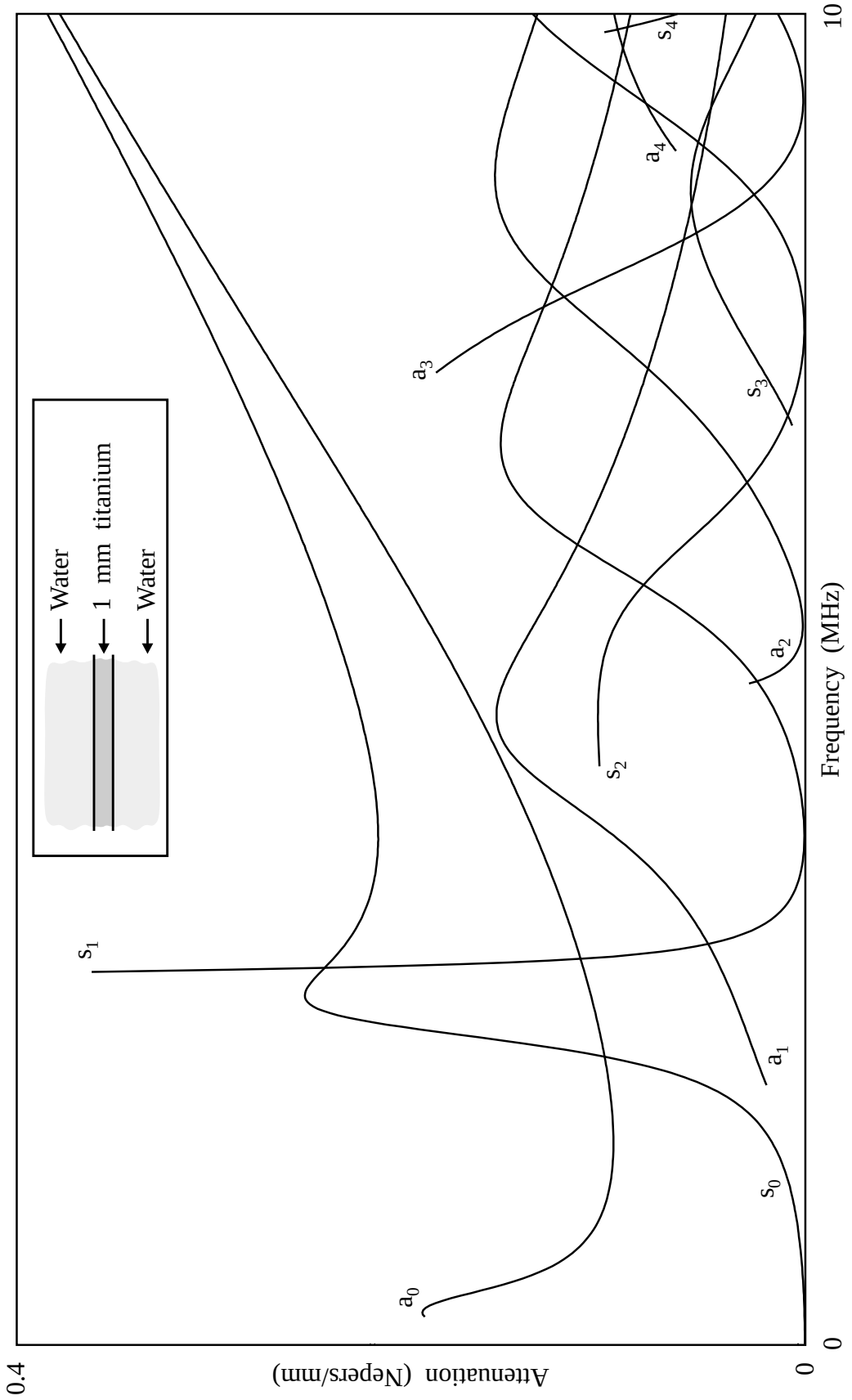

Figure 5.9 Attenuation of leaky Lamb modes in 1.0 mm thick titanium sheet in water

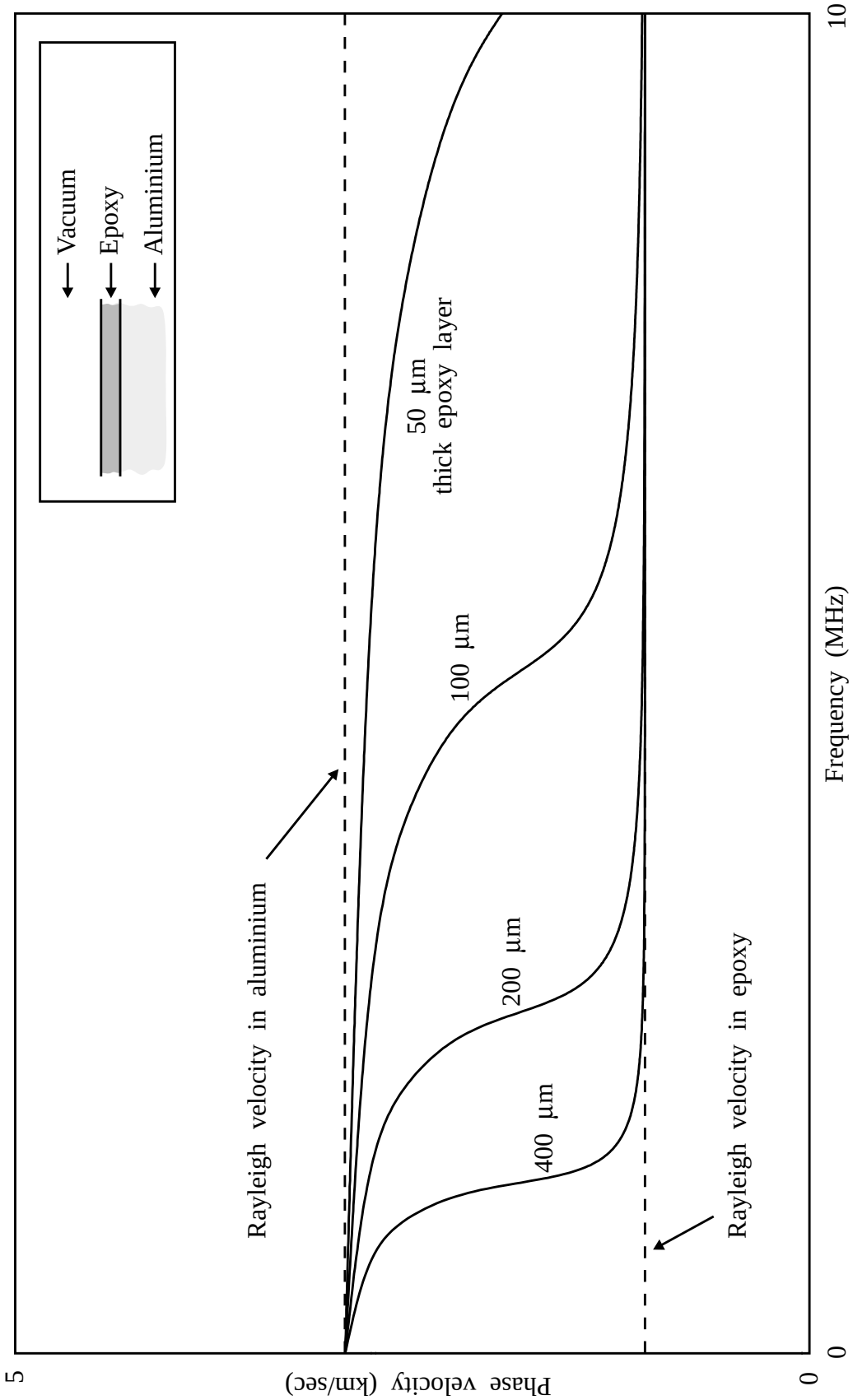

Figure 5.10 Dispersion curves for surface waves on epoxy layer on aluminium half-space

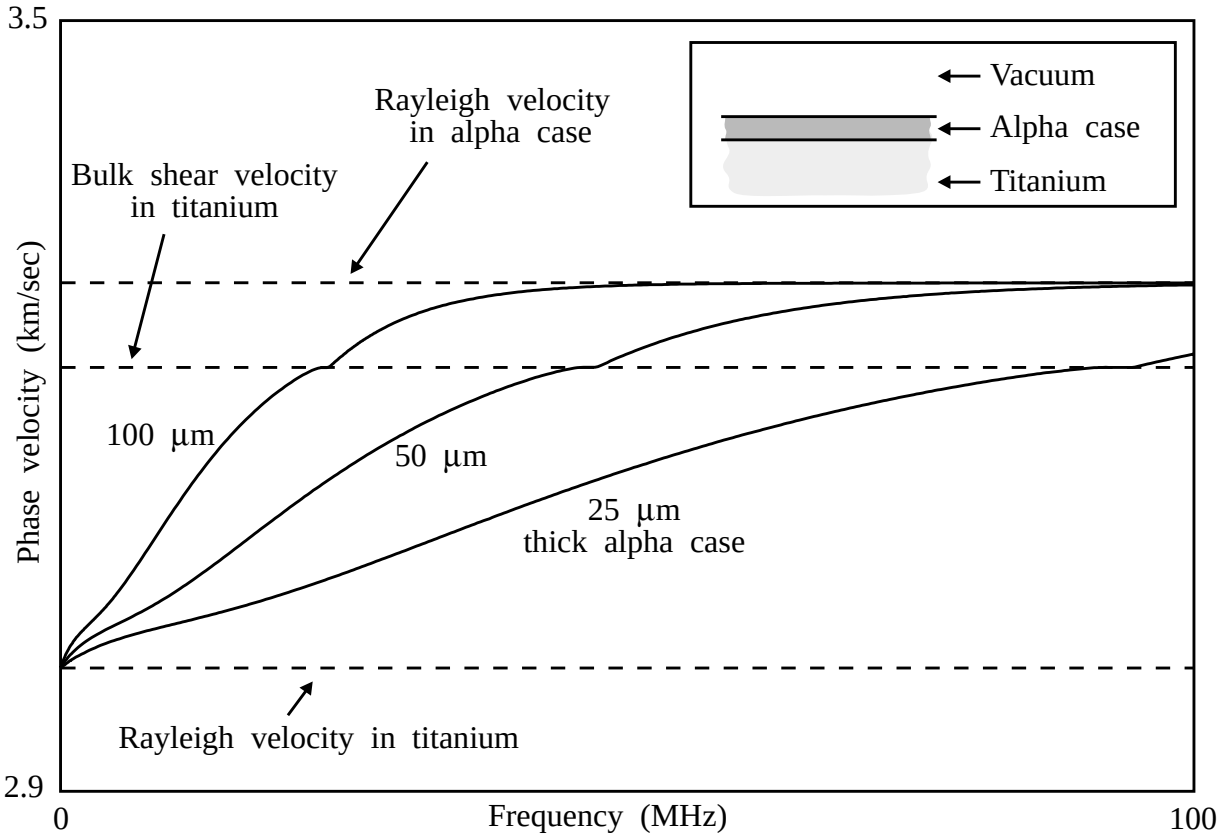

(a) Phase velocity

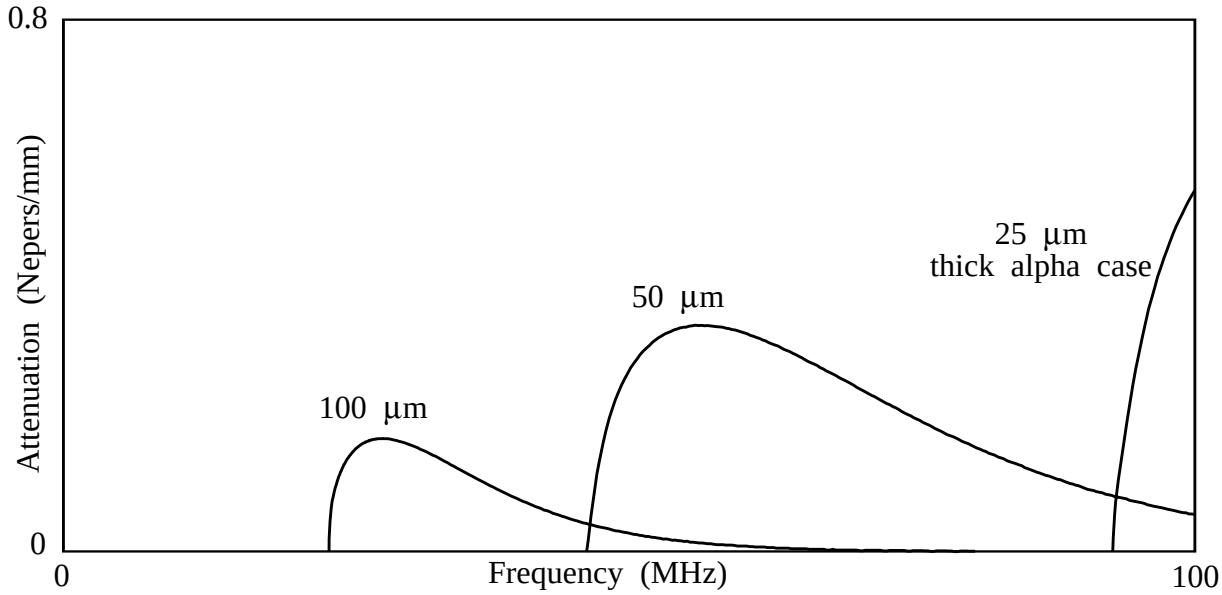

(b) Attenuation

Figure 5.11 Dispersion curves for surface waves on layer of alpha case on titanium half-space

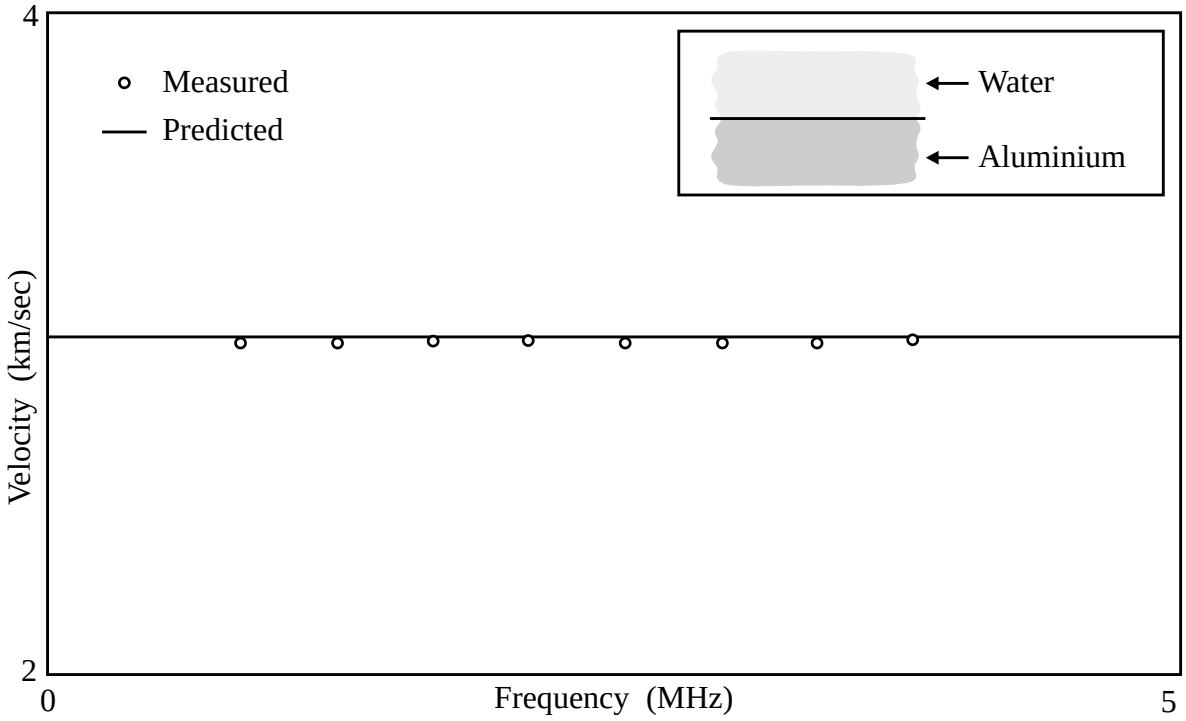

(a) Rayleigh wave on aluminium

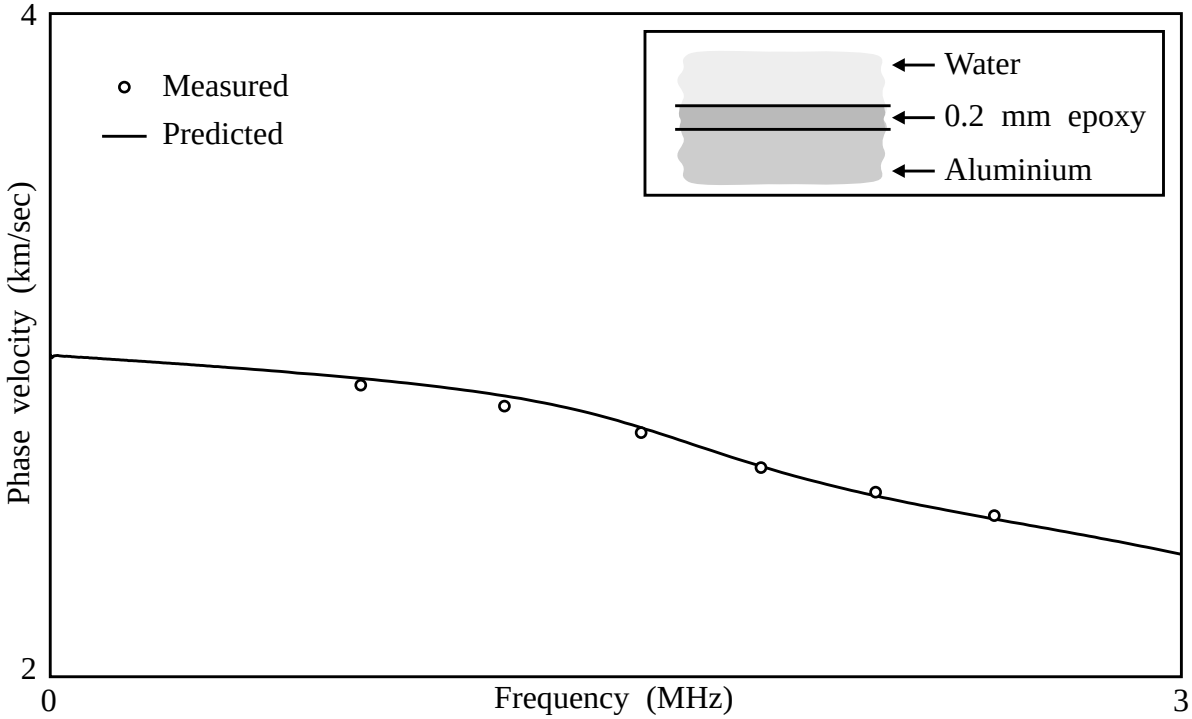

(b) Surface wave on epoxy layer on alumium

Figure 5.12 Measurements of surface waves

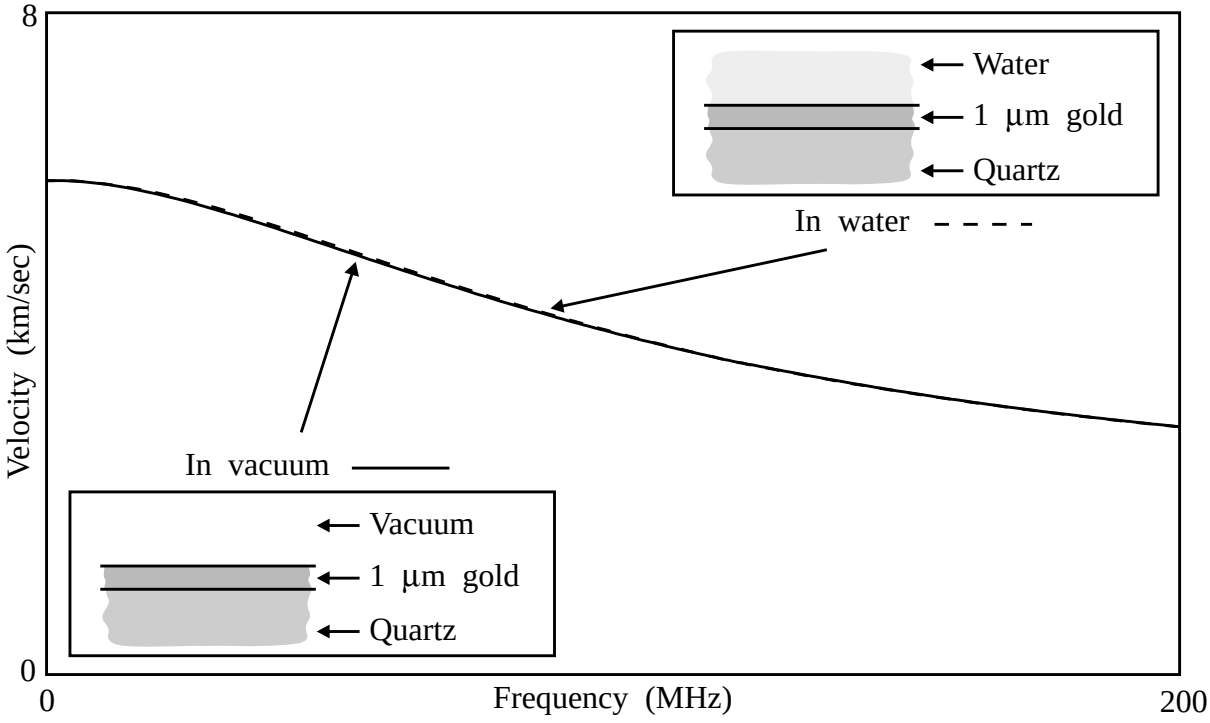

(a) Phase velocity

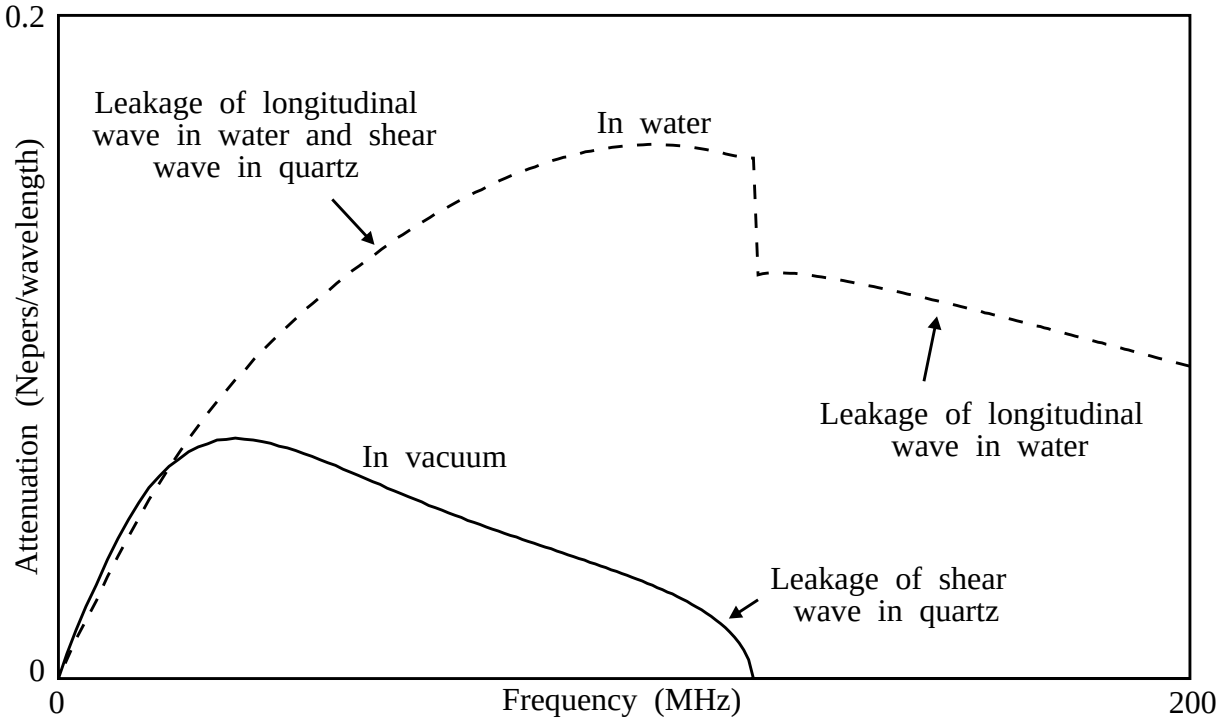

(b) Attenuation

Figure 5.13 Dispersion curves for Sezawa waves in layer of gold on fused quartz

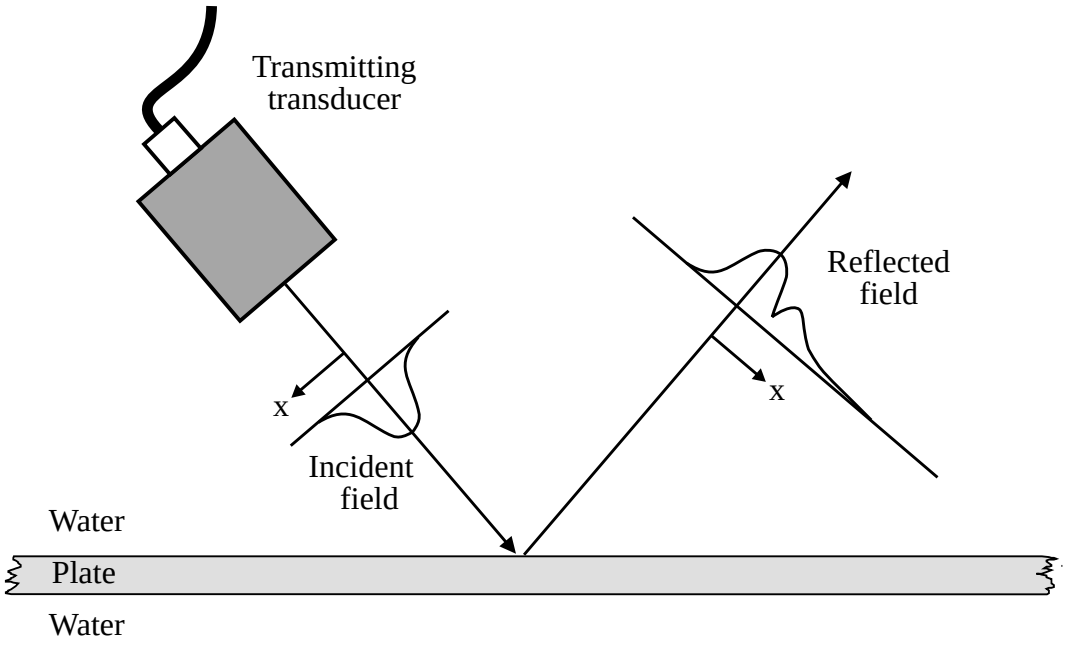

(a) Arrangement of simulation

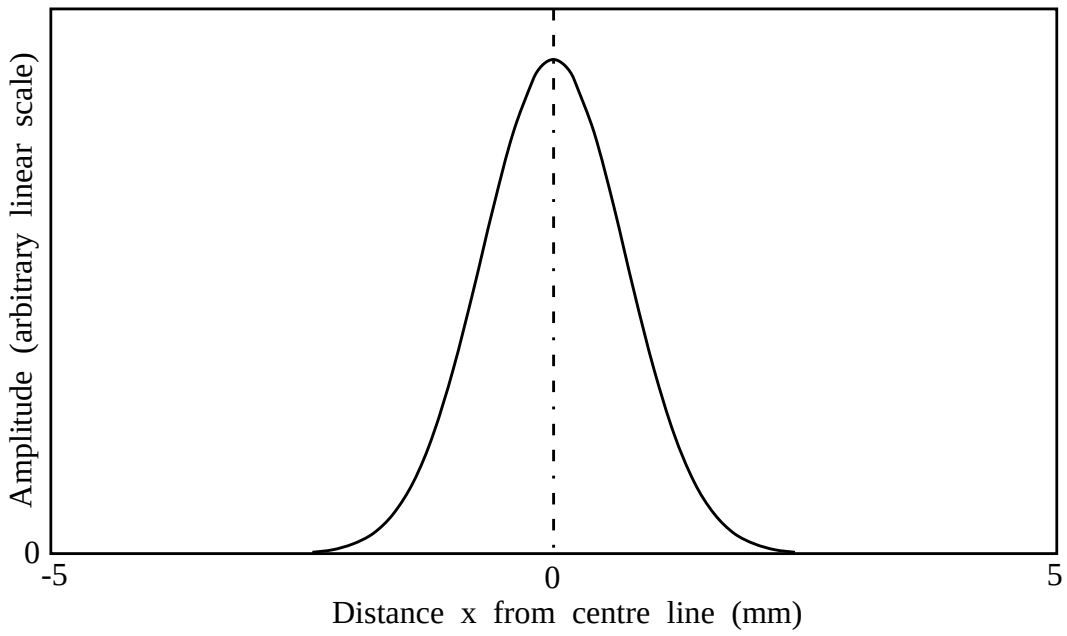

(b) Incident field profile

Figure 5.14 Simulation of near-field response using finite transducer model

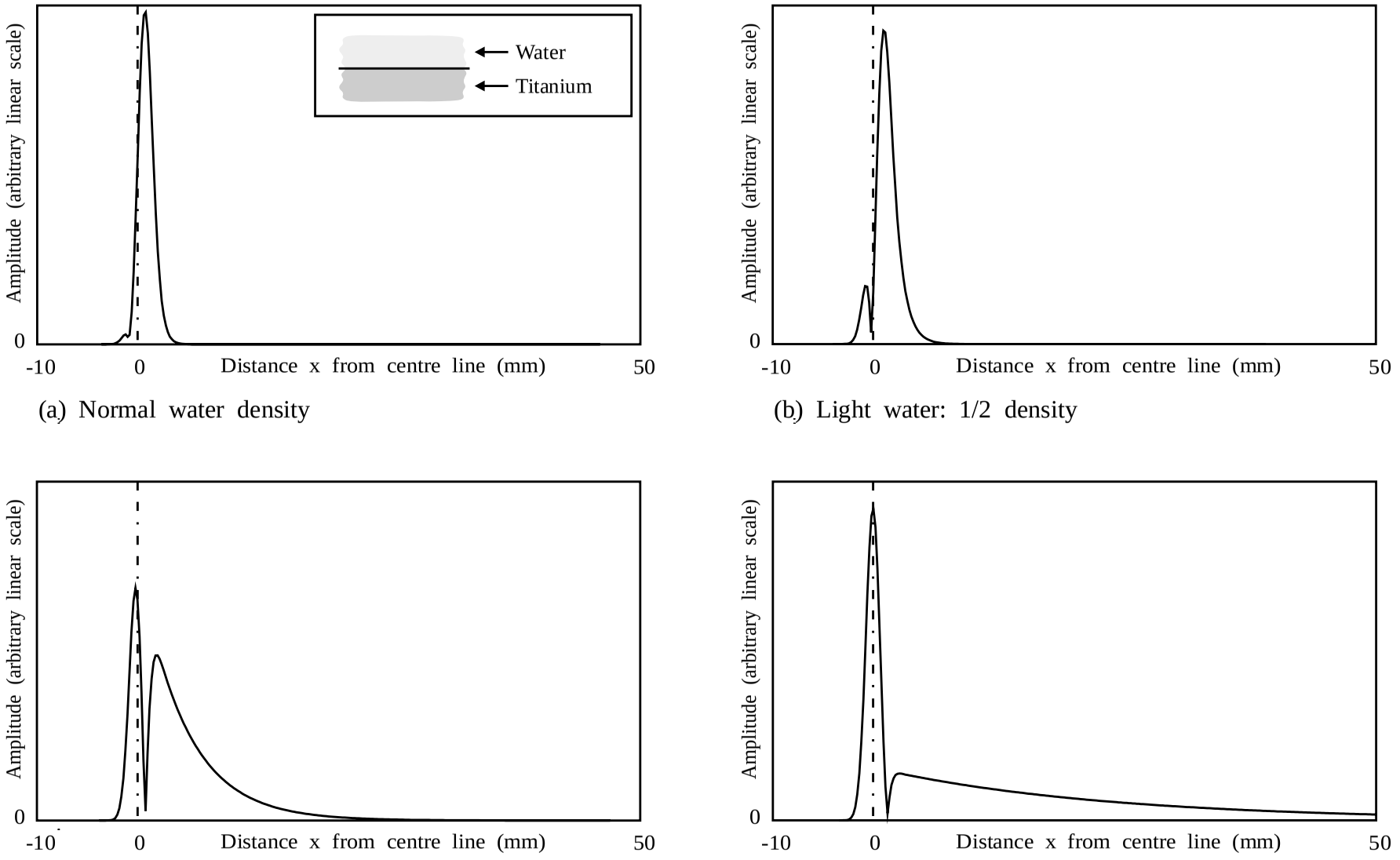

Figure 5.15 Near-field response predictions when exciting leaky Rayleigh wave in titanium - linear amplitude scale

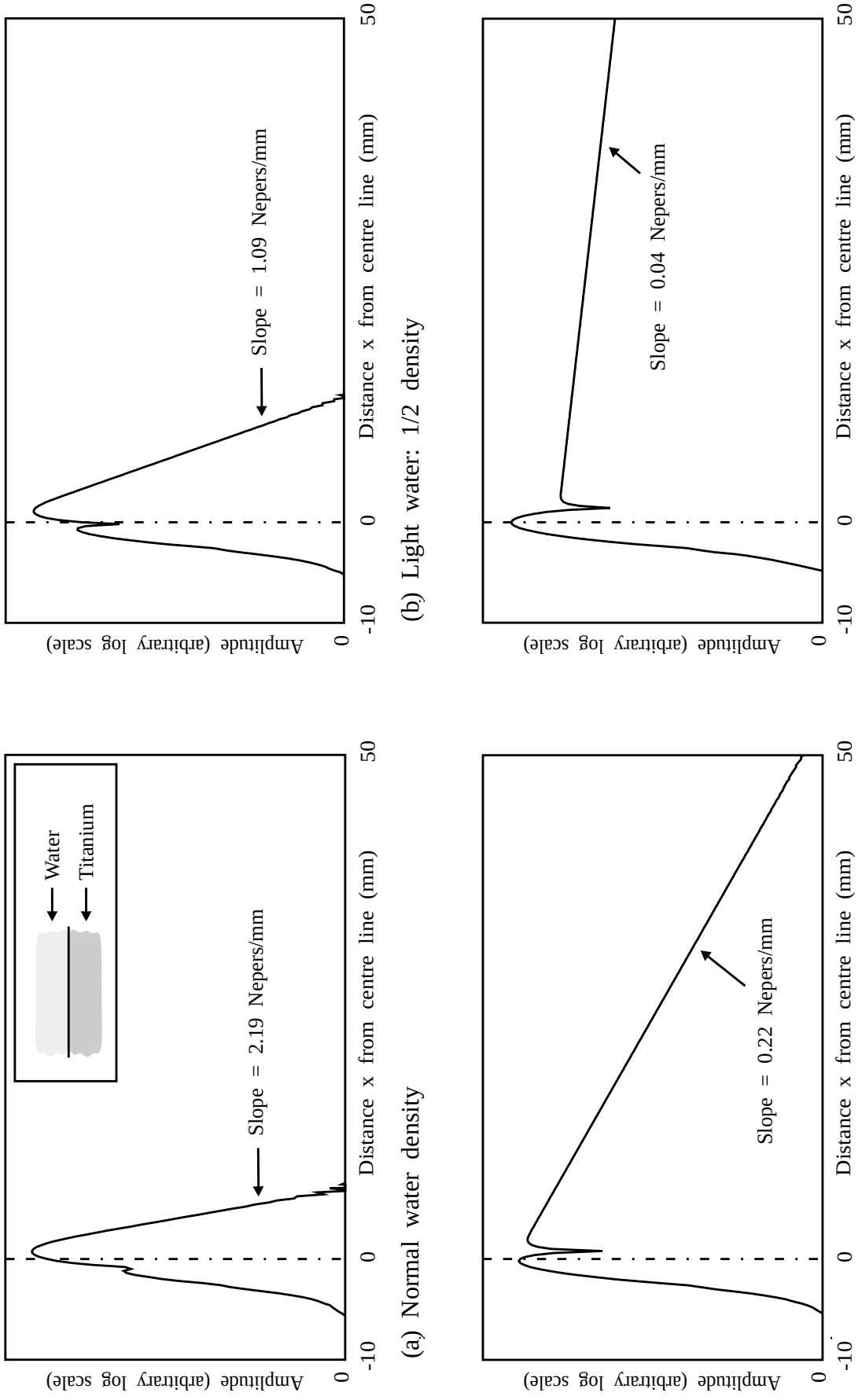

Figure 5.16 Near-field response predictions when exciting leaky Rayleigh wave in titanium - log amplitude scale

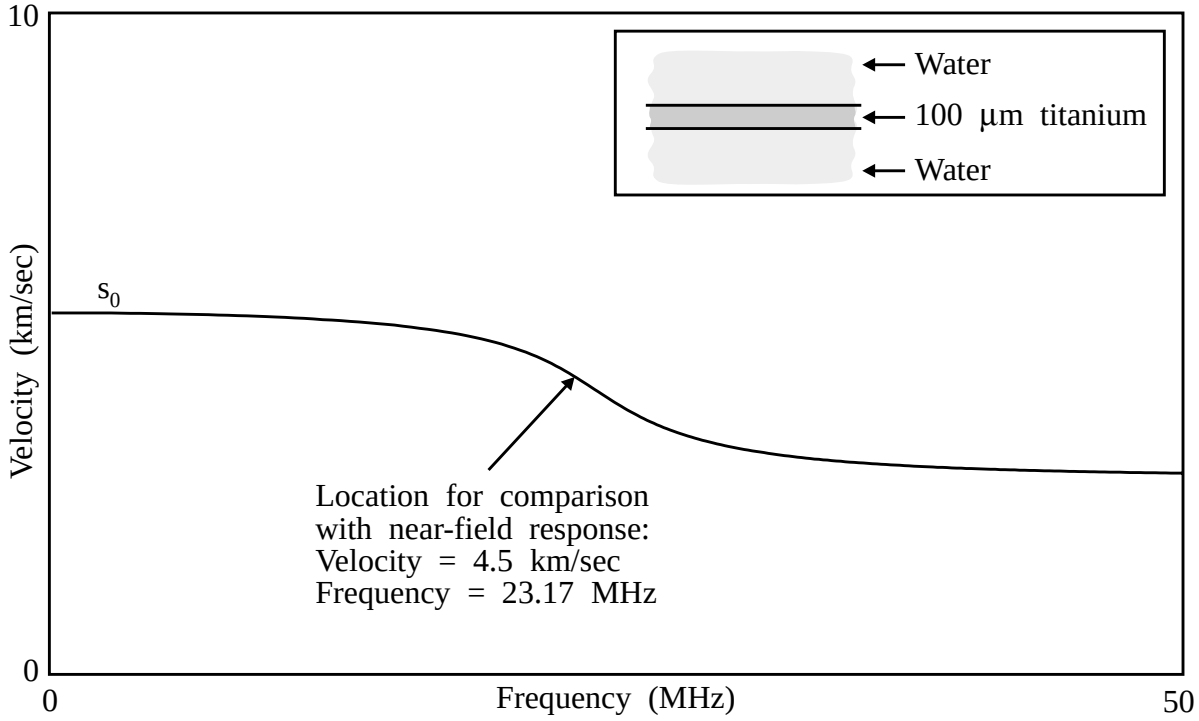

(a) Phase velocity

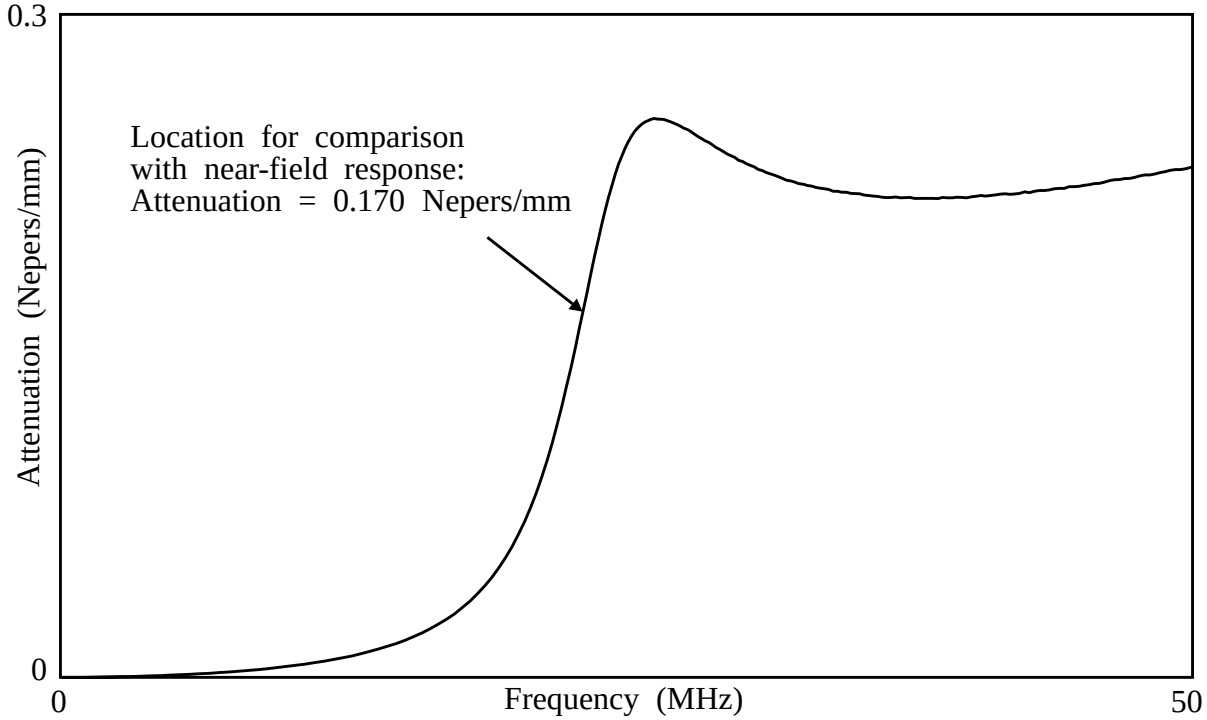

(b) Attenuation

Figure 5.17 Modal solution for leaky s_0 Lamb wave, showing location for comparison with prediction of near-field response

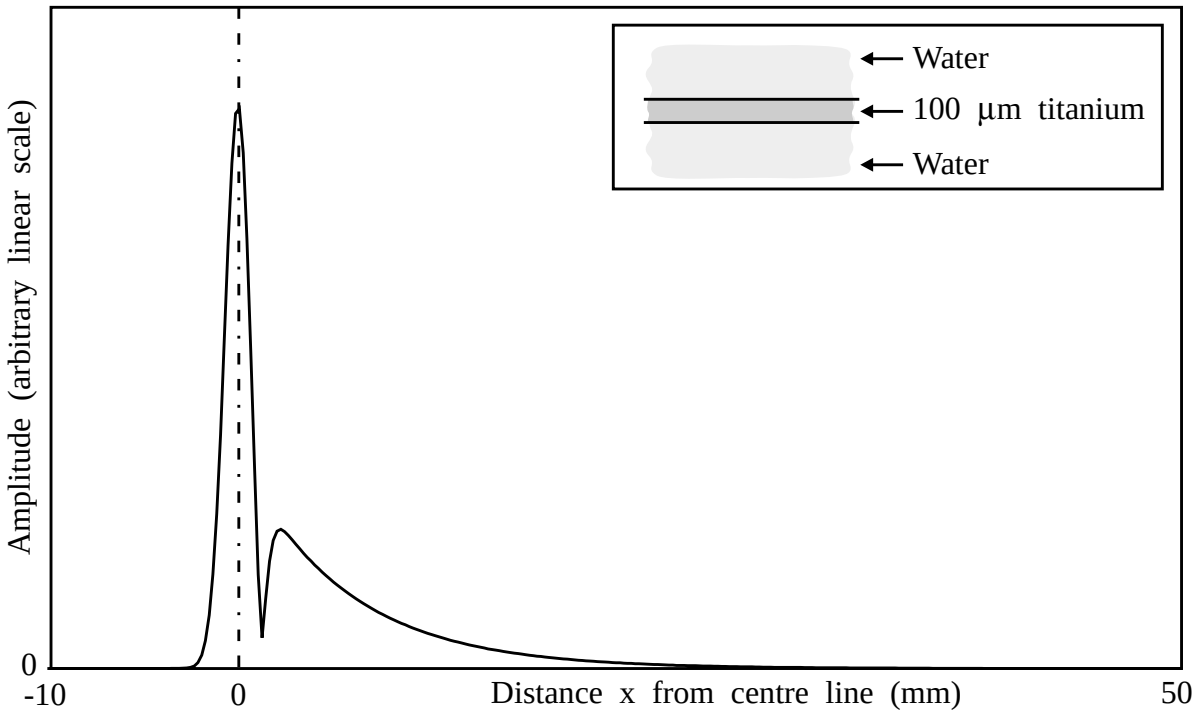

(a) Linear amplitude scale

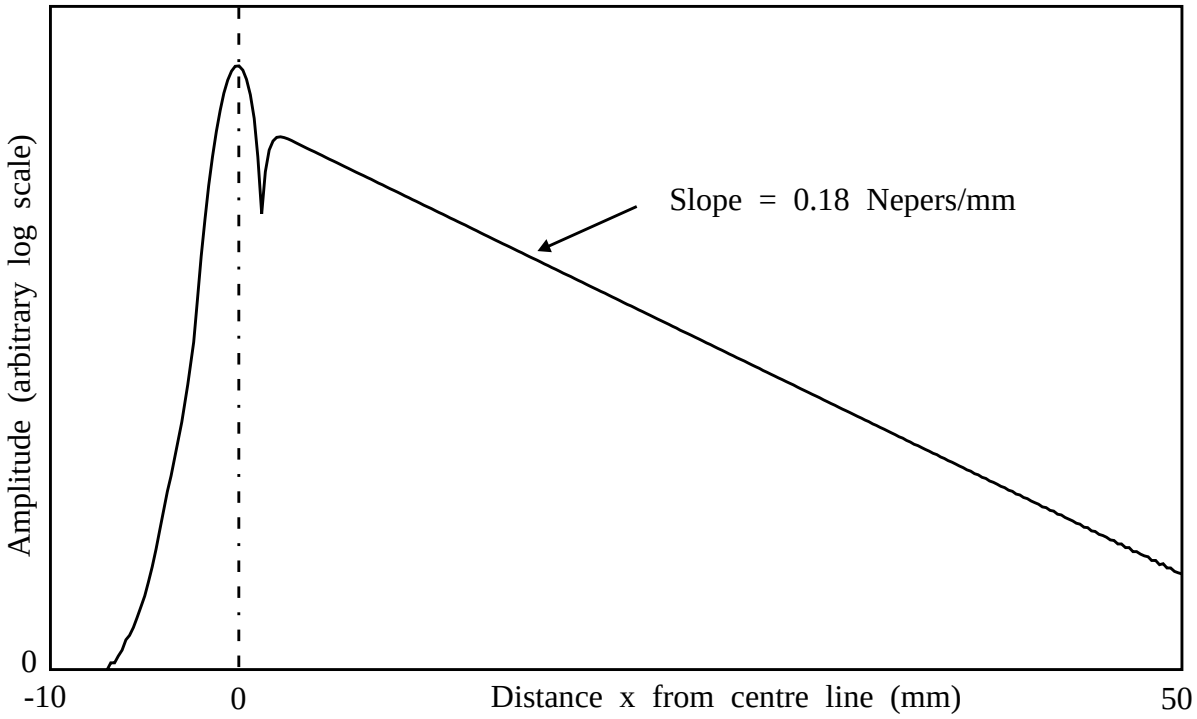

(b) Log amplitude scale

Figure 5.18 Near-field response predictions when exciting leaky s_0 Lamb wave in titanium

CHAPTER 6

Characterisation of defective joints

6.1 Introduction

Any ultrasonic method for the detection of a layer of alpha case embedded at the bondline of a diffusion bonded joint must rely on some variation of the acoustic properties of the alpha case with respect to the adherends. This chapter reports the results of a practical investigation of the material properties of alpha case, which will be needed for the model studies in Chapters 7 to 10.

In the introduction of this thesis the formation of alpha case was described as a combination of two mechanisms: first the presence of oxygen or nitrogen increases the beta transus temperature so that hard beta grains tend to transform to relatively soft alpha grains and second, the gases cause interstitial locking of the alpha grains, increasing their hardness. These mechanisms are contradictory in their effect on the hardness of the material so that it is not immediately evident whether alpha case material should be harder or softer than the uncontaminated material. This must depend on the degree of softening and hardening associated with the two mechanisms and on the proportions of alpha and beta grains in the alloy. For instance, the formation of alpha case is more likely to increase the hardness of the material if the alloy is naturally dominated by alpha grains than if it is dominated by beta grains.

This contention seems to have been observed in practice. Weglein (1988) reported two cases of measurements of bulk longitudinal velocities in titanium alloys, one in which the velocity increased by 3 % and the other in which the velocity decreased by 0.7 %. The specification of the material which was used in the former case was not stated but the latter measurements were made in the alloy Ti-6211. In his own preliminary measurements, which he made across a section of a Ti-6Al-4V diffusion bonded joint using an acoustic microscope, he also found a reduction of the surface wave velocity at the bondline. In contrast, Thompson, Margetan, Rose and Batra (1992) and Brasche, Margetan and Thompson (1992) found that the acoustic velocities of their Ti-6Al-4V specimens increased substantially when the material was contaminated with oxygen. They measured surface wave velocities on contaminated plates, finding increases of around 7-8 %.

It seems therefore that the material properties of the alpha case material must not be considered to be absolute but to depend on the specifications of the titanium alloy. Furthermore, since the growth of the alpha case is a diffusion process, it is quite reasonable to expect that the properties of the alpha case may vary gradually with depth unless saturation takes place. This is an important consideration because the ultrasonic response from a discrete layer of alpha case with homogeneous material properties may be rather different than that from a layer with gradually changing properties.

An important aspect of the research programme therefore has been to measure the acoustic properties of alpha case in the specific material being utilised for the diffusion bonds.

6.2 Preparation of specimens

In order to measure the acoustic properties of alpha case it was decided to grow thick layers of alpha case by exposing titanium sheets in air at high temperatures. Two sheet thicknesses were used, nominally 1 mm and 4 mm. Both sheets had the specification of the stock which is used for the diffusion bonding. The intention with the 1 mm sheet was to grow alpha case throughout the thickness so that through-thickness velocity measurements could be made directly to determine representative acoustic properties of the material. The intention with the 4 mm sheet was to grow a thick layer on each surface. Note that the word 'layer' is used to refer to a zone where the alpha case contamination is significant; it does not imply that the properties are constant throughout the thickness of the layer.

The treatment of the sheets was undertaken by British Aerospace. The sheets were exposed in air at 900 ^{o}C for 12 hours and 120 hours respectively. During exposure, considerable flaking of material occurred at the surfaces of the sheets. This was grit blasted from the surfaces afterwards. Consequently the 1 mm sheet reduced in thickness from 1.1 mm to approximately 0.8 mm and the 4 mm sheet reduced from 3.9 mm to about 3.7 mm.

Figure 6.1 shows micrographs of sections through the heat treated sheets. The sections were etched with a solution which was developed specifically by British Aerospace to show the presence of alpha case. It shows titanium as a dark colour and alpha case as a light colour. It is the same etch which was used to expose the alpha case in the poor diffusion bond which was discussed in Chapter 1 and illustrated in Figure 1.2. In

Figure 6.1(a) there appears to be some alpha case throughout the thickness of the 1 mm sheet but its intensity varies, the surfaces being affected considerably more than the interior. In Figure 6.1(b) the central region of the 4 mm sheet seems not to have been affected, the alpha case apparently extending about 1 mm from each surface.

It was intended also to include a range of diffusion bonded joints with different degrees of alpha case contamination as test specimens. British Aerospace have had considerable success in developing the bonding process so that they are able to produce high quality joints consistently. The plan therefore was that they would deliberately reduce the quality of the bonds by exposing the sheets to air prior to bonding. However the deliberate production of poor diffusion bonds was fraught with difficulties, predominantly associated with the selection of the appropriate degree of exposure. The result was that the 'defective' bonds were generally contaminated (or disbonded) much too severely to be used in the research, and only one suitable specimen was made available. This is the poor bond which was introduced in Chapter 1 and mentioned above. It was cut from a diffusion bonded and superplastic formed (SPFDB) specimen. It is considered to be rather heavily contaminated.

6.3 Measurements of hardness

Hardness measurements were made across the thicknesses of the heat treated specimens, the untreated material from which the heat treated specimens were made, and the poor diffusion bond. The results are plotted in Figures 6.2 to 6.4. In all cases the measurements are Vickers microhardness made using a 200g weight.

In figure 6.2 it can be seen that the hardness of the untreated 1 mm material is about 300 HV at all five test locations across the sheet. The hardness of the treated sheet varies with depth but is greater at all locations than the untreated sheet, the minimum hardness being 340 HV near the centre of the sheet and the maximum about 540 at the edges of the sheet. On average the hardness of the treated sheet is about 400 HV, 30 % greater than for the untreated material. There is no evidence of saturation of the alpha case, the hardness rising sharply at the edges of the sheet without reaching a limiting plateau.

The hardness of the untreated 4 mm sheet, in Figure 6.3, is also about 300 HV except at the two extreme test locations where it is considerably lower, presumably because the test positions were immediately adjacent to the edges of the sheet. The hardness of the treated sheet is also about 300 HV in its interior, rising to nearly 700 HV at the edges,

again without evidence of saturation. The average hardness of the treated sheet is about 365 HV.

Note that the peak hardness values at the edges of the treated 4 mm sheet are higher than at the edges of the treated 1 mm sheet. There are two possible explanations for this. One is that a greater proportion of the hard material was lost by spalling from the thin sheet than from the thick sheet. The other is that a greater concentration of alpha case developed at the surface of the thick sheet during its longer period of exposure.

The hardness of the bulk of the poor diffusion bonded joint is again about 300 HV, consistent with the untreated material, but a spike of 420 HV is clearly evident in the single measurement which was made at the bondline, as indicated in Figure 6.4. This bondline hardness value is slightly higher than the average value across the thickness of the treated 1 mm sheet. It must also be considered as a lower bound value; it is quite possible that the single hardness measurement which was made at the bondline was not at the location of the peak hardness. Furthermore the Vickers hardness measurement is not made at a point but over a small area. Therefore if there was a steep gradient of hardness at the measurement location then the measured hardness would be an underestimate of the peak hardness at that location.

The hardness measurements indicate strongly that the alpha case is not a discrete layer of homogeneous material but is a varying layer as may be expected from the gas diffusion process. They also suggest that in no case has sufficient oxygen or nitrogen been absorbed to saturate the material. Even after 120 hours exposure there is a steep hardness gradient at the edges of the 4 mm sheet. Comparing the hardness distributions with the micrographs it seems that the etch is very successful in identifying contaminated material, even at relatively low levels. The threshold for detection appears to be about 350 HV, 50 HV higher than the hardness of uncontaminated titanium.

6.4 Measurements of acoustic properties

Measurements of bulk longitudinal and shear wave velocities

Acoustic velocity measurements were made through the thicknesses of the untreated titanium sheets, the treated titanium sheets, and the poor diffusion bonded joint. The results are summarised in Table 6.1(a).

The longitudinal velocity measurements were made using an unfocused broadband transducer with a 10 MHz centre frequency, in an immersion tank. The shear velocity measurements were made using a broadband 8 MHz centre frequency shear transducer attached to the specimens with a strongly viscous coupling agent. Two shear velocity measurements were made at each location. The shear velocity 'parallel' to the rolling direction was measured with the transducer positioned so that the shear motion of the pulse was parallel to the rolling direction of the plate. The shear velocity 'normal' to the rolling direction was then made with the transducer rotated 90^{o} so that the shear motion was normal to the rolling direction. The amplitude spectrum method (Pialucha, Guyott & Cawley (1989)) was used, giving the velocity at a number of frequencies within the bandwidth of the transducer in each case. Each tabulated value is the average of these measured velocities. In no case was there any significant variation of velocity with frequency.

The accuracy of the velocity measurement was limited mainly by the accuracy of the measurement of thickness of each specimen. Thus the velocity measurements for the thin specimens were considerably less accurate than for the thick specimens. Also, the treated sheets suffered some distortion during their exposure so that their thickness measurements were not as accurate as those of the untreated sheets. In general greater confidence can be held in the measurements of longitudinal velocity than in those of shear velocity because of the quality of the received signals. It is more difficult to obtain a clean strong signal with the shear test arrangement than with the longitudinal test because of the difficulty of coupling the transducer reliably to the test specimen.

Comparing the two untreated sheets, there appears to be some variation in the properties of the raw material. The longitudinal velocity through the 1 mm sheet is some 2 % higher than that through the 4 mm sheet. The shear velocity normal to the rolling direction is also slightly higher in the 1 mm sheet than in the 4 mm sheet but the shear velocities parallel to the rolling direction are almost identical. The difference between the two shear velocity measurements in the thin sheet, indicating the degree of anisotropy, is about 4 % and in the thicker sheet, 2 %. The shear velocity is lower in the rolling direction than in the normal direction in both cases. The differences in properties between the two thicknesses of sheet are presumably due to differences in the extent of working of the material.

The fact that the shear velocity is faster in the direction normal to the plate than in the direction parallel to the plate is rather surprising at first because the stiffness is normally expected to increase in the direction in which a plate is rolled. However the plate

material which was used in these studies is not rolled solely in one direction (Bottomley (1992)). Prior to the final cold rolling of the sheets which defines the 'rolling direction', the material is hot rolled in the normal direction and it is at this stage that the microstructure is developed. Thus the elongation of the grains and the stiffening tends to be normal to the 'rolling direction'.

A significant increase of some 6 % can be seen in the longitudinal velocity in the treated 1 mm sheet over that in the untreated 1 mm sheet. The shear velocities are also increased, by 4 % and 5 %. These increases agree qualitatively with the measurements of surface wave velocities on alpha case reported by the researchers at Iowa State University (Thompson *et al.* (1992), Brasche *et al.* (1992)). It seems also that the stiffness anisotropy of the sheet has not been removed by the heat treatment, the variation of shear velocity with polarisation remaining at about 3 %. This is in agreement with metallurgical studies of the material made by British Aerospace (Bottomley (1992)). Heat treatment on its own does not affect the anisotropy of the material. However stiffness anisotropy may be reduced during superplastic forming because of the tendency for the grains to become equi-axed as the material flows.

The velocities through the treated 4 mm sheet are approximately mid-way between the velocities through the 4 mm untreated sheet and those through the 1 mm treated sheet. Again the treated sheet has retained its anisotropy, the variation of shear velocity with polarisation remaining at 2 %.

Two sets of velocities are given in the table for the poor diffusion bond, one for each adherend. Each adherend test piece was isolated from a piece of the joint by grinding off the unwanted adherend down to the bondline. As can be seen, small differences were found between the velocities in the two adherends, the longitudinal velocities differing by about 1 %. The shear velocity measurements also indicate that the anisotropy of the material is considerably lower than in the raw or heat treated sheets. The anisotropy in the first adherend is about 1 % while no anisotropy is evident in the second adherend. This observation is consistent with the loss of stiffness anisotropy during superplastic forming. The small differences between the velocities of the two adherends could be due to different degrees of straining during the superplastic forming.

Comparing the velocity measurements in the 1 mm sheets with the hardness distributions it seems that an average increase in longitudinal velocity of 6 % can be associated with the average hardness increase to 400 HV. If the velocity varies with the degree of contamination as does the hardness then much higher velocities should be expected at the

surfaces. A first linear approximation for the longitudinal velocity, obtained using the hardness and velocity data for the 1 mm untreated and treated sheets, is given by the expression:

$$c_L = 6280 + 3.7 (HV - 300) \quad m/sec \tag{6.1}$$

where c_L is the longitudinal velocity and HV is the Vickers hardness. If this approximation is accurate then the velocity at the surfaces of the sheet would be some 10-12 % higher than in the untreated material.

The expression in equation (6.1) was also modified for the 4 mm sheet in order to account for the small variations in the properties of the two thicknesses of untreated material. Accordingly the velocity in the expression was reduced by 2 % , giving:

$$c_L = 6154 + 3.63 (HV - 300) \quad m/sec \tag{6.2}$$

This equation was then applied to the 4 mm treated sheet where the average hardness is about 365 HV. The resulting prediction for the average velocity through the sheet was 6390 m/sec, about 1 % higher than the measured value of 6350 m/sec. This good agreement indicates that the simple linear approximation for the variation of the properties is reasonably representative.

An assumption of 6 % increase in longitudinal velocity for severely contaminated alpha case is therefore rather conservative. Of course the key question is the realistic degree of contamination to be expected at the bondline of a poor joint. Currently the only evidence comes from the single poor bond where a local hardness value of 420 HV implies an increase in velocity of more than 6 %.

Attempt to detect reflection from alpha case boundary

In addition to the through-thickness velocity measurements, an attempt was made to detect whether a discrete reflecting boundary existed in the interior of the treated 4 mm sheet. If the alpha case exists as a discrete homogeneous layer then at normal incidence a significant pulse should be reflected from the interface between the alpha case and the parent titanium. Both focused and unfocused transducers were employed over a range of frequencies from 10 MHz to 50 MHz but no discrete reflection could be found other than grain boundary reflections when testing at high frequencies.

Measurements of Lamb wave velocities

Lamb wave velocity measurements were made in the untreated and treated 1 mm sheets as a further study of the anisotropy of the material. For ease of testing, the first symmetric mode (s_0) was used, excited by five cycles of a 1 MHz tone burst in a Gaussian window. Coupling to the sheet was achieved by a pair of broadband unfocused transducers set in perspex angle blocks and clamped to the sheet, as illustrated in Figure 6.5. Two signals were received: the first arrival of the Lamb wave at the receiving transducer (the reference signal), followed by the arrival some time later of the same signal after it had traversed the full length of the sheet twice, reflecting from both ends (the delayed signal). The velocity was then calculated by dividing twice the length of the sheet by the difference between the arrival times of the two signals. Velocity measurements were made in the rolling direction and normal to the rolling direction. The measurements are summarised in Table 6.1(b). Also shown are the predicted Lamb wave velocities, calculated using the measured values of the through-thickness velocities and the dispersion curve model.

The measurements show once again that there is strong anisotropy in both the untreated and the treated materials. In the untreated sheet the Lamb wave was some 5 % slower in the rolling direction than in the normal direction. After treatment it seems that the anisotropy remains in the material, a difference of 3 % being evident between the velocities in the two directions. The measurements also show again significant increases in velocity in the treated material compared to the raw material. Furthermore, the predictions of the s_0 velocity which were made using the measured through-thickness acoustic properties are faster than the measured s_0 velocities, indicating that material is stiffer in the through-thickness direction than in either direction in the plane of the sheet.

Measurement of density

Density measurements were made using the 4 mm untreated and the 4 mm treated sheets. A small piece of each sheet was ground on all sides so that its dimensions could be measured accurately. In the case of the treated sheet, care was taken to remove only a few tens of microns from the exposed surfaces in order to achieve flatness without losing any significant quantity of the alpha case. The densities were then calculated from precise measurements of dimension and weight.

The densities of the two specimens are shown in Table 6.1(c). As can be seen in the values, no difference in the density of the treated sheet could be detected within the

0.2 % measurement tolerance. It was therefore concluded that there is no significant difference in density between alpha case and titanium. This conclusion is consistent with the measurements which were reported by Weglein (1988), Thompson *et al.* (1992) and Brasche *et al.* (1992), who observed differences in density of 1 % or less.

6.5 Conclusions

An investigation has been conducted in order to determine the acoustic properties of alpha case and of titanium. Sheets of titanium have been exposed in air at high temperatures and measurements of their properties have been compared with those of untreated material and of a poor diffusion bond. The study included visual examinations of etched micrographs, hardness measurements across the thicknesses of the sheets, through-thickness velocity measurements, Lamb wave velocity measurements and density measurements.

The measurements which were made on the treated sheets of titanium show that the acoustic velocity in the material increases significantly when the material is exposed to air at high temperature. It appears from the hardness measurements that saturation does not occur even when the material is heavily exposed and it is concluded that the acoustic velocity must be assumed to vary with the degree of exposure. Comparison of the micrographs with the hardness measurements shows that the etch is very effective in revealing the extent of contamination. Comparison of the hardness and through-thickness velocity measurements indicates that a peak increase in acoustic velocity of more than 6 % should be expected at the bondline of the poor diffusion bond which was used for the hardness measurements. No difference in density could be detected between untreated titanium and alpha case.

Specimen	Longitudinal velocity (m/sec)	Shear velocity with rolling direction (m/sec)	Shear velocity normal to rolling direction (m/sec)
Untreated 1 mm	6280 ± 30	3150 ± 30	3290 ± 30
Untreated 4 mm	6160 ± 10	3140 ± 20	3200 ± 20
Treated 1 mm	6650 ± 50	3310 ± 50	3420 ± 50
Treated 4 mm	6350 ± 15	3210 ± 30	3280 ± 30
DB joint, first adherend	6250 ± 30	3170 ± 30	3240 ± 30
DB joint, second adherend	6170 ± 30	3180 ± 30	3160 ± 30

(a) Bulk wave velocities

Specimen	Measured velocity in rolling direction (m/sec)	Measured velocity normal to rolling direction (m/sec)	Predicted velocity in rolling direction (m/sec)	Predicted velocity normal to rolling direction (m/sec)
Untreated 1 mm	5110	5370	5340	5520
Treated 1 mm	5310	5490	5690	5820

(b) Lamb wave velocities

Specimen	Density (kg/m^3)
Untreated 4 mm	4407 ± 10
Treated 4 mm	4403 ± 10

(c) Densities

Table 6.1 Measured acoustic properties of titanium sheets

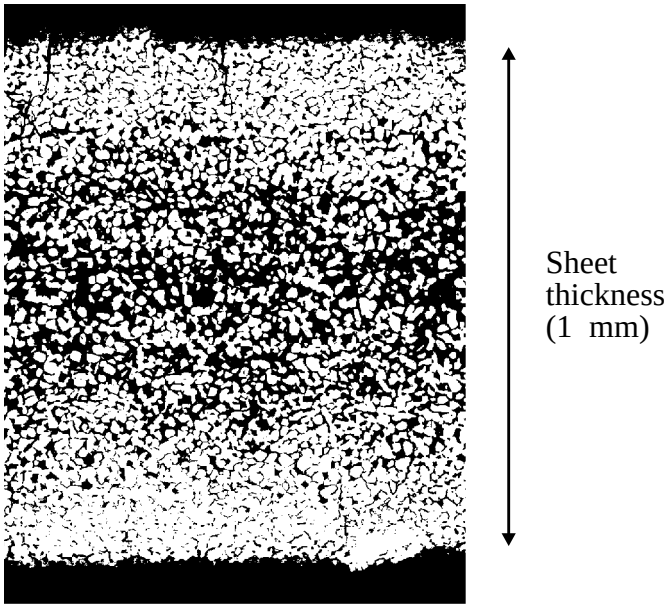

(a) Treated 1 mm thick sheet

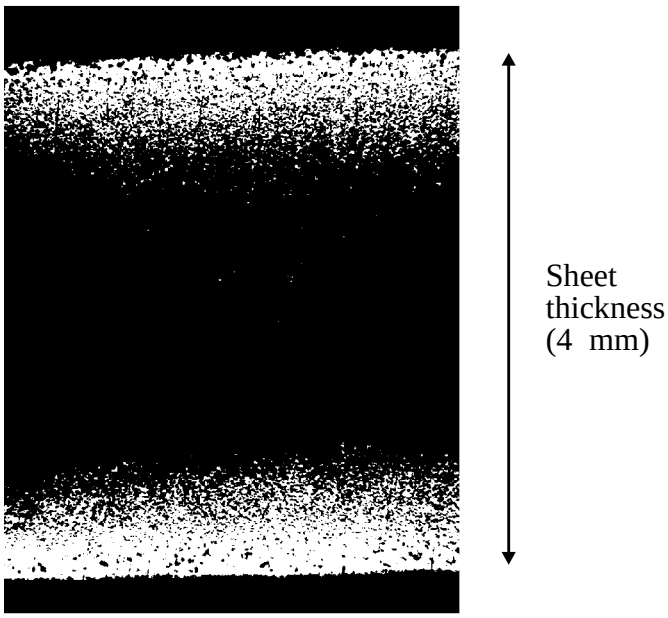

(b) Treated 4 mm thick sheet

Figure 6.1 Micrographs of sections through treated titanium sheets

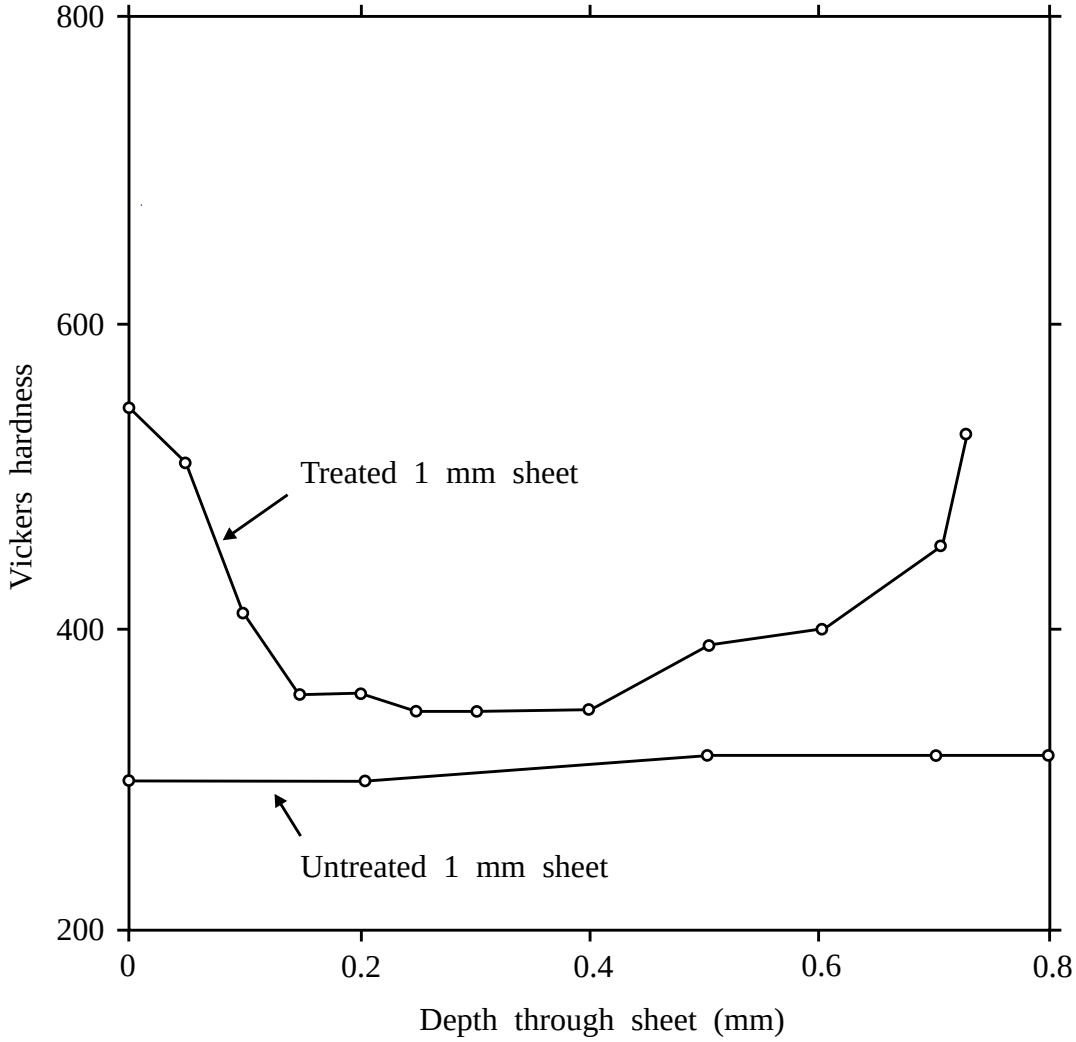

Figure 6.2 Microhardness across 1 mm thick titanium sheets

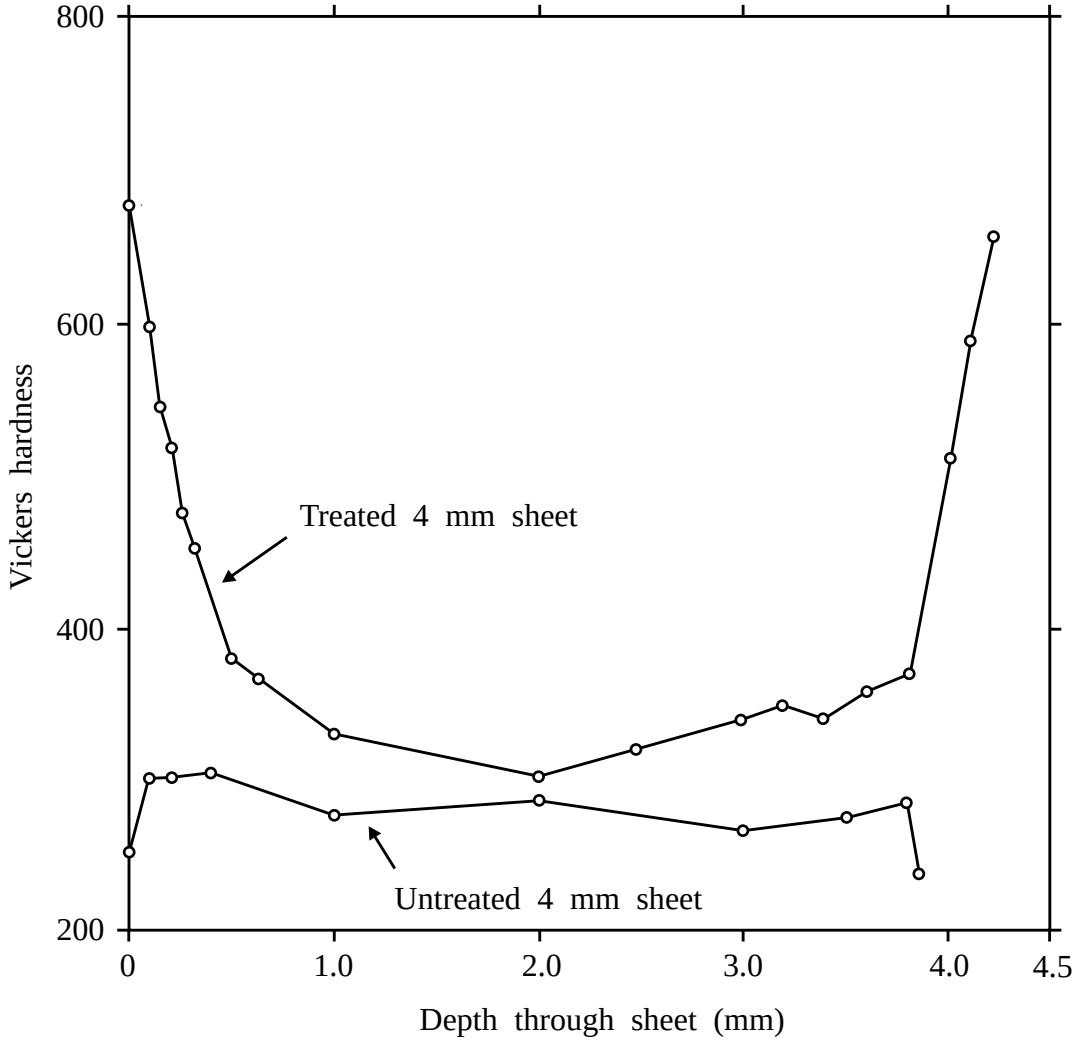

Figure 6.3 Microhardness across 4 mm thick titanium sheets

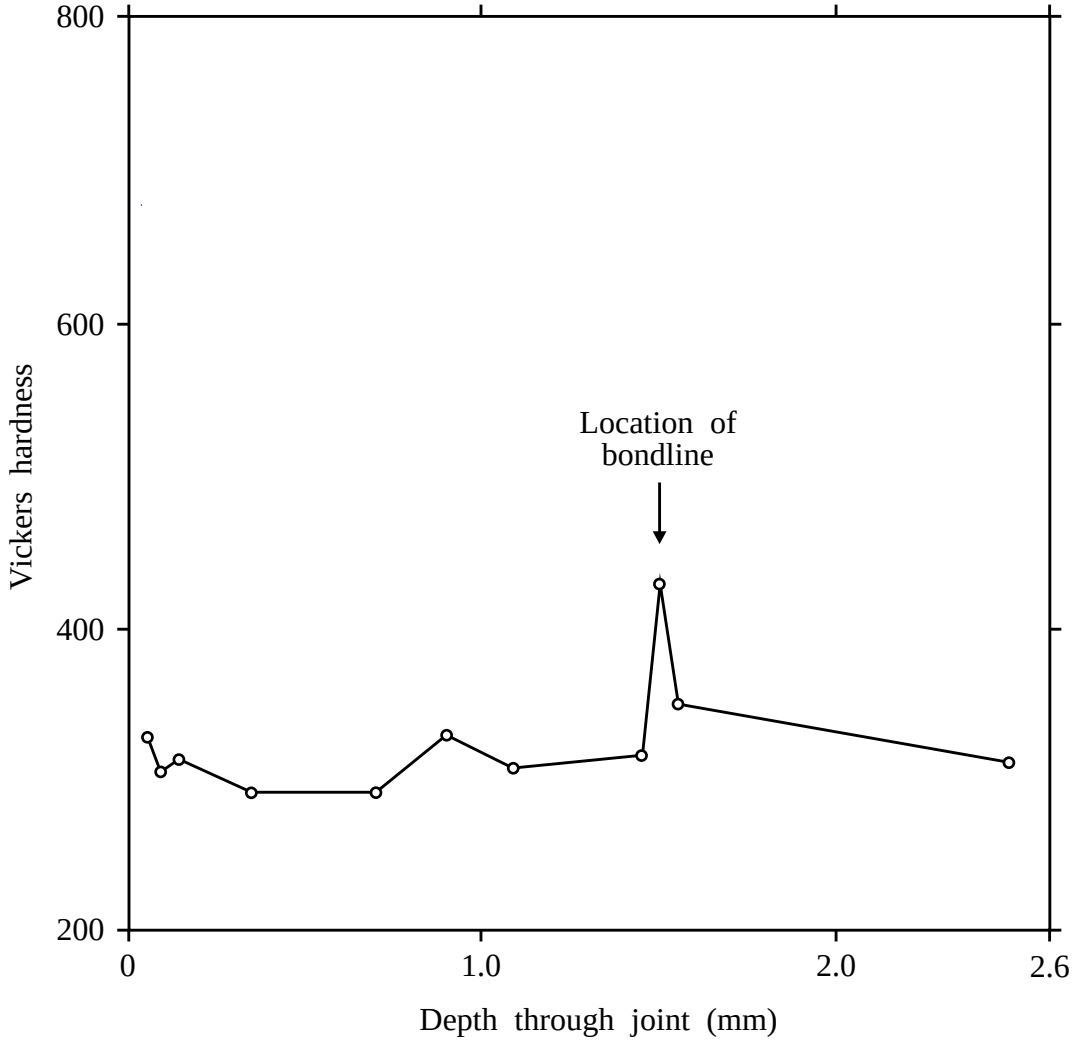

Figure 6.4 Microhardness across bondline of poor diffusion bond

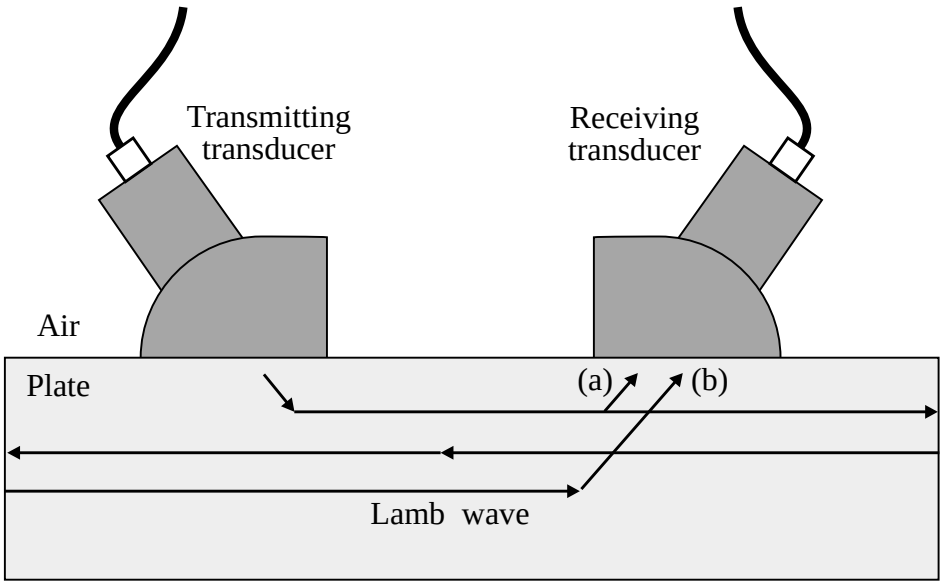

Received signals:
(a) = Reference signal
(b) = Delayed signal

Figure 6.5 Arrangement for measurement of Lamb wave velocities

CHAPTER 7

Normal incidence inspection

7.1 Introduction

In order to assess the potential of any new plate wave inspection technique it is important to have a measure of what can be achieved using the conventional approach. This chapter presents the results of two model studies which were conducted in order to determine the limits of the detectability of defects in diffusion bonded titanium using conventional normal incidence ultrasonic inspection.

The conventional ultrasonic technique for the detection of defects in plates, as introduced in Chapter 1, is to send an ultrasonic signal into the material and then to look for changes either in the transmitted signal on the other side of the plate or in reflections from the plate on the same side as the transmitter. The inspection is carried out at normal incidence, that is to say the transducers are aligned normal to the surface of the plate. For the detection of planar defects embedded in a joint whose adherends have the same acoustic properties it is clear that the latter approach, the pulse-echo method, is the preferred option. It has therefore been employed for the model studies.

The model studies each consisted of a series of simulations of normal incidence pulse-echo inspections, in which a range of inspection parameters and descriptions of the defects was employed. The simulations yielded predictions of the reflected time domain signal which would be detected by the receiving transducer. A realistic frequency response of the transmitting transducer was modelled and water coupling between the transducer and the joint was assumed.

Two model studies are reported, the first on the detection of alpha case at the bondline and the second on the detection of a planar array of voids at the bondline. The latter case is strictly outside the scope of this thesis but it was an important study because small voids are invariably present in poor bonds. It was therefore decided to include it in the presentation here.

7.2 Modelling approach

All of the response predictions were made using a model which was developed by T. Pialucha (1992). His response model was introduced and discussed in Section 5.4 of Chapter 5 where it was used as part of the validation of the modal model. It calculates the frequency domain reflection and transmission of plane waves from multilayered plates consisting of any numbers of layers of arbitrary thickness and arbitrary elastic or viscoelastic properties. An inverse Fourier transform may be applied to the frequency domain solution to yield predictions of the time domain signal which would be seen on an oscilloscope. In addition to the plane wave solutions the model may be used to simulate the response of a finite sized transducer.

In most cases a four layer model was used, as illustrated in Figure 7.1(a). The top layer was a semi-infinite half-space of water, representing the immersion coupling. The second layer represented the top adherend of the joint and the third layer, the defect at the bondline. The final layer represented the bottom adherend and was specified as a semi-infinite half-space because there was no interest in predicting any reflections from the bottom surface of the joint; indeed in practice any reflections following the bondline reflection would be gated out. The only exception to this geometry was when the defect was not described as a single layer but as multiple layers. This idealisation will be discussed in Section 7.3. In all cases the top adherend in the model was 4 mm thick. This thickness was chosen to be sufficiently large to give good separation in time of the top face echo and the bondline echo. However the materials were modelled as perfectly elastic, ignoring attenuation of the signal, so that the predictions are equally applicable to joints with other adherend thicknesses.

When simulating normal incidence response, Pialucha (1992) has shown that it is generally not necessary to include the finite dimensions of the transducer in the model (note however that it is important at certain large angles of incidence). The computation time for the finite transducer option is increased enormously over that for the plane wave model, so it was fortunate that all of the modelling reported here could be performed using the simplified infinite transducer model. This means that the predictions are for an infinitely wide plate with an infinitely wide transducer. The only significant limitation which may result from this assumption is that the predictions, which are a close match to an unfocused transducer, may underestimate the reflectivity achievable with a focused transducer.

Broadband excitation was chosen in order to give a short pulse in the time domain. The transducer response was simulated by a $\sin^6$ frequency response over the range from zero frequency to twice the centre frequency. Figure 7.1(b) shows the assumed frequency response for a 10 MHz centre frequency transducer, plotted on a linear amplitude scale. This distribution function was chosen because it is representative of the typical broadband transducer frequency response to pulsed excitation.

The reflection coefficient was defined as the amplitude of the reflection from the bondline normalised with respect to the amplitude of the reflection from the top surface of the joint. Referring to Figure 7.1(a) it is the ratio $|R_2| / |R_1|$. The paths of the pulses in the figure have been drawn at oblique angles for clarity; in all cases the predictions simulated normal incidence measurements.

7.3 Predictions of reflectivity from alpha case

In the first instance a single homogeneous layer of alpha case material was modelled at the bondline of a titanium joint. Typical acoustic properties of titanium were assumed, a longitudinal bulk velocity of 6100 m/s and a density of 4400 kg/m^3. The shear bulk velocity was not needed because it plays no part in the normal incidence response to longitudinal waves. The longitudinal velocity in the alpha case was assumed to be higher than in the parent titanium and the density was assumed to be unchanged, in accordance with the study of the material reported in Chapter 6. Two sets of results were calculated, one assuming the velocity increase to be 5 %, to 6400 m/s, and the other 10 %, to 6700 m/s. Predictions of the reflectivity from the joint were made over a range of thicknesses of the alpha case, in all cases employing a 50 MHz centre frequency transducer. Figure 7.2 shows the simulated time domain signal from one such prediction. Here the layer is 30 microns thick, the velocity of the alpha case is assumed to be 10 % higher than that of the titanium and the resulting bondline reflection is 35 dB lower than the top face reflection. Clearly a reflection of this magnitude would be detected very readily in practice.

The full sets of reflection coefficient results for the single homogeneous layer of alpha case with a 50 MHz transducer are plotted in Figure 7.3. Note that the reflection coefficient for other transducer frequencies can be deduced from the graphs because the horizontal axis is scaleable with the frequency-thickness product. Thus for example the plotted result for a 40 micron layer with a 50 MHz centre frequency transducer is applicable to an 80 micron layer with a 25 MHz centre frequency transducer.

As expected, the reflectivity vanishes when the thickness of the layer of alpha case approaches zero so that at the left of the graph the coefficient for both curves drops to minus infinity on the log scale. At the high thickness limit the response tends to that from a single interface between titanium and alpha case, the layer thickness becoming large enough so that the separate reflections from its front and back faces can be resolved. The peak of reflectivity is at about 30 microns layer thickness for both velocity assumptions. The trough at about 65 microns corresponds to resonance of the layer. Resonance of a layer occurs when standing waves can be set up in the layer, when the layer thickness is a multiple of the half wavelength of the signal. In this case the layer thickness is half of the dominant wavelength in the broadband signal of about 130 microns. Comparing the two sets of predictions it can be seen that the reflection coefficient for the 10 % faster alpha case is about 5 dB higher than for the 5% faster alpha case for all frequencies. For percentages between 5 % and 10 % it is a very good approximation to interpolate linearly on the plot.

Following these predictions two further sets of calculations were performed, assuming smoothly varying acoustic properties with depth of alpha case. The layer of alpha case was divided into a number of equal thickness sub-layers, each homogeneous. The acoustic properties of the sub-layers were specified according to a sinusoidal variation with depth, as illustrated in Figure 7.4(a). Thus the profile varied smoothly across the whole of the alpha case and blended smoothly with the adjacent adherends. In the first case the peak longitudinal velocity at the centre of the bondline was 10 % faster than in the parent material, falling gradually on each side of the bondline to the parent value at the 'edge' of the alpha case. In the second case the same profile was used but the peak velocity at the centre of the bondline was only 5 % faster than in the titanium. All of the results for the graded alpha case which are reported here were obtained using a 13 sub-layer idealisation; a convergence study using different numbers of layers confirmed that this number of sub-divisions was sufficient for the range of frequencies and thicknesses considered here.

The predicted reflection coefficients are plotted in Figure 7.5. As expected, the response from the smoothly graded alpha case is somewhat weaker than from the single layer. Now there is no upper thickness asymptote and in fact it becomes more difficult to detect the presence of the layer as its thickness increases. At first sight this observation seems surprising but it must be remembered that the peak acoustic velocity at the centre of the layer is the same for all thicknesses on each curve so that the acoustic impedance gradient decreases as the layer thickness is increased. Again the reflection coefficient for the

10 % faster alpha case is consistently higher than for the 5% faster alpha case, this time by about 6 dB.

A final study was made to examine the influence of the grading profile on the reflection coefficient. In addition to the smooth profile on each side of the bondline, a triangular profile and an intermediate profile were considered. The profiles are illustrated in Figure 7.4, in parts (b) and (c) respectively. For the triangular profile, the velocity is assumed to vary linearly with distance between the boundary with the titanium and the centre of the bondline. The intermediate profile gives a smooth blend at the interface between the titanium and the alpha case but a sharp gradient adjacent to the centre of the bondline. In reality the profile of the velocity in exposed sheets of titanium may be expected to follow the hardness profile, shown in Chapter 6, and would therefore best be modelled by the intermediate profile. However, in making a joint the surfaces of the sheets are not exposed after the bonding process has started. The diffusion of the oxygen during bonding is therefore likely to smooth out the profile so that the smooth profile would be most appropriate.

The results show that the grading profile has some influence on the reflection coefficient, particularly for large thicknesses of alpha case. At low thickness, the region of greatest interest, the largest difference between the predictions is about 2 dB. In general the reflectivity for low thicknesses is determined by the volume of the alpha case material (the area under the profile) because the wavelength is large compared to the thickness. For high thicknesses the reflectivity is governed more by local changes of acoustic impedance. Thus the reflectivity from the intermediate profile is low at low thickness because its area is relatively small but high at high thickness because of the very sharp change of gradient at the centre of the bondline.

Regarding the practical detection of an embedded layer of alpha case, the lower limit of detectability of defects will be governed by the degree and profile of the material stiffening of the alpha case, by the transducer characteristics, by the noise threshold and by any difference which may exist between the material properties of the two adherends. For small thicknesses the degree of material stiffening is extremely significant while the profile is relatively unimportant. Ideally the transducer and associated electronics should be selected to transmit a signal with a dominant quarter-wavelength which is as close as possible to the effective thickness of the alpha case. This should be possible for thicknesses down to about 20 microns using high frequency equipment, up to 60-80 MHz. Testing at higher frequencies will be limited by the grain scattering and attenuation in the adherend and so lower thicknesses of alpha case will be considerably

harder to detect. Significant levels of grain noise have been observed in the titanium sheets which have been studied in this research programme, and have also been reported by the researchers at Iowa State University (see Margetan and Thompson(1992)). In practice it seems that the noise threshold will be somewhat higher than -50 dB in high frequency measurements. Alpha case of 10-20 microns thickness would therefore be detectable only if the material stiffening was high. Finally, the reflection from a defect will be masked by a background reflection from the bondline if there is a difference between the properties of the two adherends. Fortunately the background reflection is relatively small for small differences in properties. A difference in longitudinal velocity of 1 % between the two adherends, such as was measured in the adherends of the poor diffusion bond in Chapter 6, results in a background reflection coefficient of only -59 dB.

7.4 Predictions of reflectivity from voids

The second study concerned the detection of voids at the bondline. Examination of a small number of micrographs of sections of the bondline of the poor diffusion bonded joint (one of them is shown in Figure 1.2 for example) suggests that the voids which can occur with the formation of low levels of alpha case are small, typically a few microns in diameter in the plane of the bondline and 1-2 microns normal to the bondline. These dimensions are one or two orders of magnitude lower than the wavelength in any practical normal incidence measurement of a joint.

The effect of the voiding was incorporated in the layer model by modifying the homogeneous properties of a 1 micron thick layer of material at the bondline. The stiffness across the bondline was calculated according to the 'Distributed Spring' model for penny-shaped cracks, proposed by Baik and Thompson (1984). This model gives a stiffness across the interface between two adherends corresponding to the stiffness across a layer of voids. It also predicts that even when the voids are small compared to the wavelength the stiffness is dependent not only on the area fraction of the voids but also on the void diameters in the plane of the bondline. The interface stiffness from this model was used to define the stiffness of the thin layer and the density of the thin layer was reduced from that of titanium according to the area fraction of voiding. Note that it is important to take the mass characteristics of the layer into account, even for very thin layers, when the impedance of the layer is of the same order as that of the adherends. This was shown in a theoretical analysis of interface models by Pialucha, Lowe and Cawley (1992). In this case the omission of the mass description would result in overestimation of the reflectivity. Alpha case was not included in the model.

Figure 7.7 shows the variation of the predicted reflection coefficients with the centre frequency of the broadband unfocused transducer, assuming a void diameter of 1 micron in the Distributed Spring model. Three curves are shown, each for a different area fraction of voiding. It can be seen that the reflectivity is strongly related both to the area fraction and to the transducer centre frequency. The sensitivity of the reflection coefficient to area fraction is also largely independent of frequency, the three curves being separated by about 6-8 dB over the whole frequency range. The nature of the response here is somewhat simpler than that of the embedded layer of alpha case. The layer thickness is much smaller than the wavelength of the signal (the first resonance of the layer would occur at about 3 GHz) and significant reflectivity is achieved only because the acoustic impedance of the layer differs strongly from that of the adherends.

A further set of calculations was made in order to show the influence of the void diameters on the reflectivity, in all cases assuming a 25 % void area fraction. The results, plotted in Figure 7.8, show a strong sensitivity of the reflectivity to the void diameter, with the 5 micron voids reflecting about three times as strongly as the 1 micron voids over the whole range of frequencies.

As with the embedded alpha case the practical limit of the detectability of voiding will be determined ultimately by the grain scattering noise threshold. Above this threshold the detectability will depend strongly on the void diameters and the best testing policy will simply be to work at the highest frequency which is practicable. Assuming a void diameter of 1 micron it seems that it should be possible to detect voiding down to about 20-25 % area fraction with high frequency equipment. However this assumption is probably rather conservative, the voids appearing to be elongated to some considerable extent in the plane of the bondline in the micrographs. Furthermore, unlike the embedded alpha case, there may be some variation in the extent of contamination on the scale of the spot size of the transducer so that local strong reflections may be found from concentrations of voiding even when the mean level of voiding is low.

7.5 Comparison with experimental measurements

If suitable well-characterised specimens had been available it would have been useful to make measurements of the reflectivity from bonds with a range of alpha case contaminations and a range of void sizes and distributions, for comparison with the predictions. This could also have enabled more to be discovered about the nature of the alpha case layers at the bondlines. However, as discussed in Chapter 6, the attempts to make a suite of test specimens have not been successful (to date).

Measurements on good bonds have shown no reflections whatsoever other than scattering from grain boundaries at high frequencies. Measurements on the only poor bond gave a reasonably strong reflection coefficient of -44 dB. The transducer was focused and had a nominal centre frequency of 80 MHz, although in practice the effective centre frequency was about 50-60 MHz after attenuation in the water and the adherend. Examination of micrographs of the bondline (Figure 1.2 for example) indicates that the alpha case is about 80 microns thick and that there is considerable voiding, covering between 20 % and 40 % of the bonded area. The voids are typically a few microns in diameter.

Assuming the smooth profile for the alpha case and a peak alpha case velocity somewhere between 5 % and 10 % higher than titanium, the predictions in Figure 7.5 are consistent with the measurement. Similarly, agreement is obtained between the measurement and the predictions for voiding (Figures 7.6 and 7.7) if a mean void diameter between 2 and 5 microns is assumed.

Of course these comparisons are rather approximate and are included here solely to indicate that the predictions of measurable reflectivity are consistent with the limited experimental evidence. If a range of specimens had been available for a full experimental study it would have been necessary to take into account the attenuation of the signal in the adherend (ignored in the model), the gain in reflectivity which is achieved by using a focused transducer rather than plane waves and the effects of combined alpha case and voiding.

7.6 Conclusions

Model studies based on normal incidence pulse-echo inspection have been used to simulate the reflection of ultrasonic pulses from alpha case embedded in titanium and arrays of voids in titanium. The latter case was included because of the tendency for voids to be present in poor bonds. Both types of defect present a challenge to ultrasonic testing methods. The alpha case is thin and has acoustic properties which are similar to those of the adherends and the voids, although contrasting well, are extremely small. However the fact that both of the adherends are always the same is enormously helpful because it provides the best possible testing conditions for normal incidence pulse-echo ultrasonic inspection. In a good bond there is no reflection from the bondline because the parent material is continuous across the joint. The detection of any reflection from the bondline therefore indicates the presence of a defect. Consequently it is possible to

detect features with dimensions which are more than an order of magnitude smaller than the dominant wavelength of the test signal.

Model predictions for alpha case embedded at the bondline of titanium joints have shown that it should be possible to detect layers of alpha case with thicknesses down to 20 microns or less using high frequency equipment (60-80 MHz) if the acoustic velocity of the alpha case differs from the titanium by at least 5 %.

Predictions for voiding at the bondline of titanium joints, assuming conservative void geometries, have indicated that it should be possible to detect voiding down to 25 % area fraction. The reflectivity is strongly sensitive to the diameter of the voids and so detection should be sensitive to spatial variations in void geometry.

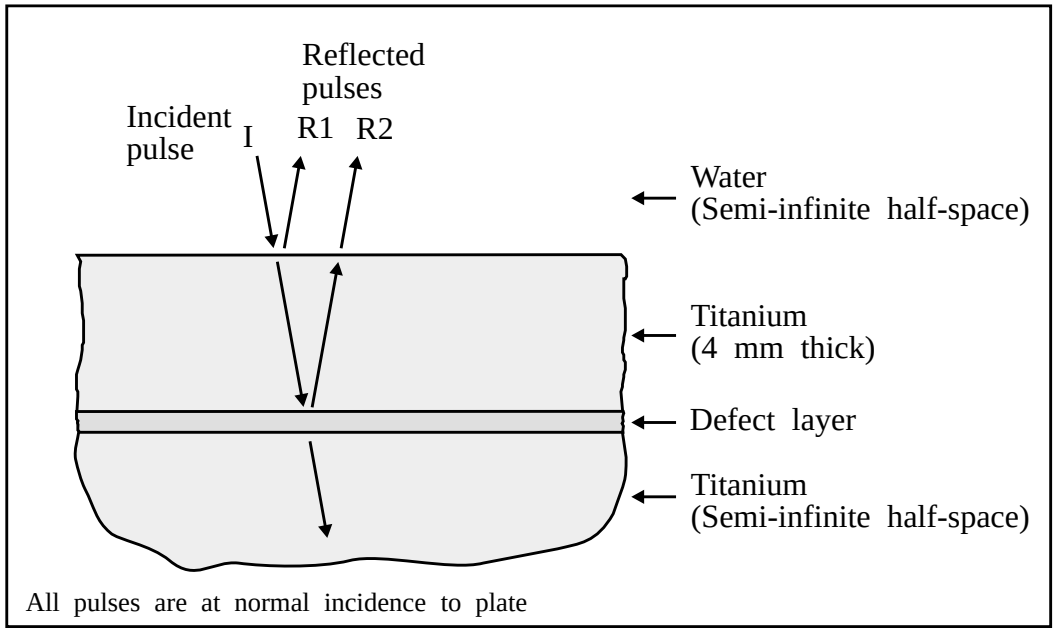

(a) Layer model

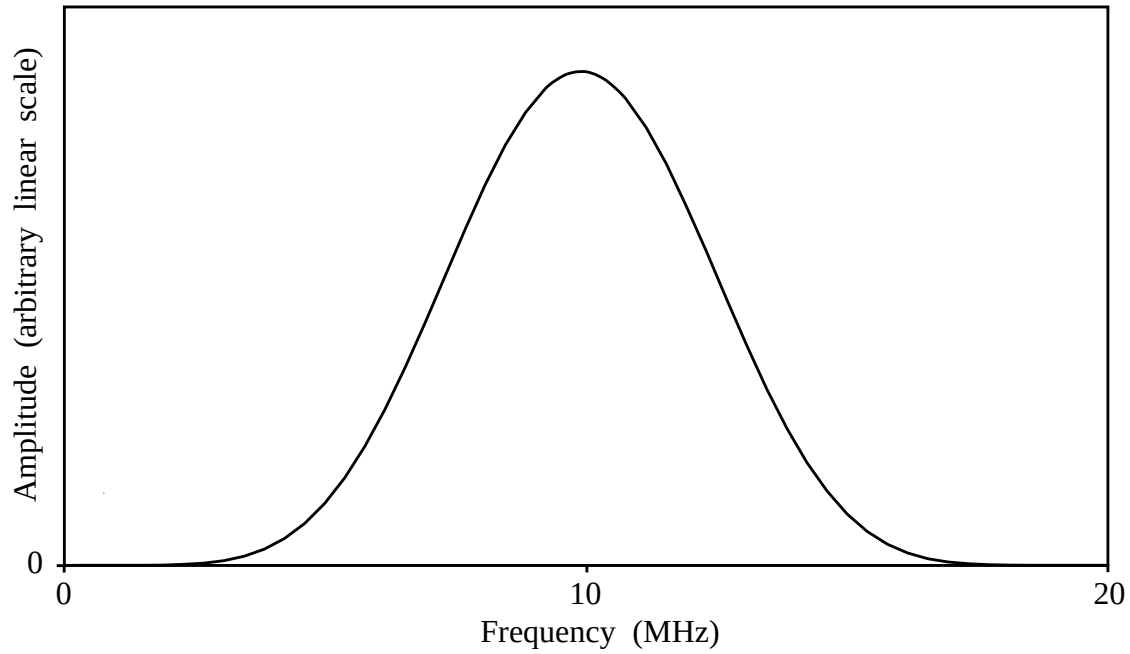

(b) Simulated frequency response of 10 MHz transducer

Figure 7.1 Model used for reflection coefficient predictions

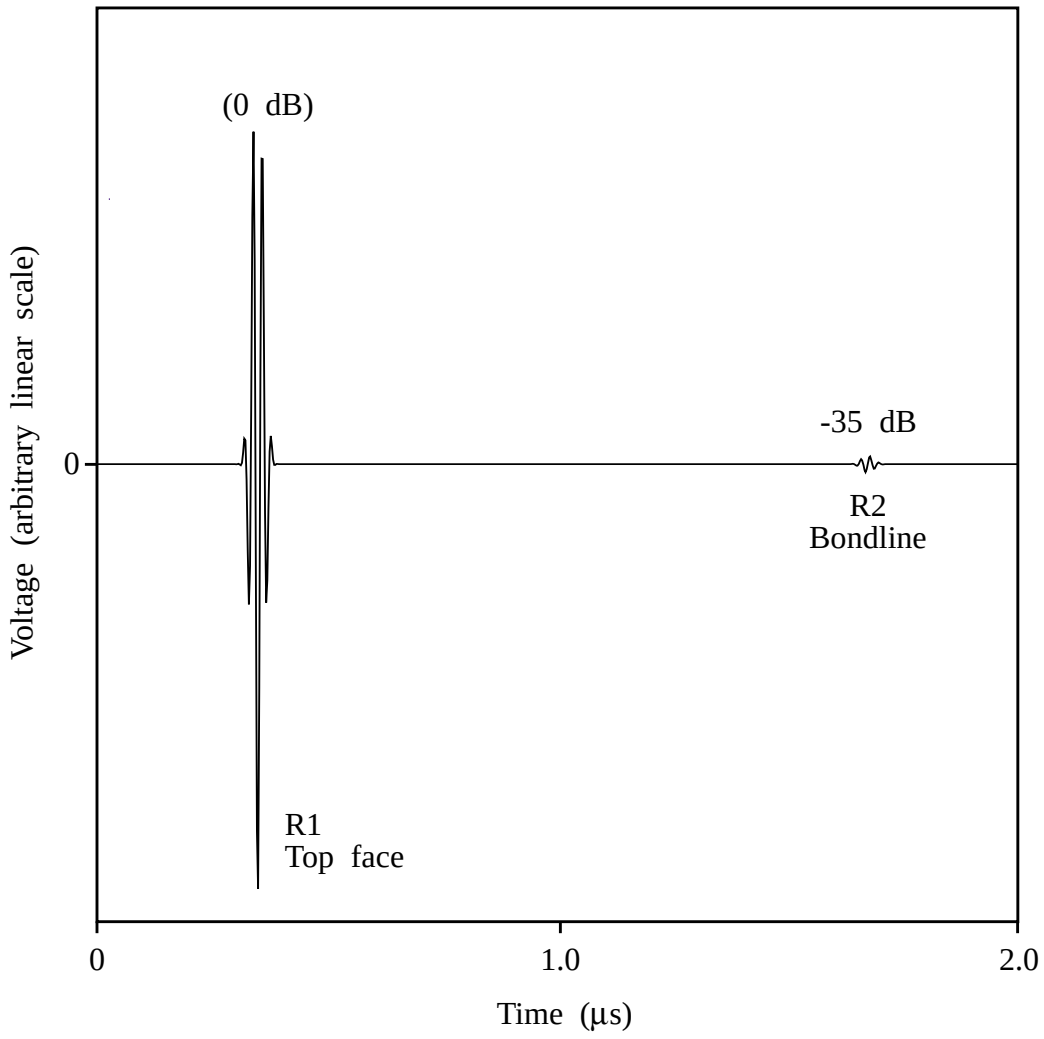

30 μm single discrete layer of alpha case with velocity 10 % faster than titanium, 50 MHz centre frequency transducer

Figure 7.2 Typical predicted normal incidence response from embedded alpha case

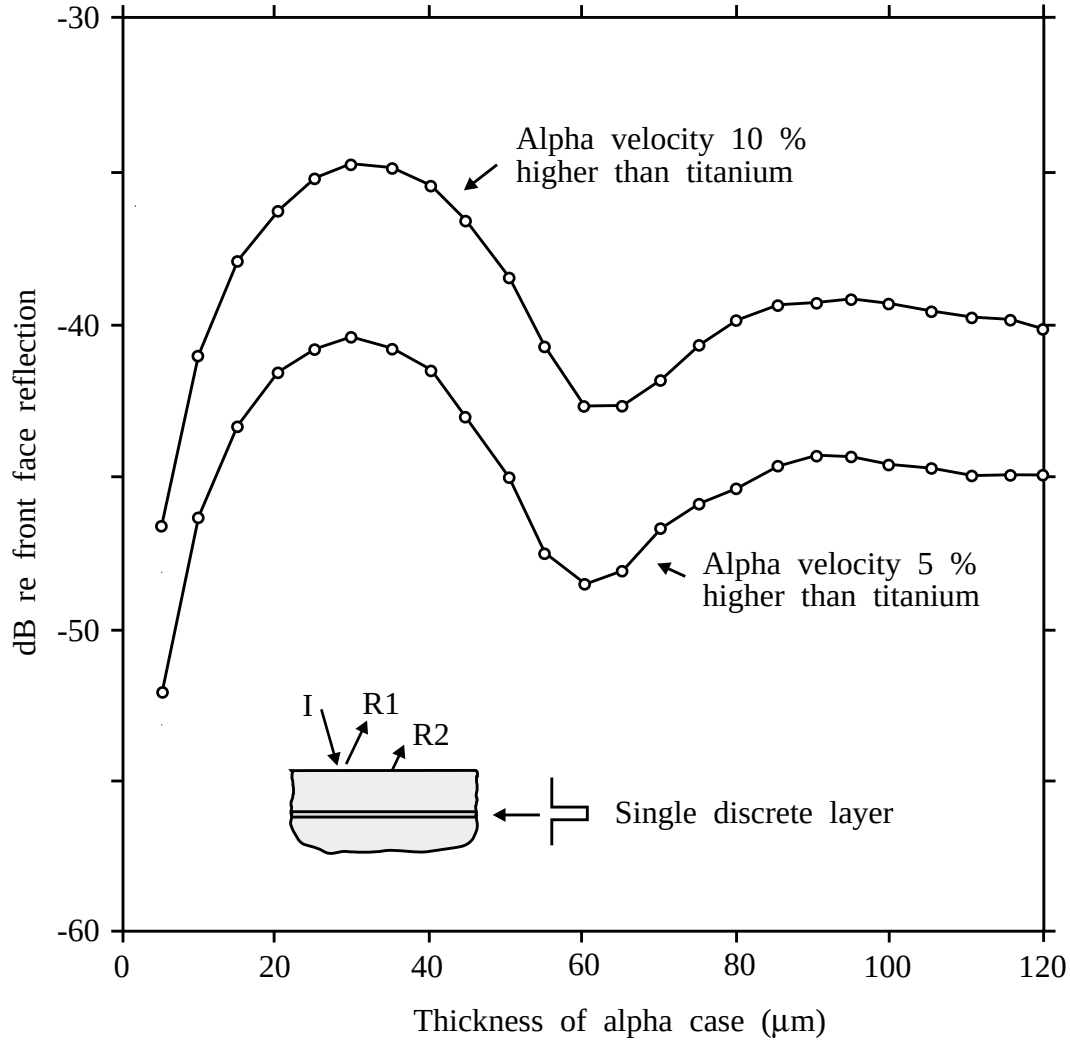

Figure 7.3 Reflection coefficient from embedded single discrete layer of alpha case, using 50 MHz transducer

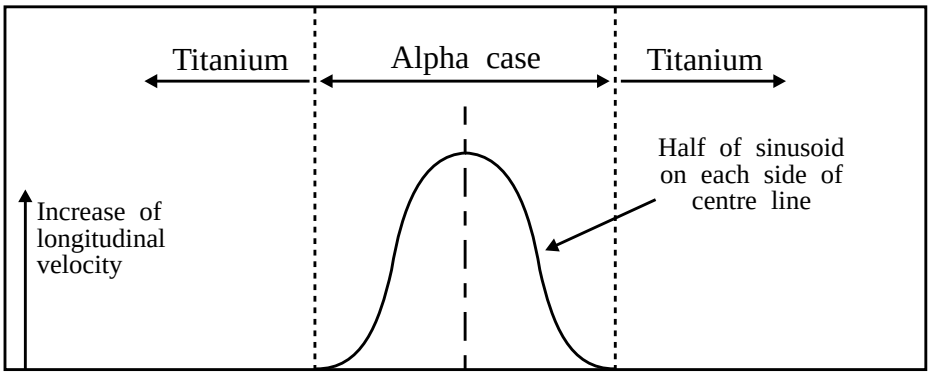

(a) Smooth profile

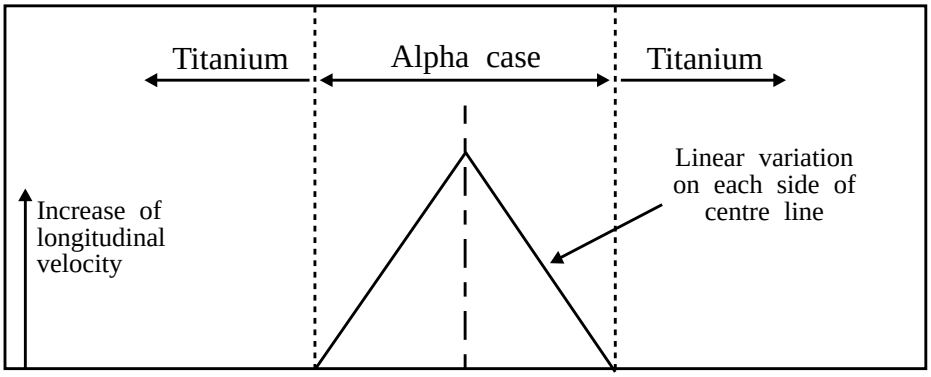

(b) Triangular profile

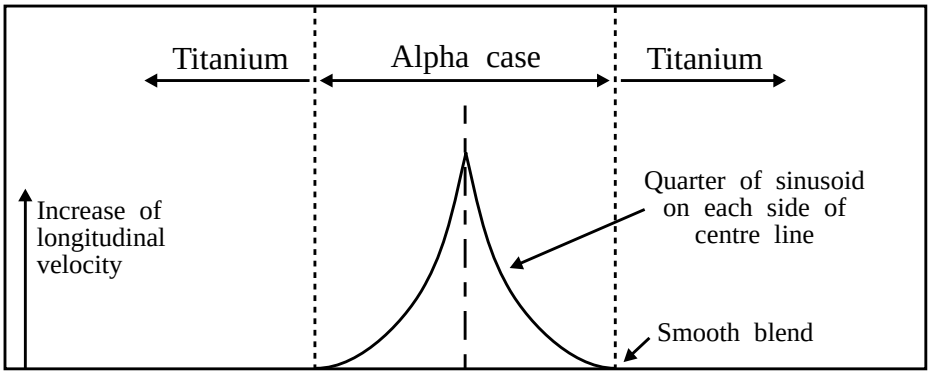

(c) Intermediate profile

Figure 7.4 Profiles of alpha case material properties used in models

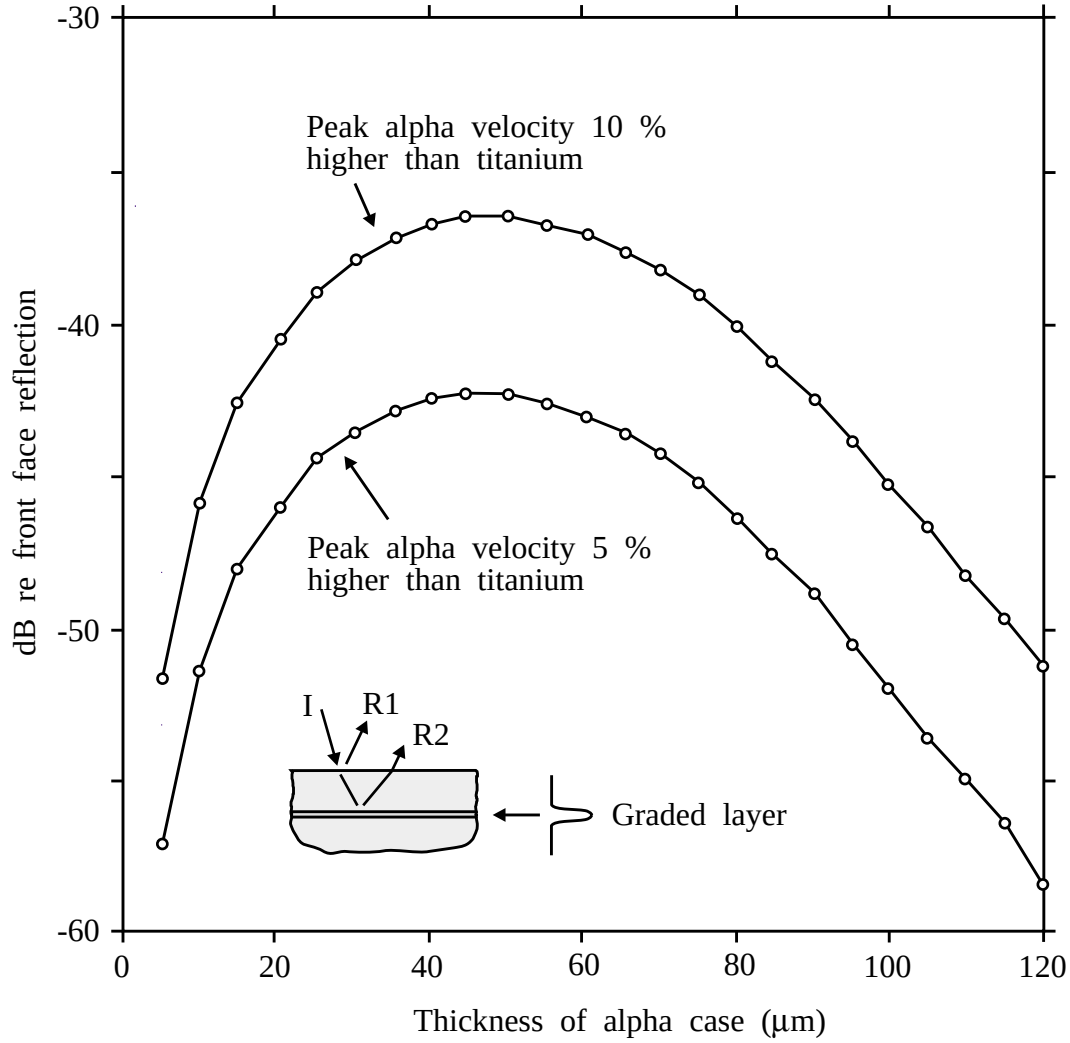

Figure 7.5 Reflection coefficient from embedded layer of alpha case with smooth profile, using 50 MHz transducer

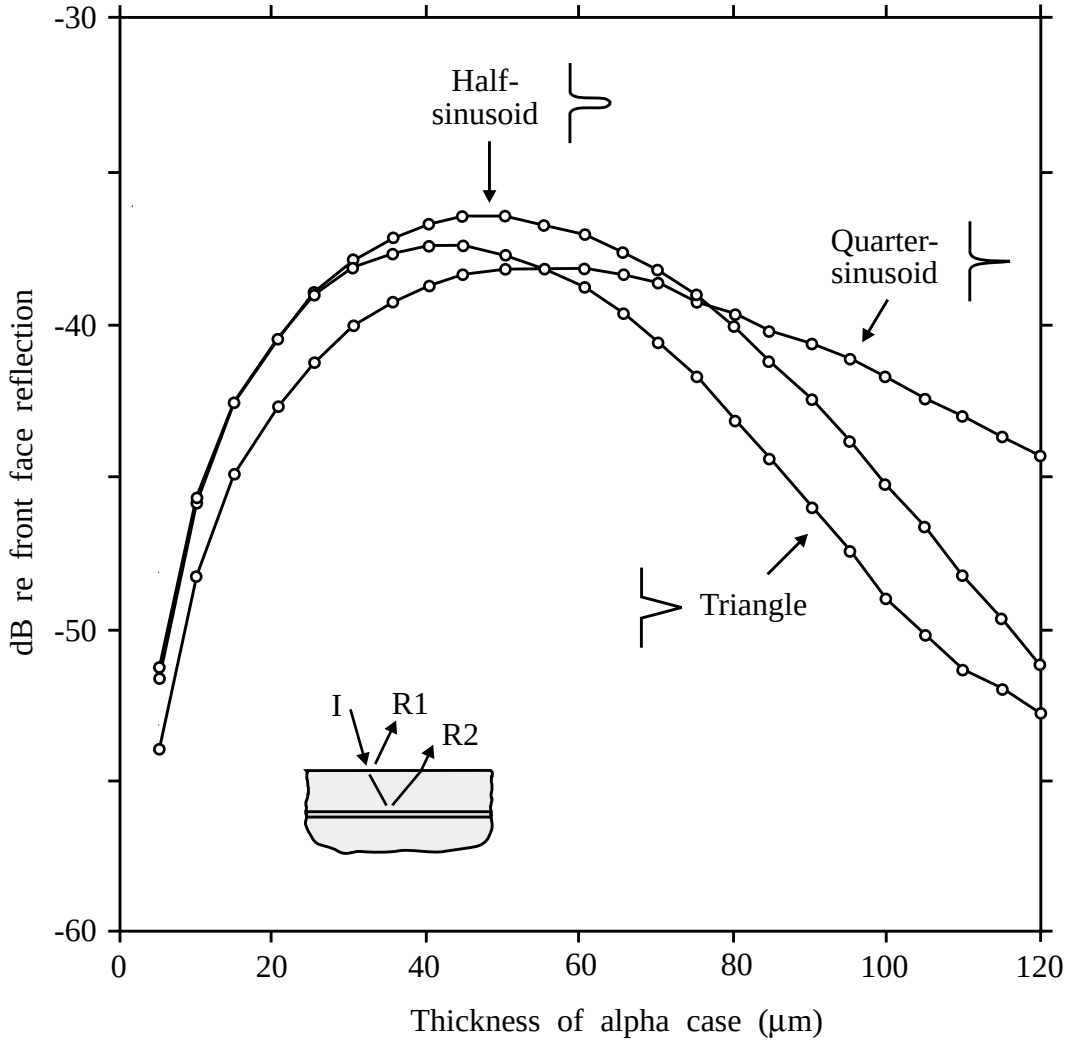

Peak alpha velocity 10 % higher than titanium in all cases

Figure 7.6 Reflection coefficient from embedded alpha case with different grading profiles, using 50 MHz transducer

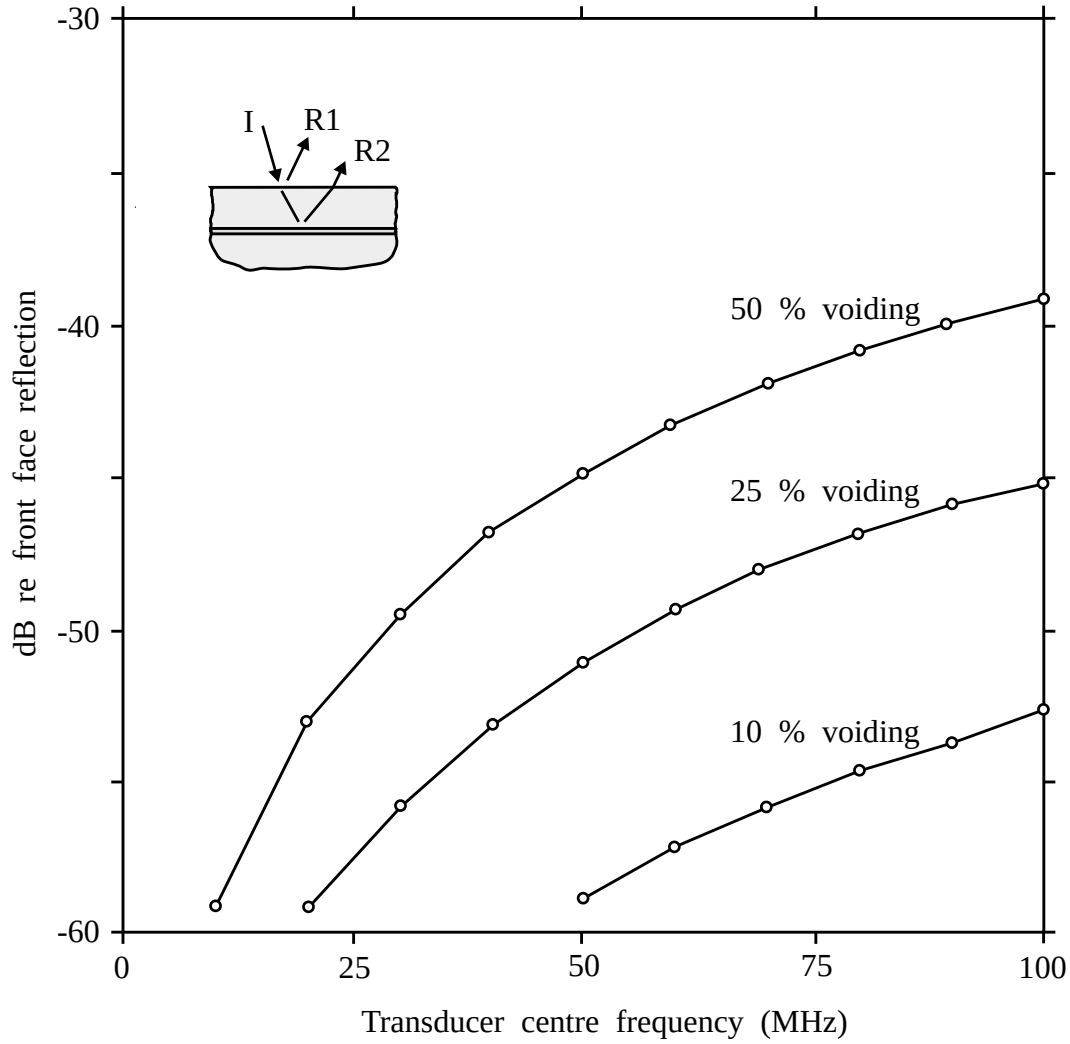

Figure 7.7 Reflection coefficient from distribution of 1 m diameter voids at bondline of joint

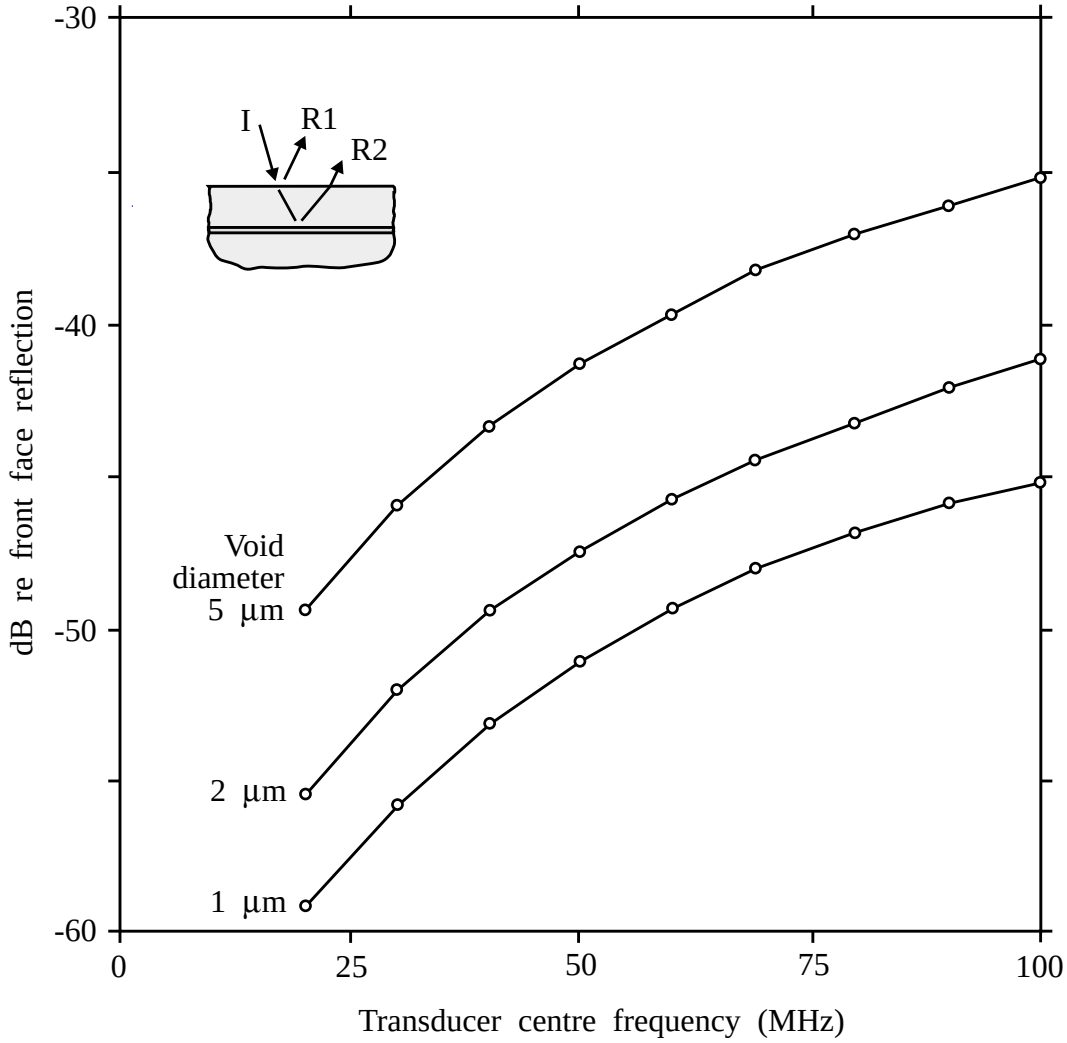

Void ratio 25 % in all cases

Figure 7.8 Reflection coefficient from distribution of voids at bondline of joint - Effect of void diameter

CHAPTER 8

Lamb wave technique

8.1 Introduction

This chapter presents the results of model studies which were made in order to assess the feasibility of using Lamb waves to detect the presence of alpha case at the bondline of a diffusion bonded joint.

The objective with the Lamb wave technique is to exploit any changes which an embedded layer of alpha case may make to the properties of the Lamb waves. For example if the velocity of a particular wave is altered by the presence of the layer then an inspection system could be based on detecting a change in the velocity of that wave. The plate waves in the defective joint are still loosely referred to as Lamb waves, although strictly speaking Lamb waves exist only in single-layer plates in vacuum, because they occupy the whole of the plate and they differ only slightly from true Lamb waves.

Clearly it is important to identify those waves which are most sensitive to the presence of the layer in order to assess the technique favourably. It is also important to take into account the sensitivity of the modes to possible variations of other parameters of the joint. Unless the other parameters of the joint are known accurately, the sensitivity of the detection of alpha case using any of these modes may be reduced or lost.

Overview

The investigation starts with a model study of the influence of alpha case and of other parameters of the joints on the dispersion curves. The modal model is used to predict the dispersion curves for a number of cases and the sensitivities of the modes to each parameter are quantified. The cases include the presence of alpha case at the bondline, both as a discrete layer and as a graded layer, alpha case offset from the centre of the joint and joints with different properties and thicknesses of adherends. The sensitivities of the modes to differences in each of the acoustic properties of the embedded layer are also predicted.

Following the parametric study, the excitation and measurement of Lamb waves is addressed. Two methods are reviewed, both involving the excitation of the waves by immersion coupling using the coincidence principle. In the first method the velocity of the wave is measured at some location downstream of the excitation point. In the second method, the 'null zone' method, the velocity or frequency of a mode is measured at the point of excitation.

The study is completed with a discussion of the implications of the model predictions. The most attractive modes for inspection are identified and the sensitivity of the technique is assessed by comparison with the sensitivity of the conventional normal incidence technique which was presented in Chapter 7.

8.2 Predictions of dispersion curves for defective joints

The reference case for the parametric study was a perfect diffusion bond with identical adherends, no embedded layers and a total thickness of 1.0 mm. The longitudinal velocity of the titanium was 6060 m/sec, the shear velocity 3230 m/sec and the density 4460 kg/m^3. The joint was assumed to be in vacuum. The reference case is therefore identical to the Lamb wave case for a single sheet of titanium which was presented in the examples in Chapter 5 and whose dispersion curves were shown in Figures 5.3 to 5.5 and 5.7.

The parametric study involved a series of calculations of the dispersion curves for variations of the parameters of the joint. In each variant case only one parameter was varied with respect to the reference case so that the influence of each parameter could be studied separately. The details of each case will be discussed in turn.

The results of the study are summarised in Figures 8.1 to 8.10 and Tables 8.1 to 8.4. The majority of the figures are plots of the dispersion curves of the joints, each showing the results of one variant and the reference case, the perfect bond. In all cases the solid lines are the dispersion curves for the perfect bond and the dashed lines for the variant case. For convenience all of the modes have been labelled with the conventional Lamb mode labels, a_0, s_0 etc., which were introduced in Chapter 5. Table 8.1 gives the values of selected velocities and frequencies of all of the cases and Table 8.2 repeats this information in the form of the percentage change of the parametric cases with respect to the reference case. In a similar fashion Tables 8.3 and 8.4 show the predictions of the through-thickness vibration frequencies of the joints. These are the frequencies of the

Lamb modes at infinite phase velocity, which would be excited using a transducer at normal incidence to the plate.

The dispersion curves may be scaled with the thickness of the joint, as discussed in general for Lamb waves in Chapter 5. Thus the predicted velocity of a mode at 1 MHz for the 1.0 mm plate would be appropriate at 0.5 MHz in a 2.0 mm plate. However all of the layer thicknesses must be scaled together. Therefore if the curves for a 1.0 mm plate with a 0.1 mm thick embedded layer are to be used to study a 2.0 mm plate then the implicit assumption is that the thickness of the embedded layer is also doubled, to 0.2 mm.

All of the predictions were made with the assumption that the plate was in vacuum and so all of the solutions are for free waves. However, as discussed and demonstrated in Chapter 5, the leaky Lamb wave velocities and frequencies for a titanium plate immersed in water are practically identical to those for the plate in vacuum, with minor exceptions. The parametric study is therefore applicable to inspection arrangements in which water is used as a coupling medium between the transducers and the plate. For completeness the solutions for leaky Lamb waves in a 1.0 mm plate are included in the tables in this chapter.

Single discrete layer of alpha case ('bad' bond)

For this set of predictions it was assumed that there was a layer of alpha case at the bondline of the joint. The layer was 0.1 mm thick and it was centrally positioned in the joint. The total thickness of the joint remained 1.0 mm so the two equal adherends were each 0.45 mm thick. The layer was assumed to be homogeneous with both longitudinal and shear velocities 10 % faster than in the titanium. The density was unchanged. The idealisation is therefore broadly in line with the results of the material study of Chapter 6 but is a rather severe case. The alpha case is fairly thick, is assumed to be discrete rather than graded and has a relatively high variation of its acoustic properties from the raw material. In a sense this case is also a reference case, being the basic idealisation of a poor diffusion bond. In the comparisons it will be referred to as the 'bad' bond case.

The dispersion curves for the reference case and for the variant are shown in Figure 8.1. Here the sensitivities of each of the modes to the presence of the layer can be seen immediately.

The first symmetric mode, s0, shows some sensitivity to the presence of the layer at low and medium frequencies in the figure, the change to the mode being an increase in velocity. At the low frequency limit the increase in velocity is to be expected from the nature of the mode. The wave is characterised by uniform stresses through the thickness of the plate, according to the plane stress analysis which was discussed in Chapter 5. Its velocity is therefore governed by an average value of the stiffness of the plate across its thickness. Indeed reference to Tables 8.1 and 8.2 shows the velocity increase of the wave to be 57 m/sec, about 1 %, which is consistent with such an analysis.

As the frequency is increased, the s_0 mode shows increasing sensitivity to the presence of the layer. At intermediate frequency-thickness products of 2-3 MHz-mm, it shows its greatest sensitivity, when the deformations of the plate are concentrated around the bondline. The deformations can be seen in the plots of the mode shapes in Figure 8.2 which have been calculated for a frequency-thickness product of 2.5 MHz-mm. At this location on the dispersion curve (indicated in Figure 8.1) the component of the displacement in the direction along the plate is no longer constant across the section, as it would be at the low frequency limit, but is much larger at the centre of the plate than elsewhere. The most useful revelation however is the peak in the strain energy density at the centre of the plate, indicating that the energy of the wave is concentrated in this region. The velocity of the mode is some 4 % higher than that of the reference case at this frequency-thickness.

As the frequency is raised further the s_0 mode is increasingly Rayleigh-like, the energy concentrating near the surfaces of the plate. It is therefore no surprise that the sensitivity of the mode to the presence of a centrally positioned layer diminishes. Clearly in the high frequency limit the mode must be completely insensitive to the properties at the centre of the plate.

In contrast, the first antisymmetric mode, a_0, shows no sensitivity to the layer at the low frequency limit and in general it shows very little sensitivity throughout its frequency range. This is consistent with the antisymmetric nature of the wave. At very low frequency it is characterised by bending of the plate and is therefore largely insensitive to the alpha case because of the location of the layer in the region of the neutral axis where there is very little strain. At intermediate frequencies the velocity of the mode is slightly higher than in the reference case but the mode is still antisymmetric and is still dominated by bending behaviour. At high frequencies the arguments which applied to the symmetric mode s_0 apply equally to the antisymmetric mode and in the limit the wave is completely insensitive to the embedded layer.

The higher order modes also show variations in their sensitivity to the layer. In general the mode shapes of a Lamb mode vary considerably along the length of the dispersion curve and, whereas they can be described in terms of integer multiple half-wavelengths at the normal incidence limit (infinite phase velocity), their compositions are much more complex at other locations. Indeed the number of 'half-waves' in the shapes of each mode increases as the frequency is increased. Consequently it is not surprising that the modes tend to have sensitive regions and insensitive regions, corresponding to relatively strong and relatively weak deformations near the bondline.

Of the higher order modes, mode s_2 shows the strongest sensitivity to the embedded layer within the range of velocity and frequency in the figure. At 6 MHz the presence of the layer causes an increase in velocity of 240 m/sec, about 4 % of the velocity of 6700 m/sec. On the frequency axis the difference is about 340 kHz, a 6 % increase, at this velocity. The mode shapes of s_2 at this location for the plate with the embedded layer are shown in Figure 8.3 and the location on the dispersion curve is indicated in Figure 8.1. As should be expected, the mode shapes show that the strain energy density is relatively high at the centre of the plate.

It is interesting to observe also that mode s_2 can be extremely insensitive to the presence of the layer. At normal incidence it is the least sensitive of the first four of the higher order modes, showing less than one tenth of a percent variation from the reference case. The normal incidence cut-off frequencies are tabulated in Table 8.3 and the percentage changes with respect to the reference case, in Table 8.4. The reason for its insensitivity is that it consists of two half-wavelengths of a shear wave through the thickness of the plate so that the stress at the centre of the plate is zero. The other three modes in the table consist of odd numbers of half-wavelengths through the thickness and do not have zero stresses at the centre. Mode a_1 consists of half a wavelength of a shear wave, mode s_1 of half a wavelength of a longitudinal wave and mode a_2 of one and a half wavelengths of a shear wave.

Graded layer of alpha case

In the context of the influence of the presence of alpha case on the Lamb waves in a plate, the variation of the alpha case properties across the layer is considered to be a detail. The Lamb waves are likely to be influenced by the volume of the alpha case material and by the average material properties; the profile is almost certainly of secondary importance. The majority of the parametric study was therefore based on

single embedded layers of homogeneous alpha case material. However in order to demonstrate the secondary nature of the profile it was decided to make one set of predictions using a graded layer.

A rather simple idealisation was chosen, in which the 0.1 mm thick layer was divided into three sub-layers of equal thickness. The central sub-layer was given 10 % faster longitudinal and shear velocities and the two adjacent layers were given 5 % faster longitudinal and shear velocities. The profile was therefore the simplest case of the triangular distribution which was modelled in the normal incidence reflectivity studies of Chapter 7.

The dispersion curves for this system are shown in Figure 8.4. Comparison of the curves with those of the reference case reveals again the sensitivity to the presence of the layer and, as was expected, the modes vary from the reference case in the same manner as they did for the single embedded layer in Figure 8.1. Furthermore, the variations are consistent with the assumption that the Lamb modes are influenced by the average material properties of the alpha case. The average acoustic velocities over the three sub-layers are 6.7 % faster than in the titanium, two thirds of the value for the 'bad' bond. Comparison of the velocities of s_0 at low frequency, in Table 8.1, shows that the effect of this case on the velocity is exactly two thirds of that of the 'bad' bond case. Similar ratios are also found when comparing all of the other results in the tables.

Alpha case offset from centre of joint

Figure 8.5 shows the dispersion curves for an asymmetric joint in which there is an embedded layer of alpha case and the two adherends are not of equal thickness. The 0.1 mm layer of alpha case is identical to that for the 'bad' bond except that it is offset from the centre line of the joint by 0.05 mm. One adherend is therefore 0.4 mm thick and the other is 0.5 mm thick. This case addresses the possibility that slight thinning may occur in one of the adherends, perhaps during superplastic forming, even though the adherends were expected to be the same thickness. Clearly if the two adherends are markedly different then any trends which are identified here would be much exaggerated but of course in such cases the asymmetry would be anticipated.

The dispersion curves show practically the same sensitivities to the presence of the offset layer as they did for the central layer. Comparing the tabulated velocities of s_0 at low frequency for this case and the 'bad' bond (Table 8.1), there is no difference at all within the given precision of 1 m/sec. Comparing the frequencies at 10 km/sec phase velocity,

in the same table, the two cases can be seen to agree to within a few kHz. At normal incidence the cut-off frequencies (Table 8.3) again agree to within a few kHz, the largest difference being 16 kHz for the a_2 mode. In conclusion therefore it appears that a small offset of the alpha case from the centre line of the bond has an insignificant effect on the dispersion curves.

Good bond with thicker adherends

In a sense this case is trivial because the frequency axis of the Lamb wave dispersion curves is known to scale linearly with the thickness of the plate. A 1 % increase in the thickness of the plate must therefore result in a 1 % reduction of the frequency for every point on each dispersion curve. However it is useful to plot this variant because it illustrates the strong sensitivity of the modes to the thickness of the plate. The changes of the dispersion curves can be seen to be of a similar order to those of the 'bad' bond, yet they are brought about by a very small change to the adherends.

Good bond with different acoustic properties

There are two further variants of the acoustic properties of a perfect bond which are also trivial cases. They have not been plotted here but their results can be summarised very simply. In the first case, if the bulk longitudinal and shear velocities of a single layer plate in vacuum are increased by a certain percentage then both the velocities and the frequencies of each mode are increased by that percentage. In the second case, if the density of a single layer plate in vacuum is changed then there is no change at all to the dispersion curves. These two deductions can be made without recourse to numerical analysis, by examination of Lamb's equations (see Lamb (1917) or Viktorov (1970)).

Good bond with unmatched adherends

One of the realistic possibilities with diffusion bonds is that there may be small differences between the properties of the adherends. In fact the measurement of the properties of the two adherends of the poor diffusion bond in Chapter 5 revealed a 1 % difference between their acoustic velocities, arising perhaps from differences in their strain histories during superplastic forming. Another possibility is that the two adherends may be anisotropic and may be bonded such that their rolling directions are not parallel. Whereas a small degree of anisotropy is unlikely to affect the validity of the analysis, provided that the appropriate material properties are used, the difference in the properties between two adherends may be quite significant. A set of dispersion curves was

therefore calculated for a good bond in which one of the adherends had 1 % faster longitudinal and shear velocities than the reference values. The adherends were of equal thickness and there was no embedded layer.

The results are shown in Figure 8.7. They show a general trend of an increase in velocity for all of the modes, as would be expected if the bulk velocities of the whole of the plate were increased. Indeed, the velocity of s_0 at low frequency is increased by exactly 0.5 %, consistent with the average values of the properties of the plate. There is also an increase in frequency which can be seen clearly in the normal incidence cut-off frequencies in Tables 8.3 and 8.4. The frequencies all increase by exactly 0.5 %, again consistent with the average properties of the plate. In conclusion it seems that the modes are rather sensitive to the properties of the adherends, as revealed in the previous case, but that they have no particular sensitivity to a small degree of asymmetry.

Layer with faster longitudinal velocity

The final three cases of the parametric study have been included simply to show independently the influence of the three acoustic properties of the layer on the dispersion curves. In all three cases a 0.1 mm thick layer was assumed to be embedded centrally in the joint, so that the geometry was identical to that of the 'bad' bond.

In the first case the longitudinal velocity of the layer was increased by 10 %, the shear velocity and density being identical to the adherends. The results are plotted in Figure 8.8. The trends in the dispersion curves reflect the modes which are sensitive to the presence of the alpha case and whose composition is dominated by longitudinal wave components. This can be seen very clearly in the values of the cut-off frequencies. The shear modes a_1, s_2 and a_2 are completely insensitive to the change whereas the longitudinal mode s_1 is quite strongly affected. Of particular interest are the relatively small changes to the lowest order modes a_0 and s_0.

Layer with faster shear velocity

In the second case illustrating independently the influence of the acoustic properties of the embedded layer, the shear velocity of the layer was increased by 10 %, the longitudinal velocity and density being identical to the adherends. The results are plotted in Figure 8.9. Now a different pattern of influence can be seen in the curves, revealing those modes whose composition is dominated by shear waves. Amongst them can be seen the low order modes a_0 and s_0.

Layer with higher density

In the final case illustrating independently the influence of the acoustic properties of the embedded layer, the density of the layer was increased by 10 %, the longitudinal and shear velocities remaining identical to the adherends. The results are plotted in Figure 8.10. There is no change to the velocity of s_0 at low frequency but in general most modes show some sensitivity to the increase in density. The direction of change is also not uniform, some modes showing increases in frequency (or velocity) and some showing decreases. For the problem being addressed here, the detection of alpha case, it seems that the density of the layer is no different from the density of the adherends and so this information is not required. However, in general, if an embedded layer has a different density it is clear that this influences the dispersion curves even though the density plays no part in the true Lamb wave solutions.

The increase in frequency of a curve when the density of the layer is increased seems surprising when considered in the context of the principles of vibration theory, the frequencies of vibrating structures decreasing when masses are increased. However, the analogy is not strictly correct in the case of Lamb waves. Consider the Lamb wave dispersion curves for a single layer. The curves depend only on the bulk velocities of the material and the thickness. On the other hand vibration frequencies depend on density (or mass) and stiffness. The stiffness and density of the material are accounted for implicitly in the dispersion curves because they define the bulk velocities, according to equation (2.9), but they are not prescribed separately. An increase in density, without changing the bulk velocities, is therefore accompanied by an increase in stiffness. Accordingly, in the case considered here, both the stiffness and the mass of the layer of alpha case are increased.

8.3 The measurement of Lamb waves

If Lamb waves are to be used to exploit any of the sensitivities which have been observed in the model study it is important to be able to measure the velocities and frequencies of the waves in a selective manner. There are two aspects to this. First, a method of excitation should ideally be employed in which the energy can be focused on a particular location on the dispersion curve diagram so that particular waves can be launched. Second, a method of measurement should be used which can determine accurately the velocities and frequencies of the modes.

The excitation of Lamb waves

The selective excitation of Lamb waves can be achieved with considerable success using the coincidence principle which was discussed in Chapter 5, Section 5.2 and was illustrated in Figure 5.6. The principle states that an incident wave in a coupling medium may be used to excite a plate wave if the component of its wavenumber in the direction along the plate matches the wavenumber of the plate wave. This means that waves with high phase velocities are excited and received using small angles of incidence and waves with low phase velocities using large angles.

Ideally the coincidence principle could be used to excite a wave at a precise location on a dispersion curve by using an infinitely wide plane wave transducer and a single frequency signal. In practice of course this is not possible. Waves do not leave the face of a finite transducer solely in the normal direction but are spread over a range of angles. The transducer cannot therefore be aligned to excite plate waves of a single velocity, its energy can only be centred on a particular velocity. Similarly it is not possible to work with a single frequency, only with a range of frequencies.

However it is possible to direct the energy into a small zone of the dispersion curve diagram by controlling the angle of the transducer and the frequency of the signal. The practical excitation of plate waves using the coincidence principle is illustrated in Figure 8.11. Typically an unfocused transducer is used, with water coupling to the plate. The velocity of the centre of the excitation zone is defined by the angle of incidence of the transducer and the velocity range of the excitation zone results from the beam spreading characteristics of the transducer. The frequency of the excitation zone is determined by the frequency characteristics of the signal. Clearly by selecting the angle of incidence and the input signal it is possible to place the excitation zone at the desired location on the dispersion curve diagram.

The frequency range of the excitation zone may be minimised by using a long tone burst. Additionally, at a later stage in the measurements, when a signal is received, windowing in the frequency domain may be used to limit the examination of the received signal to the frequency of interest. The velocity range of the excitation zone decreases as either the test frequency or the transducer diameter is increased. Additionally, an array of parallel 'fingers', like a comb, may be used to partially shade the ultrasonic beam in the coupling medium in order to limit the transmission of energy to a particular wavelength (see Viktorov (1970)).

Remote measurement of velocity

The obvious way to measure the velocity of a plate wave is to measure the time it takes to travel a known distance. A typical scheme is illustrated in Figure 8.12(a). A receiving transducer is set at the same angle to the plate as the transmitter, some distance downstream, so that it detects a leaking signal from the plate. A second signal is then recorded at a known distance further downstream and the velocity is calculated from the separation distance and the time difference between the two signals.

If the wave is dispersive then the shape of the signal changes as it propagates and the calculation of the time difference is not so straightforward. However, measurements can be made by comparing the two signals in the frequency domain, using for example the amplitude spectrum method (Pialucha, Guyott and Cawley (1989)). Indeed this technique can usefully be employed to determine the velocity of a dispersive wave at a number of frequencies within the range of frequency of the signal.

A second difficulty arises if the excitation zone covers more than one mode, in which case more than one wave may propagate along the plate. Alleyne (1991) discussed the difficulties associated with multimode signals and developed a method of measuring the modes separately in the received signal. A general discussion of the long range propagation and measurement of Lamb waves may also be found in his thesis.

A third consideration is the attenuation of the waves. As was discussed in Chapter 5, Lamb waves can exhibit considerable attenuation in water, so that it may not be possible to detect them at remote locations. One technique to avoid this difficulty is to use local immersion only, at the positions of the transducers (Alleyne (1991)). An alternative of course is to receive the signal as close to the transmitter as possible. In the extreme, a signal may be received by another part of the transmitting transducer, as is the case when a defocused acoustic microscope is used to measure surface wave velocities (see Weglein (1985) for example).

The accuracy of the measurement of the velocities of plate waves using such techniques is generally determined by the mechanical considerations such as the precision of the positioning of the transducers and the degree of flatness of the plate. Accuracies of better than 1 % can typically be achieved (Alleyne (1991)).

Point measurement of velocity or frequency

An alternative approach, one which is extremely attractive for the inspection of diffusion bonds, is the 'null zone' technique. With this technique the fact that a wave has been excited is detected by a measurement at the location of excitation. Proponents of the application of this technique to plate waves have included Mal, Bar-Cohen and co-workers who have successfully measured Lamb waves over a wide range of the dispersion curves for adhesive joints and have demonstrated excellent agreement with the theoretical curves. See Mal, Xu and Bar-Cohen (1989) for example.

The technique works by exploiting the interference of the specular reflection of the excitation signal from the plate with the leaking field immediately downstream of the transmitter, which occurs when plate waves are excited. The mechanism is illustrated in Figures 8.12(b) and 8.13. Figure 8.12(b) shows the arrangement of a pair of transducers with their centre lines meeting at a point on the plate. Figure 8.13(a) shows the dispersion curves for the s_0 mode for a good bond (the reference case) and for the 'bad' bond. Figure 8.13(b) shows a prediction of the reflected field from the good bond using a 10 mm diameter transducer, at a frequency of 2.5 MHz (infinite tone burst) and an angle of incidence of 21.119 degrees. The prediction was made in exactly the same manner as was described in the validations in Section 5.4 of Chapter 5, using the response model which was developed by Pialucha (1992). Since the angle and frequency correspond to a position on the dispersion curve, in part (a) of the figure, a wave is excited in the plate and it leaks energy downstream of the centre line of the reflected beam. The leakage is out of phase with the specular reflection and so causes some cancellation of the received signal, the extent of the cancellation clearly depending on the size of the receiver.

If the transducers are swept through a range of angles, as shown in Figure 8.12(b), and are excited with a narrow band signal, then the angles at which modes exist can be determined by detecting the minima in the reflection amplitude, corresponding to the null zones when the cancellations occur. Simulations of the amplitude of the received signal from such a sweep are shown for the good bond and for the bad bond in Figure 8.14(a), for a single frequency of 2.5 MHz (infinite tone burst), assuming a pair of 10 mm diameter transducers. The difference between the locations of the minima for the two joints corresponds to the difference between their velocities at this frequency, which can be seen in Figure 8.13(a). Similarly, if the angles of the transducers are fixed and a frequency sweep is performed then the frequencies of the modes may be located, as illustrated for the same cases in the simulation in Figure 8.14(b). Again the difference

between the locations of the minima can be seen to correspond to the difference between the frequencies of the dispersion curves.

8.4 Discussion

The idea of using Lamb waves for the inspection of the material at the bondline in bonded plates is not new. As was discussed in Chapter 1, a number of researchers have worked in this field, in particular with regard to adhesively bonded aluminium joints. Reviews may be found in Dewen (1991) or Dewen, Lowe and Cawley (1992). The problems which the researchers have addressed are the evaluation of the thickness and acoustic properties of the adhesive and the properties of the interfaces between the adhesive and the adherends. The acoustic properties of the adhesive give an indication of its strength (the cohesive properties) and the interface properties reveal the quality of its attachment to the adherends (the adhesive properties).

The main progress in this field has been achieved by Mal, Bar-Cohen and co-workers. Mal, Xu and Bar-Cohen (1989) generated dispersion curves for adhesive joints and compared them with measurements. Karim, Mal and Bar-Cohen (1990) and Xu, Mal and Bar-Cohen (1990) reported the development of an inversion algorithm which could be used to determine the cohesive properties and the adhesive thickness of a joint from the Lamb wave dispersion curves. Bar-Cohen and Mal (1990) used the algorithm to determine these properties from experimentally constructed dispersion curves. Mal, Xu and Bar-Cohen (1990) also calculated dispersion curves for joints in which one of the interfaces between the adhesive and the adherends was assumed to be unbonded and they suggested that the inversion of measured Leaky lamb wave data may be used to detect this extreme case of poor adhesion.

The developers of the inversion technique have achieved some success in the detection of the cohesive properties of joints when the other parameters are well characterised. However a parametric study by Dewen, Lowe and Cawley (1992) indicated that the dispersion curves for realistic aerospace joints are rather sensitive to small changes in the properties of the adherends. They concluded that Lamb waves are unlikely to offer any significant advantage over normal incidence inspection techniques.

The task of inspecting diffusion bonded joints differs from that of adhesive joints because of the nature of the objective. In an adhesive joint the adhesive layer is known to be present and the primary objective is to detect its homogeneous properties. In a diffusion bonded joint the primary objective is to detect whether a layer is present at all. The latter

task is clearly simpler in principle. However the layer thickness of the alpha case to be detected is likely to be much smaller than the thickness of the adhesive in an adhesive bond and, furthermore, the acoustic impedance of alpha case differs only slightly from the titanium adherends. Therefore, although Lamb waves have been studied quite extensively in the context of adhesive joints, it is not immediately evident from such results what level of sensitivity may be achieved if the technique is applied to diffusion bonds.

Considering the modelling study which is presented in this chapter, the implications for the development of an inspection technique are not promising. The dispersion curves show some sensitivity to the presence of a centrally embedded layer of alpha case so in principle the inspection should be possible. The curves are also insensitive to a small offset of the layer from the centre of the joint which would be an advantage in practice because of the realistic possibility of slight differences between the thicknesses of the two adherends. They are also insensitive to the profile of the acoustic properties of the alpha case, depending only on the average properties and the thickness of the layer. This is an advantage when the objective is to detect the presence of the layer but proves clearly that the method could not be used to characterise the layer. However the serious drawback which was demonstrated by the predictions is that, as was found in the studies of adhesive joints, the dispersion curves are much more sensitive to the bulk velocities of the adherends and the overall thickness of the joint than they are to the properties of the embedded layer.

In identifying the best modes for an inspection scheme it is important therefore to consider the nature of the sensitivities of the modes to the bulk velocities of the adherends and to the thickness of the joint. In the former case the dispersion curves are affected in both the frequency and velocity axes and in the latter case, solely in the frequency axis. In general it is to be expected that the material properties of the adherends are likely to be known more precisely than the thickness of the joint. Consequently in practice the frequency axis of the dispersion curves for a good bond will be less well known than the velocity axis. It follows that the best testing locations on the dispersion curve diagram are the regions of modes which show strong sensitivity to the embedded layer and have low dispersion.

Following this argument, the obvious candidate is the first symmetric mode, s_0, at very low frequency. It shows some sensitivity to the presence of the layer and is insensitive to small variations in the thickness of the joint. However the sensitivity is not strong, the velocity increasing by only 1 % when a 0.1 mm thick layer of alpha case is embedded in

a 1.0 mm thick joint. This percentage is typical of the error margin which can be achieved in careful velocity measurements on ideal specimens in the laboratory. Furthermore if the adherends were thicker but the alpha case remained at 0.1 mm thickness then the sensitivity would be reduced, roughly in linear proportion. Thus the increase in velocity would be 0.1 % for a 10 mm thick joint.

There is greater sensitivity to the presence of the layer in the s_0 mode and in the s_2 mode at the two locations marked in Figure 8.1 at which the mode shapes were calculated. In both cases the sensitivity is about 4 % for a 0.1 mm thick layer in a 1.0 mm thick joint, four times that of the s_0 mode at low frequency. However unfortunately the modes are strongly dispersive at these locations and so they are very sensitive to the thickness of the joint. Any inspection method which utilised them would therefore have to include a separate, extremely accurate, measurement of the thickness of the joint. This presents a serious difficulty, as discussed in the context of adhesive joints by Dewen (1991). In order to detect the layer in the joint considered here, it would be necessary to know the thickness of the joint to an accuracy better than 1 %. Worse still, in order to detect the same thickness of layer in a 10 mm joint it would be necessary to know these quantities to an accuracy of better than 0.1 %.

By comparison, the use of normal incidence ultrasonics is considerably more attractive. The case of the 0.1 mm thick layer in a 1.0 mm thick joint is very much an upper bound description of a poor joint, the layer being relatively thick and the joint relatively thin. According to the analysis of Chapter 7 such a layer would be detected rather easily using the conventional pulse-echo inspection technique.

8.5 Conclusions

Model studies have been conducted to investigate the potential of utilising Lamb waves for the detection of an embedded layer of alpha case in a diffusion bonded joint.

A parametric study was undertaken using the modal model in order to determine the sensitivity of the Lamb waves to the presence and properties of the layer and also to other parameters associated with a joint. Although the sensitivity to the presence of the layer was not strong, the study revealed the modes which are most sensitive and led to the identification of the most suitable locations on the dispersion curves for the inspection. It also revealed however that the modes are strongly sensitive to the properties of the adherends, specifically to their bulk acoustic velocities and to the total thickness of the joint.

The practical potential of utilising Lamb waves is further ill-fated by the success of the conventional normal incidence method. Comparing the two methods, the best sensitivity which could be achieved using the Lamb wave technique falls far short of that which is possible using the normal incidence technique. Furthermore, the Lamb wave technique would be more complicated to implement in practice than the conventional method.

It was therefore concluded that the Lamb wave inspection scheme could work in principle but its sensitivity to the presence of the embedded layer falls short of normal incidence testing and it suffers from unwanted sensitivity to other properties of the joint.

	Velocity at zero frequency (km/sec)	Frequency at velocity of 10 km/sec (MHz)			
Case	Mode s_0	Mode a_1	Mode s_1	Mode s_2	Mode a_2
Good bond (Reference case)	5.466	1.975	2.814	4.353	4.970
Layer of alpha case ('bad' bond)	5.523	2.012	2.853	4.413	4.996
Graded layer of alpha case	5.504	2.000	2.841	4.393	4.988
Alpha case offset from centre of joint	5.523	2.011	2.853	4.417	4.998
Good bond with thicker adherends	5.466	1.955	2.786	4.309	4.920
Good bond with unmatched adherends	5.493	1.989	2.828	4.385	4.997
Layer with faster longitudinal velocity	5.485	1.975	2.841	4.415	4.970
Layer with faster shear velocity	5.496	2.012	2.828	4.341	4.996
Layer with higher density	5.466	1.994	2.831	4.318	4.959
Good bond in water	5.466	1.975	2.649	4.351	4.970

Table 8.1 Predicted Lamb mode velocities and frequencies at selected locations on dispersion curves

	Change of velocity at zero frequency (%)	Change of frequency at velocity of 10 km/sec (%)			
Case	Mode s_0	Mode a_1	Mode s_1	Mode s_2	Mode a_2
Good bond (Reference case)	0	0	0	0	0
Layer of alpha case ('bad' bond)	1.04	1.87	1.40	1.40	0.53
Graded layer of alpha case	0.69	1.29	0.96	0.93	0.36
Alpha case offset from centre of joint	1.04	1.84	1.38	1.48	0.56
Good bond with thicker adherends	0.00	-1.00	-1.00	-1.00	-1.00
Good bond with unmatched adherends	0.50	0.72	0.51	0.75	0.56
Layer with faster longitudinal velocity	0.34	0.00	0.96	1.43	0.01
Layer with faster shear velocity	0.54	1.87	0.48	-0.27	0.53
Layer with higher density	0.00	0.95	0.59	-0.79	-0.21
Good bond in water	0.00	-0.01	-5.88	-0.03	0.00

Table 8.2 Percentage change of selected velocities and frequencies of Lamb modes with respect to reference case

	Frequency at normal incidence (MHz)			
Case	Mode a_1	Mode s_1	Mode s_2	Mode a_2
Good bond (Reference case)	1.615	3.030	3.230	4.845
Layer of alpha case ('bad' bond)	1.643	3.083	3.232	4.926
Graded layer of alpha case	1.635	3.067	3.231	4.901
Alpha case offset from centre of joint	1.643	3.082	3.237	4.910
Good bond with thicker adherends	1.599	3.00	3.198	4.797
Good bond with unmatched adherends	1.623	3.045	3.246	4.869
Layer with faster longitudinal velocity	1.615	3.083	3.230	4.845
Layer with faster shear velocity	1.643	3.030	3.232	4.926
Layer with higher density	1.630	3.057	3.200	4.884
Good bond in water	1.615	3.030	3.230	4.845

Table 8.3 Predicted frequencies of Lamb modes at normal incidence

	Change of frequency at normal incidence (%)			
Case	Mode a_1	Mode s_1	Mode s_2	Mode a_2
Good bond (Reference case)	0	0	0	0
Layer of alpha case ('bad' bond)	1.76	1.76	0.06	1.67
Graded layer of alpha case	1.21	1.21	0.03	1.16
Alpha case offset from centre of joint	1.71	1.71	0.21	1.34
Good bond with thicker adherends	-1.00	-1.00	-1.00	-1.00
Good bond with unmatched adherends	0.50	0.50	0.50	0.50
Layer with faster longitudinal velocity	0.00	1.76	0.00	0.00
Layer with faster shear velocity	1.76	0.00	0.06	1.67
Layer with higher density	0.90	0.90	-0.92	0.80
Good bond in water	0.00	0.00	0.00	0.00

Table 8.4 Percentage change of frequencies of Lamb modes at normal incidence with respect to reference case

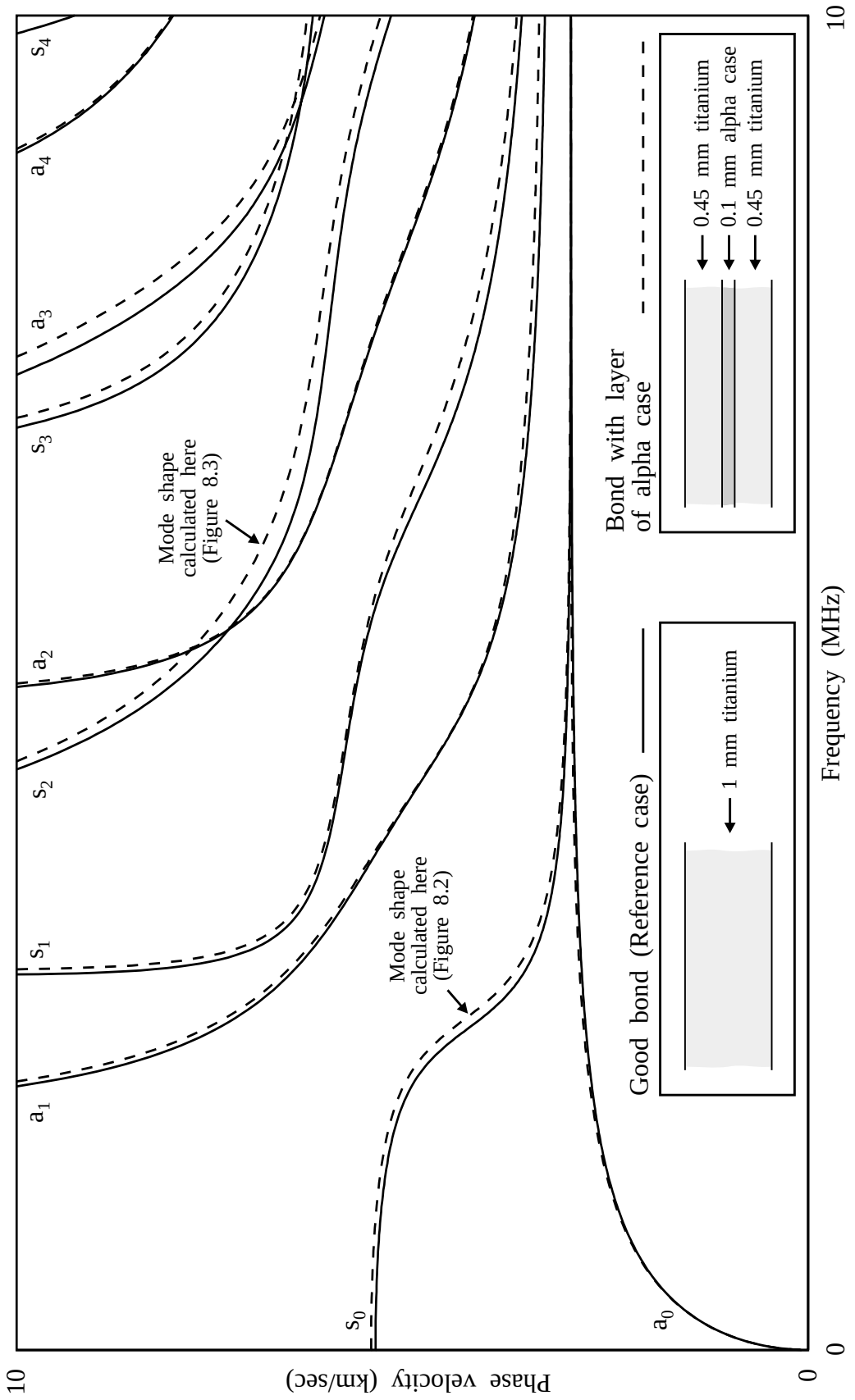

Figure 8.1 Lamb wave dispersion curves for titanium - influence of: Layer of alpha case

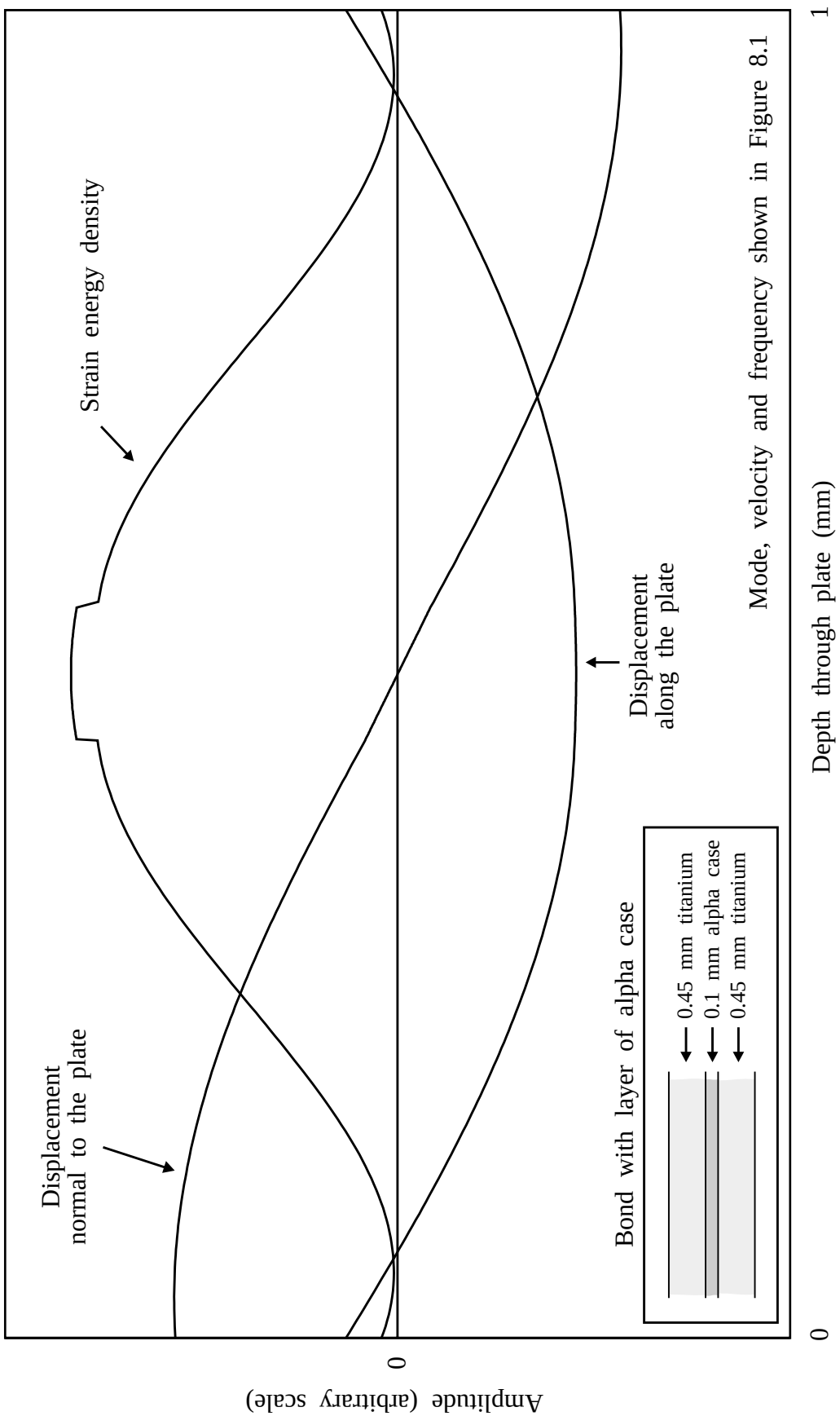

Figure 8.2 Mode shapes of Lamb mode s_0 for plate with embedded layer of alpha case

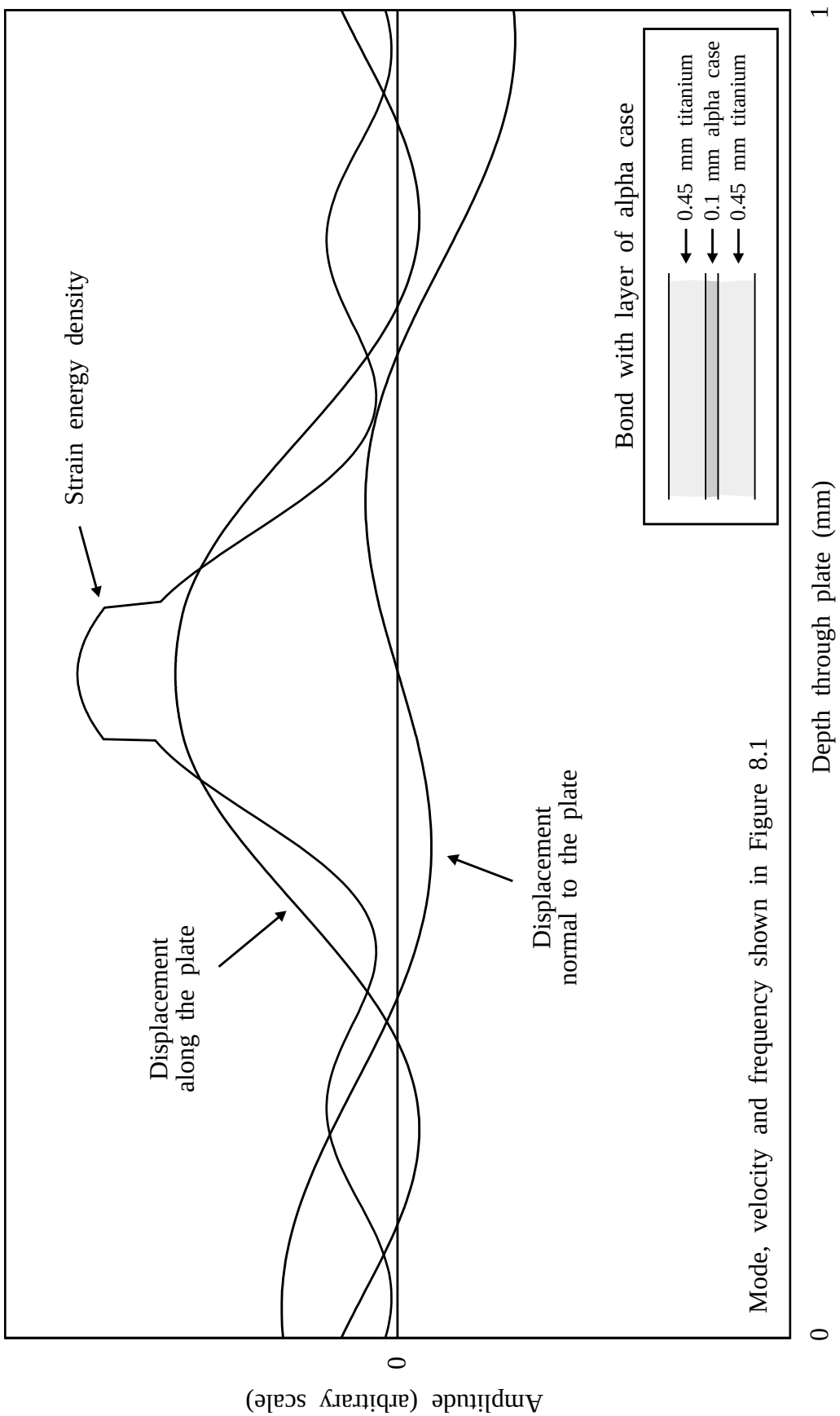

Figure 8.3 Mode shapes of Lamb mode s_2 for plate with embedded layer of alpha case

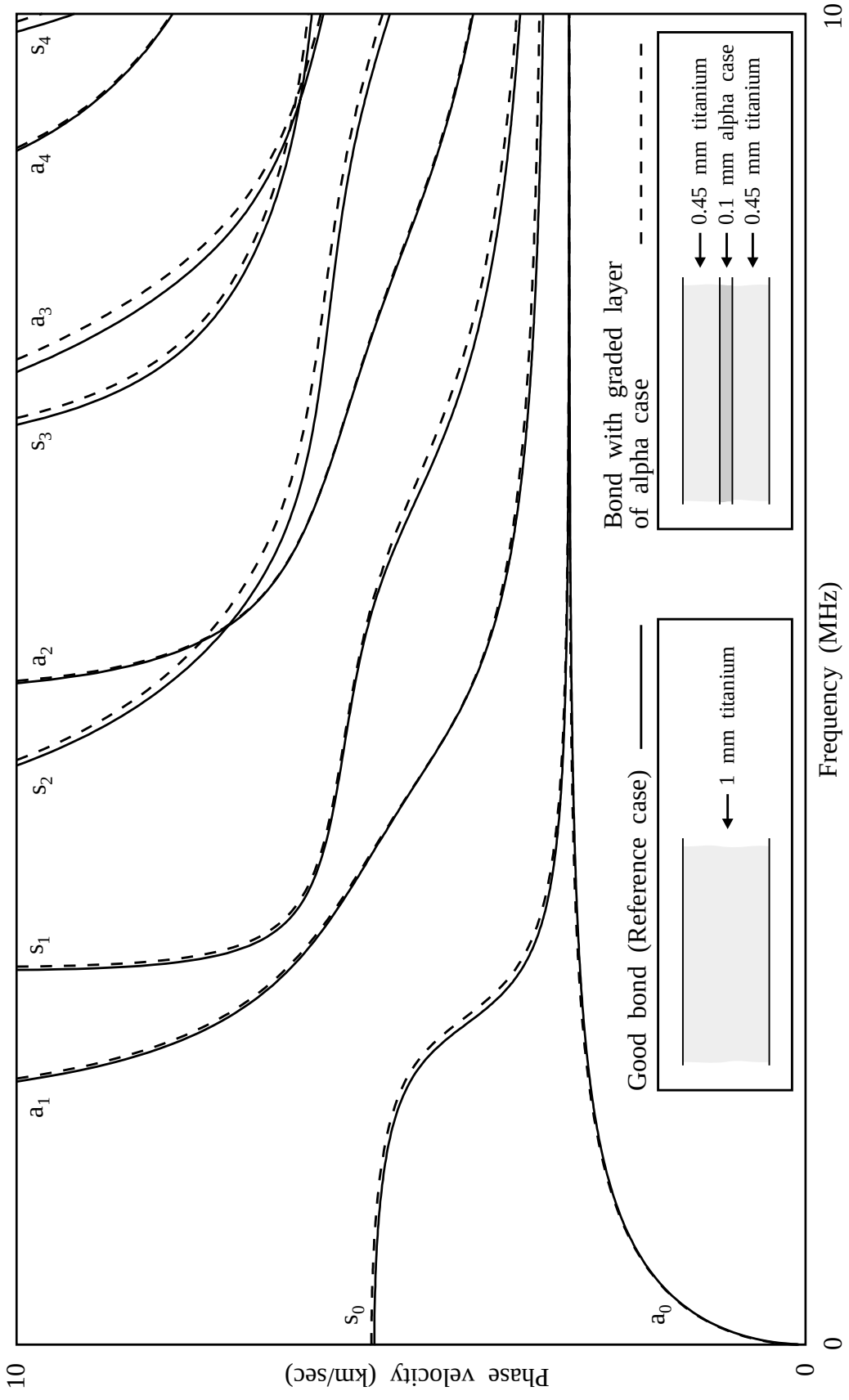

Figure 8.4 Lamb wave dispersion curves for titanium - influence of: Graded layer of alpha case

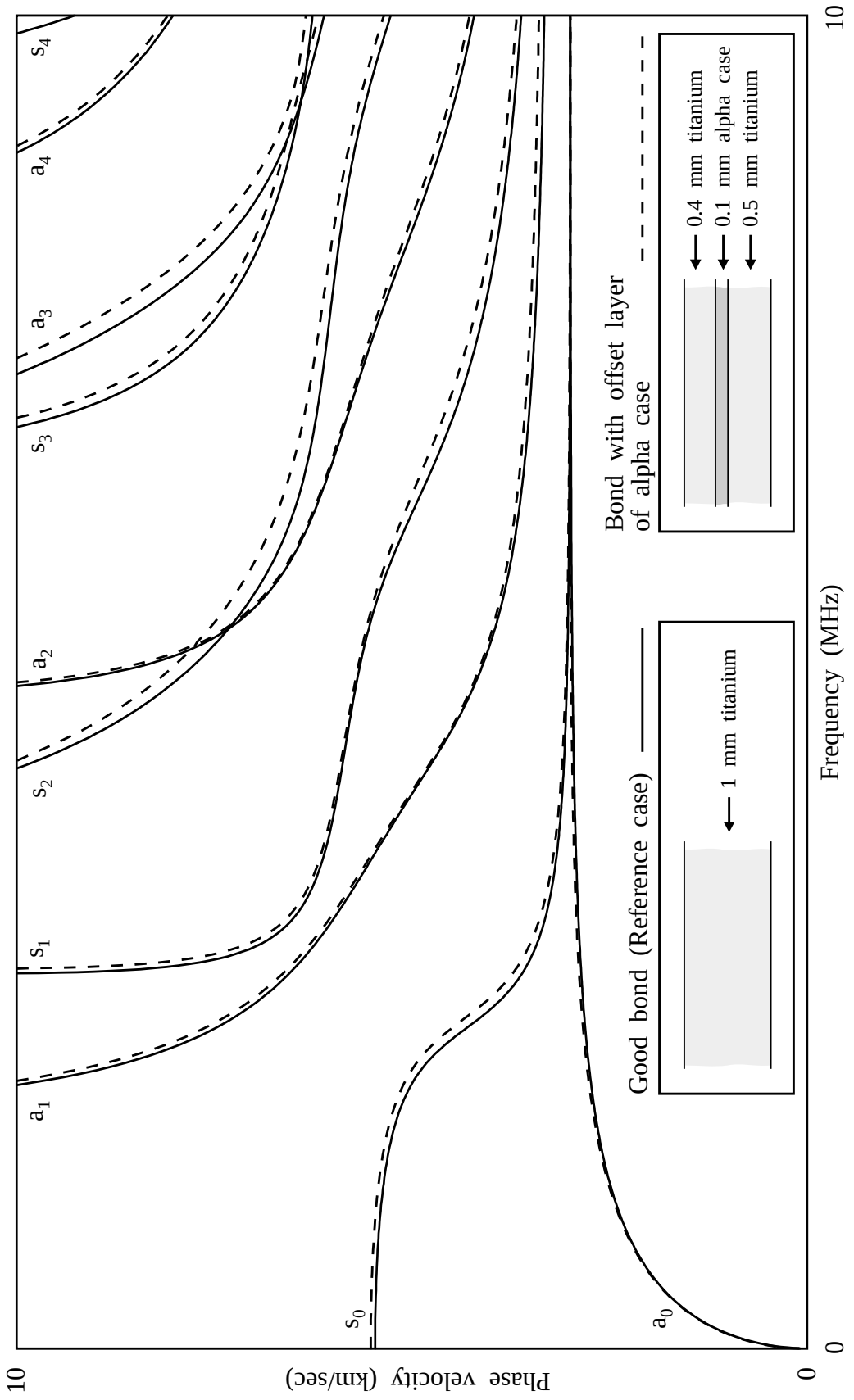

Figure 8.5 Lamb wave dispersion curves for titanium - influence of: Alpha case offset from centre of joint

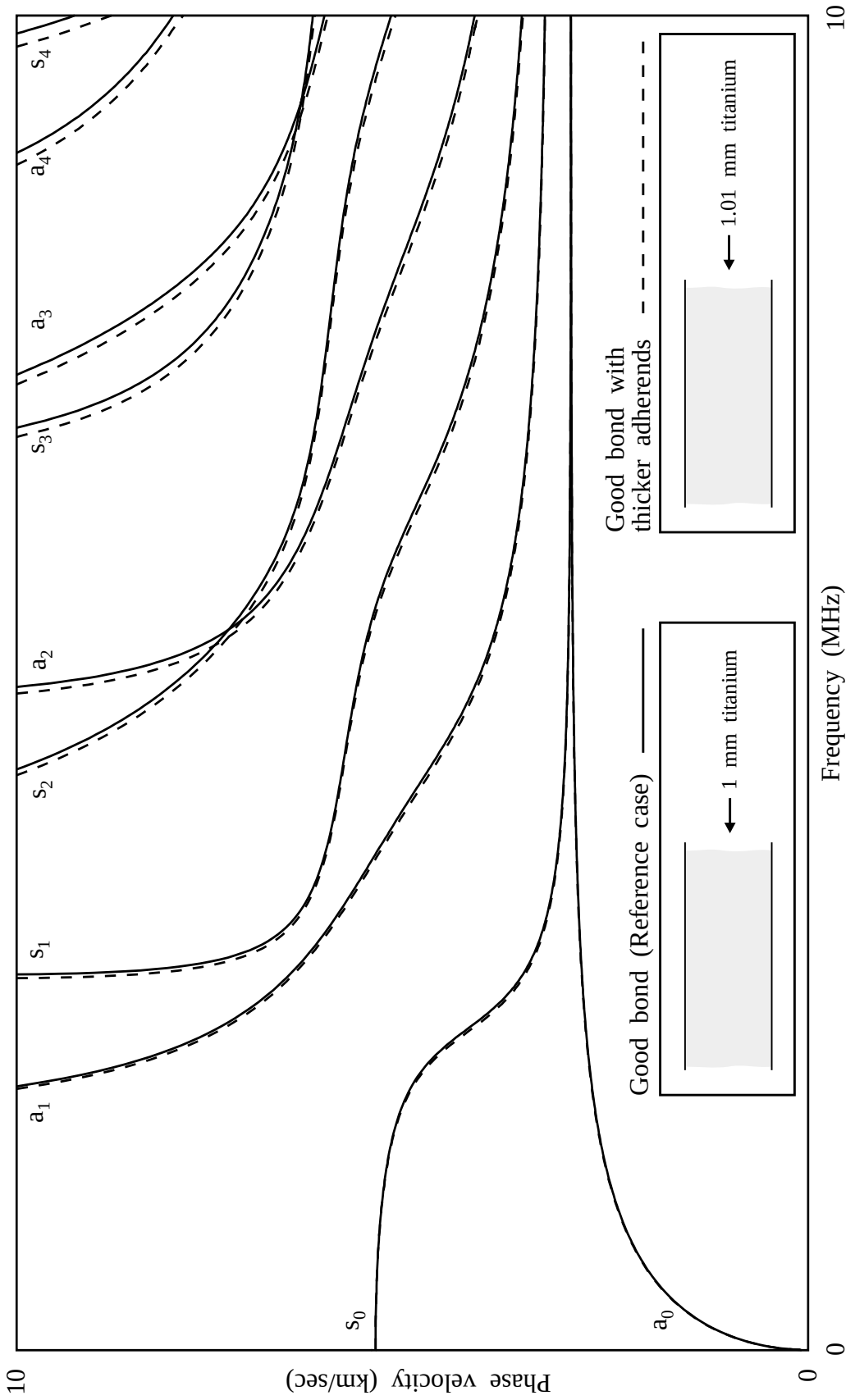

Figure 8.6 Lamb wave dispersion curves for titanium - influence of: Thicker adherends

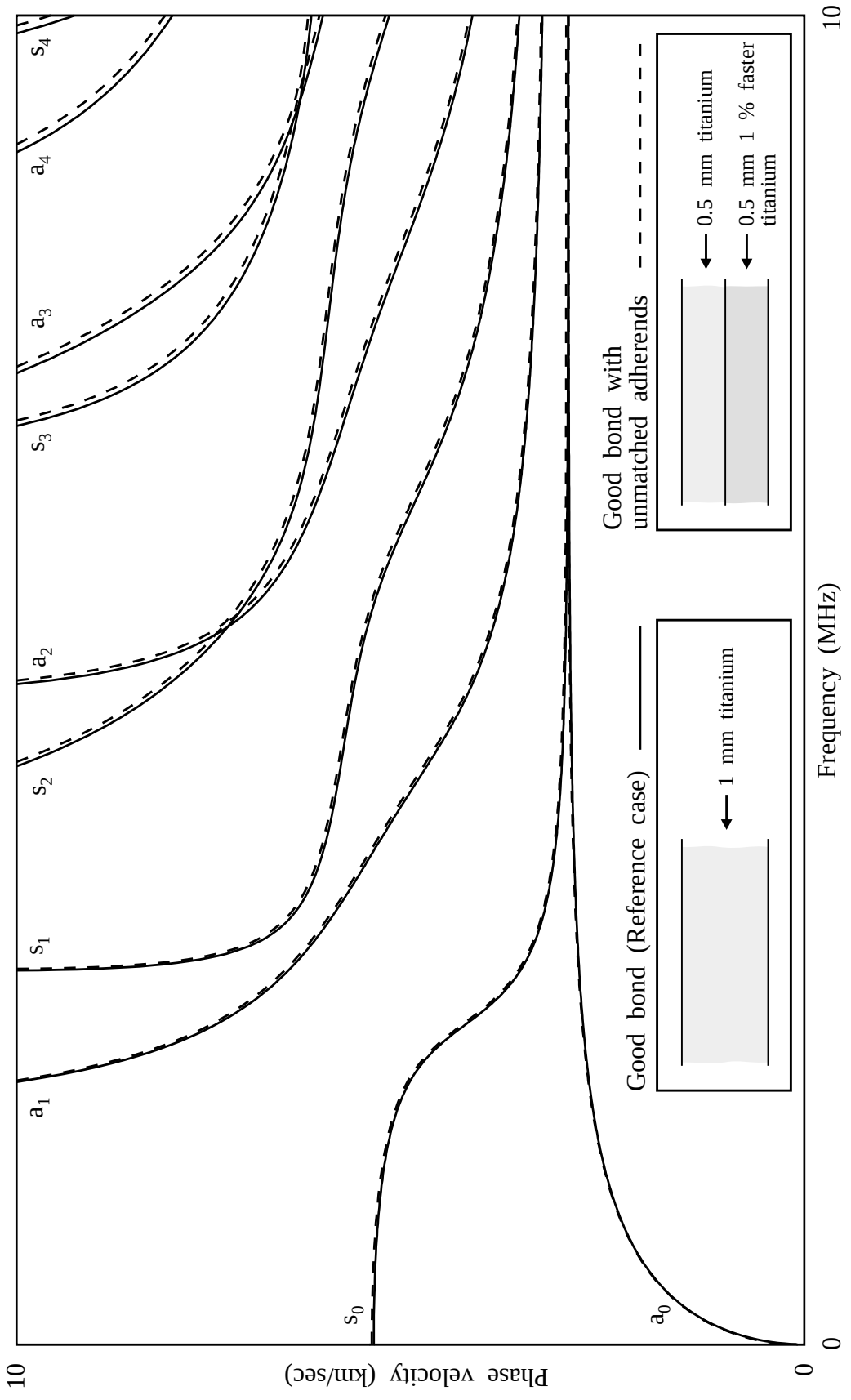

Figure 8.7 Lamb wave dispersion curves for titanium - influence of: Unmatched adherends

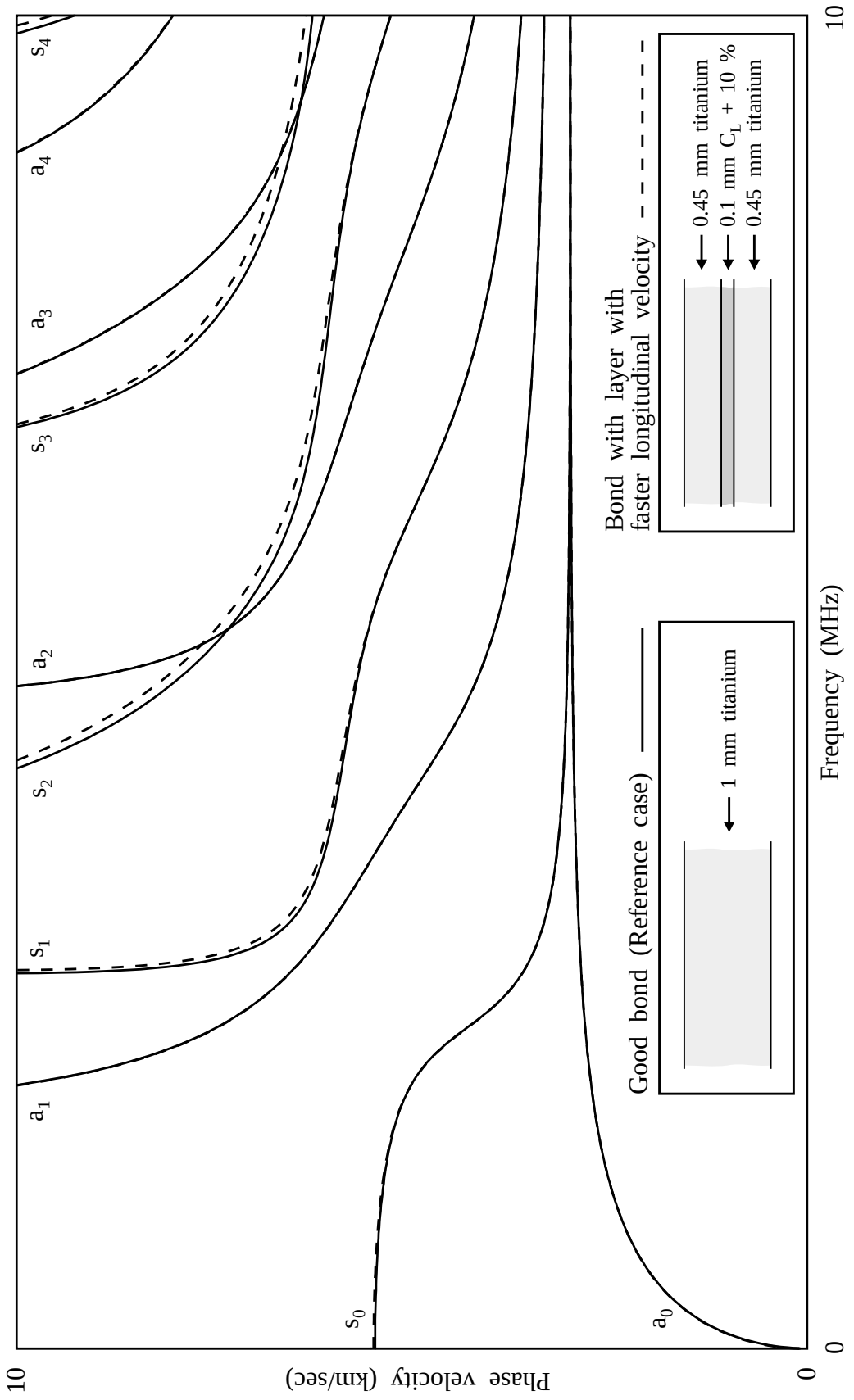

Figure 8.8 Lamb wave dispersion curves for titanium - influence of: Layer with faster longitudinal velocity

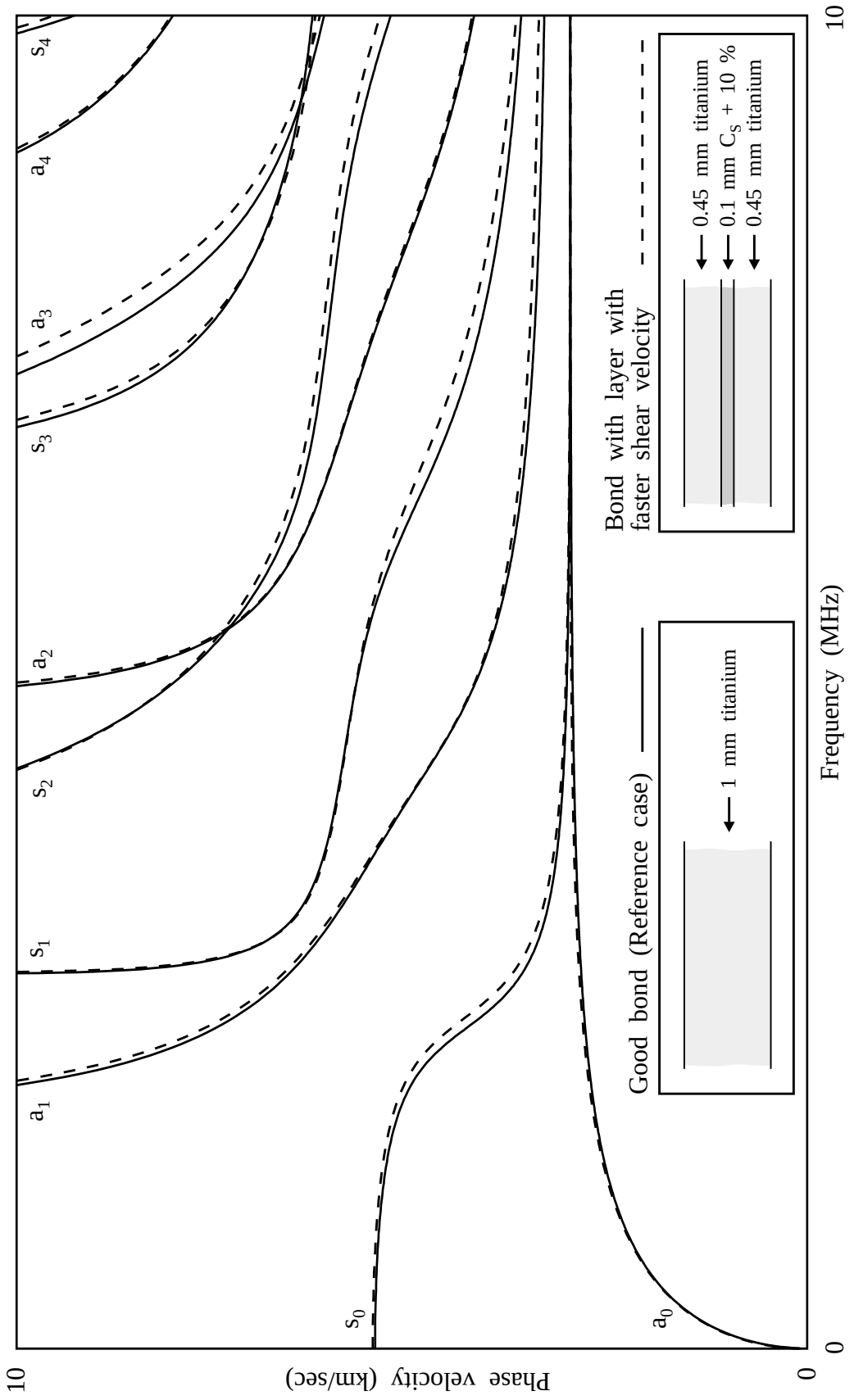

Figure 8.9 Lamb wave dispersion curves for titanium - influence of: Layer with faster shear velocity

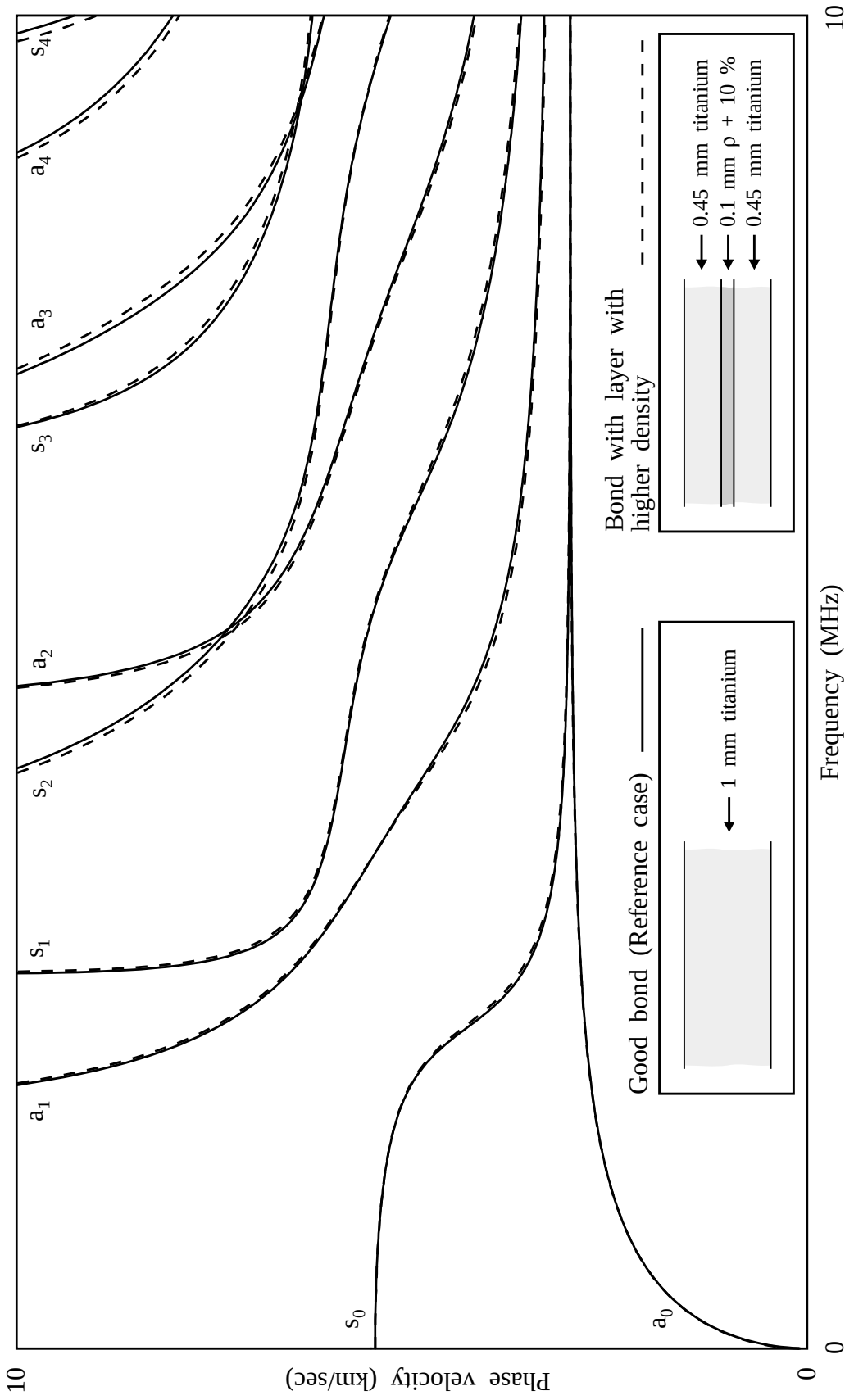

Figure 8.10 Lamb wave dispersion curves for titanium - influence of: Layer with higher density

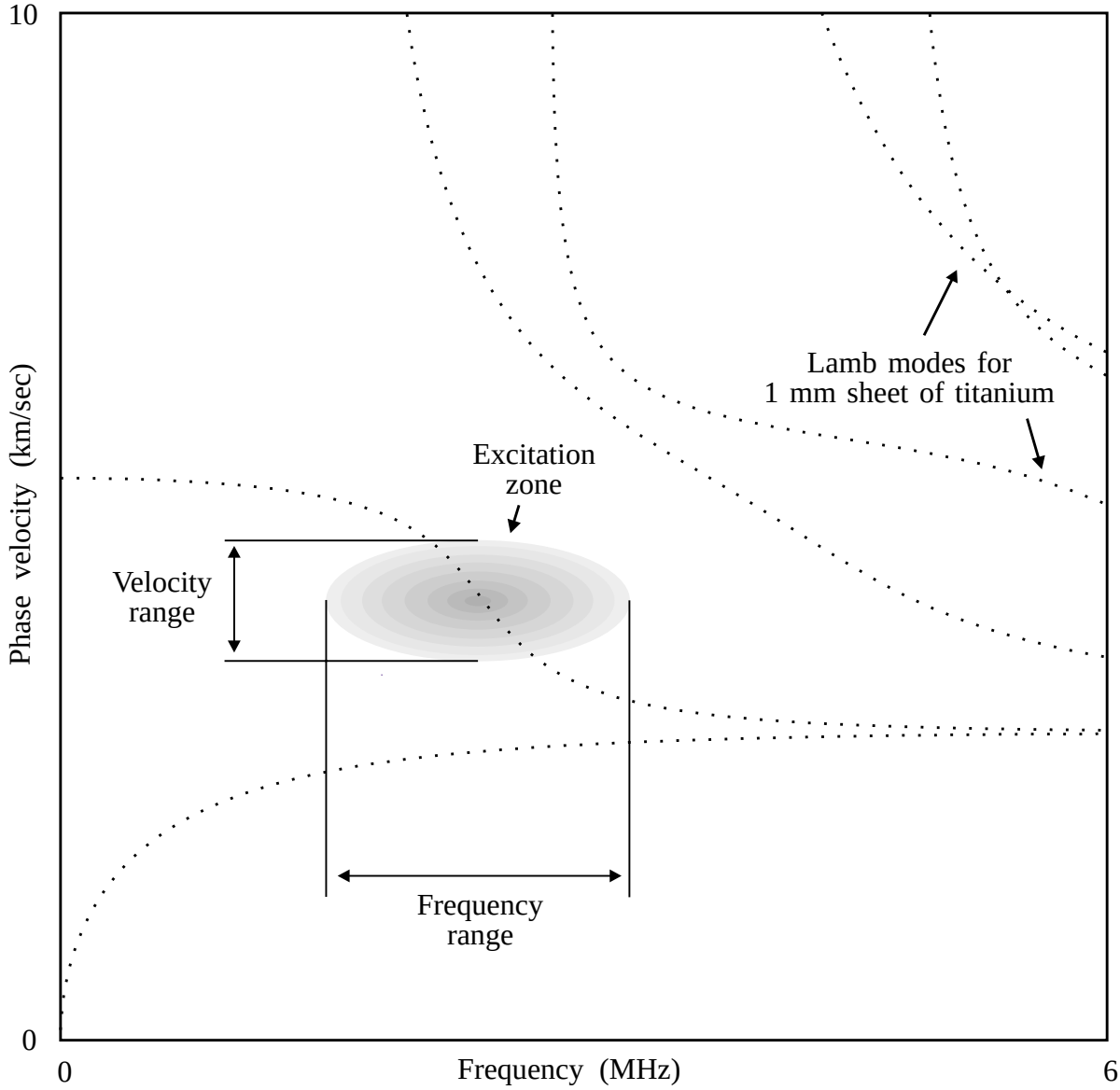

Figure 8.11 Selective excitation of Lamb modes using the coincidence principle

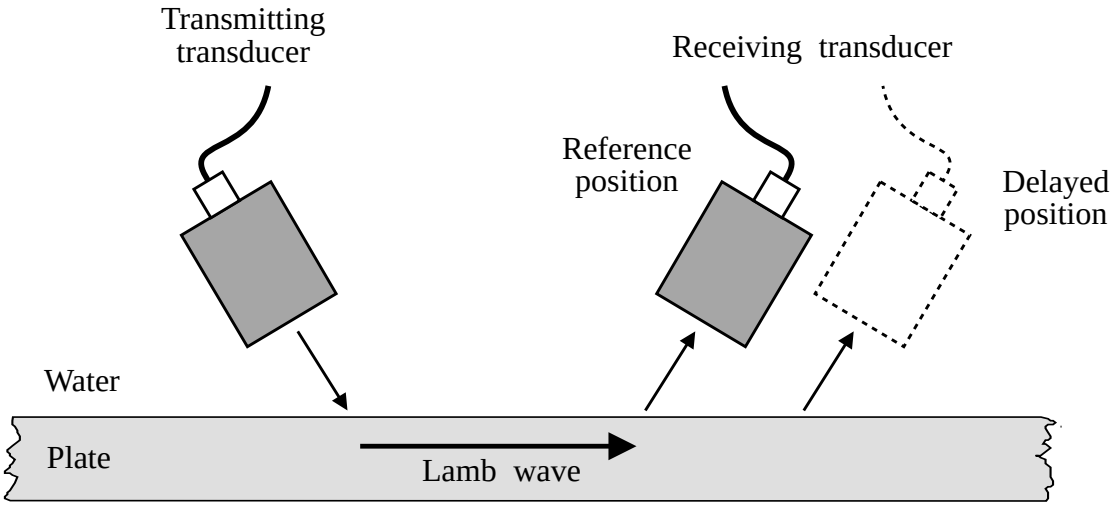

(a) Remote measurement of velocity

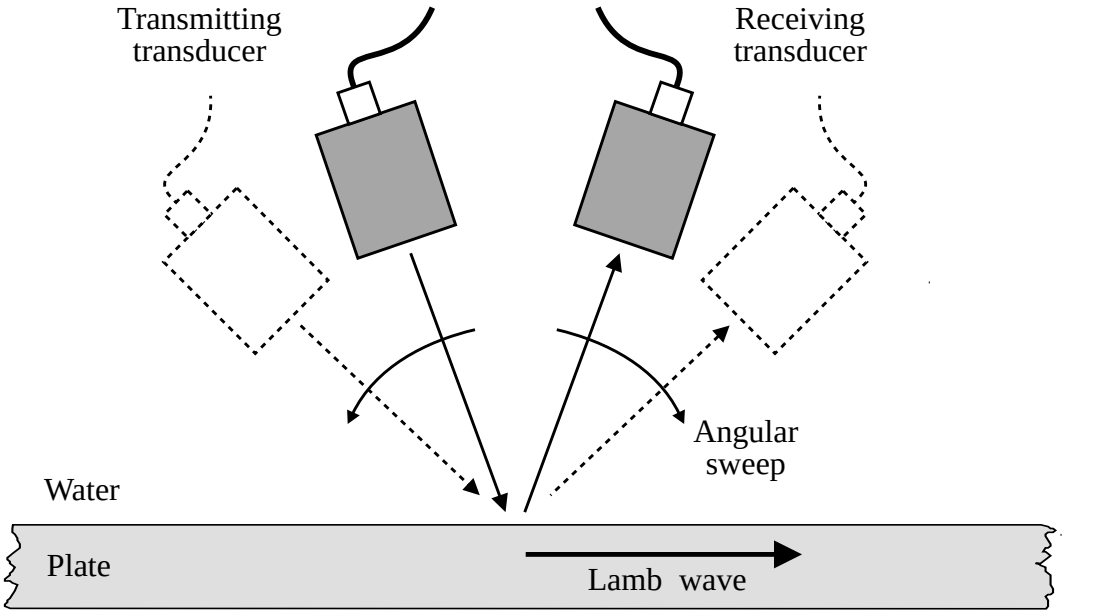

(b) Point measurement of velocity by null zone technique

Figure 8.12 The measurement of Lamb wave velocities

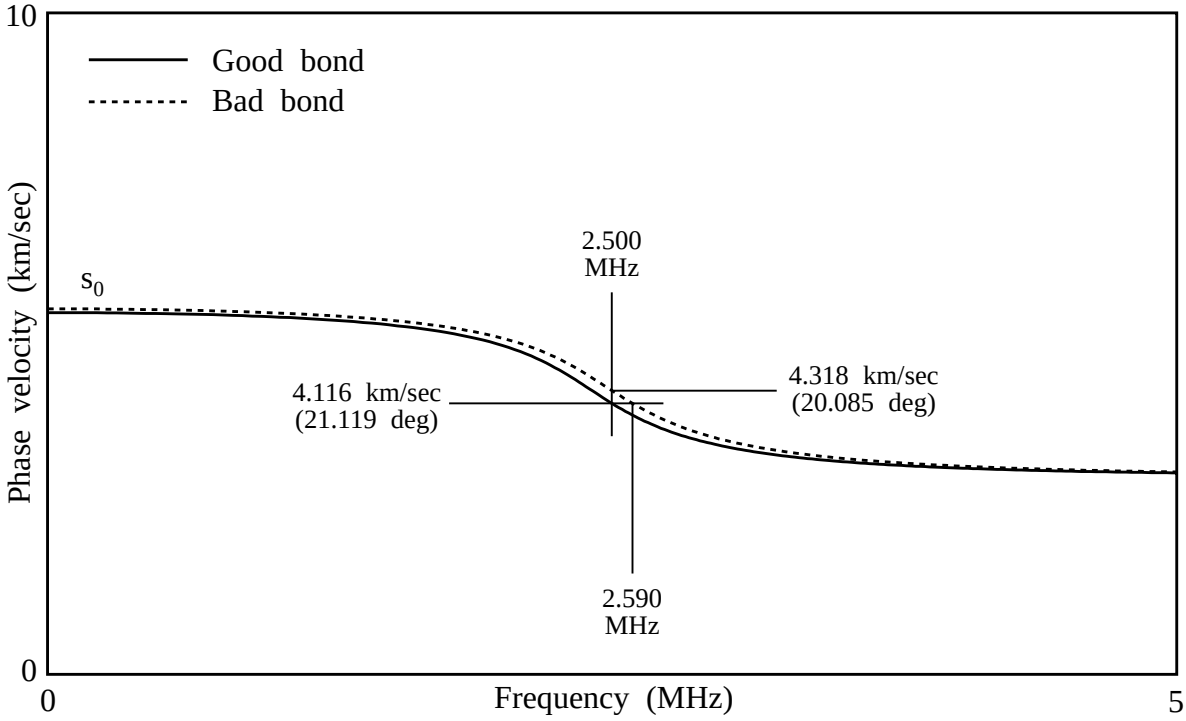

(a) Modal predictions of leaky s_0 for good and bad bonds

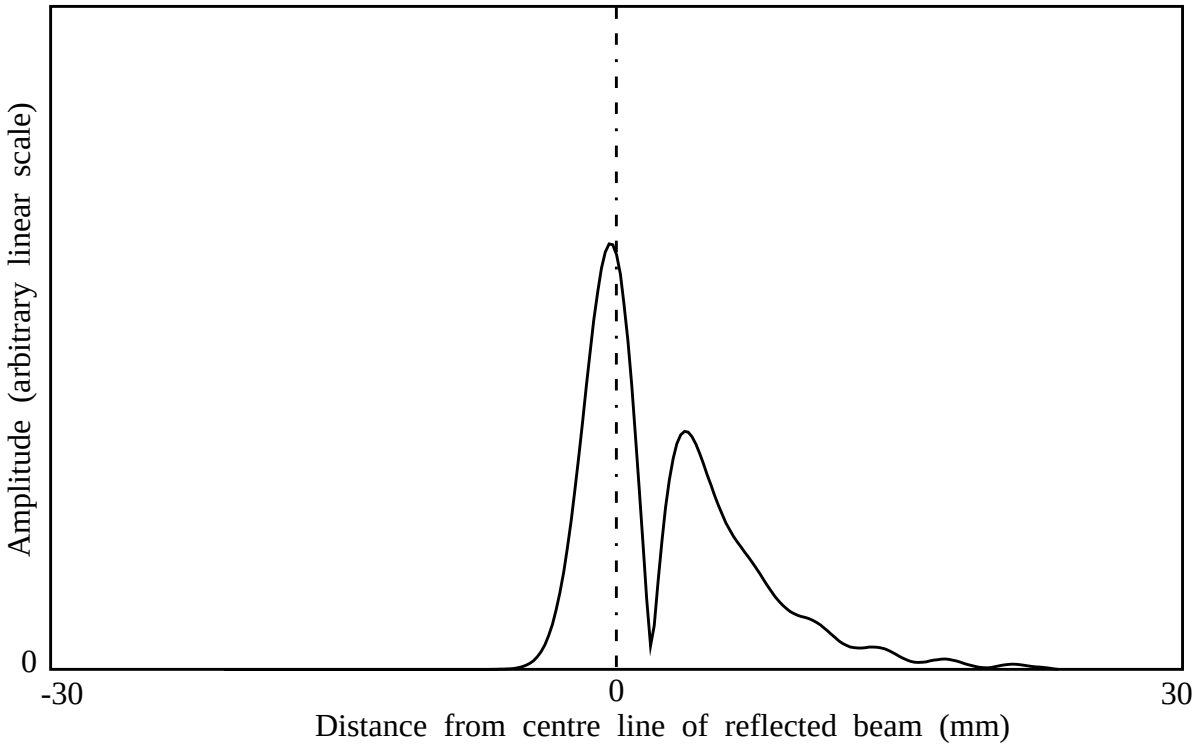

(b) Near-field response from good bond, at 2.500 MHz, 21.119 degrees

Figure 8.13 Modal and field predictions of leaky s_0 wave in diffusion bonded joint

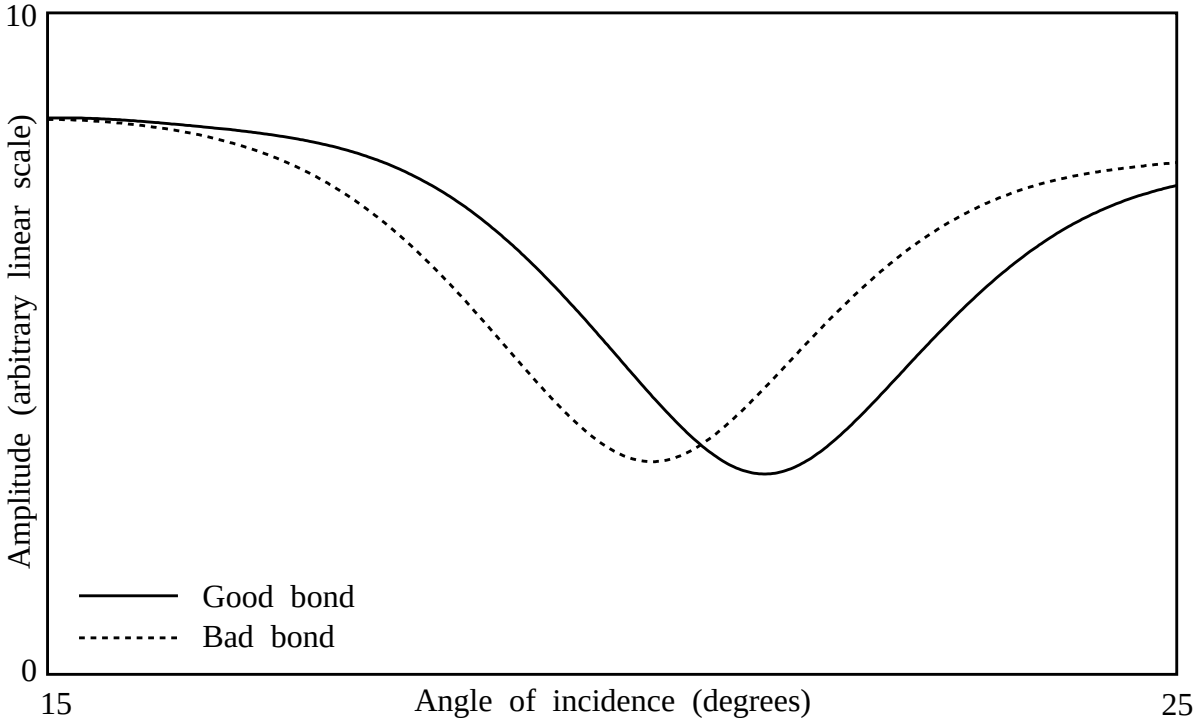

(a) Amplitude of received signal using angular sweep at frequency of 2.500 MHz

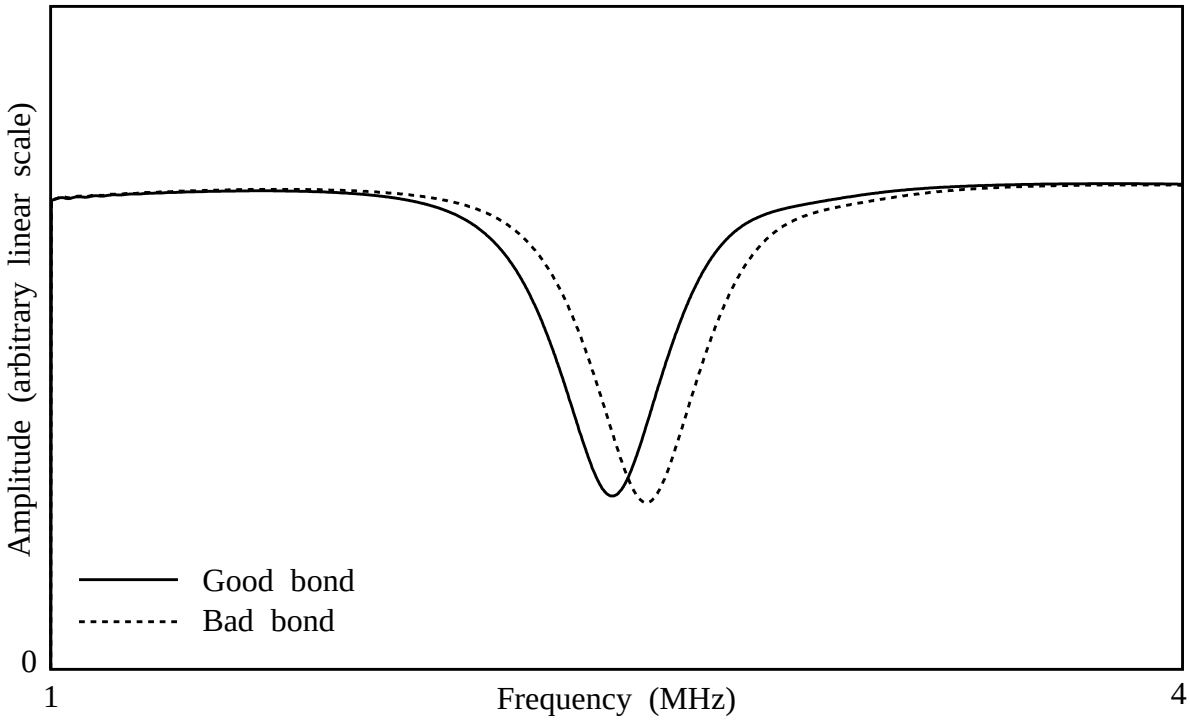

(b) Amplitude of received signal using frequency sweep at angle of 21.119 degrees

Figure 8.14 Simulation of null zone measurement of leaky s_0 wave in good and bad diffusion bonded joints

CHAPTER 9

Interface wave technique

9.1 Introduction

This chapter presents the results of model studies which were made in order to investigate the possibility of using some form of interface wave for the detection and characterisation of alpha case at the bondline of a diffusion bonded joint.

The objective with the interface wave inspection technique is to excite and detect a wave which travels along the bondline. In principle there are two major attractions of this technique when compared to the Lamb wave technique. First, if there is no alpha case at the bondline then there is no interface and so it will not be possible to excite the wave. The existence of the alpha case is therefore determined simply by the existence of the wave, not by small variations in its properties as was the case for the Lamb wave technique. Second, an interface wave whose energy is concentrated at the bondline is likely to be much more sensitive to the properties of the embedded layer and less to the properties of the adherends. If a layer of alpha case is found to exist, it may therefore be possible to characterise it by measuring the properties of the interface wave, even if the properties of the adherends are not known precisely.

It is well known that waves can exist at the interface between two semi-infinite half-spaces, for example the Stoneley and leaky Stoneley waves which were discussed in Chapter 5. It is possible that such an interface wave could be utilised for the inspection of the interface between an adherend and the embedded layer if the layer was very thick or if the frequency was very high, so that the depth of penetration of the interface wave was much smaller than the thickness of the layer. However the smallest wavelengths of acoustic waves which could be propagated through the thickness of an adherend in practice (about 40 microns for a shear wave at 80 MHz) are not significantly smaller than the thickness of an embedded layer of alpha case, even in a very poor bond. It is therefore unreasonable to expect that an interface wave with a sufficiently small depth of penetration could be generated for the inspection of alpha case. A second type of interface wave must therefore be considered in which the wave travels along the layer of alpha case, in principle rather like a Lamb wave. In this case the wave is strictly not an

interface wave because it is not confined to a single interface. However it will be referred to as an interface wave because it propagates along the interface layer.

Overview

The study starts with the examination of the excitation and measurement of leaky interface waves. If the rate of leakage of the waves is mild then the coincidence principle and the null zone technique may be used successfully. However it is shown that if the waves leak strongly then such methods may not be valid.

Next, the study addresses the simplest form of interface wave, that at a single interface between two different materials. Modal predictions are made for several pairs of materials and are compared with near-field response simulations.

The investigation then proceeds to the much more difficult case of the interface waves which travel along an embedded layer. Dispersion curves, attenuation curves and mode shapes are predicted for a layer of alpha case embedded in titanium. The modal predictions are analysed and compared with predictions of plane wave reflection coefficients and with simulations of the near-field response.

A final set of predictions shows the influence of variations of the properties of a joint on the dispersion curves. The variant cases include different acoustic properties of the alpha case and of the adherends.

The study is completed with a discussion of the implications of the model predictions. The potential for the practical use of interface waves for inspecting diffusion bonded joints is examined and conclusions are drawn.

9.2 Approach for the excitation and detection of interface waves

If the rate of leakage of a plate wave is mild then the coincidence principle may be used to excite and receive the wave and the null zone technique may be used successfully to measure its velocity and frequency. However if the leakage is strong then considerable complications emerge, based on fundamental differences between the modal and the response characteristics of the system. The excitation and detection of interface waves is therefore presented in two parts. First the case of the mildly leaking waves is examined and it is shown that the basic principles which were introduced for the measurement of Lamb waves may be applied to an embedded interface or layer. Then the complications

of the strongly leaking waves are addressed and the implications for the measurements are discussed. These discussions are followed by a model illustration of strongly leaking plate waves and the section is completed with the overall conclusions about the measurement of interface waves.

Mildly leaking interface waves

Mildly leaking interface waves at an embedded interface or in an embedded layer in a joint may be excited and received using the coincidence principle, in a similar manner to the method which was discussed for Lamb waves in Section 8.3 of Chapter 8. The approach is illustrated in Figure 9.1, using an embedded layer as an example.

The excitation of a particular wave is achieved by the selection of the angle of incidence of the transmitting transducer and the frequency characteristics of the ultrasonic signal. The angle of the transmitting transducer in the coupling medium (water in the illustration) must be such that the refracted beam, either longitudinal or shear, within the top adherend arrives at the layer at the appropriate angle to excite the wave. The wave propagates along the layer, leaking energy back into the adherends as it travels. Some of the energy subsequently leaks back into the water and can be detected by the receiving transducer.

As with the Lamb wave method, two approaches are possible in principle for the measurement of the interface wave. A long-range measurement may be made at some distance downstream of the point of excitation, as illustrated in part (a) of the figure. In this case the velocity of the wave may be determined by receiving two signals a known distance apart. Alternatively, a point measurement may be made at the location of excitation, as shown in part (b) of the figure. In this case the velocity or frequency at which the mode is excited may be measured using the null zone technique, as discussed in Section 8.3 of Chapter 8.

Clearly the method is restricted to interface waves whose phase velocity is faster than the bulk shear velocity in the adherend material and which leak energy as they travel. Interface waves whose velocity is slower than the bulk shear velocity in the adherend could only couple with inhomogeneous waves in the adherend so they could not be excited using the coincidence principle and, furthermore, they would not leak energy into the adherends.

Strictly speaking, the study of any wave propagation properties of a multilayered plate should take account of all of the layers of the system. In general it is not valid simply to identify those layers in which there is a particular interest. The investigation of the modal properties of a joint in which there is an embedded layer of alpha case should therefore include the finite dimensions of the adherends and the presence of the coupling medium. However, the influence of the parts of the joint which are remote from the embedded layer are only significant in practice if reflections of the signals from such boundaries are taken into account. Referring to Figure 9.1(a), the dashed line shows a reverberating signal within the top adherend. If the signal which is detected at the receiving transducer includes some part of this reverberation then any relevant modal predictions of the system would have to include the finite dimensions of the top adherend. However if it is possible to resolve the response from the bondline, gating out any other reflections, then it is valid to idealise the system as the embedded layer surrounded by semi-infinite half-spaces of the adherend material. The behaviour of the layer, and indeed the received leaking signal, is then independent of the thickness of the adherends. This is a very attractive feature of interface waves when applied to bondline inspection.

Strongly leaking interface waves

In the description of the measurement of leaky Lamb waves in Chapter 8 it was demonstrated that the minima of the reflection coefficient may be used to determine accurately the frequency and velocity at which mildly leaking plate waves propagate, according to the null zone technique. Indeed some researchers (Mal, Xu and Bar-Cohen (1989) and (1990) for example) have used the reflection coefficient minima in order to measure the dispersion curves for leaky Lamb waves.

The leaky Lamb wave dispersion curves for a metal plate in water differ only slightly from the true Lamb wave curves, and the rate of leakage of energy into the water is relatively small. In this circumstance good agreement may be expected between the response measurements and the modal predictions. However if the acoustic impedance of the half-spaces is much closer to that of the layer then the dispersion curves may differ greatly from the Lamb modes. Furthermore, as observed by Nagy and Adler (1989) and Chimenti and Rokhlin (1990), the same good agreement between the response measurements and the modal predictions cannot necessarily be assumed. The work by Chimenti and Rokhlin is particularly interesting in this context. They analysed the behaviour of plates in water and demonstrated the divergence of the loci of the reflection coefficient minima from the Lamb wave dispersion curves as the density of the water

was increased. They also showed theoretically that the conditions for plane wave reflection coefficient minima are fundamentally different from the conditions for plate wave propagation, and that exact agreement is only achieved in the zero density limit.

The principal reason for lack of agreement between the plane wave reflection coefficient minima and the modal predictions is that they are based on quite different boundary conditions. A reflection coefficient minimum occurs when the transmission of the energy of an incident wave through the plate is a maximum. The boundary conditions for the system therefore are that there is an incoming wave in one half-space and an outgoing wave in the other half-space, the other wave components in the half-spaces being zero or small. On the other hand the boundary conditions for the existence of a mode, which were shown in Figure 2.8, are that there are no incoming waves in either half-space although outgoing waves may occur in both half-spaces, corresponding to leakage of the plate wave.

Mathematically, as discussed by Chimenti and Rokhlin, the plane wave reflection coefficient may be described by a complex function whose zeroes yield the response minima and whose poles (given by zero values of the denominator), yield the modal properties. Specifically, in their example of a plate immersed in water, they defined the complex function in the form:

$$R = \frac{(AS - Y^2)}{(S + iY)(A - iY)} \tag{9.1}$$

where R is the reflection coefficient, the terms A and S relate to symmetric and antisymmetric Lamb waves, and Y is linearly dependent on the density of the water. Clearly when Y is zero, corresponding to the case of the plate in vacuum, the numerator and the denominator are identical and consequently there is no difference between the conditions when the poles and the zeroes of the function occur. However when Y is not zero then the conditions for the poles may be different from those for the zeroes.

The plane wave reflection coefficient minima may be predicted using an infinite plane wave response model. The minima will also be revealed in finite transducer simulations and in practice because the finite field consists of the summation of infinite plane waves over a range of angles of incidence, much of the energy being concentrated in the 'central' waves of the field, those whose angle of incidence is approximately that of the transducer. Thus the 'central' waves of the field will be transmitted through the plate and

the peripheral waves will be reflected, the result being an overall reduction of the amplitude which is measured by the receiver.

The reflectivity may also be perturbed when the conditions are appropriate for plate wave propagation. In general a leaky plate wave emits a plane wave at a specific angle on both sides of the plate, the angle being determined precisely by the velocity of the wave. The plane wave reflection coefficient may therefore be affected at this angle. In practice however, when the field is finite, the plate wave is detected by a mechanism which occurs in the near-field. The mechanism, as discussed in Section 8.3 of Chapter 8, is the interference of the leaking plate wave with the specular reflected beam, the result again being an overall reduction of the amplitude which is measured by the receiver. Clearly the simulation of this mechanism requires a finite transducer response model.

There is also a difficulty with the excitation of strongly leaky waves, concerning the coincidence principle. The coincidence principle is based on the coupling of the incident wave in the half-space to the plate wave, the angle of the incident wave being selected so that the wavenumbers match in the plate wave direction. However the coupling is limited to the real part of the wavenumber and makes no allowance for the imaginary part of the wavenumber which describes the attenuation of the plate wave. The correct coupling of the complex wavenumbers across the interface, as discussed in detail in Section 3.3 of Chapter 3, is therefore not achieved. If the attenuation is weak, for example in the case of a metal plate in water, then reasonable coupling may be achieved and the omission of the imaginary part of the coupling can be ignored. However if the attenuation is strong then the coupling may be very poor and in extreme cases it may not be possible to excite very leaky modes with any significant amplitude by this method.

In summary, there are two possible causes of minima of the reflection coefficient. Minima may exist either when the transmissibility of the plate is a maximum or when a plate wave is excited and its leaking field interferes with the point reflection of the beam. If the attenuation of the wave is weak then these mechanisms occur under practically identical conditions of frequency and angle of incidence, and their distinction is unnecessary. If the attenuation is strong then each of these mechanisms may occur under different conditions. Furthermore, the excitation of a plate wave depends on the coupling of the incoming wave in the half-space with the plate wave, poor coupling occurring when the attenuation is strong. It may therefore not be possible in practice to excite very leaky waves using the coincidence principle.

The practical implication of this analysis in the context of embedded layers is that it may not be possible to make direct measurements of strongly leaky waves. The first problem is that the excitation of the waves is likely to be very weak because of poor coupling. Then, even if a wave is successfully launched, the remote measurement technique will not be possible because of the rapid rate of decay of the wave. Measurements will therefore have to be made at the point of excitation. The difficulty here is that the other mechanism, the reflection minimum due to the strong transmission of plane waves, is likely to dominate the response. In principle the conditions for the strong transmission mechanism and for the mode are expected to be slightly different so that ideally it should be possible to measure the two effects separately. In practice however the influence of the strong transmission will be detected over a finite range of angle and frequency because of the spatial and frequency spread of the beam. It may not therefore be possible to identify the comparatively weak influence of a propagating wave. Furthermore, under conditions where there is good separation of the frequencies or angles of the minima of the two mechanisms, the attenuation of the mode is expected to be particularly strong. Consequently the mode will be particularly difficult to excite.

It is therefore concluded that if the modes are strongly leaky then the measurement technique should address the response behaviour rather than the modal behaviour. Measurements should be made of the minima which are associated with the strong transmission of energy through the layer, in the knowledge that these are related indirectly to the modal properties and are likely to be equally sensitive to the parameters of the system.

Example: influence of water density on leaky s_0 Lamb wave

Some calculations have been performed in order to illustrate the significance of the density of the water on leaky Lamb waves. The s_0 mode in a 1 mm thick sheet of titanium was studied, at its most dispersive region, shown in Figure 9.2(a). This is the same location on the dispersion curve as was chosen for the null zone simulation study in Section 8.3 of Chapter 8. Modal solutions and near-field response predictions were calculated for a range of densities. In all cases a constant angle of incidence of 21.119 degrees (constant velocity of 4116 m/sec) was assumed and the frequency was varied. The response model developed by Pialucha (1992) and described in Section 5.4 of Chapter 5 was employed for the response calculations.

Figure 9.2(b) shows the variation of the modal frequency and of the frequency of the minimum of the plane wave reflection coefficient for a range of densities. At very low

density the two predictions agree closely but divergence is evident as the density is increased, the modal frequency rising and the response frequency falling. For the normal density of water of 1000 kg/m^3, the separation is about 10 kHz, some 0.4% of the modal frequency of 2.5 MHz. For a density of water of 5000 kg/m^3, the separation is about 80 kHz, 3 % of the modal frequency.

Figure 9.3(a) shows the near-field response for the 5000 kg/m^3 'heavy' water case. A 10 mm diameter transmitting transducer was modelled and the reflected field was calculated at a total water path length of 10 mm. The amplitude of the field in front of the transmitting transducer was assumed to have Gaussian variation across the beam, as discussed in Chapter 5 and illustrated in Figure 5.14(b). Three cases are shown, one for the response at the modal frequency, one at the frequency of the plane wave reflection coefficient minimum and one at a 'remote' frequency, about 50 kHz higher than the modal frequency. In each case the transducer was excited by a single frequency tone (an infinite toneburst).

In all three fields, a non-specular reflection is evident, the strongest distortion of the beam occurring at the frequency at which the plane wave reflection coefficient is minimum. The dominant mechanism in the distortion of the field therefore appears to be the strong transmission (and consequent weak reflection) of the 'central' plane wave components of the finite beam, those whose angle of incidence is approximately that of the transducer. The modal calculations predicted the attenuation of the leaky wave to be 2.38 Nepers/wavelength which corresponds to a loss of amplitude of about 80 % per mm travelled, or 99.9 % over 5 mm. It is clear therefore that if there is any significant modal contribution to the field, it is restricted to the region within the beam, where the point reflection is strong. The fact that the distortion of the field due to strong transmission occurs over a range of frequencies is not surprising because of the beam spreading properties of the transducer.

Finally, Figure 9.3(b) shows the results of simulations of null zone measurements in which the excitation frequency was varied, the angle of incidence remaining fixed. Two cases of finite transducers were considered, one in which the receiver was 10 mm in diameter and the other in which it was 2 mm in diameter. In each case the receiver was placed on the centre line of the reflected beam, shown by the dashed line in Figure 9.3(a), at a total distance in water of 10 mm from the transmitter. The same 10 mm diameter transmitter, described above, was employed in both cases. For completeness, the plane wave reflection coefficient is also included in the plot and the frequency of the modal solution is indicated.

The results show again the significant difference between the frequency of the reflection coefficient minimum and the modal frequency. They also show small differences between the minima for the three response predictions. These differences arise because each of the finite receivers covers a different extent of the reflected field. Referring to Figure 9.3(a), it is apparent that the reflection amplitude which is detected by a finite receiver may vary significantly with the transducer's diameter. Furthermore, in practice, the location of the transducer with respect to the centre line of the reflected beam is also likely to be influential on the measurements.

Conclusions concerning the measurement of interface waves

It is concluded that if the rate of leakage of a plate wave is mild then the coincidence principle may be used to excite and receive the wave and the null zone technique may be used successfully to measure its velocity and frequency, just as with the measurement of Lamb waves which was discussed in Chapter 8.

However if the modes are strongly leaky then the behaviour is much more complicated. It may be very difficult to excite the waves using the coincidence principle and it may not be possible to detect them because of their strong attenuation and the presence of the separate transmission mechanism dominating the near-field. In this circumstance the measurement technique should therefore address the response behaviour rather than the modal behaviour. Measurements should be made of the minima which are associated with the strong transmission of energy through the layer, in the knowledge that these are related indirectly to the modal properties and are likely to be equally sensitive to the parameters of the system.

9.3 Waves at a single interface between titanium and alpha case

Before tackling the case of the modal properties of an embedded layer, it is instructive to examine the modal properties of the simpler geometry, the single interface between two different materials. This geometry would be relevant in practice if tests could be performed at sufficiently high frequencies that the different reflections from the top and bottom surfaces of the embedded layer could be resolved separately in which case any waves travelling along either interface could be studied. It would also be directly appropriate if interface waves were to be used to inspect bonds between different materials.

The geometry which was modelled was the interface between a semi-infinite half-space of titanium and a semi-infinite half-space of alpha case. The longitudinal velocity of titanium was assumed to be 6060 m/sec, the shear velocity 3230 m/sec and the density 4460 kg/m^3. The alpha case was assumed to have 10 % faster longitudinal and shear velocities (6666 and 3553 m/sec respectively) but to have the same density as the titanium. Both of the materials were assumed to be perfectly elastic.

For interest, three cases were considered, with varying values of the density of the titanium. In the first case the titanium was modelled with one tenth of its density, in the second with half of its density, and in the third with its correct density.

In the first case, where the density of the titanium was one tenth of its correct value, an interface wave was predicted with a velocity of 3360 m/sec and an attenuation of 0.0056 Nepers/wavelength. These properties are independent of frequency. At 10 MHz the attenuation per unit distance is 0.0168 Nepers/mm, corresponding to a 2 % loss of amplitude per mm travelled. Since the velocity of the wave is slower than the longitudinal bulk waves in both media and slower than the shear bulk wave in the alpha case, all three of these bulk wave components of the interface wave are inhomogeneous, retaining energy at the interface like a Rayleigh wave. However the fourth component, the shear wave in the titanium is homogeneous. The interface wave may therefore be excited by an incoming shear wave in the titanium and may also leak a shear wave into the titanium. This leakage explains the predicted non-zero attenuation of the wave. The angle of incidence of the excitation wave and of the leaky wave is 74 degrees.

When the density was increased to half of its correct value the properties of the interface wave were found to change. The velocity of the wave increased by 4 % to 3496 m/sec and the attenuation increased by almost an order of magnitude, to 0.0535 Nepers/wavelength, indicating that the leakage of energy is strongly sensitive to the density. In this case a 10 MHz wave would decay at 0.153 Nepers/mm, corresponding to a 14 % loss of amplitude per mm travelled. However the nature of the wave has not changed, all of the components remaining inhomogeneous with the exception of the leaking shear wave in the titanium. The angle of incidence of an excitation wave and of the leaky wave is now 67.5 degrees.

Mode shapes for the half-density case are plotted in Figure 9.4, for a frequency of 10 MHz. The plots show the variations of the displacements and stresses in the alpha case material only. Shapes have not been plotted for the titanium side of the interface because there is no identifiable wavefront propagating parallel to the interface on this

side. Although there is an inhomogeneous longitudinal wave in the titanium, its contribution to the field is minimal. The field in the titanium is therefore dominated by the leaking shear wave whose amplitude is constant with distance from the interface, only the phase varying spatially. The mode shapes show that the effective depth of the wave in the alpha case is approximately 1 mm, three times the wavelength of 0.35 mm at this frequency. This depth-to-wavelength ratio is similar to that of a Rayleigh wave.

When the density of the titanium is increased to its correct value, it is no longer possible to find a propagating wave solution. Pilant (1972) reported the conditions for the existence of all types of plane strain interface waves between pairs of half-spaces and observed a 'hidden' region in the solution space for which the solution of Stoneley's interface wave equation is imaginary and there is no propagating wave. The hidden region covers materials whose densities are almost equal and whose shear velocities are almost equal. The case which is considered here falls in the hidden region. There is therefore no propagating interface wave between titanium and alpha case half-spaces.

Near-field response predictions

Near-field response calculations were made for the three cases considered above, for comparison with the modal solutions. The predictions were again made using the response model which was developed by Pialucha (1992) and which was described in Section 5.4 of Chapter 5. A modification was made however, to introduce an idealised finite shear wave transducer, so that the interface wave could be excited from within the titanium half-space. The simulation is illustrated in Figure 9.5. The finite transducer is embedded in the titanium half-space and it emits a shear wave beam rather than a longitudinal wave beam. In reality an embedded transducer, either shear or longitudinal, would propagate a complex field of both shear and longitudinal waves into the titanium. In the model however, the interest is simply to generate a finite width shear beam in order to observe the excitation of the interface wave. Therefore the modelling of the transducer has not been developed to simulate the more complex field which would be associated with a real embedded transducer. A 10 mm diameter transducer was assumed in all cases, operating at a single tone of 10 MHz.

The results for the first two cases are plotted in Figures 9.6 and 9.7 respectively. In each figure, part (a) shows the reflected shear field (as shown schematically in Figure 9.5) when the angle of incidence of the transducer is appropriate for the excitation of the interface wave, and part (b) shows the amplitude of the reflections received by a 10 mm diameter finite transducer, as a function of the angle of incidence. The receiver was

placed on the centre line of the reflected beam, shown by the dashed line in part (a) of each figure, at a total distance in the titanium of 10 mm from the transmitter. The infinite plane wave reflectivity has been included in the plots too, for comparison.

In the first case, in which the density of the titanium is one tenth of its correct value, the leakage of the interface wave is rather small and the leaky shear wave can be seen clearly on the downstream side of the reflected beam, in Figure 9.6(a). The attenuation of the leaky signal was calculated from the slope of the log of the field amplitude, in the same manner as was described in Section 5.4 of Chapter 5, giving an attenuation of 0.061 Nepers/mm in the plane of the field. When projected onto the plane of the interface, by multiplying by the cosine of the angle of the beam (74 degrees), this value agrees exactly with the modal prediction of 0.0168 Nepers/mm.

Note also that the distortion of the reflected beam can be attributed entirely to the excitation of the interface wave. Plane shear waves at angles of incidence greater than the critical angle for shear waves in the alpha case substrate are reflected totally. Since the angle of the transducer of 74 degrees is significantly greater than the critical angle of 65.4 degrees, the vast majority of the energy of the field in front of the finite transmitter is reflected from the interface. The transmission mechanism which was discussed in Section 9.2 in the context of leaky Lamb waves is therefore not present and cannot be responsible for the distortion of the field.

Looking at the amplitude of the reflected signal as a function of angle of incidence, in Figure 9.6(b), a minimum can clearly be identified at 74 degrees, in agreement with the modal solution. As discussed above, the infinite plane wave reflectivity shows no evidence of the existence of the mode because all of the energy of plane waves is reflected when the angle of incidence is greater than the shear wave critical angle of 65.4 degrees (shown on the plot). The identification of this mode is therefore not possible with infinite plane waves but requires the finite transducer simulation in order to generate the near-field interference between the specular reflection and the leaking wave.

In the second case, in which the density of the titanium is half of its correct value, the attenuation of the interface wave is much larger and consequently the field, shown in Figure 9.7(a), does not extend significantly on the downstream side of the beam. However considerable distortion of the beam is evident. The minimum of the reflection coefficient, in Figure 9.7(b), is now at 67.5 degrees, again in agreement with the modal prediction. Note that the plane wave reflectivity at sub-critical angles of incidence is considerably lower than in the previous case, in Figure 9.6(b). This is because the

acoustic impedances of the two materials are better matched in this case and so there is greater transmission of energy into the alpha case.

Figure 9.8 shows the predictions for the third case, in which the titanium was given its correct density. Part (a) of the figure shows three reflected fields, for different angles of the transducer. Part (b) shows the amplitude of the reflections received by a 10 mm diameter finite transducer, as a function of the angle of incidence, and the infinite plane wave reflectivity.

The first observation is that there is no longer a minimum in the reflection amplitude, indicating that no interface mode is excited within this angular range. This is in agreement with the modal analysis of the system. The second observation is that, although specular reflections may be expected when there is no interface wave, some distortion of the reflected fields is evident, particularly at the angle of incidence of 65 degrees. The obvious explanation for this behaviour is that the reflectivity of plane waves varies strongly with the angle of incidence, as shown in part (b) of the figure, so that plane wave components of the finite field with large angles of incidence are reflected much more strongly than those with small angles of incidence. It should therefore not be expected that the composed field will reflect perfectly. The strongest distortion of the field, at a transducer angle of 65 degrees, occurs when the gradient of the reflectivity is largest. The variation in the reflectivity can also be seen in the magnitudes of the reflected fields. The strengths of the fields increase substantially as the angle of the transducer is increased, as does the plane wave reflectivity.

9.4 Waves in a layer of alpha case embedded in titanium

This section examines the second type of interface wave, waves which travels along an embedded layer. These interface waves are likely to be much more relevant to the inspection of the embedded layer of alpha case than the waves at a single interface because the layer is very thin and consequently in practice it will not be possible to propagate waves separately along each of the two interfaces.

The system which was chosen for the study of the modal properties of an embedded layer was a 0.1 mm thick layer of alpha case between two semi-infinite half-spaces of titanium. The longitudinal velocity of titanium was assumed to be 6060 m/sec, the shear velocity 3230 m/sec and the density 4460 kg/m3. The alpha case was assumed to have 10 % faster longitudinal and shear velocities (6666 and 3553 m/sec respectively) but to have the same density as the titanium. The embedded layer was therefore identical to that

which was studied in the context of Lamb waves in Chapter 8. As discussed in Section 9.2, the external boundaries of the adherends do not need to be included in the modal model because of the judicious gating of the ultrasonic signals. The modal properties will therefore be independent of the dimensions of the joint and of the properties of any medium which is used for coupling between the transducer and the joint.

Figure 9.9 shows the predicted dispersion curves for the system for frequencies up to 100 MHz. For convenience the modes have been labelled 1 to 9. As with the Lamb wave dispersion curves there is an infinite number of modes, further modes being introduced to the diagram as the frequency is increased. However it is apparent immediately that the shapes of the dispersion curves for the embedded layer differ strongly from the Lamb wave curves which would be generated if the half-spaces on either side of the layer were vacuum rather than titanium. It is therefore not appropriate to think of the modes simply as leaky Lamb modes, as can be done when a plate is immersed in water; the addition of the stiff, solid half-spaces transforms the curves radically.

Besides the shapes of the dispersion curves, the first important difference between the interface modes and the Lamb modes is that all of the interface modes leak energy strongly into the surrounding material as they travel along the layer. Their amplitudes therefore diminish rapidly with distance travelled. The rate of decay is shown in Figure 9.10 in Nepers/mm travelled along the layer, from which it can be seen that the lowest leakage within the diagram is of mode 1 at its lowest frequency. The attenuation here is 1.3 Nepers/mm, corresponding to a loss of about 70 % of the amplitude of the wave in each mm travelled. The second least leaky mode is mode 6 which attenuates at 3.2 Nepers/mm at its lowest frequency in the diagram, losing about 95 % of its energy in each mm travelled. There is also a general trend for the attenuation of the modes to decrease with frequency, the main exceptions being modes 1 and 2 which have relatively low attenuation at both low and high frequencies. This trend can be seen clearly in the plots of attenuation in Nepers/mm in Figure 9.10 and is even more pronounced if the attenuation is assessed in Nepers/wavelength.

The second important difference is that the dispersion curves for the interface waves have been plotted with ends which are not necessarily at the boundaries of the diagram or at infinity. In calculating the curves, each mode was identified by a velocity sweep at 100 MHz and the curve was generated by decreasing the wavenumber (decreasing frequency direction in Figure 9.9). Modes 1 and 6 were found to have clearly identified low frequency limits. In both cases the velocity at low frequency decreases with

decreasing frequency and the limit is reached when the velocity drops to the bulk velocity of the titanium half spaces. For mode 1 this is the bulk shear velocity in titanium and for mode 6, the bulk longitudinal velocity. The curves have therefore been calculated close to these values, down to 11 MHz and 29 MHz respectively. No propagating solutions could be found for these modes at lower frequencies. For all of the other modes the limit is practical. The solution of the modal equations can be extremely difficult and time-consuming when the attenuation is very high. Furthermore, the results are of dubious practical worth when the attenuation is of the order of tens of Nepers/mm. The curves were therefore generated only for their regions of lowest attenuation. The generation of each curve was terminated arbitrarily when the solution became slow as the attenuation became very large. To give an indication of the strength of the attenuation at these termination points, the lowest attenuation is 12 Nepers/mm, for mode 2. This corresponds to a loss of 99.9994 % of the amplitude of the wave in each mm travelled.

The mode shapes of mode 1 are shown in Figure 9.11. Part (a) of the figure shows the shapes near the low frequency end of the curve, at 12 MHz, and part (b) shows the shapes at very high frequency, at 1 GHz. The shapes have been plotted through the thickness of the 0.1 mm thick layer of alpha case. For clarity, the displacement mode shapes have been plotted as solid lines and the stress mode shapes as dashed lines.

The mode shapes show that mode 1 is essentially a shear wave travelling along the layer. The predominant motion is normal to the layer and the shear stress is much larger than the other stress components. The wave would therefore appear, like a bending wave, as an undulation propagating along the layer. The wave can also be seen to change with frequency. At low frequency the dominant displacement and stress components are approximately uniform across the thickness of the layer whereas at high frequency they each develop a peak at the centre of the layer, decreasing towards the interfaces with the titanium. The motion of the low frequency wave therefore involves the whole of the layer but as the frequency increases the motion becomes concentrated at the centre of the layer. This is consistent with the variation of the velocity of the wave. At the lowest frequency the velocity is equal to the bulk shear wave velocity in the titanium adherends. The shear wave motion in the whole of the layer can therefore couple, in the low frequency limit, with bulk shear waves travelling along the two half-spaces. At very high frequency the velocity of the mode tends to the bulk shear velocity in the alpha case. This is consistent with the concentration of the motion of the wave at the centre of the layer. The increasing concentration of the motion at the centre of the layer as the frequency increases is also consistent with the predicted reduction of the rate of leakage of the wave.

The mode shapes of modes 2 and 3 are shown in Figure 9.12, in parts (a) and (b) respectively, at their lowest frequencies. Mode 2 has a high value of displacement parallel to the layer throughout the thickness of the layer. Its two direct stress components are also approximately constant across the layer. It is therefore a first order extensional mode, rather like an s_0 Lamb mode which is constrained by the adjacent half-spaces. Mode 3 is clearly a second order mode, fitting in perfectly as the next mode in the series after mode 2. Each of its displacement and stress components shows an increase in the order of its shape, the constant shapes being replaced by half-wavelengths and the half-wavelengths by full wavelengths. Although not presented here, the progression of the series was found to continue with modes 4 and 5.

The mode shapes of mode 6 are shown in Figure 9.13. As with mode 1, the shapes are plotted for two frequencies, part (a) near the low frequency end of the curve, at 30 MHz, and part (b) at very high frequency, at 1 GHz.

The mode shapes show that mode 6 is essentially a longitudinal wave travelling along the layer. The predominant motion is parallel to the layer and the direct stress in this direction is much larger than the other stress components. The characteristics of the mode are very similar to those for mode 1, except that the wave is a longitudinal wave rather than a shear wave. At low frequency the dominant displacement and stress components are approximately uniform across the thickness of the layer whereas at high frequency they each develop a peak at the centre of the layer, decreasing towards the interfaces with the titanium. The motion of the low frequency wave therefore involves the whole of the layer but as the frequency increases the motion becomes concentrated at the centre of the layer. This is again consistent with the variation of the velocity of the wave. At the lowest frequency the velocity of the wave is equal to the bulk longitudinal wave velocity in the titanium adherends and at very high frequency the velocity of the wave tends to the bulk longitudinal velocity in the alpha case.

The mode shapes of modes 7 and 8 are shown in Figure 9.14, in parts (a) and (b) respectively, at their lowest frequencies. These two modes appear to be the next in a series of modes of increasing order following mode 6, each of the displacement and stress components showing an increase in the order of its shape with respect to the previous. Indeed, although not presented here, the series is continued with mode 9 and with further modes which can be found at higher frequencies.

Finally, it appears that the categorisation of the modes according to symmetry and antisymmetry or shear and longitudinal motions, as is applied to Lamb waves, is not the most appropriate approach here. The analysis of the plane wave components of the nine modes indicates that they can be categorised very clearly into two groups according to the manner in which they leak energy. The amplitudes of the plane shear waves leaving the layer for modes 1 to 5 are considerably larger than the amplitudes of the plane longitudinal waves. Furthermore, the plane longitudinal waves are inhomogeneous below the phase velocity of 6060 m/sec. The leakage of energy from these modes is therefore entirely by shear waves. In contrast, the amplitudes of the longitudinal waves leaving the layer for modes 6 to 9 are much larger than the amplitudes of the shear waves. Accordingly, although in principle both longitudinal and shear waves could leak in this region of the solution space, these modes are characterised by leakage of longitudinal waves.

Comparison of interface modes with Lamb modes

For interest a few cases were studied in which the density of the titanium was varied, in order to see how the dispersion curves develop between the Lamb wave curves and the interface wave curves. Some of the results are plotted in Figure 9.15. Part (a) of the figure shows the curves for the case in which the density of the titanium is one hundredth of the correct density, part (b) for one tenth of the correct density and part (c) for half of the correct density. Part (d) shows the case for the correct density, already shown in Figure 9.9, for reference.

As expected, the curves for the case with the lowest density of titanium are extremely close to the Lamb wave curves for a plate in vacuum. The only significant difference is in the 'a_0' mode at low frequency, a region of the curve which was already known to be particularly sensitive to the presence of non-vacuum half-spaces (see discussion about leaky Lamb waves in Chapter 5).

Following the a_0 mode through the three low density cases, it seems that the mode is modified progressively as the density is increased. Its low velocity region becomes less pronounced but it remains continuous across the whole frequency range of the plot. When the titanium has the correct density however, there is no propagating mode at zero frequency, the nearest mode to a_0 being interface mode 1 which only exists above a threshold frequency. At first sight it seems that there may be an inconsistency here because smooth changes may be expected when the density is varied yet discrete differences are evident. However, recalling the investigation of Section 9.3 of the

interface wave at a single interface, a major change was found when the density of the titanium was varied. It was found that an interface wave may exist when the density of the titanium is low but does not exist when the density of the titanium is identical to that of the alpha case. Indeed, returning to the present study, the a_0 mode converges on the interface wave velocity at high frequency in all three of the low density cases. However when the correct density is used, mode 1 is asymptotic to the bulk shear velocity in the alpha case. It must be accepted therefore that discrete and fundamental changes may occur in the nature of the curves as the density is varied and consequently that the interface wave modes cannot be categorised simply as extreme forms of leaky Lamb modes.

Examination of the other modes shows further discrete changes in the nature of the curves. This is particularly clear in case (b) in which breaks are just apparent in three of the modes. Following the progression of these 'breakaway' modes through from this case to case (c) and then to case (d), it seems that they develop ultimately into the high velocity group of interface modes. Finally, it seems that the interface wave mode 2 is most closely related to the Lamb mode s_0, an observation supported by the similarity in their mode shapes.

Comparison of interface modes with minima of reflection coefficients

A study was made of the plane wave reflectivity from the embedded layer in order to determine whether minima of the reflection coefficient would occur at the angles of incidence and frequencies of the modes or would differ, as discussed in Section 9.2. Furthermore, if the loci of the major reflection minima differed significantly from the modes, indicating strong transmission of energy through the layer, then it was important to determine whether any separate, perhaps minor, minima could be identified with the excitation of the modes.

Two sets of plane wave reflection coefficients were calculated, one in which a shear wave was incident and the reflected shear wave was measured, and the other in which a longitudinal wave was incident and the reflected longitudinal wave was measured. In each case a sweep of frequency from 0 to 100 MHz was performed and the minima were identified from the resulting spectrum. The process was repeated for a range of angles of incidence of the waves, up to 90 degrees. Thus the complete area of the dispersion curves of Figure 9.9 was covered in both cases, for all velocities above the bulk velocities in the titanium. For the shear wave case the bulk velocity is 3230 m/sec and for the longitudinal wave case it is 6060 m/sec. The results are shown for shear waves in

Figure 9.16 and for longitudinal waves in Figure 9.17, together with the dispersion curves. The angles of incidence of the shear and longitudinal waves are indicated on the right hand sides of the plots.

Before discussing the results, it should be mentioned that the quality of the minima was found to vary considerably over the solution space, the minima being sharp in some cases and rather vague in others. An example of very good minima is shown in Figure 9.18(a) and an example of poor minima, in Figure 9.18(b). The good minima in the figure were found using shear waves at a large angle of incidence of 40 degrees, when there are no homogeneous longitudinal waves present. The poor minima in the figure were encountered at 22 degrees (about 9000 m/sec phase velocity), again with shear waves. In this example the five minima can just be identified, although the frequencies of all but one of them are indistinct. However in some cases in this angular region the minima were found to vanish as the angle of incidence of the sweep was advanced. This resulted in discontinuities of the loci of the minima, evident in Figure 9.16.

One reason for the complication of the reflection coefficient spectra is that at velocities above the bulk longitudinal velocity of the titanium, both shear and longitudinal waves may be reflected from the layer. Minima in the shear wave reflection coefficient, for example, may therefore be associated either with maxima in the reflection of longitudinal waves or with maxima in the transmitted energy. The former case is of course not of interest here; it relates to another aspect of the behaviour, the balance of the longitudinal and shear wave components in the response. In many cases confirmation of the frequency was therefore found by examining the transmission coefficient. This of course has its complications too because both shear and longitudinal waves may be transmitted.

A second reason for complication of the spectra is the interaction of adjacent minima when the loci (or dispersion curves) are close together. This was particularly evident at the lowest phase velocities in Figure 9.16 where two of the loci appear to converge at about 30 MHz. The loci are sharp at lower frequencies but vague at frequencies above this value.

The results for the shear wave minima show that their loci differ significantly from the dispersion curves. A pattern can be seen however, in which four of the loci of the minima converge on four of the low velocity modes, modes 2 to 5, as the frequency increases. The remaining locus is relatively close to mode 1 but convergence is not demonstrated, the locus appearing to converge instead on mode 2. As discussed above, the result is rather inconclusive however because the minima for this locus were poorly

defined at all frequencies above about 30 MHz. The convergence of loci on modes is consistent with the reduction of the attenuation of the modes with frequency. The association of the shear wave minima with the low velocity modes is also consistent with the fact that the leakage of these particular modes occurs entirely by shear waves.

The loci of the longitudinal wave minima also differ significantly from the dispersion curves. Here it appears that the minima may converge on two of the high velocity group of modes, modes 6 to 9. Indeed, further calculations of both the modal solutions and the reflection coefficients at frequencies up to 200 MHz confirmed that this is the case, the minima converging on modes 6 and 7. Furthermore, additional longitudinal reflection coefficient minima appear at the higher frequencies, converging on the other high velocity modes. Again the association of the longitudinal wave minima with the high velocity modes is consistent with the fact that the leakage of these modes occurs predominantly by longitudinal waves.

Near-field response predictions

Near-field response predictions were made for two locations in the solution space, one in the shear-dominated region and the other in the longitudinal-dominated region. The locations are identified in Figures 9.16 and 9.17 respectively. The predictions were made using a spatially realistic simulation of a joint, including a finite thickness adherend and water coupling.

The geometrical arrangement for the simulations is shown in Figure 9.19. The upper adherend was 10 mm thick, the alpha case 0.1 mm thick and the lower adherend was a semi-infinite half-space of titanium, there being no interest in predicting the reflections from the lower surface of the joint. The finite transducer was located in a semi-infinite half-space of water above the joint.

Figure 9.19 also shows a schematic illustration of the paths of the finite ultrasonic beams and the received field. The general case is shown, in which both the longitudinal and the shear waves in the adherend are homogeneous and both a shear and a longitudinal wave are reflected and transmitted each time a beam encounters an interface. The reflected field which is illustrated therefore contains four contributions in addition to the front face reflection R1. The first reflection to be received, R2, is the shear-shear contribution from the bondline, involving shear beams only. The final reflection, R4, is the longitudinal-longitudinal contribution, involving longitudinal beams only. Between these two are two other combinations, the shear-longitudinal and the longitudinal-shear

beams which contribute at the same location in the field to make the reflection R3. Although not shown in the illustration, additional contributions to the field would be received further downstream due to subsequent reverberations of the signal in the upper adherend and reflections from the lower boundary of the lower adherend. In practice such reflections would be ignored by gating the signal, as discussed in Section 9.2.

A 10 mm diameter transducer was modelled in the first simulation, operating at a single tone of 25 MHz. Two cases were considered. In the first case the transducer was placed at an angle of incidence of 23.7 degrees in the water so that the refracted shear wave in the titanium was incident on the bondline at an angle of 61.1 degrees. This angle corresponds to the locus of the reflection coefficient minimum at the location shown in Figure 9.16. In the second case the angle in water was reduced by one degree to 22.7 degrees, resulting in a reduction of the angle in the adherend by 3.9 degrees to 57.2 degrees. The intention of the second case was to provide a reference reflection, when there is no minimum, for comparison.

The field predictions are presented in Figure 9.20. The full fields are shown in part (a) of the figure and enlargements of the bondline reflections in part (b). The solid line is for the first case when the angle was appropriate for the reflection coefficient minimum and the dashed line is for the 'off-angle' case. The distortion of the reflected beam can be seen very clearly in the first case, corresponding to the transmission of much of the energy of the beam through the layer. In the off-angle case however the reflected beam is specular. The positions of arrival of the bondline reflections agree perfectly with trigonometric calculations of the beam paths, the off-angle reflection whose angle was smaller arriving slightly closer to the front face reflection. There are no other contributions to the field because in both cases the transducer angle is larger than the critical angle for longitudinal waves and so there are no homogeneous longitudinal waves in the adherend.

The second simulation used a 5 mm diameter transducer, operating at a single tone of 100 MHz. Again two cases were considered, one corresponding to the locus of the reflection coefficient minimum at the location shown in Figure 9.17, and the other at a half-degree smaller angle. The angles in water were 12.1 and 11.6 degrees respectively and the longitudinal angles in the adherend were 59 and 55.3 degrees respectively.

The field predictions for the second simulation are presented in Figure 9.21, again using solid lines for the first case and dashed lines for the off-angle case. All of the possible contributions to the field are now present in both cases and their positions again agree

with calculations of the beam paths. In the first case the shear-shear contribution to the field is specular but the contributions involving longitudinal waves are distorted. All of the off-angle contributions are specular.

According to the discussion in Section 9.2, minima in the reflected field may occur either when the transmissibility of the plate is a maximum or when a mode is excited. The simulations which have been presented here were made at locations on the loci of the plane wave reflection coefficient minima, shown in Figures 9.16 and 9.17, and therefore addressed the former category. The distortion is strong because the 'central' plane wave components of the finite beam, those whose angle of incidence is approximately that of the transducer, are transmitted through the layer whereas there is significant reflection of the plane wave components at other angles. In both cases the plane wave reflection coefficient minima were sharp (as in the 'good' case in Figure 9.18(a)) and so the contrast between the reflection amplitudes of the 'central' and the 'off-angle' components was strong.

An important question is whether separate near-field minima can also be found at frequencies and angles which match locations on the dispersion curves. The presence of such minima may then indicate the excitation of modes. Of course it should be expected that the minima may be very weak because of the strong attenuation of the modes and the consequent poor coupling of the incoming waves with the modes.

An attempt was made to find such minima, using embedded shear wave transducers, introduced in Section 9.3 and illustrated in Figure 9.5, and, similarly, embedded longitudinal wave transducers. The reflected fields were predicted at several frequencies and angles which matched locations on the dispersion curves and which were remote from the loci of the plane wave reflection coefficient minima. Pairs of transducers were also used to predict the measurement of the amplitude of the received signal, performing frequency sweeps in the same manner as for the infinite plane wave study. However no evidence was found of the excitation of the modes. It was concluded that, as discussed in Section 9.2, there was insufficient coupling between the incident wave and the attenuating mode for significant energy to be transferred to the mode. Perhaps this is not surprising when it is considered that the attenuation of the modes is typically greater than 10 Nepers/mm at the locations on the dispersion curves where there is good separation from the loci of the plane wave reflection coefficient minima. This rate of attenuation corresponds to more than 99.99 % loss of amplitude per mm travelled.

9.5 Sensitivity of interface waves to the properties of the joint

One of the potential attractions of interface waves which was stated at the start of this chapter was that they may be particularly sensitive to the properties of the embedded layer and insensitive to the properties of the adherends. They could therefore be used, not solely to detect the layer, but to characterise it.

Unfortunately it is clear at this stage in the investigation that it will not be possible to excite and measure the interface waves because of the extreme attenuation of the modes. The analysis of the variant cases in which the influence of the different parameters of a joint are studied would therefore appear to be futile. However it seems that the reflection coefficient minima which are associated with the transmission of plane waves through the layer may be measurable and could in principle be used to characterise the layer. Since the minima are related indirectly to the modal properties of the system, the parameters of the joint which affect the dispersion curves are likely to affect the loci of the reflection coefficient minima. For this reason, and for the completeness of the investigation, it was therefore considered useful to conduct the parametric study.

Considering the cases which were assessed in Chapter 8, some of the results are evident immediately. The dispersion curves are completely insensitive to the total thickness of the joint because of the proposal to gate the ultrasonic signals in practice and the consequent nature of the system which was modelled. For the same reason they are completely insensitive to the location of the layer within the joint and would even be insensitive to tapered adherends.

The curves are rather sensitive however to the thickness of the embedded layer, the frequency axis of the dispersion curves scaling linearly as with Lamb waves. Thus for example, referring to the curves in Figure 9.9, the cut-off frequency of 11 MHz for mode 1 in the 100 micron thick layer would be at 22 MHz in a 50 micron layer.

Alpha case with slower bulk velocities

Figure 9.22 shows the effect of varying the values of the acoustic velocities of the alpha case material on the dispersion curves. The solid lines show the dispersion curves for the reference case, originally plotted in Figure 9.9, of the 0.1 mm thick layer of alpha case with 10 % faster longitudinal and shear bulk velocities. The dashed lines show the curves for the same system but with only a 5 % increase in the bulk velocities of the alpha case.

All of the modes show substantial reductions in their velocities, indicating their strong dependence on the properties of the layer. Indeed in the cases of modes 1 and 6, the reduction could have been foreseen because of the bounded nature of the curves. The velocity of mode 1 must always lie between the shear velocity in the adherend, at low frequency, and the shear velocity of the layer, at high frequency. Similarly the velocity of mode 6 must lie between the longitudinal velocities of the two materials. A second important observation concerning these two modes is that their cut-off frequencies have approximately doubled.

Graded layer of alpha case

Figure 9.23 shows the dispersion curves for a graded layer of alpha case, the solid lines again showing the reference curves and the dashed lines, the variant curves. The graded layer was exactly that which was studied in the context of Lamb waves, in Chapter 8. Thus the 0.1 mm thick layer was divided into three sub-layers of equal thickness. The central sub-layer was given 10 % faster longitudinal and shear velocities and the two adjacent layers were given 5 % faster longitudinal and shear velocities. The profile was therefore the simplest case of the triangular distribution which was modelled in the normal incidence reflectivity studies of Chapter 7.

In general the curves lie between the reference case and the first variant case (the alpha case with slower bulk velocities), as would be expected if a single layer was modelled using the average properties of the three sub-layers. There are some exceptions however, modes 7, 8 and 9 being almost the same as the first variant case and the divergence of mode 3 from the reference case actually increasing very slightly. This suggests that these modes are dominated by the material near the surfaces of the layer and are not sensitive to the central portion of the layer. Indeed the mode shapes of the strain energy density for these four modes (not shown here) support this observation, the energy being strongly concentrated at the edges of the layer.

Adherends with faster bulk velocities

Figure 9.24 shows the effect of varying the values of the acoustic velocities of the adherend material. The dashed lines in this plot show the dispersion curves for the system with a 1 % increase in the bulk longitudinal and shear velocities of the titanium. An uncertainty of this order in the bulk properties of the titanium is consistent with the variations in the measurements of the material which were reported in Chapter 6.

The curves show some changes from the reference case but the differences are small, particularly in the low velocity modes. The variant curve for mode 1 is present but is completely obscured by the reference curve. In fact it differs slightly at its low frequency end, the cut-off frequency and velocity both being slightly higher than in the reference case.

The case of a layer between unmatched adherends has not been calculated, the present variant case sufficiently demonstrating the general insensitivity of the modes to the properties of the adherends. If the adherends are unmatched and there is no embedded layer, in a good bond, then there is no mode at the interface, as discussed in Section 9.3

9.6 Discussion

Previous work

Previous work in the application of interface waves to nondestructive testing has addressed both single interface geometries and embedded layers.

In the category of single interface geometries, Lee and Corbley (1977) made predictions and performed calculations for interface waves travelling along the boundaries between pairs of different metals, including aluminium, steel and titanium, with a view to characterising the boundary conditions at the interfaces between such materials in interference-fit components. In the perfect contact cases they found free wave solutions with some materials and leaky solutions with others, the leaky solutions having low values of attenuation, and they obtained good agreement between theory and experiment. Kumar (1983) was also interested in characterising the interface boundary conditions between components, in this case of the same material. He studied the interface between two half-spaces of steel for different boundary conditions, finding free wave solutions when the contact was imperfect. In the context of adhesively bonded joints, some researchers have investigated the possibility of using an interface wave at the boundary between the adhesive and the adherend, operating at sufficiently high frequencies and bondline thicknesses to be able to ignore the second adhesive-adherend boundary. Claus and Kline (1979) found an experimental correlation between the attenuation of true Stoneley waves and the surface roughness of the adherend. Pilarski (1985) proposed the use of such interface waves to inspect the adhesion quality.

In the category of embedded layers, a number of researchers have investigated the use of guided waves which travel along a flexible layer between two stiff half-spaces without leaking energy, a particular interest again being the inspection of adhesive joints. Such waves have the advantage that they can propagate over long distances but are only useful if access is possible to the ends of the layer because they can neither be excited nor received through the adherends. Rokhlin, Hefets and Rosen (1980 and 1981) and Rokhlin (1986) demonstrated experimentally that a guided wave travelling along a layer of adhesive between two half-space adherends may be used to determine the material properties of the adhesive (the cohesive properties) at various states of cure.

Nagy and Adler (1989) and Nagy, Rypien and Adler (1990) additionally considered other modes of the adhesive joint system, including both leaky shear and leaky longitudinal modes which could in principle be excited and received through the adherends. Their ultimate interest was to detect both poor cohesion and poor adhesion in joints. They predicted and measured transmission coefficient maxima through the adhesive layer, obtaining generally good agreement. They also anticipated divergence of these maxima from the modal solutions at locations where the predicted leakage was strong. Such divergence was discussed in Section 9.2 of this chapter and by Chimenti and Rokhlin (1990).

Interface waves at a single interface

In the present investigation it has been found that there is no propagating interface wave between half-spaces of titanium and alpha case. This category of wave could not therefore be utilised for the inspection of the diffusion bonded joints, even if testing could be conducted at sufficiently high frequencies that the finite thickness of the layer could be ignored.

However the study which was made using 'light' titanium showed that in cases where a leaky wave does exist at a single interface it is potentially very useful, supporting the findings of the previous workers. The attenuation of the wave was found to be very sensitive to the degree of acoustic mismatch between the half-spaces. Moreover the value of the attenuation was found to be low in general, even when the acoustic contrast was relatively small. Accordingly it was found in the simulations that such a wave could be excited readily using the coincidence principle and could be detected accurately using the null zone technique.

Furthermore, a bonus with the measurement of waves at a single interface is the fact that there is only one mechanism which can be associated with a reflection minimum, unlike the complications of the embedded layer. A minimum in the reflection coefficient must be associated with the modal properties of the system because the transmission mechanism which was discussed in Section 9.2 cannot exist at the conditions when the mode is excited. The angle of incidence is significantly larger than the critical angle for shear waves in the stiffer half-space and consequently infinite plane waves are reflected totally.

Leaky waves at a single interface may be useful for the inspection of diffusion bonded joints where the materials of the two adherends are different. In such cases the conventional normal incidence inspection technique would not be optimal because a signal would always be reflected from the bondline, even in a good joint, obscuring any small reflections from defects. However an interface wave may be rather sensitive to the properties local to the bondline, particularly if the technique exploits the dependence of the effective depth of the wave on the frequency. Other joints which could potentially be inspected by such waves are joints in which an interface layer is known to exist but may need to be characterised, such as diffusion brazed joints and, as mentioned above, adhesive joints.

Interface waves in an embedded layer

Regarding the second category of geometry, the embedded layer, the nature of the present investigation differs fundamentally from the work on adhesive joints. The embedded layer of alpha case is stiffer than the titanium adherends whereas in an adhesive joint the embedded layer is less stiff than the adherends. The properties of the alpha case are also very similar to those of the adherends unlike the large difference in the acoustic impedances which is normal in an adhesive joint. Moreover, the primary task addressed here is to detect the presence of a layer which may be extremely thin. In an adhesive joint the layer is known to exist and the task is to characterise it.

The predictions are not promising. All of the modes are leaky, which is an attraction in principle because it means that they could be excited and received through the adherends. However the attenuations in all cases are extremely strong and it would be impossible to contemplate any remote measurement of the velocity of the modes at a location downstream of the point of excitation. In fact, even at the point of excitation, the simulations indicate that incident waves in the adherend are unable to excite the extremely attenuative modes. The inspection therefore addresses the detection of minima

in the point reflection which are caused, not by the modal properties of the system, but by the different (although associated) mechanism of maxima in the transmission of energy through the layer.

As far as the detection of the presence of the layer is concerned, the exploitation of these minima clearly offers no advantage over normal incidence inspection. In order to detect a minimum in the reflected signal using the null zone technique it would be necessary to detect significant reflections over a range of angles or frequencies. In a good joint there would be no reflection from the bondline. In a bad joint the presence of the layer would be indicated, not by the minimum of the reflection, but by the fact that reflections could be found at other angles or frequencies.

If the layer is known to exist and its characterisation is required, then the measurement of the minima appears to be more attractive. The dispersion curves are rather sensitive to the properties of the layer and rather insensitive to the properties of the adherends. Assuming, very reasonably, that the loci of the minima are as sensitive as the modes, such reflection measurements could therefore be used to examine the properties of the layer. However, the measurements would be feasible only when the alpha case is relatively thick and has good acoustic contrast with the titanium. Referring to the reflection coefficient minima in Figures 9.16 and 9.17, a transducer with a centre frequency of at least 25 MHz would be required in order to characterise the low frequency loci. If the layer was 50 microns thick then the same information would require a transducer with a centre frequency of 50 MHz. Since the upper frequency limit in practice is no higher than 80 MHz (see discussion in Chapter 7), the thinnest layer which could be examined would be at least 30 microns thick.

9.7 Possible alternative inspection strategy

It is clear from this investigation and from the Lamb wave study which was reported in Chapter 8 that plate waves are not attractive either for the detection or for the characterisation of the embedded layer. The conventional technique, the measurement of reflectivity at normal incidence, is therefore currently the most sensitive approach. Fortunately the investigation of the conventional method revealed that in principle it is extremely well suited to the detection of alpha case and it also has the benefit of simplicity of application. It may therefore not be necessary to pursue any other alternatives.

However another ultrasonic approach, the oblique incidence reflectivity method, has not been considered for this inspection problem to date and it is possible that it may offer significantly greater sensitivity than the normal incidence technique. Although the method utilises pairs of transducers at oblique angles of incidence in exactly the same arrangement as was discussed in the context of modal inspection, the method is fundamentally different. Instead of identifying the frequency and angular conditions at which changes can be observed in the reflectivity, the method is based on the measurement of the amplitude of the reflected signal at a particular frequency and angle. It is therefore much more closely related to the normal incidence technique, the only difference being the selection of appropriate oblique angles in order to maximise the sensitivity.

The method has been studied widely in the context of the characterisation of adhesive joints. For example Pialucha (1992) addressed the inspection of the interface between the adhesive and an adherend using oblique incidence measurements. A review is also presented by Cawley, Pialucha and Lowe (1993). In fact the task of characterising an adhesive joint by this method is difficult; the layers of the joint are known to exist and the measurement system must rely on detecting changes in the amplitude of the reflectivity. In the present case the task is somewhat simpler; as with the normal incidence measurements, the reflection only exists if the layer is present. It would therefore appear that the method is well suited to the detection of the embedded layer.

Such an investigation into oblique incidence response is outside the scope of this thesis. However one possibility which could be explored is to measure the reflectivity from the layer using waves which are incident on the layer at super-critical angles. Super-critical angles are angles of incidence in the adherend which are larger than the angle at which the transmitted wave in the layer becomes inhomogeneous. The method could use either shear or longitudinal waves. The use of shear waves offers the advantage that any longitudinal waves which are reflected or transmitted are inhomogeneous so that the received signal is simple, just as in the near-field simulations in Section 9.4. It may be simpler however to make measurements of longitudinal waves because the angle of incidence of the transducer will be smaller.

Taking an incident shear wave as an example, if the layer is infinitely thick then total reflection of the shear wave takes place at super-critical angles but if the layer has finite thickness then the reflectivity is dependent on the properties of the layer, the layer thickness and the angle of incidence. This is illustrated in Figure 9.25(a) which shows the predicted reflection coefficient for shear waves for several thicknesses of alpha case

and for the full range of angles. It can be seen that the reflectivity at super-critical angles is very much larger than at normal incidence and is rather sensitive to the thickness of the layer. Furthermore, the positions of the curves in the horizontal direction in the plot will depend on the material properties of the alpha case because the critical angle is defined by the bulk velocity of the layer.

The 'tunnelling' mechanism which permits the transmission of some energy through the thin layer at super-critical angles is illustrated in Figure 9.25(b). Here it can be seen that, even if the shear wave in the layer is inhomogeneous, it may transmit energy into the lower adherend. In order for energy not to be transmitted, the depth of penetration, the depth in which the majority of the energy of the inhomogeneous wave is retained, must be smaller than the thickness of the layer. The exponential function which describes the decay of the wave with the depth from the interface is dependent on the wavenumber in the direction along the layer and on the frequency, as discussed in detail in the derivation in Chapter 2 (see Section 2.5). Accordingly, the depth of penetration of the inhomogeneous wave reduces with both the angle of incidence in the adherend and with the frequency.

9.8 Conclusions

Model studies have been conducted to investigate the potential of using interface waves for the inspection of an embedded layer of alpha case in a diffusion bonded joint.

A study of the interface wave which travels along the boundary between two different materials indicated that in general such a wave shows good potential for nondestructive testing. A single, leaky non-dispersive mode may exist between certain pairs of materials. It may readily be excited and received and is sensitive to the properties of the materials in the region of the interface. However it could only be utilised in embedded layers if its depth of penetration was significantly smaller than the thickness of the layer. This would require tests to be conducted at extremely high frequencies for very thin layers. Moreover it was found that such an interface wave does not exist in the specific case of the interface between titanium and alpha case.

A study of the modal properties of a layer of alpha case embedded in titanium revealed that there is an infinite family of these interface waves just as there is with Lamb waves. However the nature of the modes is substantially different. The dispersion curves bear little resemblance to the Lamb wave curves and all of the waves leak energy strongly into the adherends. In general the dispersion curves are sensitive to the properties of the layer

and insensitive to the properties of the adherends. However the strong attenuation of all of the modes precludes any form of remote measurement of wave velocities. Point reflection measurements made at the same location as an incident signal may be used to detect spectral or angular minima which are associated (though not directly) with the modal properties of the system. The conditions for these minima could in principle be used to characterise a layer which is known to exist although they are clearly inappropriate for the detection of the presence of the layer. However with realistically thin layers of alpha case and small acoustic contrasts between the materials, the frequencies of the minima are likely to be too high for practical exploitation.

It is therefore concluded that interface waves offer no practical potential for the inspection of alpha case in diffusion bonded titanium.

Leaky waves at a single interface may be useful for the inspection of diffusion bonded joints where the materials of the two adherends are different. In such cases the conventional normal incidence inspection technique would not be optimal because a signal would always be reflected from the bondline, even in a good joint, obscuring any small reflections from defects. However an interface wave may be rather sensitive to the properties local to the bondline, particularly if the technique exploits the dependence of the effective depth of the wave on the frequency. Other joints which could potentially be inspected by such waves are joints in which an interface layer is known to exist but may need to be characterised, such as diffusion brazed joints and adhesive joints.

Finally, an oblique incidence response measurement technique is proposed for investigation. An initial study indicates that it may offer strong sensitivity to both the presence and the nature of embedded stiff layers.

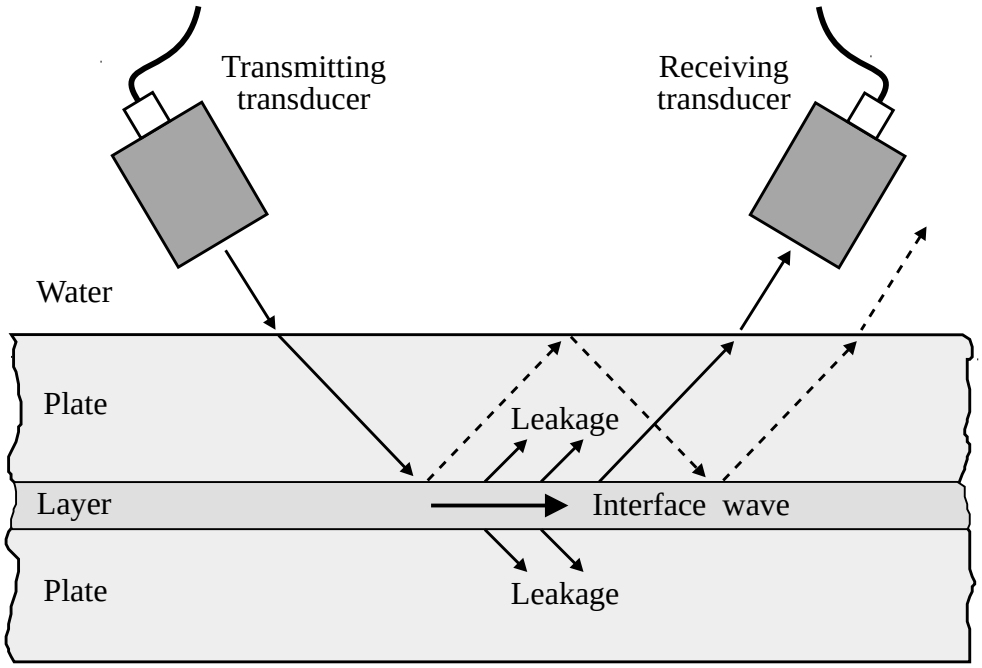

(a) Measurement of leakage downstream

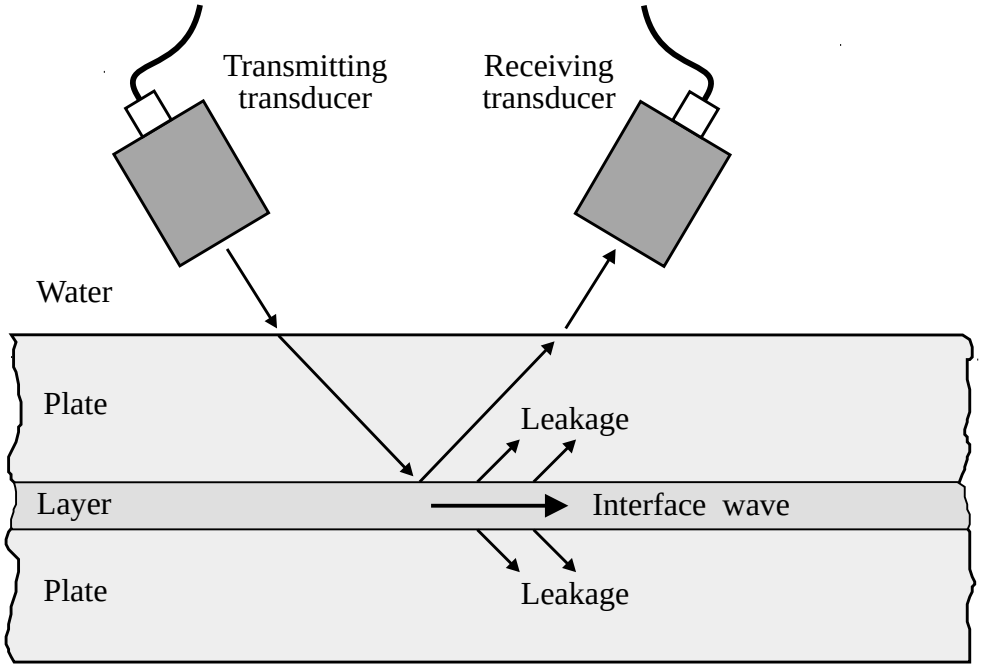

(b) Measurement of null zone

Figure 9.1 The excitation and detection of interface waves

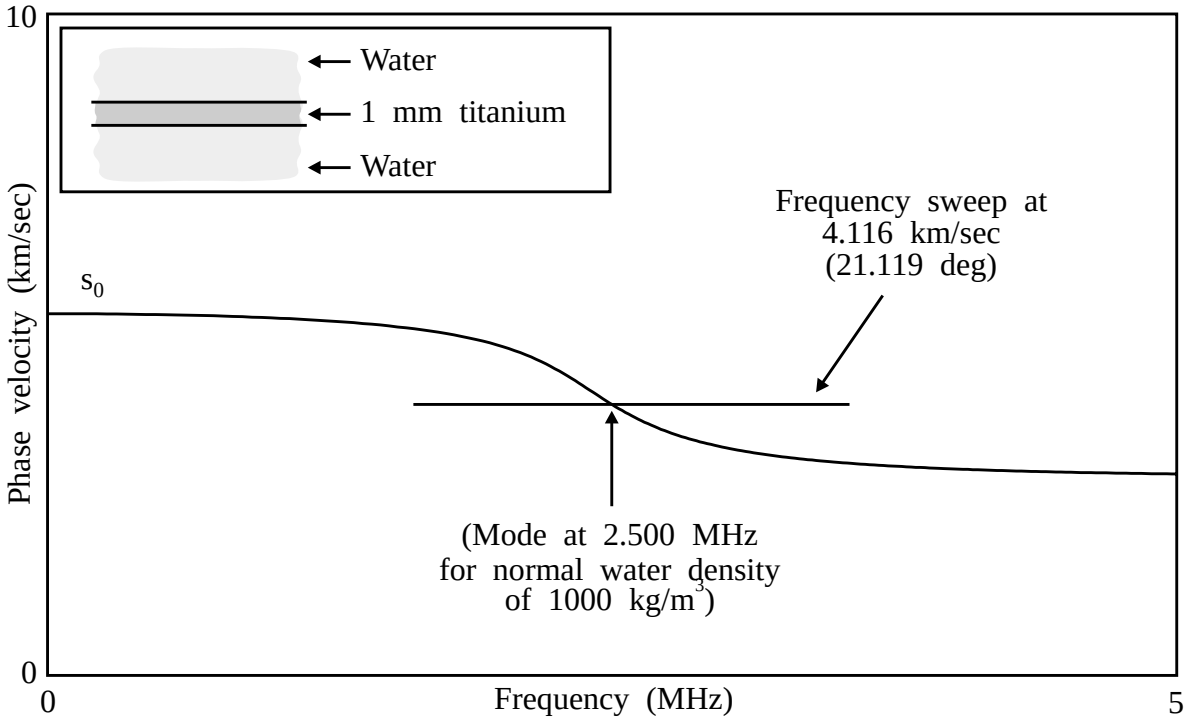

(a) Dispersion curve for leaky s_0 wave and location of frequency sweep

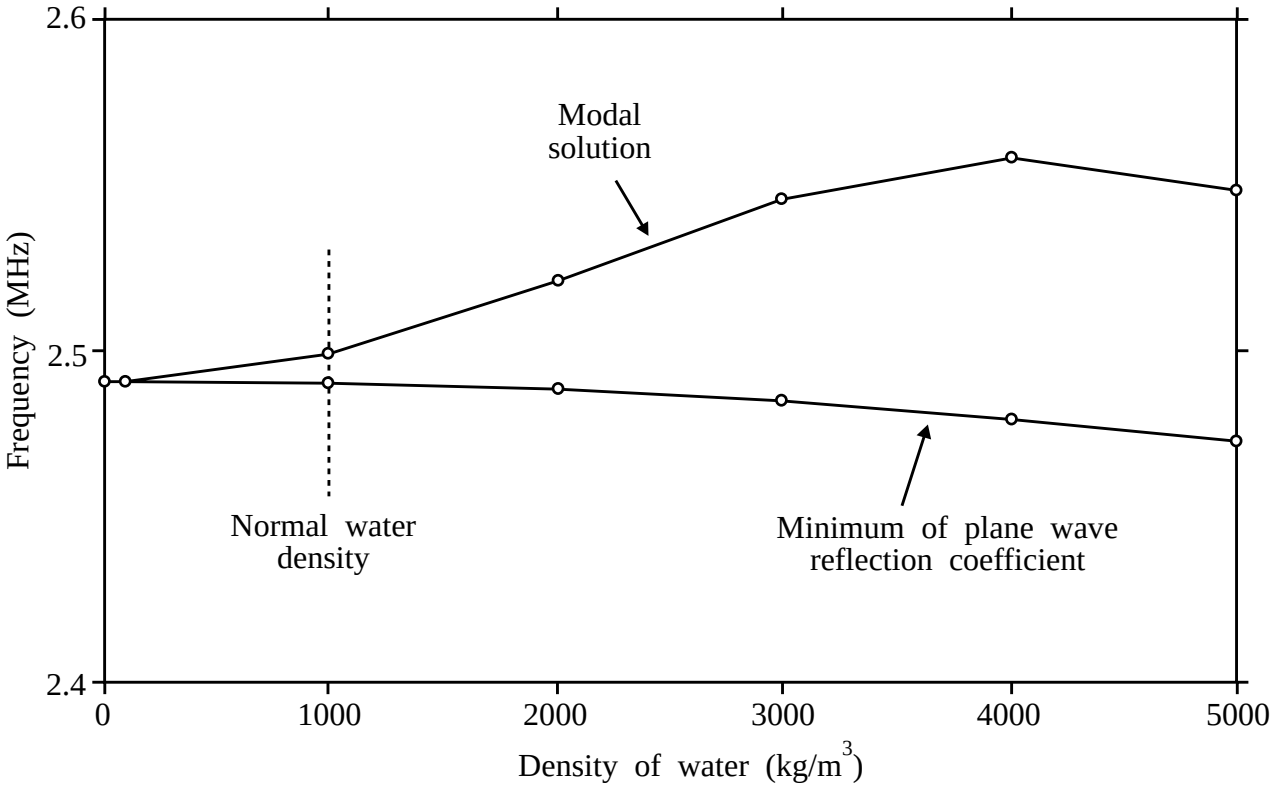

(b) Variation of modal and response frequencies with density of water

Figure 9.2 Comparison of modal solution and reflection coefficient minimum for leaky s_0 wave

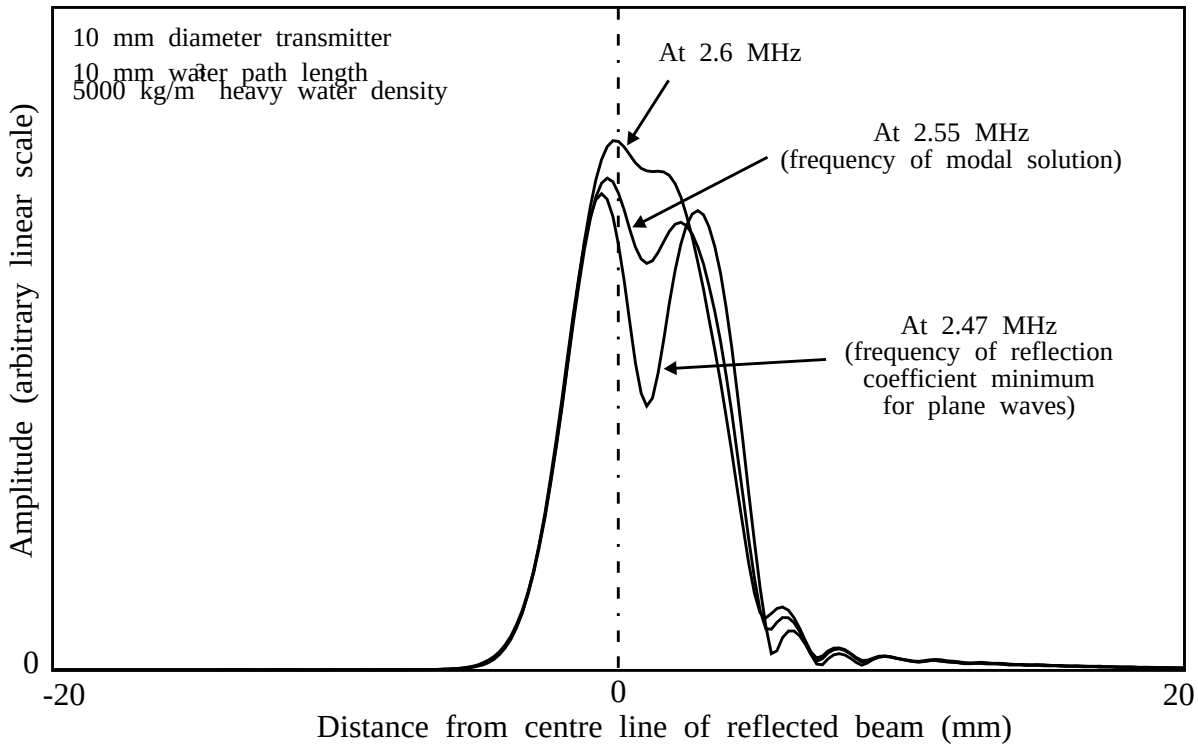

(a) Near-field response at 21.119 degrees at a selection of frequencies

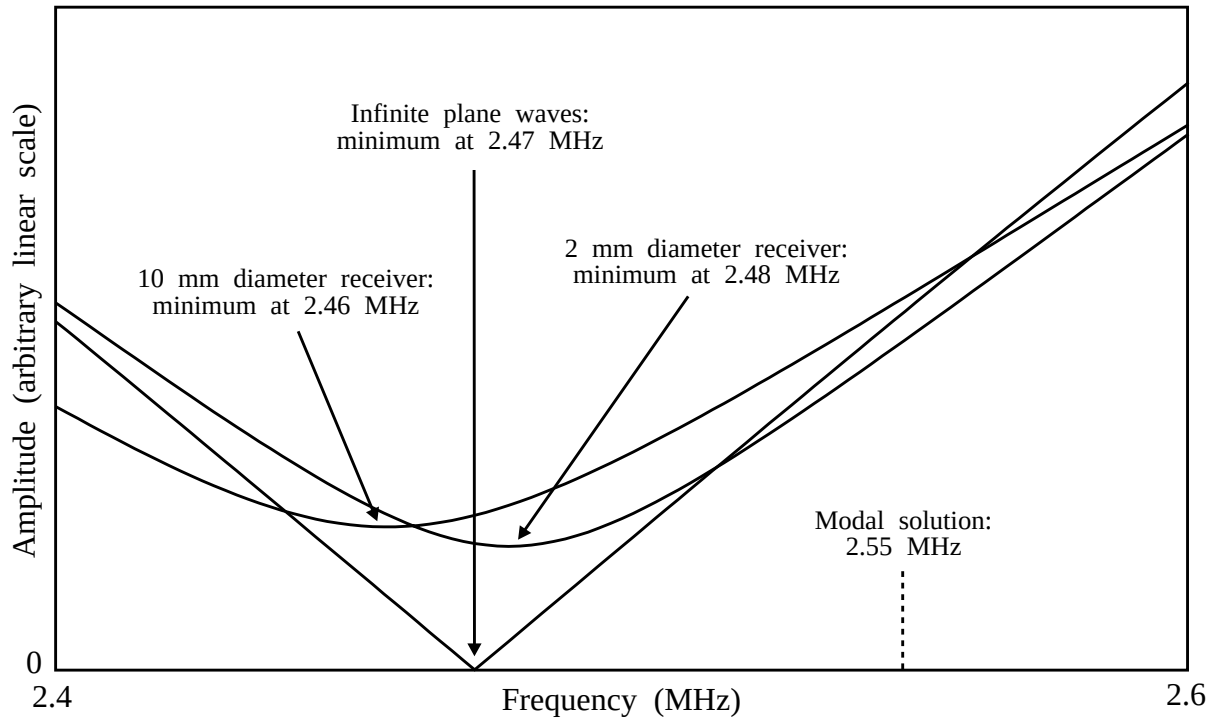

(b) Amplitude of received signal using frequency sweep at angle of 21.119 degrees; effect of varying transducer diameter

Figure 9.3 Near-field response and simulation of null zone measurements for s_0 wave in 'heavy' water

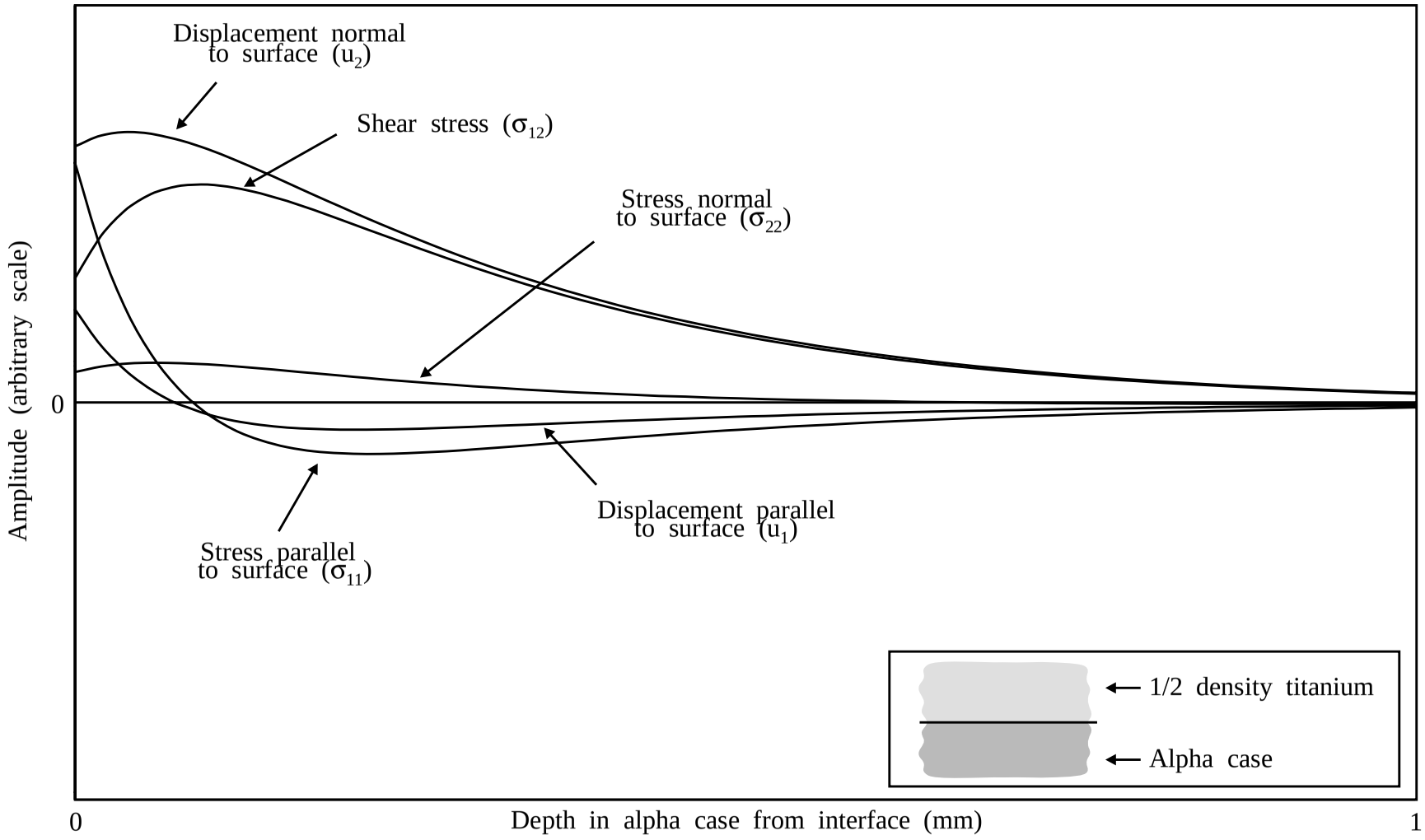

Figure 9.4 Interface wave between 'light' titanium and alpha case at 10 MHz - Mode shapes of guided part, in alpha case

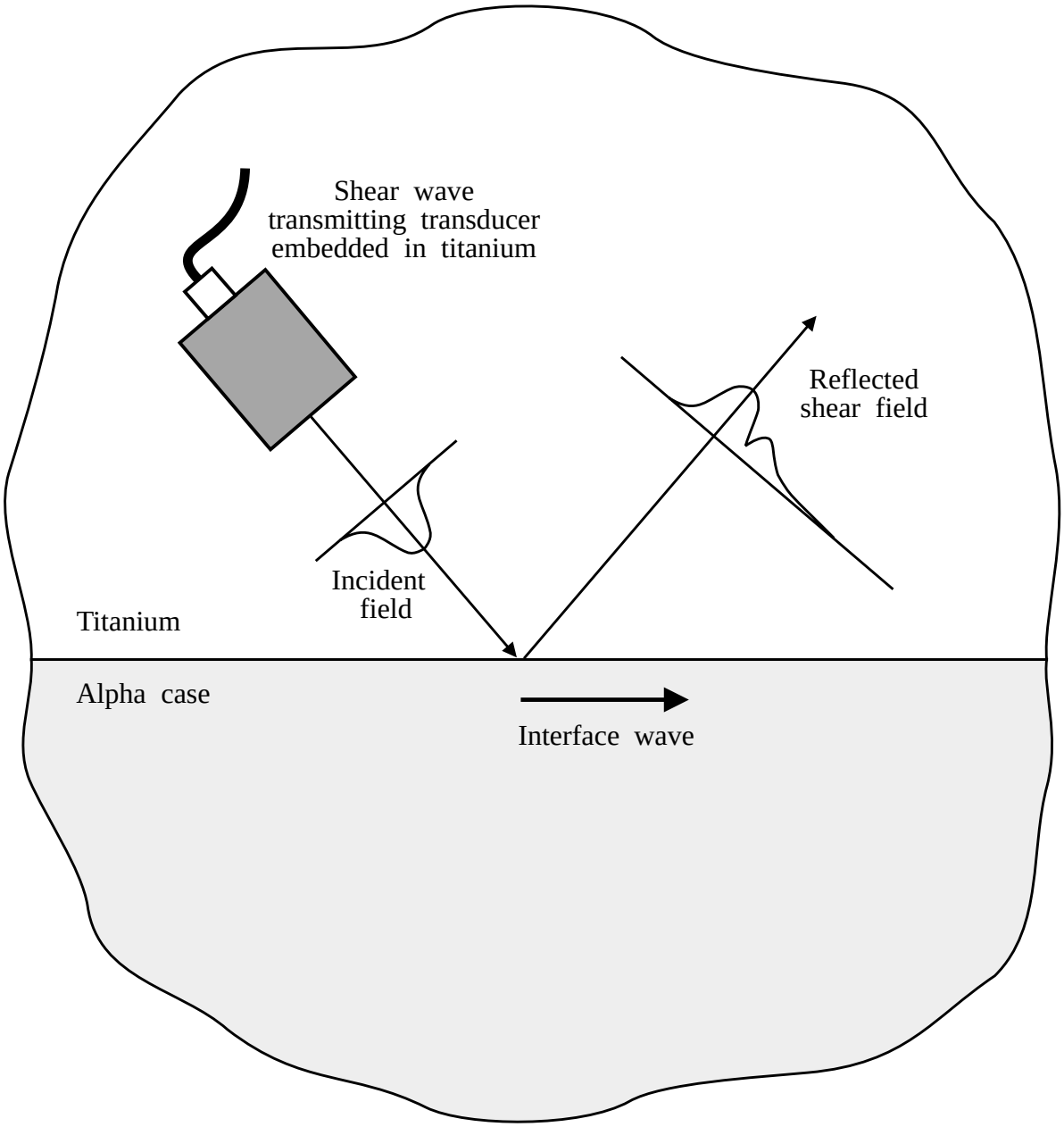

Figure 9.5 Simulation of embedded shear wave transducer for studying the excitation of interface waves

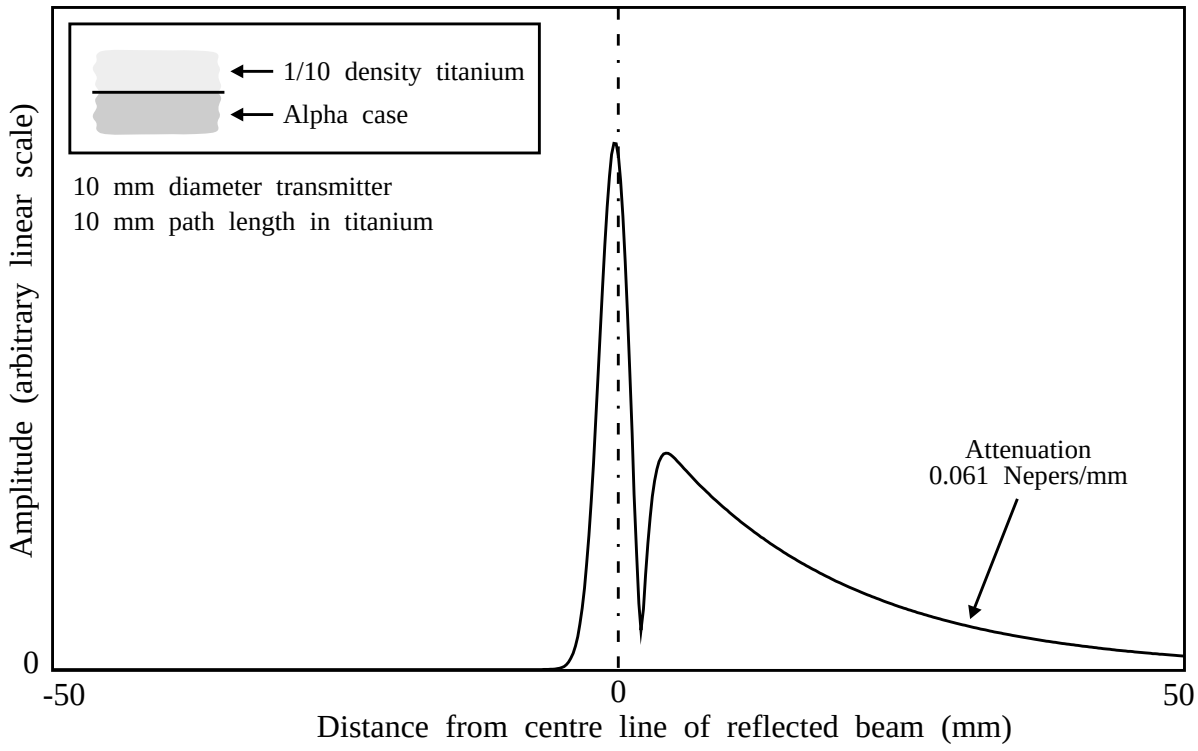

(a) Near-field response at 74 degrees and 10 MHz

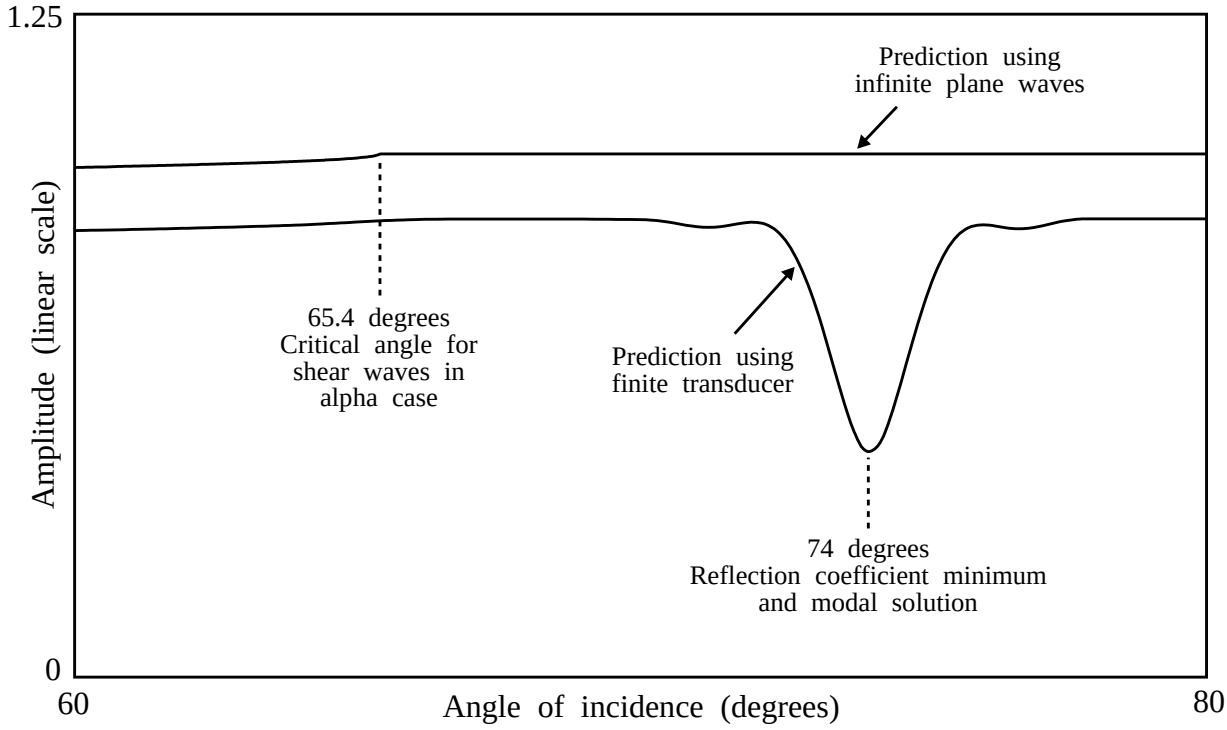

(b) Amplitude of received signal using angular sweep at frequency of 10 MHz

Figure 9.6 Predicted near-field response from interface between 1/10 density titanium and alpha case

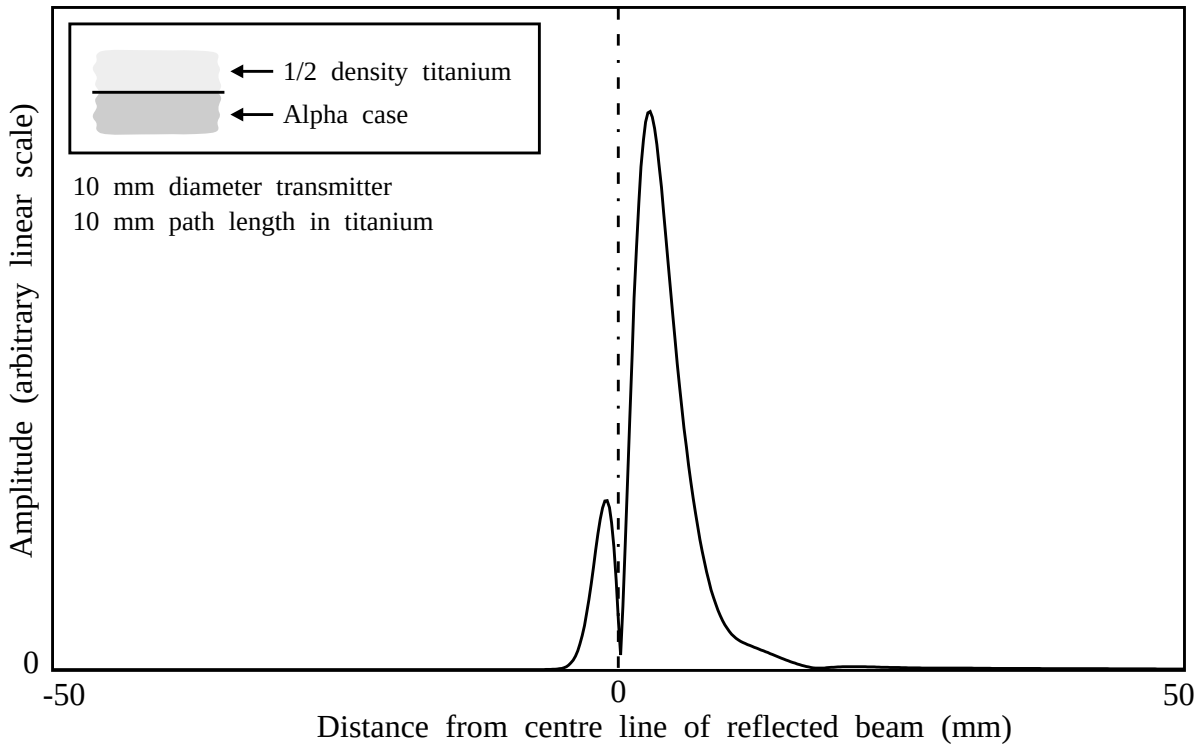

(a) Near-field response at 67.5 degrees and 10 MHz

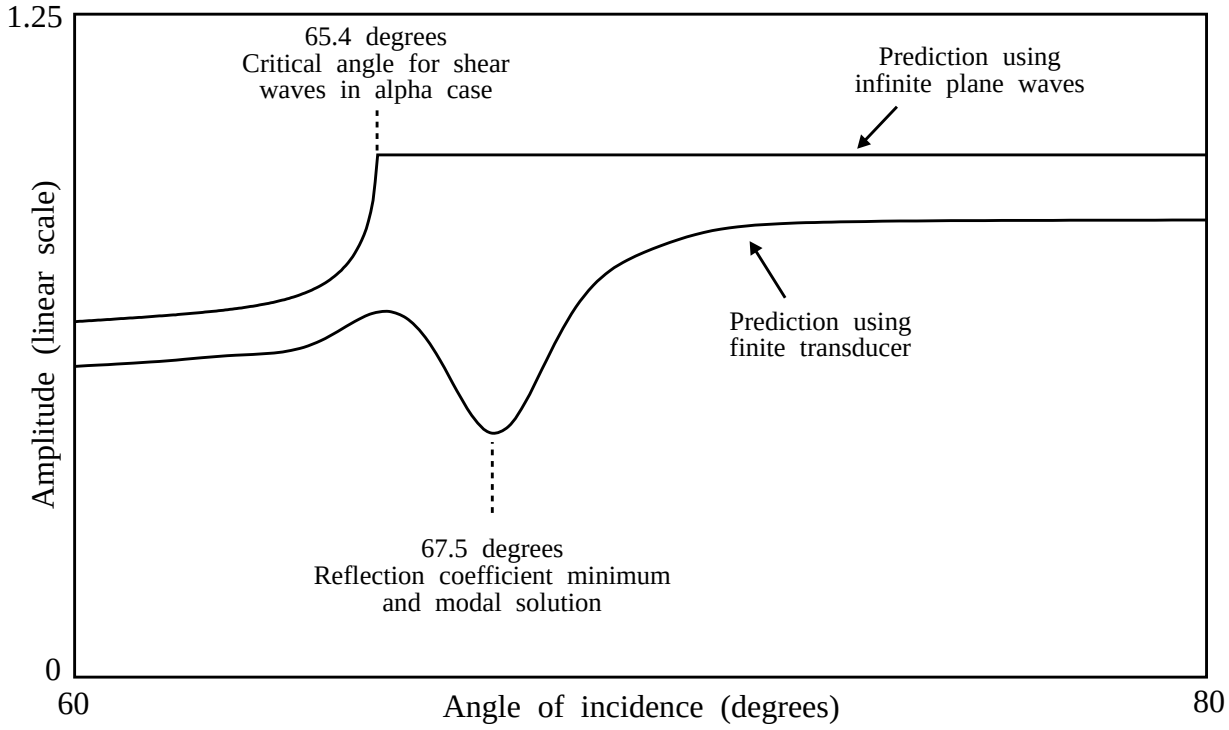

(b) Amplitude of received signal using angular sweep at frequency of 10 MHz

Figure 9.7 Predicted near-field response from interface between 1/2 density titanium and alpha case

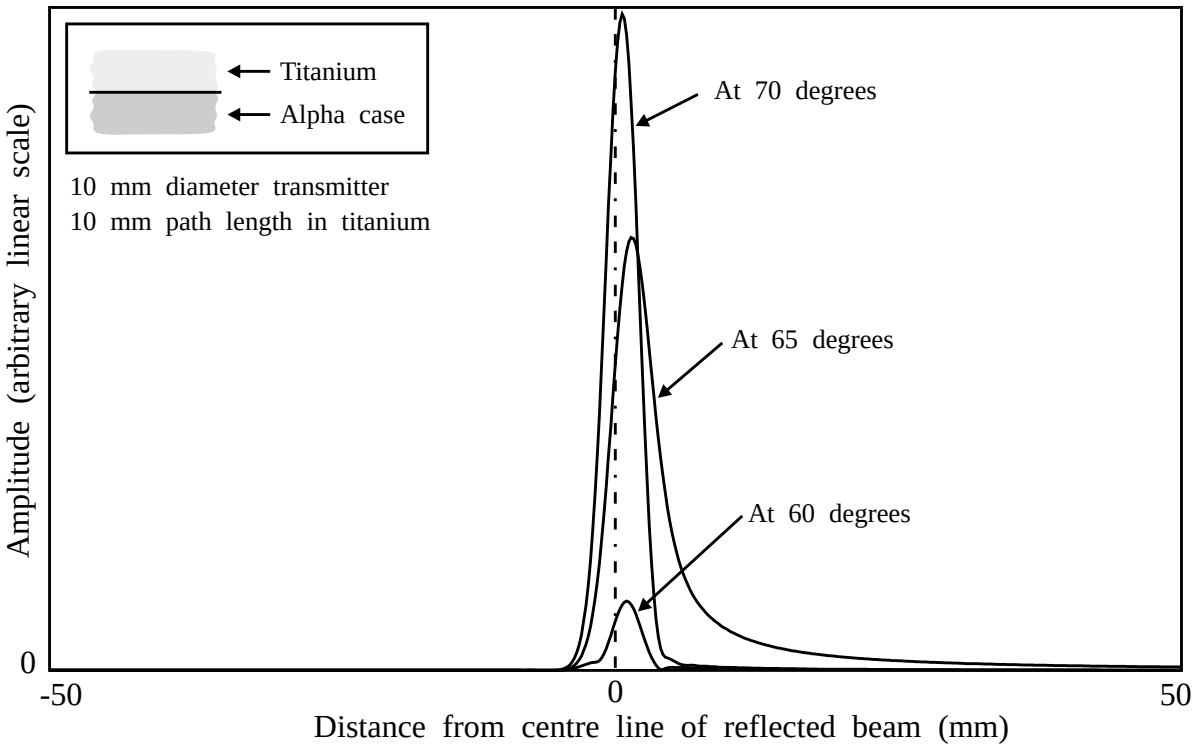

(a) Near-field response at 10 MHz and various angles

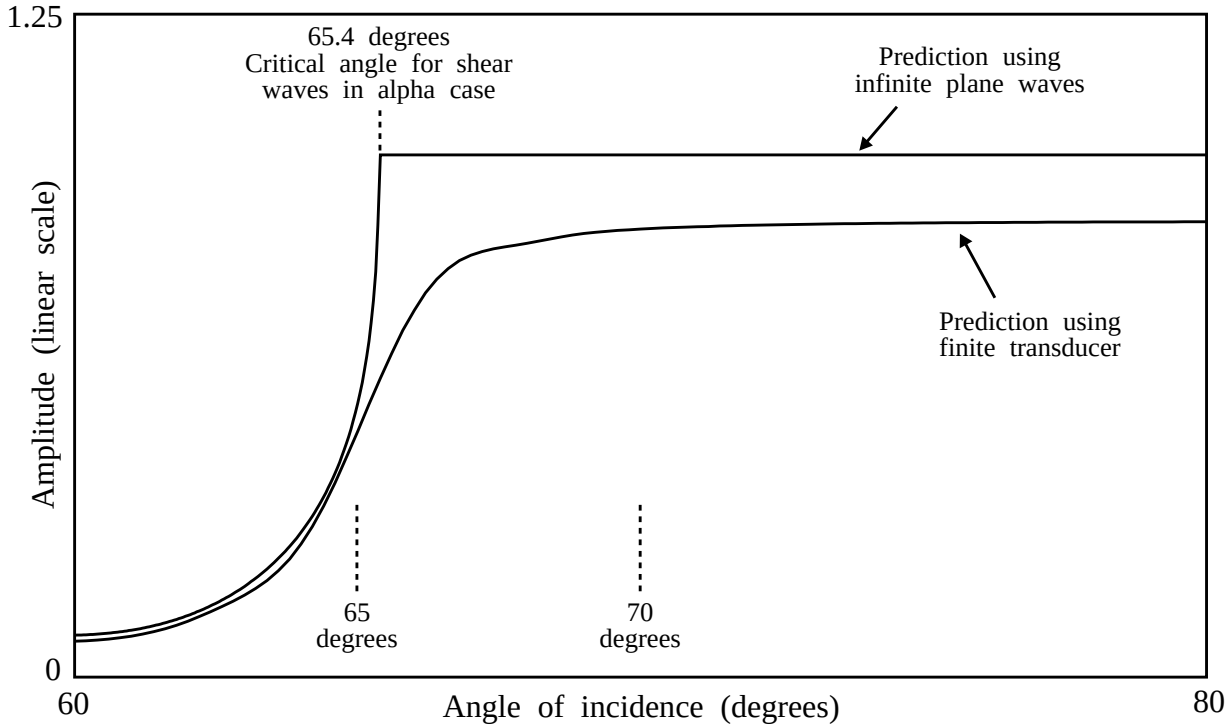

(b) Amplitude of received signal using angular sweep at frequency of 10 MHz

Figure 9.8 Predicted near-field response from interface between titanium and alpha case

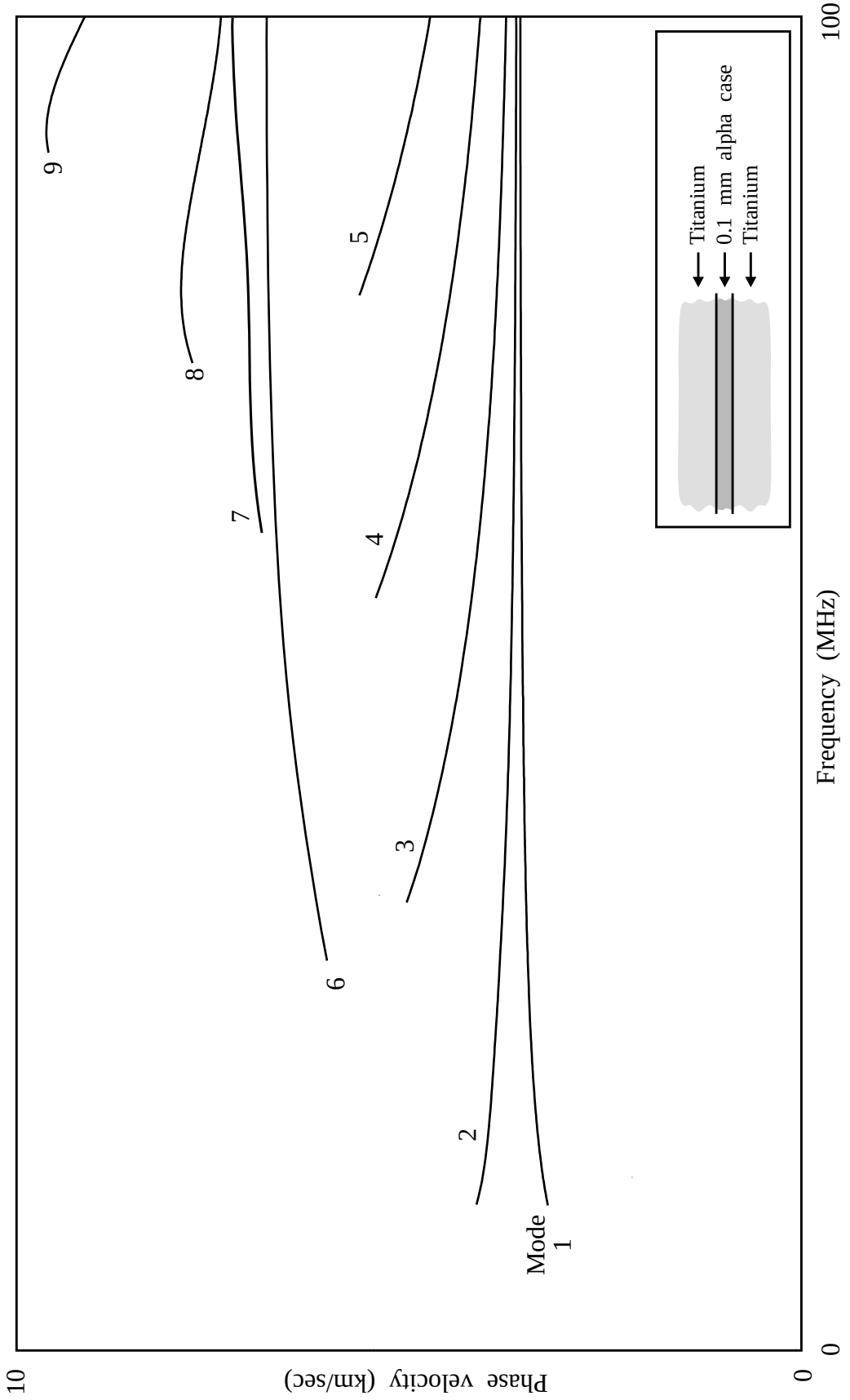

Figure 9.9 Interface wave dispersion curves for layer of alpha case embedded in titanium

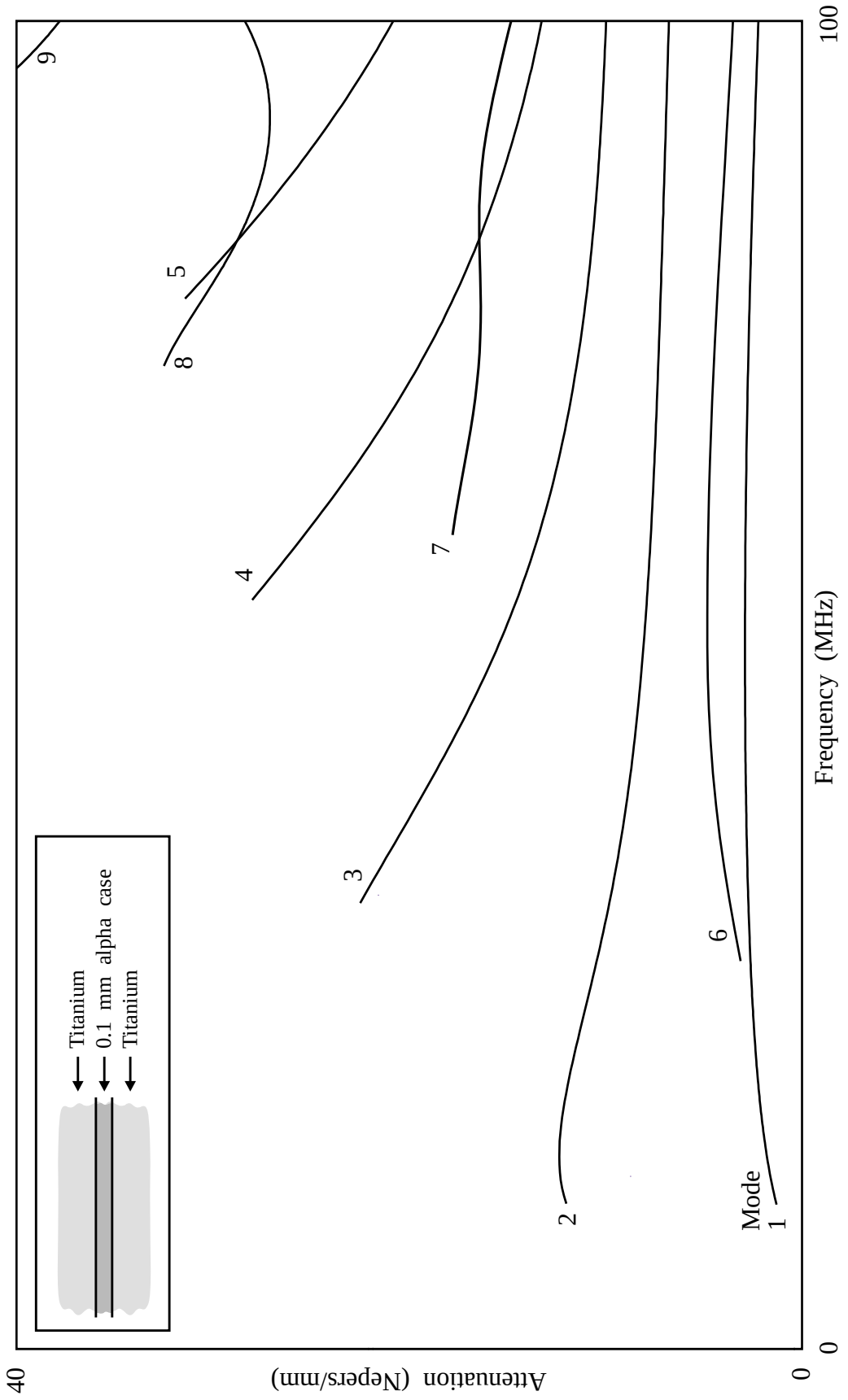

Figure 9.10 Attenuation of interface waves in layer of alpha case embedded in titanium

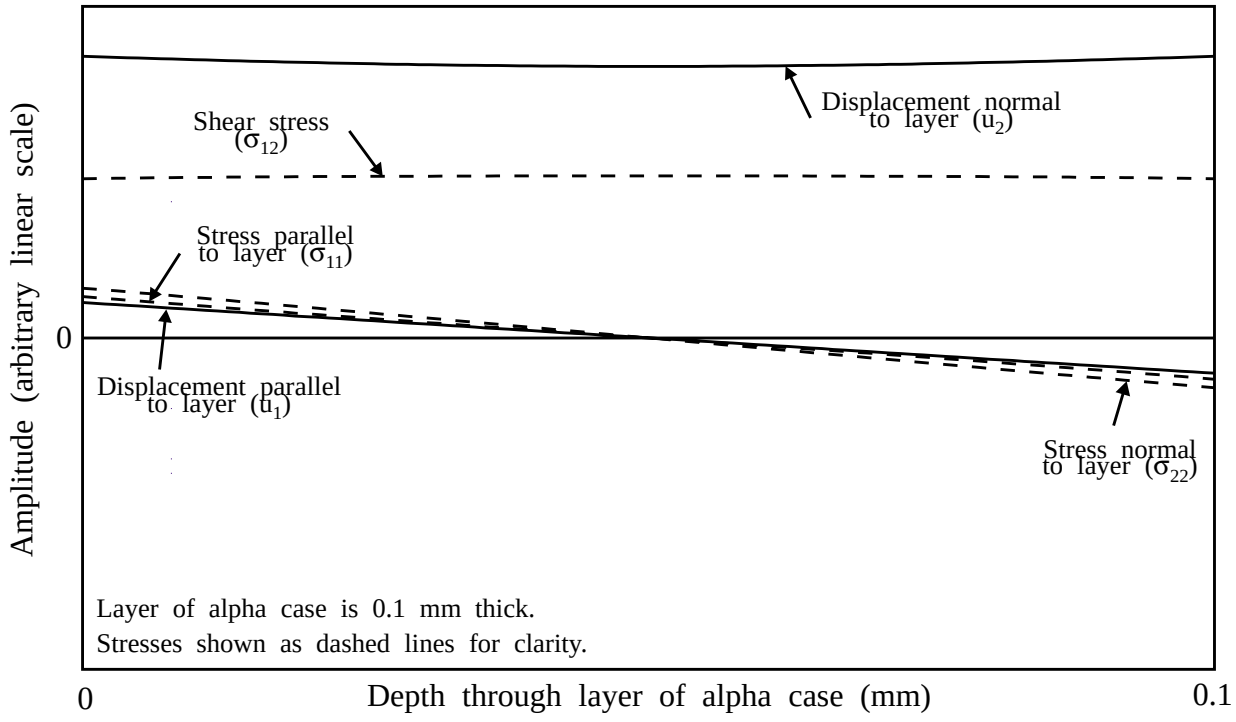

(a) At low frequency (12 MHz)

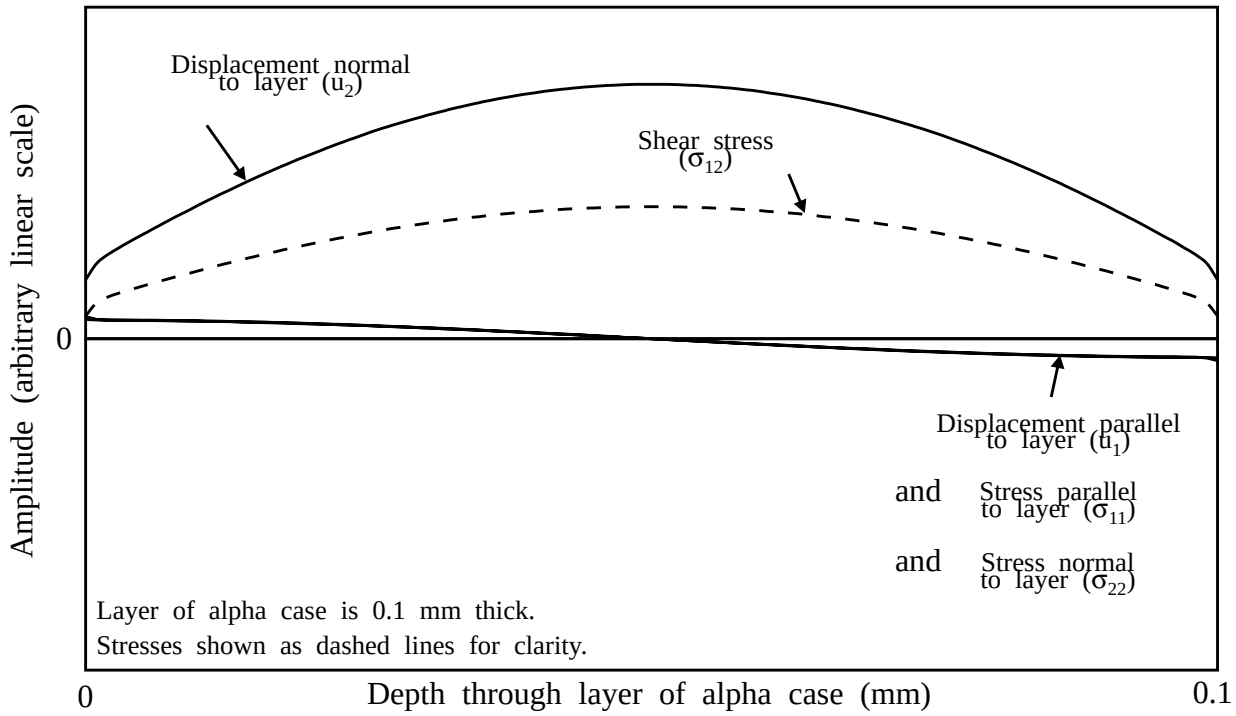

(b) At High frequency (1 GHz)

Figure 9.11 Mode shapes of interface mode 1

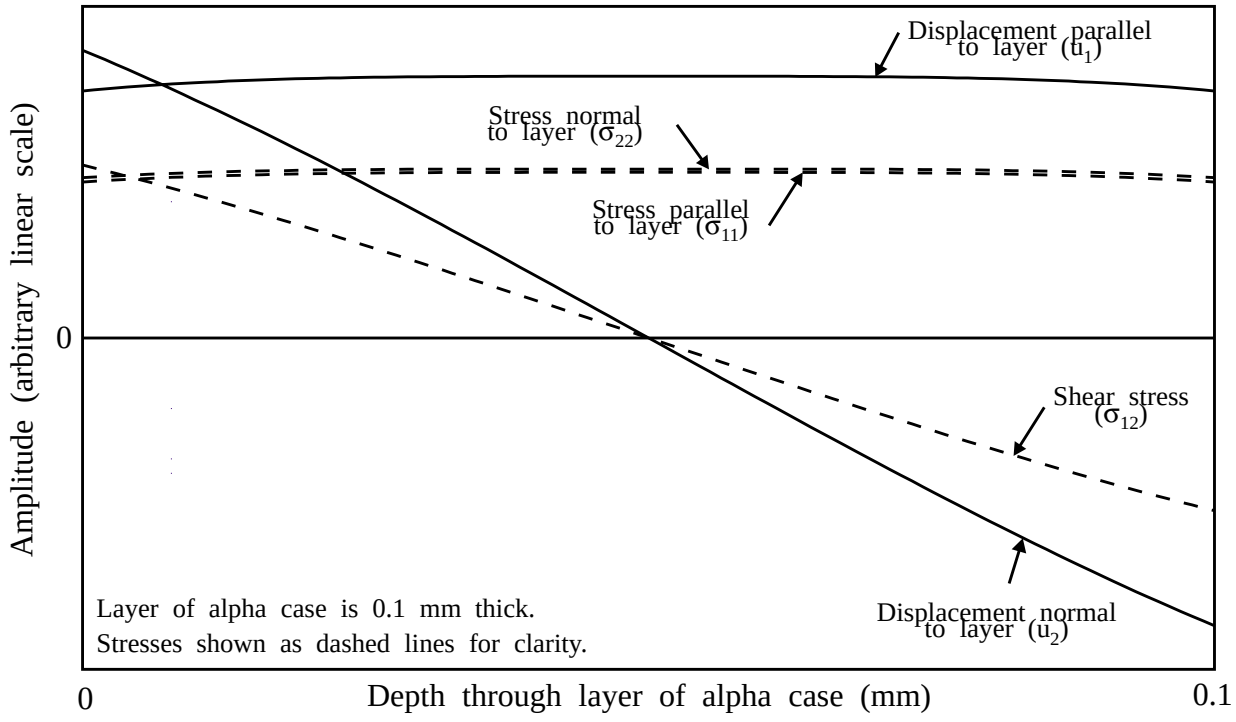

(a) Mode 2 at low frequency (12 MHz)

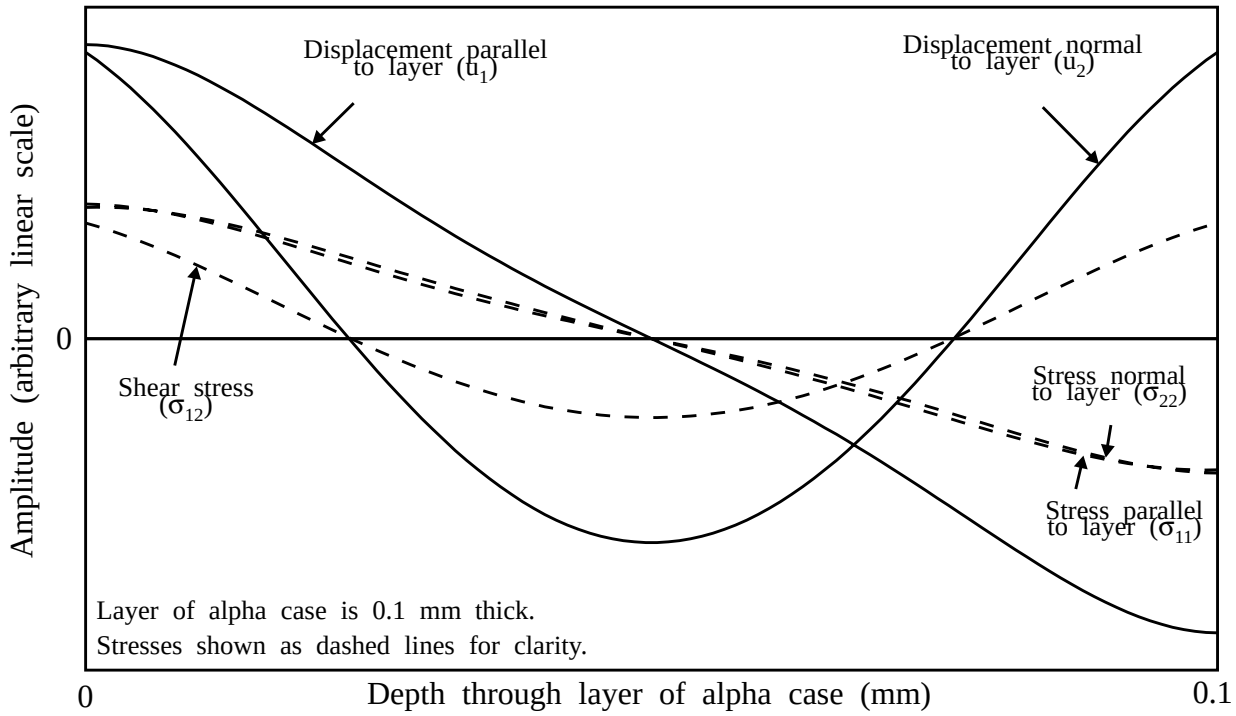

(b) Mode 3 at low frequency (34 MHz)

Figure 9.12 Mode shapes of interface modes 2 and 3

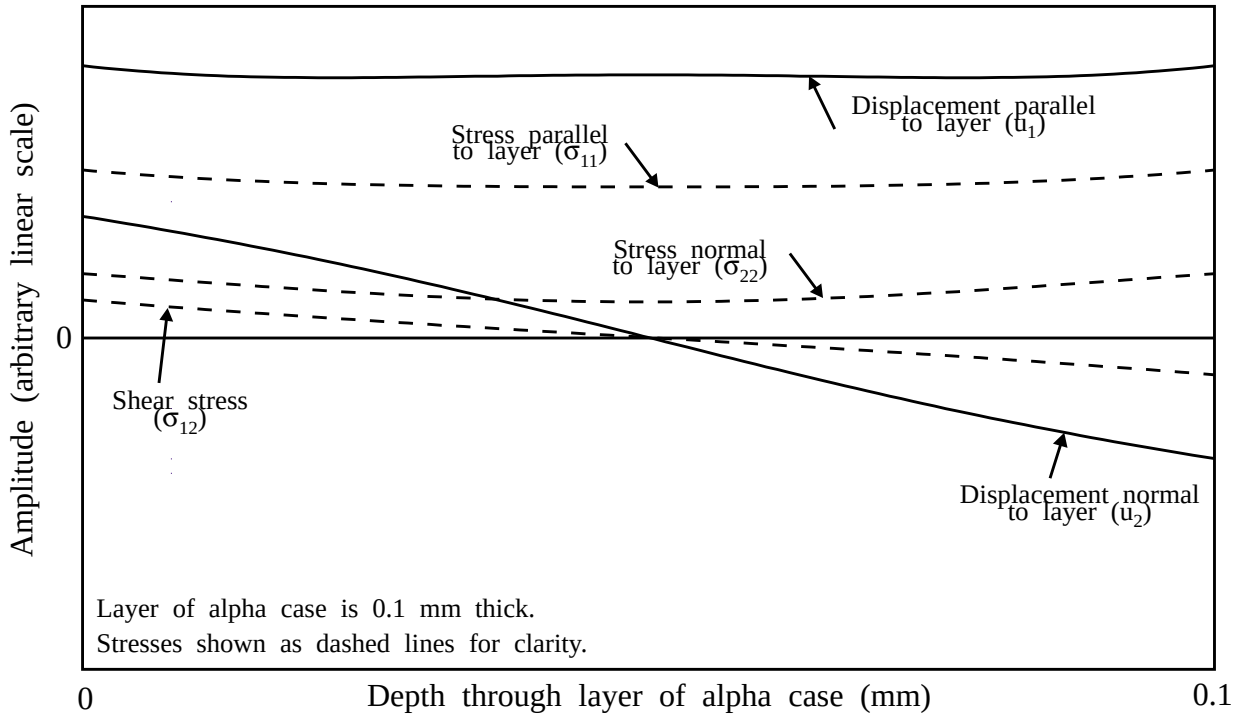

(a) At low frequency (30 MHz)

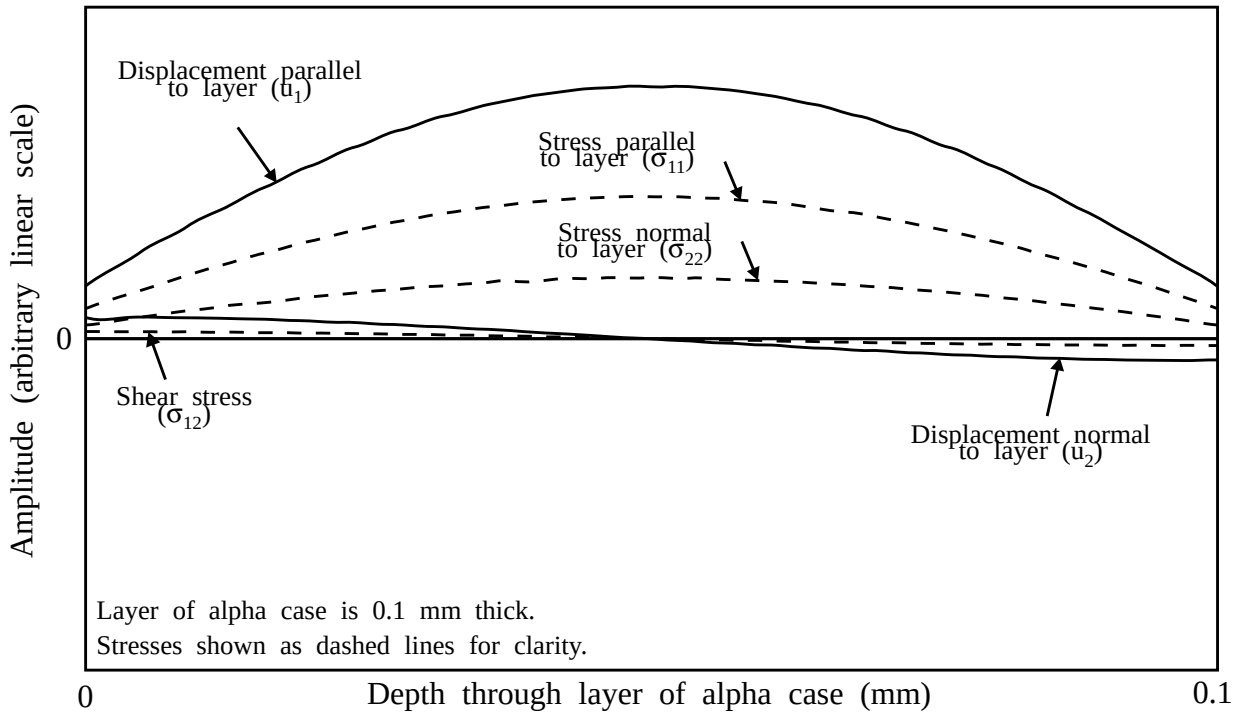

(b) At High frequency (1 GHz)

Figure 9.13 Mode shapes of interface mode 6

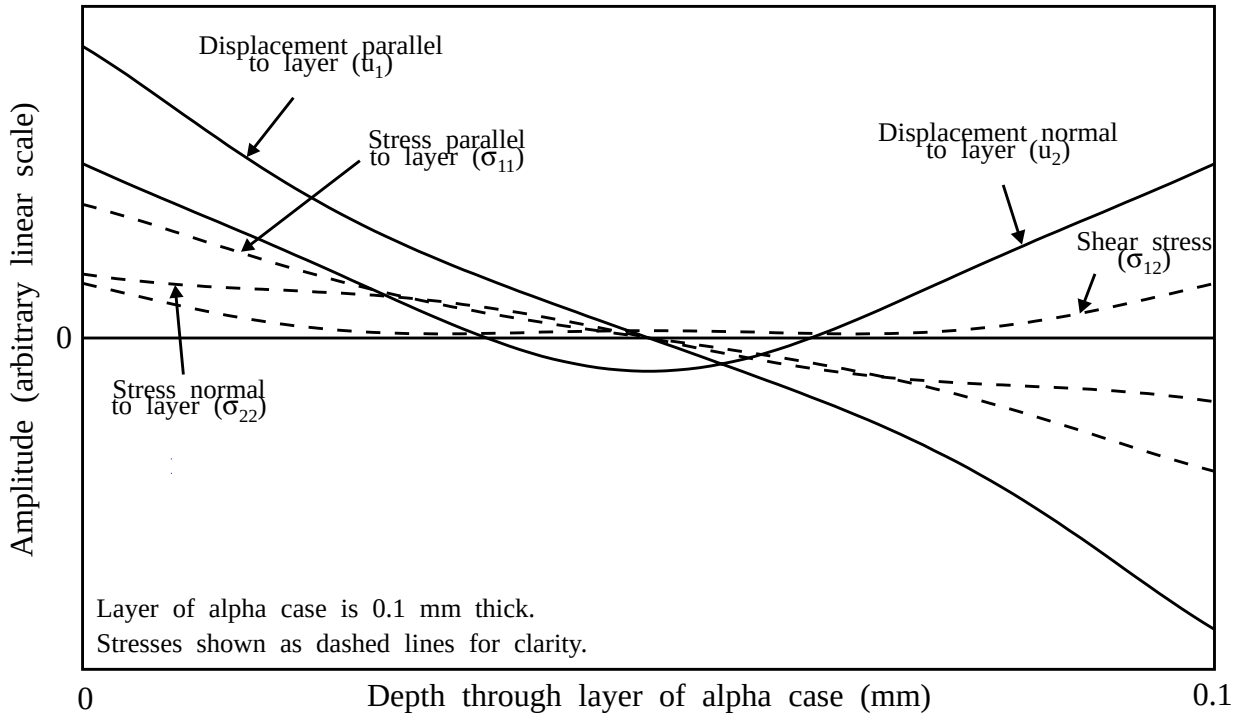

(a) Mode 7 at low frequency (60 MHz)

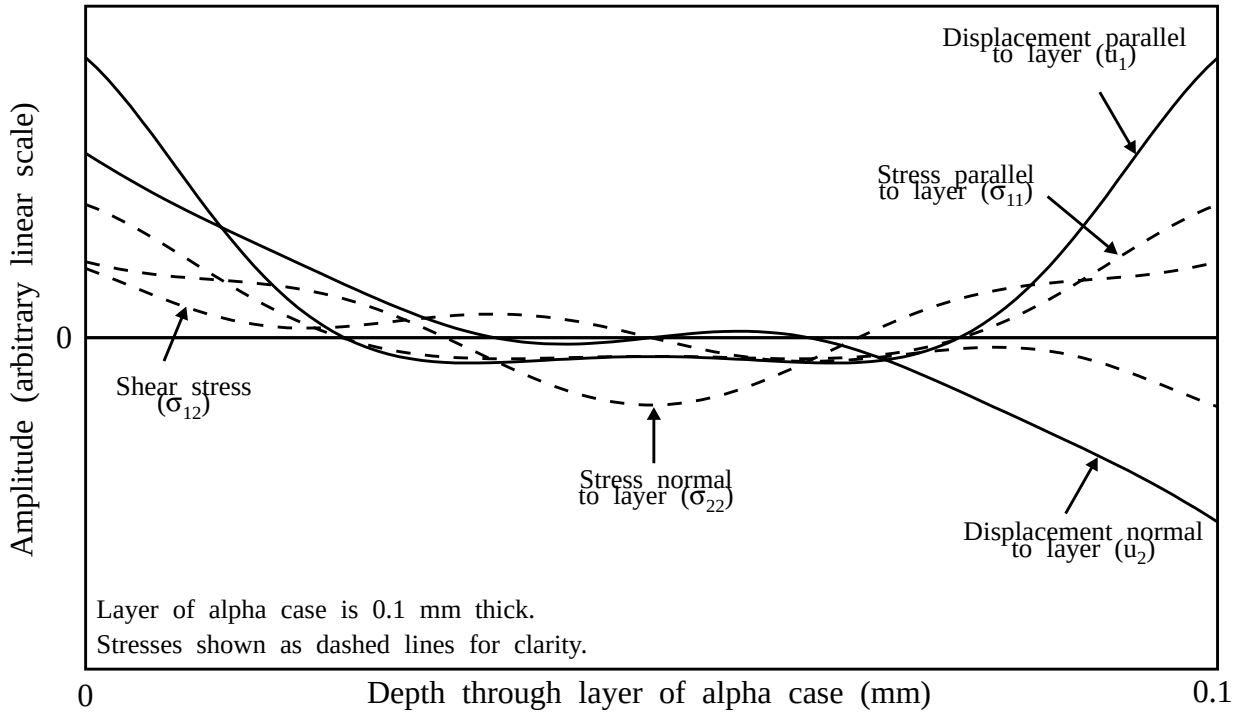

(b) Mode 8 at low frequency (75 MHz)

Figure 9.14 Mode shapes of interface modes 7 and 8

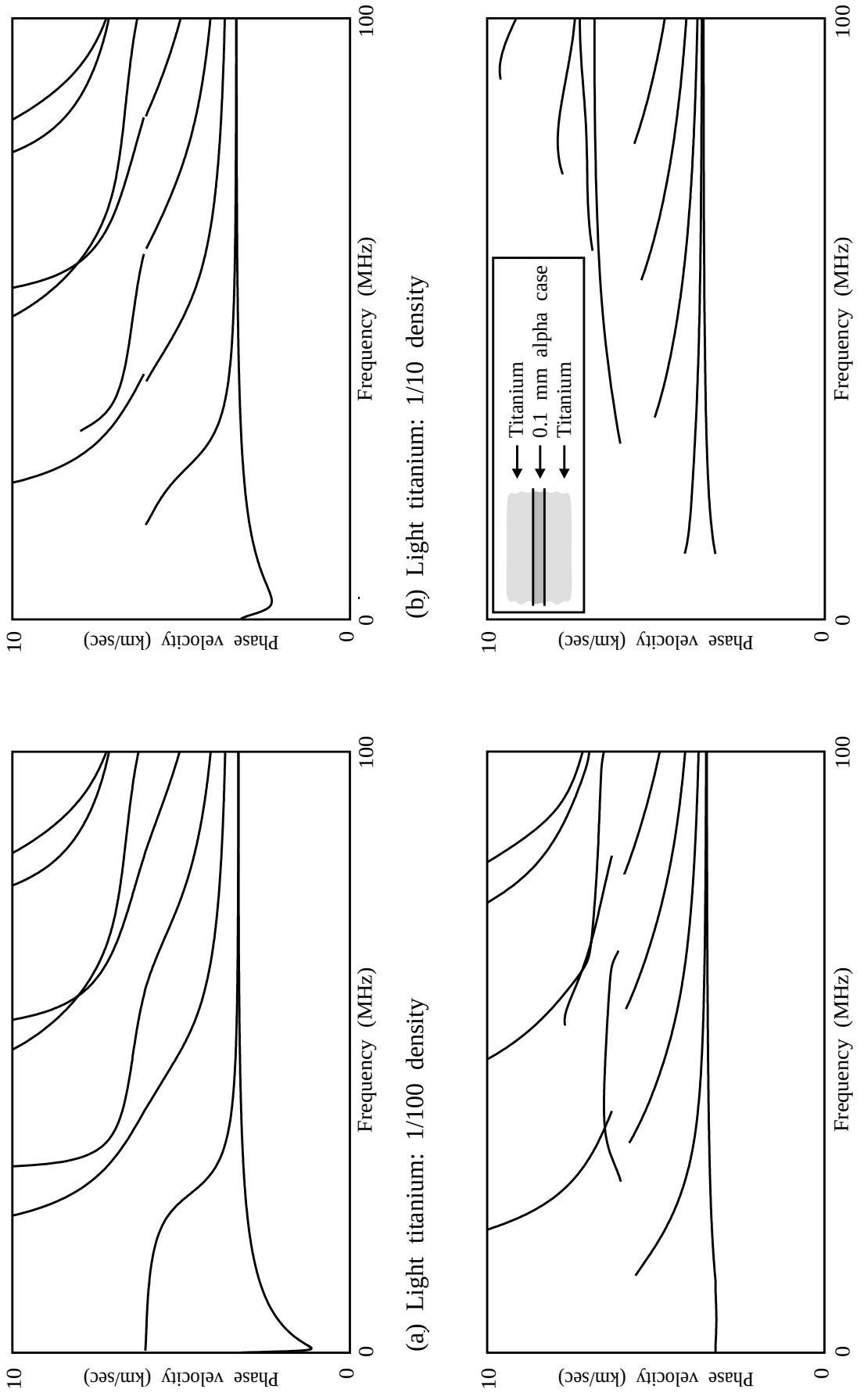

Figure 9.15 Interface wave dispersion curves for layer of alpha case embedded in 'light' titanium

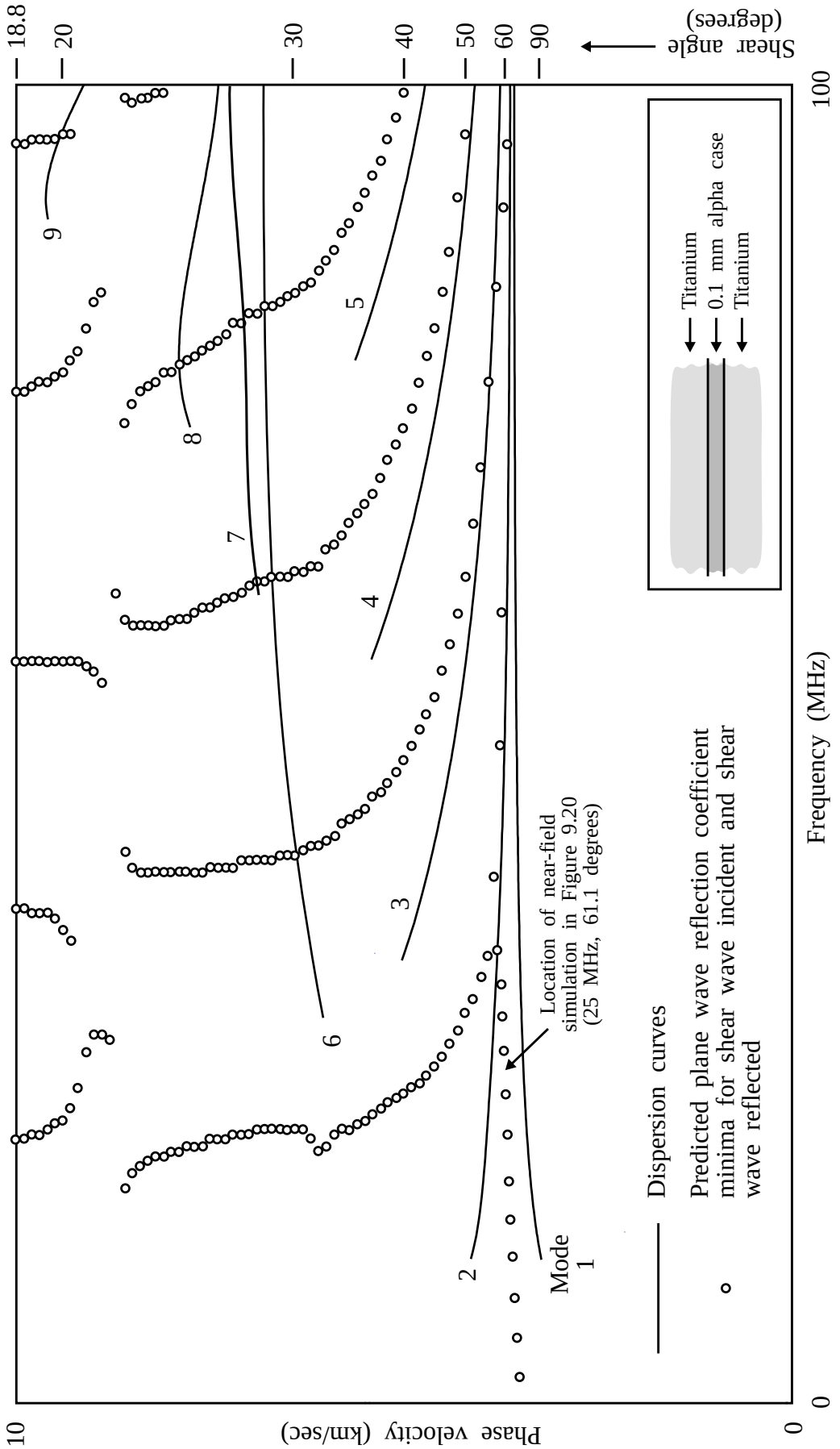

Figure 9.16 Comparison of dispersion curves and shear wave reflection coefficient minima

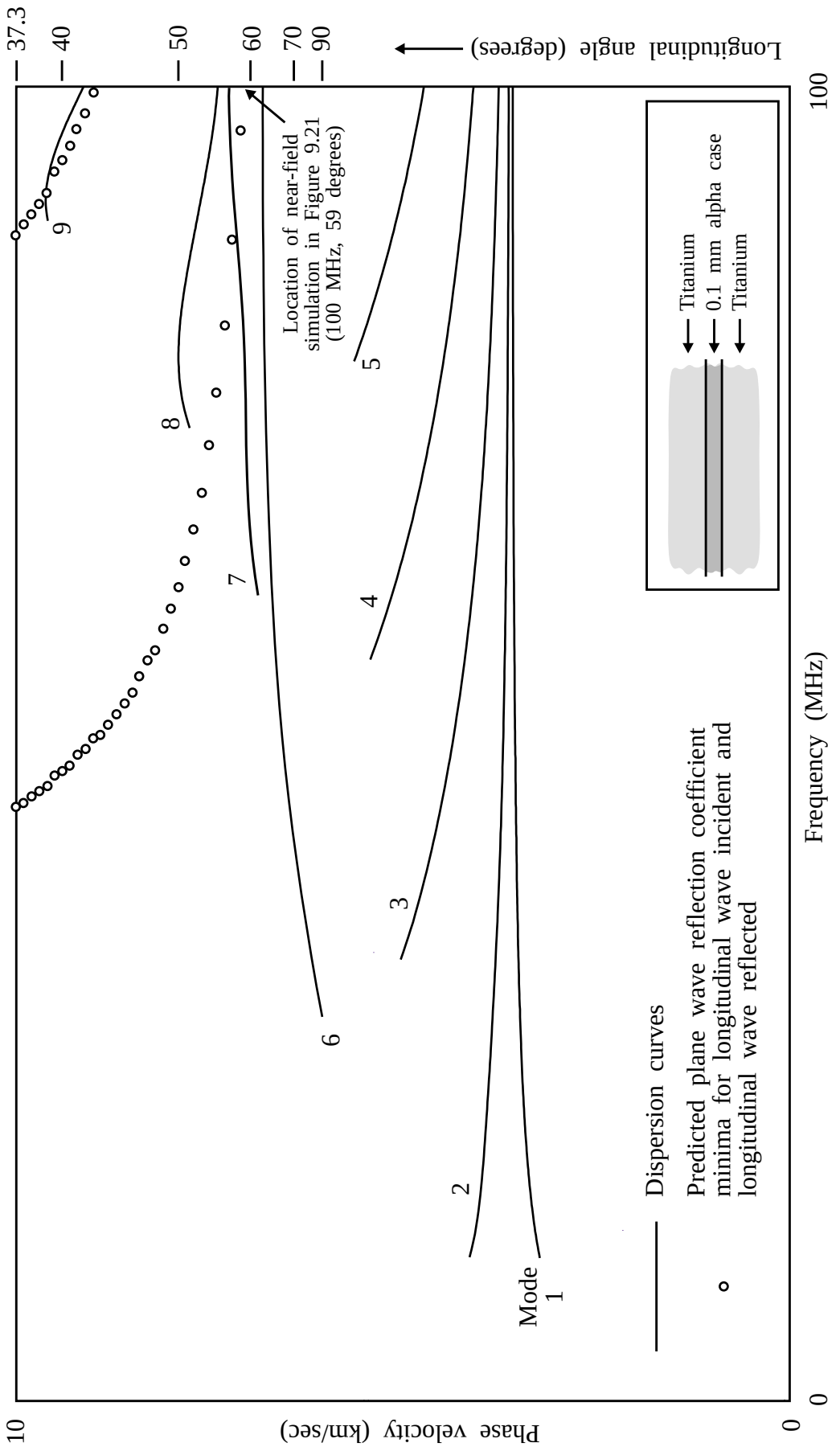

Figure 9.17 Comparison of dispersion curves and longitudinal wave reflection coefficient minima

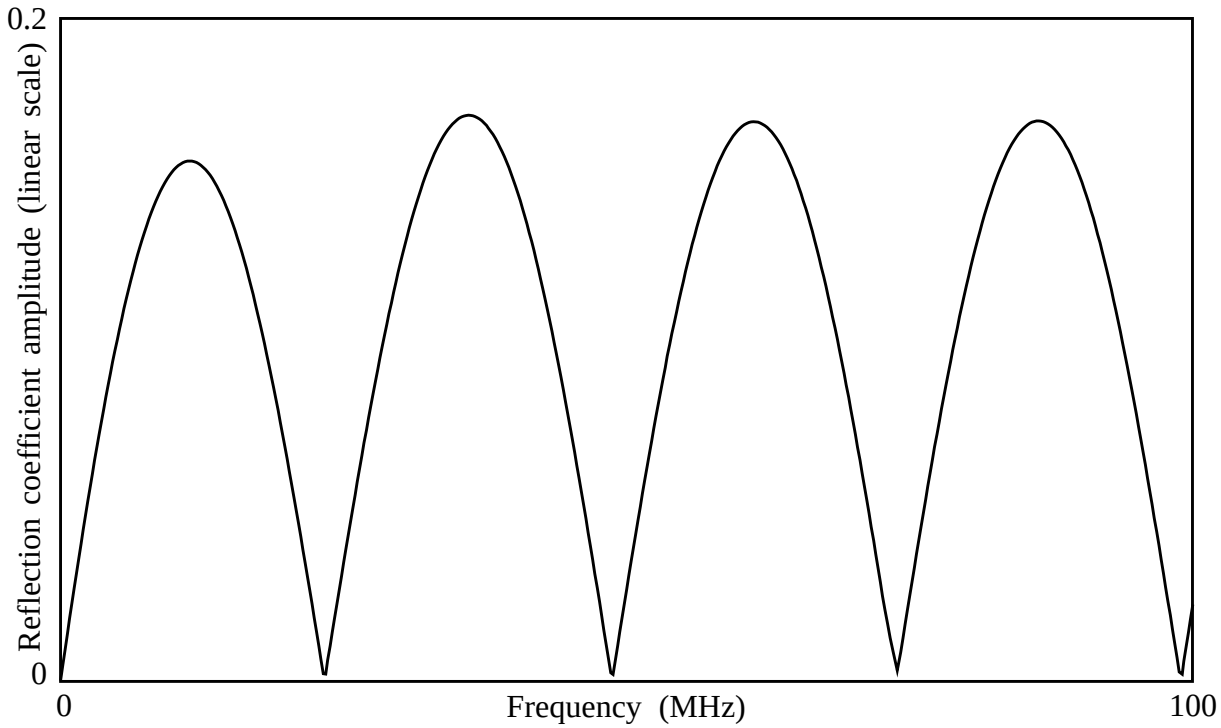

(a) Example of good minima: Shear waves, frequency sweep at 40 degrees

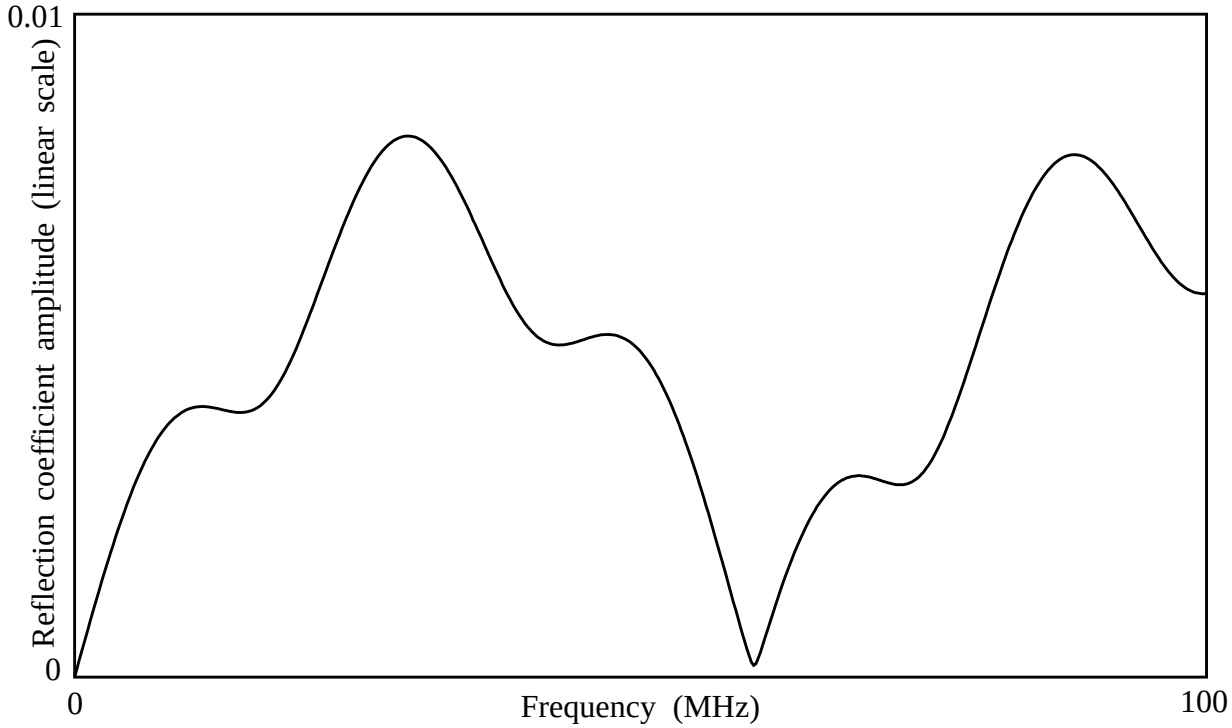

(b) Example of poor minima: Shear waves, frequency sweep at 22 degrees

Figure 9.18 Examples of predicted plane wave reflection coefficients

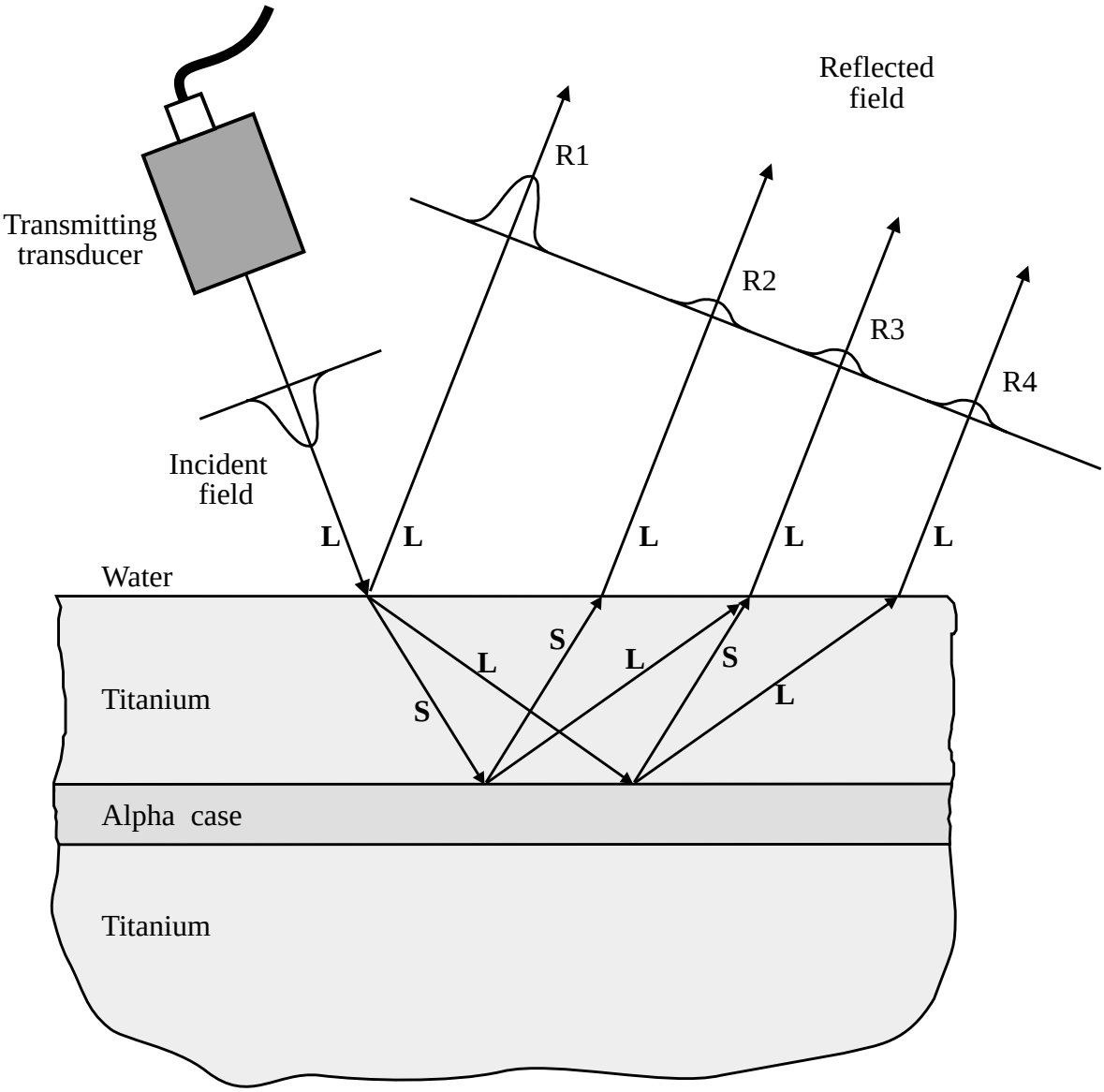

L = longitudinal wave
S = shear wave

Figure 9.19 Arrangement for modelling of near-field response from embedded layer

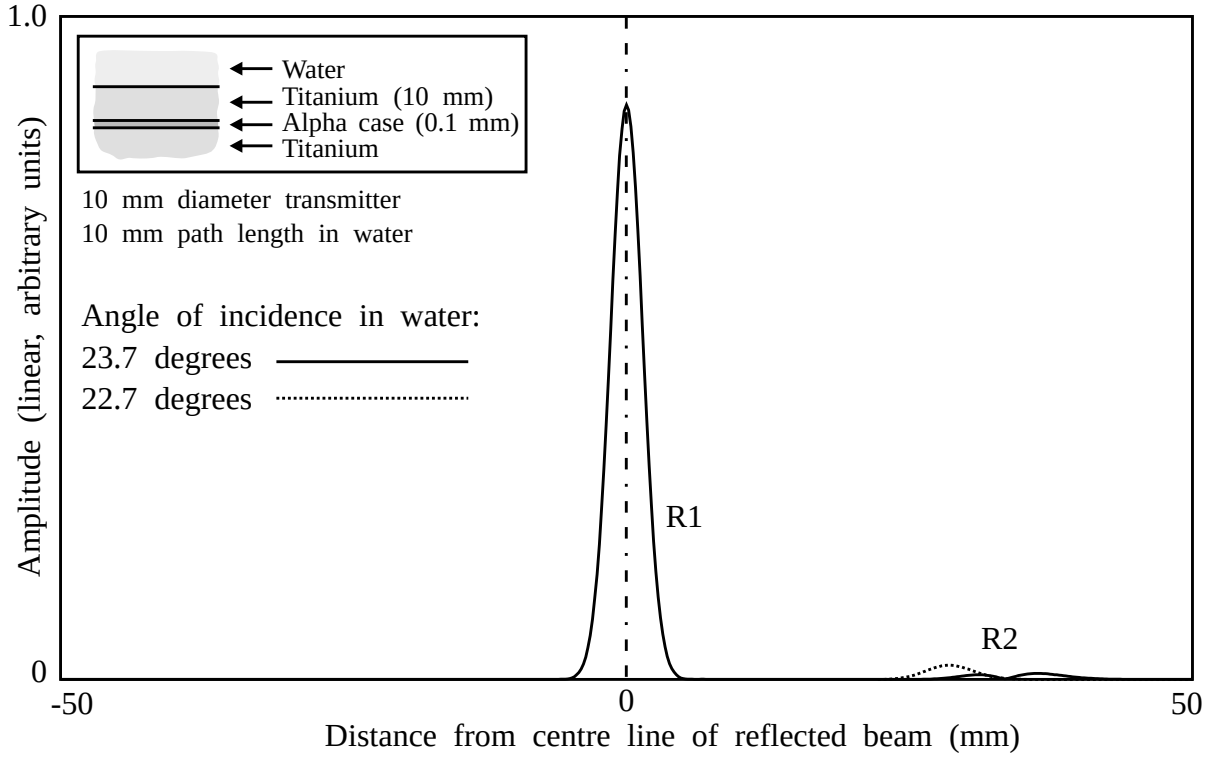

(a) Near-field response at 25 MHz

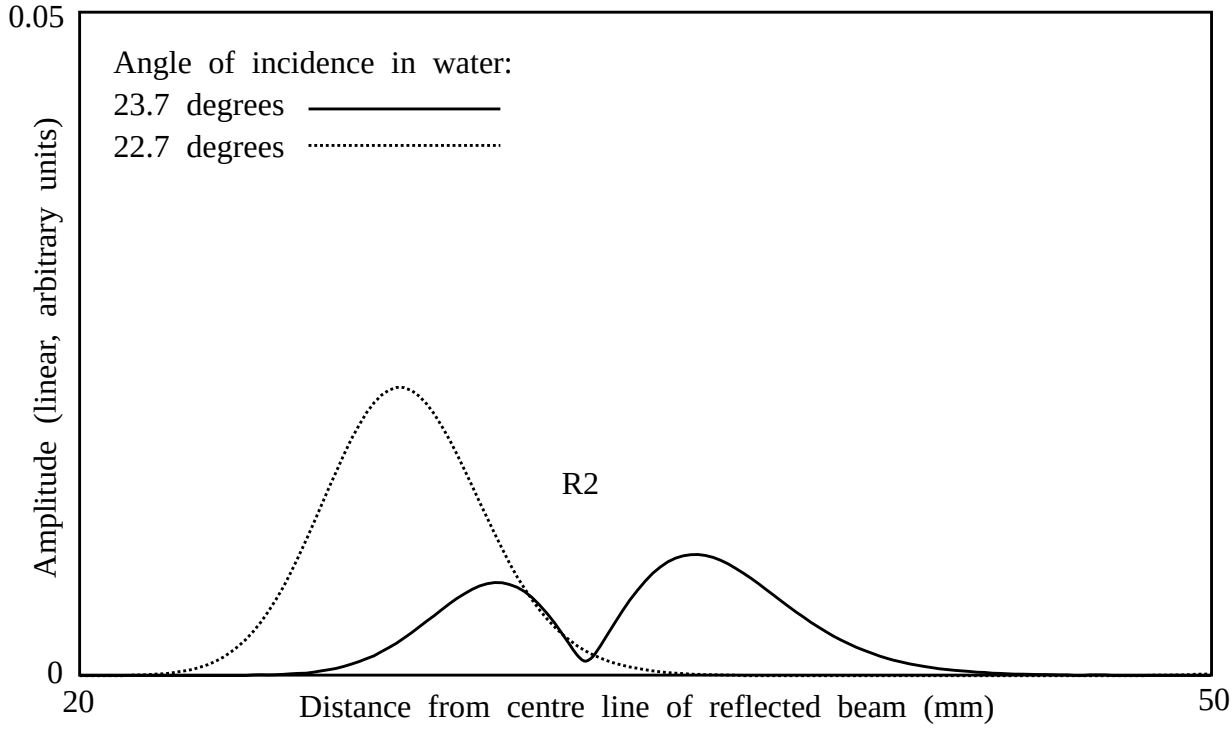

(b) Detail of bondline reflection (X 20 amplitude magnification)

Figure 9.20 Predicted near-field response from layer of alpha case - shear wave at 25 MHz

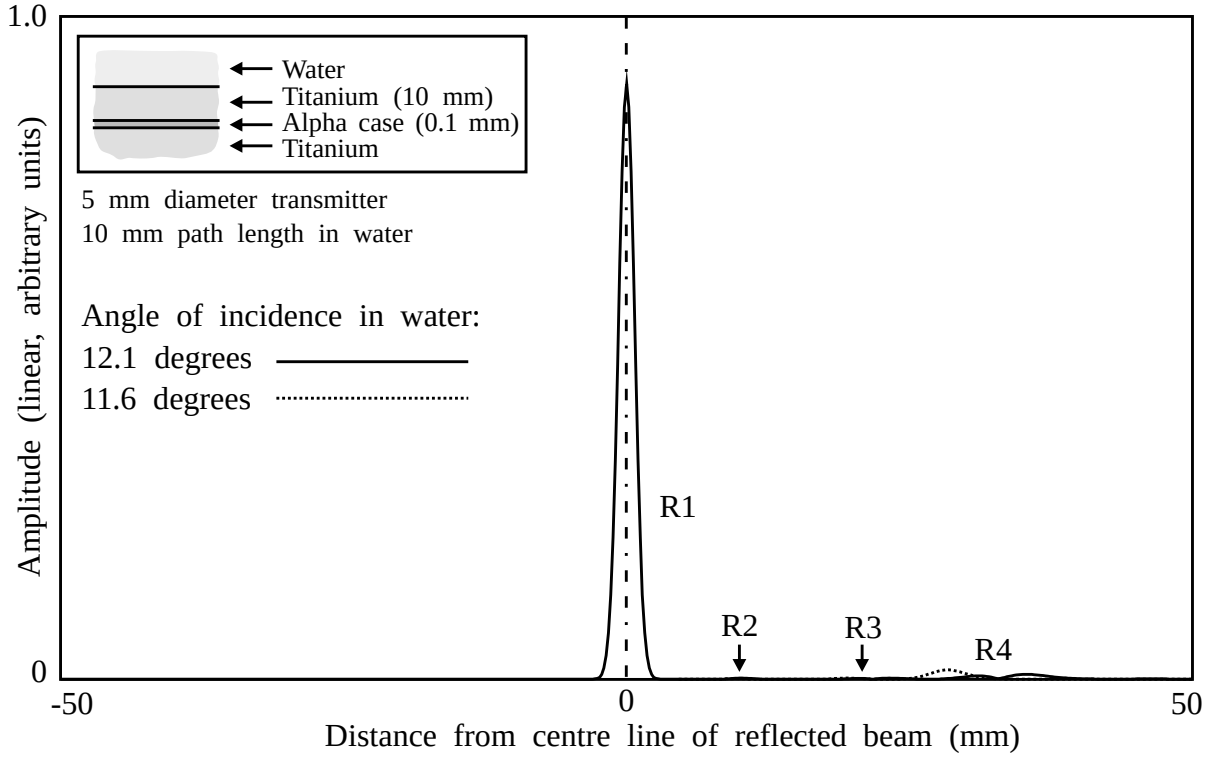

(a) Near-field response at 100 MHz

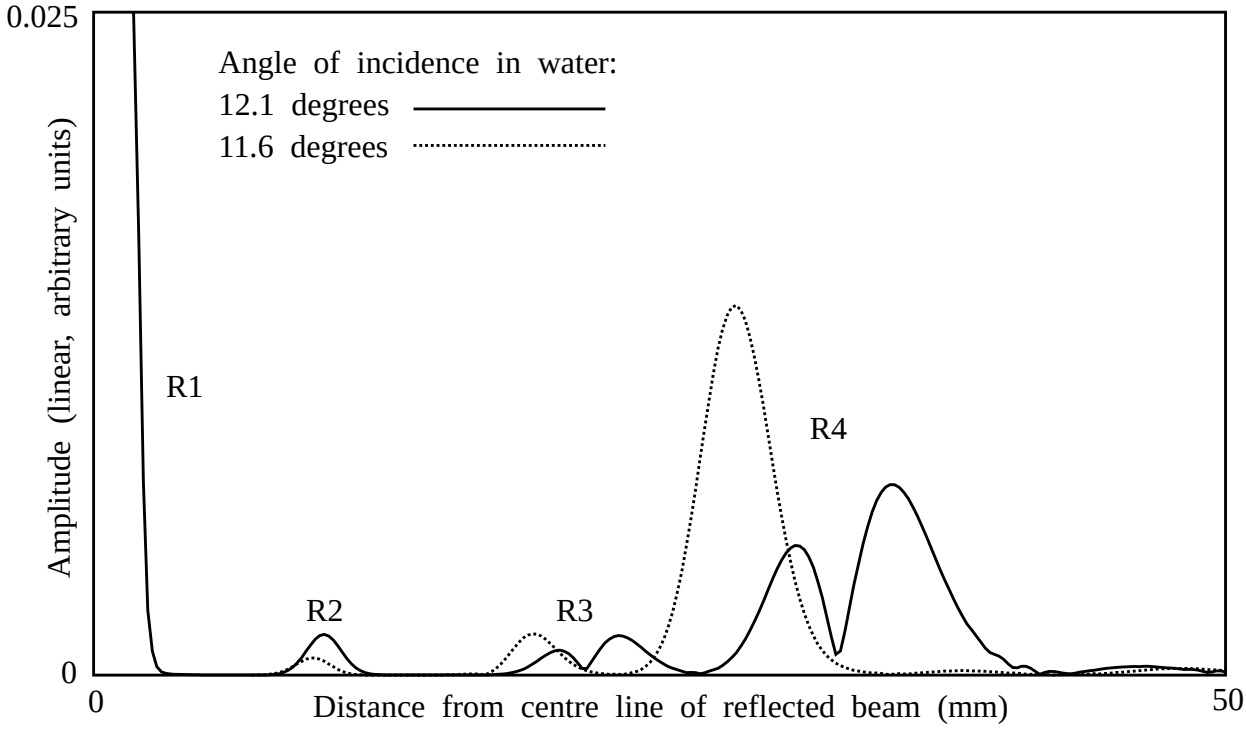

(b) Detail of bondline reflection (X 40 amplitude magnification)

Figure 9.21 Predicted near-field response from layer of alpha case - longitudinal wave at 100 MHz

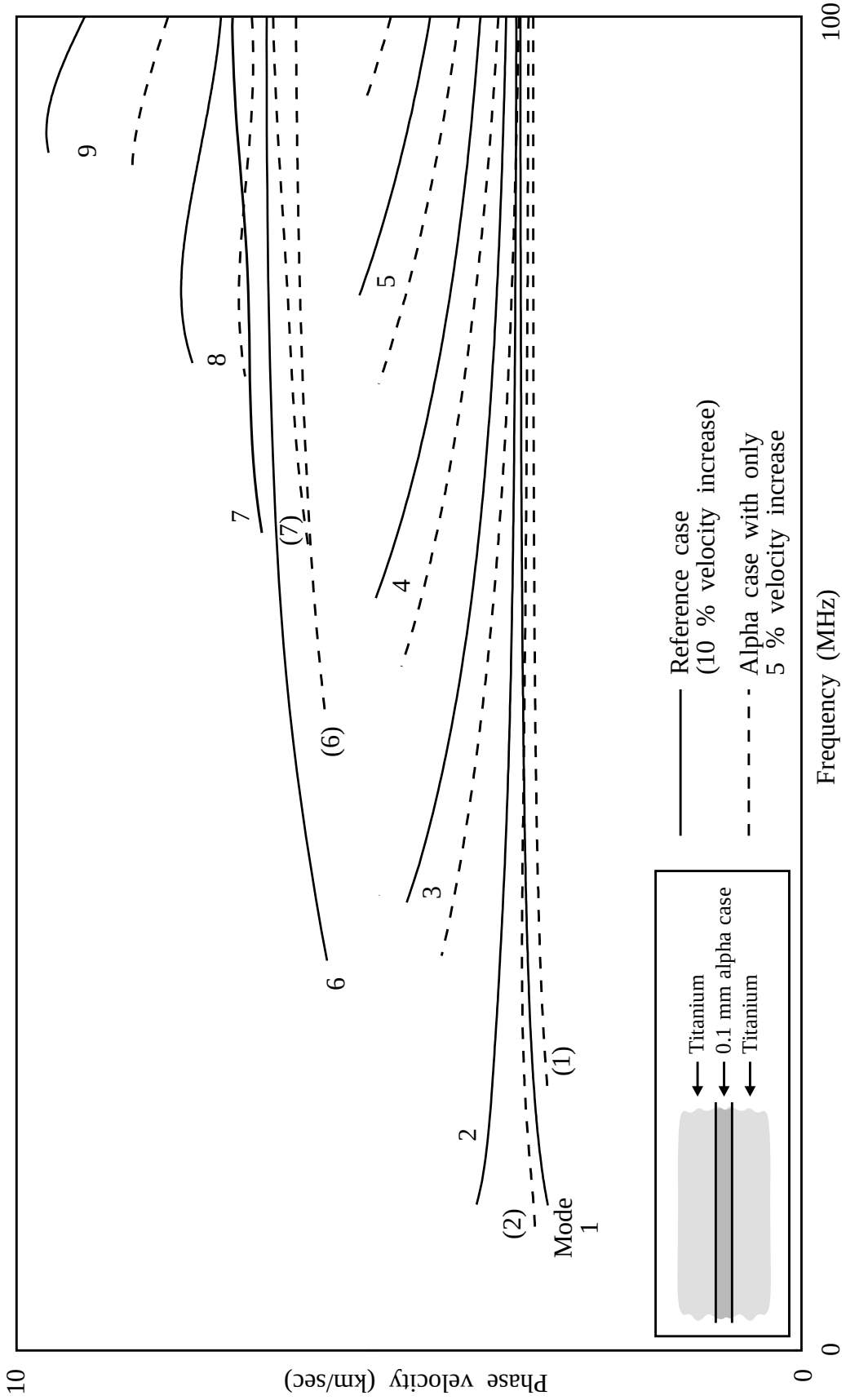

Figure 9.22 Interface wave dispersion curves for layer of alpha case embedded in titanium - influence of: Alpha case with smaller velocity increase

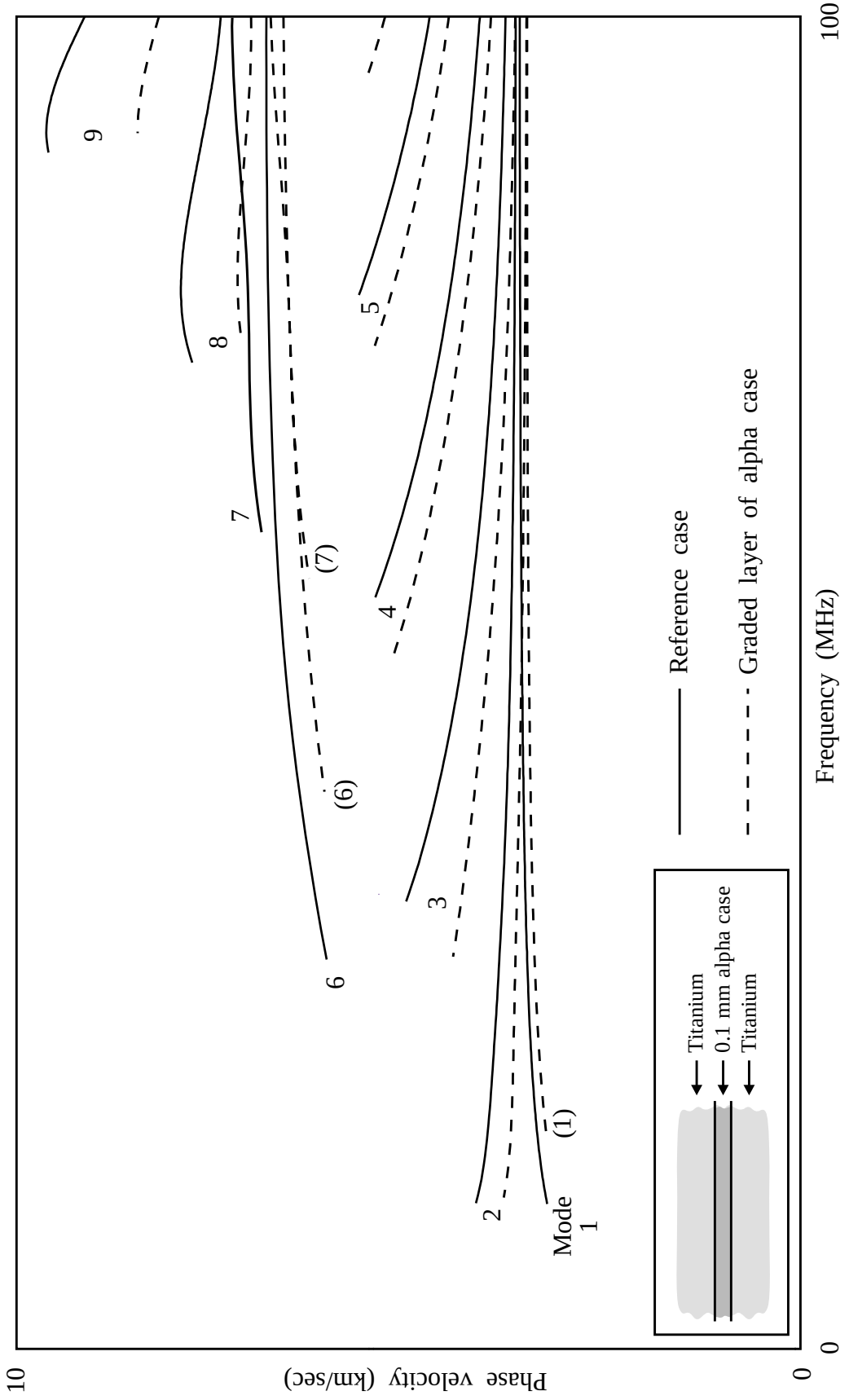

Figure 9.23 Interface wave dispersion curves for layer of alpha case embedded in titanium - influence of: Graded layer of alpha case

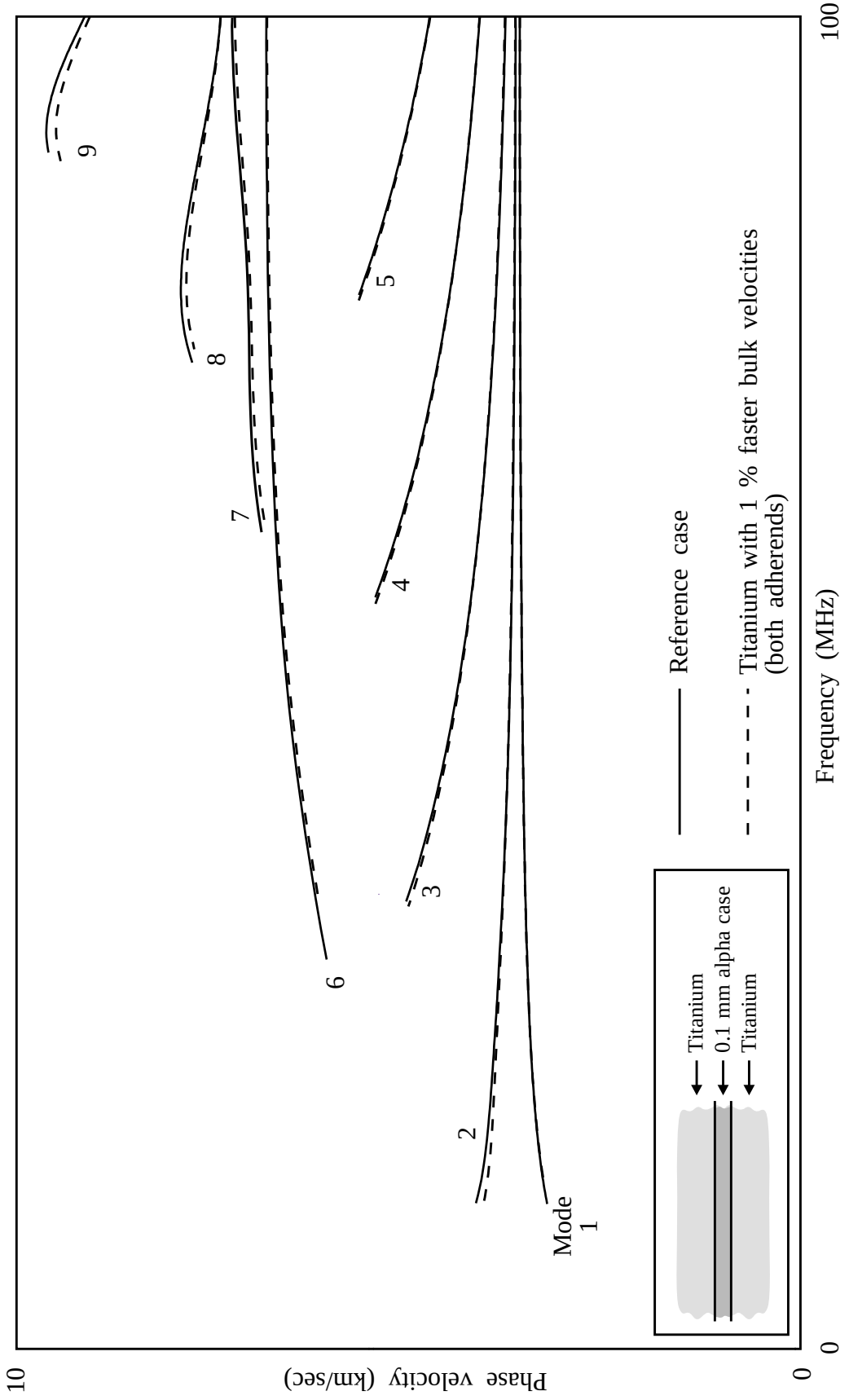

Figure 9.24 Interface wave dispersion curves for layer of alpha case embedded in titanium - influence of: Adherends with faster bulk velocities

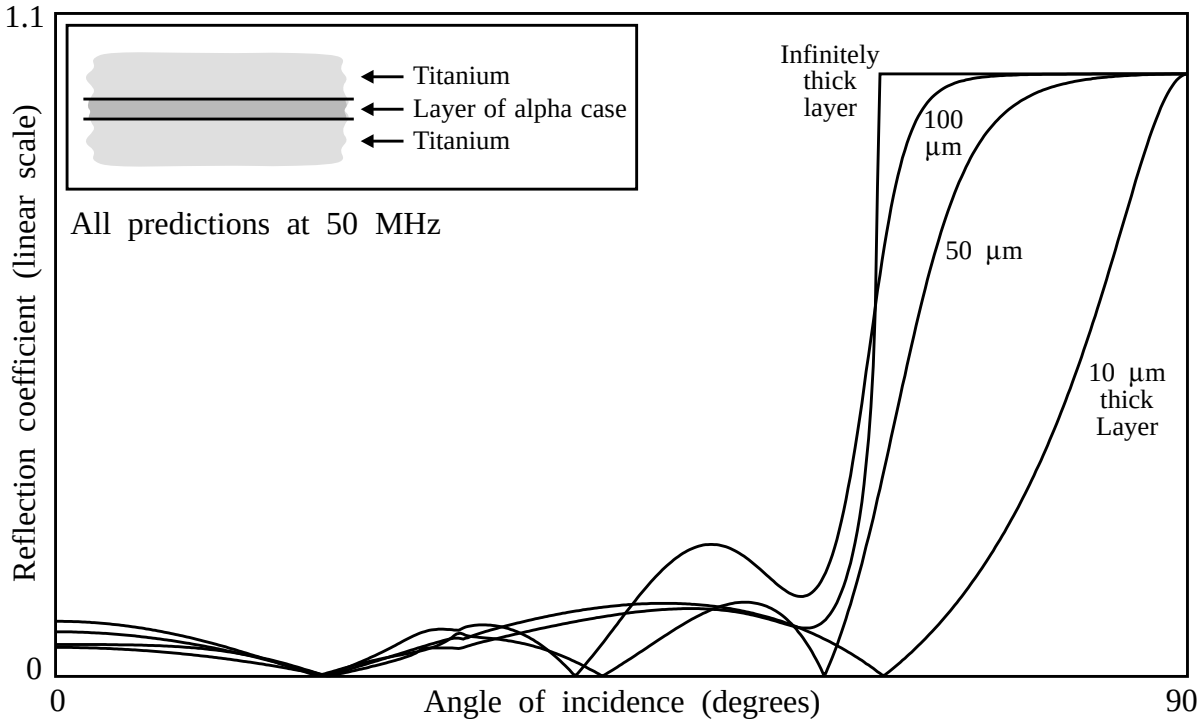

(a) Plane shear wave reflection coefficient for embedded layer of alpha case

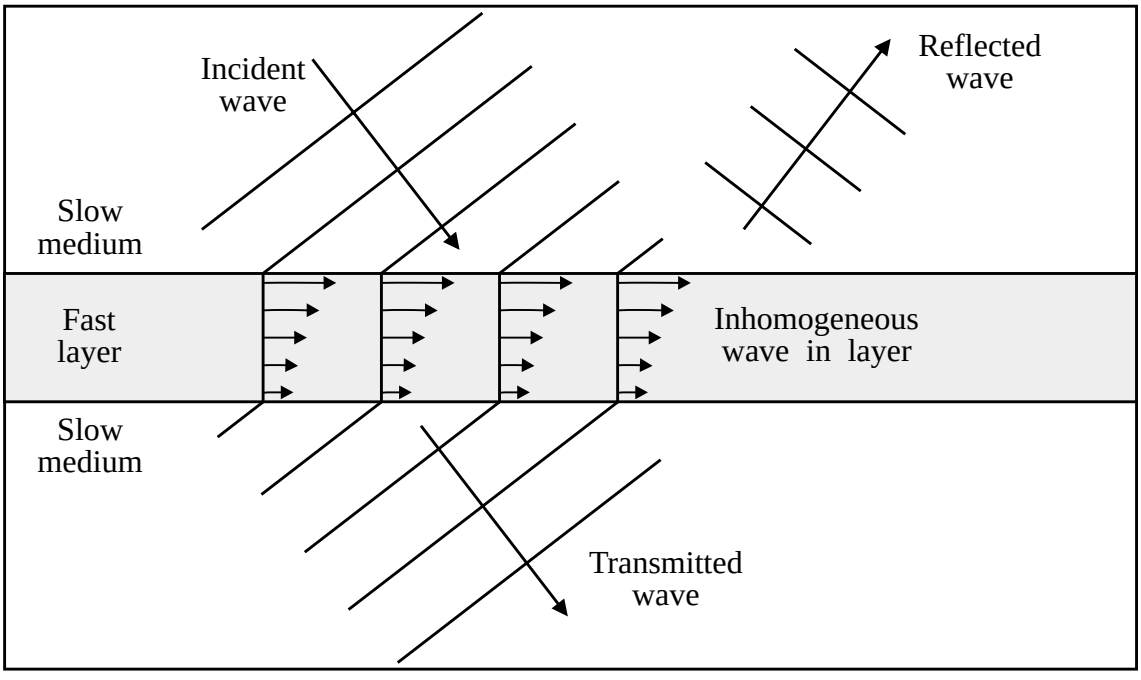

(b) Transmission of energy through thin fast layer at super-critical angles of incidence

Figure 9.25 Inspection of embedded stiff layer by oblique incidence reflectivity

CHAPTER 10

Conclusions

10.1 Review of thesis

Diffusion bonding, the joining of two surfaces by the diffusion of material across the interface, has the attractions of very high strength and minimal distortion of the components. Recent developments of the diffusion bonding process in the aircraft industry has further exploited the process by the diffusion bonding and superplastic forming of sheets of titanium to create cellular structural components. Along with these developments has been the necessary research into inspection methods for quality control during production. An important inspection problem is the detection of a brittle layer of a phase of the titanium alloy, known as alpha case, which can occur at the bondline if air is present during bonding.

The conventional ultrasonic technique for the detection of defects in plates is to send an ultrasonic pulse into the material and then to look for changes either in the transmission or in the reflection of the signal. In the case of an embedded layer the most sensitive option is to look at the reflected signal, using a single transducer for both transmission and reception, positioned so that the signal path is normal to the surface of the plate. Typically a broadband piezo-electric transducer with a focused beam and a short duration pulse excitation is used for this form of inspection. The conventional approach is very effective for detecting large changes in acoustic impedance such as voids or inclusions but its sensitivity is limited when the defects are small or their properties are similar to those of the plate.

An alternative approach to normal incidence inspection is to consider some form of ultrasonic wave which propagates along the plate. This is very attractive in principle because the energy in certain waves travelling along a plate may be concentrated at the bondline so that the wave propagation properties may be sensitive to the properties at the bondline. Therefore an inspection method based on plate waves may potentially offer greater sensitivity to an embedded layer of alpha case than normal incidence testing. However the drawback in devising such an inspection method is that the waves propagating along a plate are very much more complicated than the bulk waves which are utilised in conventional normal incidence testing.

The objective of this thesis was to investigate whether such ultrasonic plate waves could be used for the detection of alpha case, and if so, whether they could offer improved sensitivity over the conventional normal incidence approach.

A major part of the research was the development of a modelling tool to be used to perform the feasibility studies. A comprehensive modal model was developed for the prediction of the behaviour of waves propagating along multilayered plates and was implemented in a computer code.

The theory for the model was developed in two stages, in Chapters 2 and 3. In the first stage a formulation was derived for free waves, waves which propagate indefinitely along the plate without losing energy. This class of waves includes, for example, Lamb waves which exist in elastic plates in vacuum and Stoneley waves which carry energy along the interface between two different materials. In the second stage the formulation was extended to include attenuating waves which lose energy as they travel. The energy may be lost by material damping, when the material is not perfectly elastic, or by leakage from the plate into the adjacent media. An example of a wave which leaks is a leaky Lamb wave in a plate which is immersed in water. The development of the theory concluded with the expression of a characteristic function whose inputs are the physical description of the multilayered plate, a value of frequency and a value of wavenumber, and whose result must be zero for a plate wave to exist.

The implementation of the theory into the computer model was described in Chapter 4. Some of the difficulties of solving the characteristic function were discussed and systematic numerical procedures were developed. Algorithms were then developed for the generation of dispersion curves and mode shapes. The dispersion curves describe the variations of the velocities, frequencies and attenuations of the waves, and the mode shapes describe the profiles of the displacements and stresses of a wave through the thickness of the plate. The completed model may be used to predict both free and leaky wave solutions in plate systems of any numbers of layers of isotropic elastic or viscoelastic materials.

The validation of the model was addressed in Chapter 5. Examples of the application of the model were presented and the modal solutions for a number of layered systems were discussed. Comparisons were also made with known analytical solutions, with solutions predicted by other models and with experimental measurements. The validation exercise

demonstrated the versatility and accuracy of the model and its suitability for the research task.

The acoustic properties of the materials were investigated in Chapter 6. An experimental study was undertaken in which alpha case was grown on sheets of titanium by exposing them to air at high temperature. The acoustic properties of both treated and untreated materials were measured and the variation of the alpha case contamination with depth from the exposed surfaces was assessed by measuring hardness profiles. It was found that the longitudinal and shear velocities of bulk waves in the alpha case varied with the depth but that in all cases they were faster than those in the titanium, typical measured increases being between 5 and 10 percent. No difference in density could be detected between alpha case and titanium.

Model studies of normal incidence reflectivity were made in Chapter 7, in order to quantify the sensitivity of the conventional inspection technique. Reflectivity measurements of defective joints were simulated, using a response model and assuming a variety of alpha case properties and property profiles. The study also included a brief examination of the reflectivity from arrays of voids at the bondline, voids frequently accompanying alpha case in poor bonds. The investigation was limited to model studies; unfortunately it was not possible to obtain suitable defective bonded joints for experimental confirmations.

The first of two plate wave approaches for inspection, the Lamb wave technique, was assessed in Chapter 8. This method relies on the detection of changes which the embedded layer may make to the properties of the Lamb waves in the bonded plate. Dispersion curves were predicted for good joints and for defective joints. The predictions were used to determine the sensitivity of the Lamb waves to the potential defects and to other parameters associated with the joints. This resulted in the identification of the most sensitive modes which could be used for inspection. The means of excitation and measurement of Lamb waves were discussed and the Lamb wave method was assessed by comparison with the conventional normal incidence inspection method.

The second plate wave approach, the interface wave technique, was assessed in Chapter 9. This method relies on the excitation and detection of waves which travel along the embedded layer, leaking energy into the adherends. Two types of interface wave are possible in principle: waves which are restricted to a single interface between the titanium and the alpha case, and waves which occupy the whole of the embedded

layer. Wave propagation predictions were made for both of these cases and the nature of the waves was analysed. The sensitivity of the waves to the properties of the embedded layer and of the adherends was investigated by a parametric study. Methods were considered for the excitation and measurement of interface waves and their potential for inspection was discussed.

10.2 Summary of findings

Conventional normal incidence technique

The model studies of normal incidence reflectivity demonstrated that the conventional inspection technique performs particularly well when looking for an embedded planar layer such as a layer of alpha case in a diffusion bonded joint. Since both of the adherends are identical there is no reflection from the bondline of a good joint. Any reflection from the bondline must therefore be associated with some form of defect, and a planar layer tends to reflect energy back towards the transducer rather than scattering it in other directions. Consequently it is possible to detect features with dimensions more than an order of magnitude smaller than the dominant wavelength of the test signal.

The model predictions for alpha case embedded at the bondline of titanium joints showed that it should be possible to detect very thin layers of alpha case using high frequency equipment. The lower limit of thickness was predicted to be about 20 microns, using the highest practicable frequencies of 60-80 MHz, provided that the acoustic velocity of the alpha case differs from the titanium by at least 5 %. Furthermore, the predictions for voiding at the bondline of titanium joints indicated that it should be possible to detect voiding down to about 25 % area fraction. This additional contribution to the reflectivity is a significant consideration in practice because of the tendency for voids to be present in poor bonds along with alpha case.

The strong sensitivity of the normal incidence technique to the presence of alpha case is a very positive conclusion from the practical point of view. The thickness of alpha case which can be detected, according to the predictions, is considerably thinner than the layer which was evident in the very poor bond (the only badly bonded specimen which was available), and may be associated with relatively low levels of contamination. Of course, concerning the development of a plate wave inspection technique, the task is particularly challenging because significant further improvements would have to be demonstrated in order for the new technique to be viable.

Lamb wave technique

The Lamb wave modelling study revealed that the dispersion curves show some sensitivity to the presence of a centrally embedded layer of alpha case so that in principle the inspection of diffusion bonded joints should be possible using this technique.

Unfortunately however, because the Lamb waves occupy the whole of the bonded joint, the curves are affected by variations in the properties of any part of the joint. Accordingly, the curves are much more sensitive to global parameters such as the thickness of the joint and the properties of the adherends than they are to the presence of a very thin layer of alpha case. They are also insensitive to the profile of the acoustic properties of the alpha case, depending only on the average properties and the thickness of the layer, and consequently the method could not be used to characterise the layer.

The practical potential of utilising Lamb waves is further ill-fated by the success of the conventional normal incidence method. Comparing the two methods, the best sensitivity which could be achieved using the Lamb wave technique falls far short of that which is possible using the normal incidence technique. Furthermore, the Lamb wave technique would be more complicated to implement in practice than the conventional method.

It was therefore concluded that the Lamb wave inspection scheme could work in principle but its sensitivity to the presence of the embedded layer falls short of normal incidence testing and it suffers from unwanted sensitivity to other properties of the joint.

Interface wave technique

The model studies of the interface wave which travels along the boundary between two different materials indicated that in general such a wave shows good potential for nondestructive testing. A single, leaky non-dispersive mode may exist between certain pairs of materials. It may readily be excited and received and is particularly sensitive to the properties of the materials in the region of the interface. However it could only be utilised in embedded layers if its depth of penetration was significantly smaller than the thickness of the layer. This would require tests to be conducted at extremely high frequencies for very thin layers. Moreover it was found that such an interface wave does not exist in the specific case of the interface between titanium and alpha case.

In general, a leaky wave at a single interface may be useful for the inspection of diffusion bonded joints where the materials of the two adherends are different. In such cases the conventional normal incidence inspection technique would not be optimal because a signal would always be reflected from the bondline, even in a good joint, obscuring any small reflections from defects. However an interface wave may be rather sensitive to the properties local to the bondline, particularly if the technique exploits the dependence of the effective depth of the wave on the frequency. Other joints which could potentially be inspected by such waves are joints in which a relatively thick interface layer is known to exist but may need to be characterised, such as diffusion brazed joints and adhesive joints.

The model studies of the interface waves which travel along the embedded layer showed that there is an infinite family of these waves just as there is with Lamb waves but that the nature of the modes is substantially different. The dispersion curves bear little resemblance to the Lamb wave curves and all of the waves leak energy into the adherends. As anticipated, the dispersion curves are sensitive to the properties of the layer and insensitive to the properties of the adherends, a major attraction compared with the Lamb wave technique.

Unfortunately the attenuation of the modes is too strong for the remote measurement of the wave velocities to be considered. The alternative, point reflection measurements made at the same location as an incident signal, may be used to detect minima either in a sweep of frequency or in a sweep of the angular position of the transducers. These minima are associated with the modal properties of the system although they do not correspond directly to the frequencies or velocities of propagating waves.

The identification of the minima is an inappropriate method for the detection of the presence of the layer because minima can only be found by measuring reflections at adjacent angles or frequencies. If such reflections can be measured then they indicate directly the presence of the layer and there is no need to find the minima. However the conditions when minima occur could in principle be used to characterise a layer which is known to exist. Unfortunately in the current application this approach is unlikely to be practicable because the frequencies of the minima for realistic joints are too high.

It is therefore concluded that interface waves offer no practical potential for the inspection of alpha case in diffusion bonded titanium.

Possible alternative inspection strategy

Although it has been concluded that the plate wave techniques offer no advantage over the conventional normal incidence technique, it is possible that a method based on oblique incidence reflectivity may be worth pursuing.

Such an investigation into oblique incidence response is outside the scope of this thesis. However one possibility which could be explored is to measure the reflectivity from the layer using waves in the adherend which are incident on the layer at super-critical angles. An initial study has indicated that this approach may offer strong sensitivity to both the presence and the nature of embedded stiff layers and further investigation is recommended.

References

Abo-Zena, A. *Dispersion function computations for unlimited frequency values.* Geophys. J.R. Astr. Soc., Vol 58, 1979, pp 91-105.

Achenbach, J.D., Epstein, H.I. *Dynamic interaction of a layer and a half-space.* J. Eng. Mech. Div., ASCE, 1967, pp 27-42.

Adler, E.L., de Billy, M., Quentin, G. *Evaluation of friction-welded aluminium-steel bonds using dispersive guided modes of a layered substrate.* J. Appl. Phys., Vol. 68, 1990, pp 6072-6076.

Adler, E.L., Sun, I-H. *Observation of leaky Rayleigh waves on a layered half-space.* IEEE Trans. Sonics and Ultrasonics, Vol. SU-18, No. 3, 1971, pp181-184.

Alleyne, D.N. *The nondestructive testing of plates using ultrasonic Lamb waves.* PhD thesis, University of London, 1991.

Anderson, O.L. *Determination of some uses of isotropic elastic constants of polycrystalline aggregates using single-crystal data*. In Physical Acoustics, Vol. III, Part B, Ed. Mason W.P. and Thurston R.N., Academic Press, New York, 1965, pp 43-95.

Angel, Y.C., Achenbach, J.D. *Reflection and transmission of elastic waves by a periodic array of cracks.* J. Appl. Mechanics, Vol. 52, 1985, pp 33-41.

Alsop, L.E. *The leaky-mode period equation - a plane-wave approach.* Bull. Seism. Soc. Am, Vol. 60, 1970, pp 1989-1998.

Baik, J.M., Thompson R.B. *Ultrasonic scattering from imperfect interfaces: a quasi-static model.* J. Nondestr. Eval., Vol. 4, 1984, pp 177-196.

Bar-Cohen, Y., Mal, A.K. *Characterization of adhesive bonding using leaky Lamb waves.* Review of Progress in Quantitative NDE, Vol 9, 1990, pp 1271-1277.

Bendec, F., Peretz, M., Rokhlin S.I. *Ultrasonic Lamb wave method for sizing of spot welds.* Ultrasonics, 1984, pp 78-84.

Bond, L.J., Som, A.K., Shiloh, K., Taylor, K.J. *Diffusion bond inspection using a pulsed digital reflection acoustic microscope.* Review of Progress in Quantitative NDE, Vol 9, 1990, pp 1339-1346.

Bottomley, I. British Aerospace, plc. Private communication, 1992.

Brasche, L.J.H., Margetan, F.J., Thompson, R.B. *Sample preparation techniques and material property measurements of hard alpha titanium samples*. Review of Progress in Quantitative NDE, Vol 11, 1992, pp 1733-1738.

Brekhovskikh, L.M., Goncharov V. *Mechanics of continua and wave dynamics.* Springer-Verlag, Berlin, 1985.

Broomfield, R.W. *Application of advanced joining techniques to titanium alloys.* In Designing with Titanium, Institute of Metals, 1986, pp 69-75.

Cawley, P., Pialucha, T.P., Lowe, M.J.S. *A comparison of different methods for the detection of a weak adhesive/adherend interface in bonded joints.* In press, in Review of Progress in Quantitative NDE, 1993.

Chimenti, D.E., Nayfeh, A.H., Butler, D.L. *Leaky Rayleigh waves on a layered halfspace.* J. Appl. Phys., Vol. 53, 1982, pp 170-176.

Chimenti, D.E., Rokhlin, S.I. *Relationship between leaky Lamb modes and reflection coefficient zeroes for a fluid-coupled elastic layer.* J. Acoust. Soc. Am., Vol. 88, 1990, pp 1603-1611.

Claus, R.O., Kline, R.A. *Adhesive bondline interrogation using Stoneley wave methods.* J. Appl. Phys., Vol. 50, 1979, pp 8066-8069.

Clayton, E., Derrick, G.H. *A numerical solution of wave equations for real or complex eigenvalues.* Aust. J. Phys., Vol. 30, 1977, pp 15-21.

Deschamps, M., Roux, J. *Some considerations concerning evanescent surface waves.* Ultrasonics, Vol 29, 1991, pp 283-287.

Dewen, P.N. *The nondestructive evaluation of the cohesive properties of adhesively bonded joints.* PhD thesis, University of London, 1991.

Dewen, P.N., Lowe, M.J.S., Cawley, P. *The determination of the cohesive properties of bonded joints using Lamb wave data - a feasibility study.* Submitted to J. Nondestr. Eval., 1992.

Dunkin, J.W. *Computation of modal solutions in layered elastic media at high frequencies.* Bull. Seism. Soc. Am, Vol. 55, No. 2, 1965, pp 335-358.

Evans, R.B. *The decoupling of seismic waves.* Wave Motion, Vol. 8, 1986, pp 321-328.

Farnell, G.W., Adler, E.L. *Elastic wave propagation in thin layers.* Physical Acoustics, Principles and Methods, Vol. IX, Ed. Mason W.P. and Thurston R.N., Academic Press, New York, 1972, pp 35-127.

Frederick, C.L., Worlton, D.C. *Ultrasonic thickness measurements with Lamb waves.* Nondestructive Testing, 1962, pp 51-55.

Gilbert, F. *Propagation of transient leaking modes in a stratified elastic wave guide.* Rev. Geophys, Vol. 2, 1964, pp 123-153.

Guo, N., Cawley, P. *Lamb waves for the NDT of composite laminates.* Review of Progress in Quantitative NDE, Vol 11, 1992, pp 1443-1450.

Habeger, C.C., Mann, R.W., Baum G.A. *Ultrasonic plate waves in paper.* Ultrasonics, 1979, pp 57-62.

Haskell, N.A. *Dispersion of surface waves on multilayered media.* Bull. Seism. Soc. Am, Vol. 43, 1953, pp 17-34.

Hosten, B. *Bulk heterogeneous plane waves propagation through viscoelastic plates and stratified media with large values of frequency domain.* Ultrasonics, Vol 29, 1991, pp 445-450.

Karim, M.R., Mal, A.K., Bar-Cohen, Y. *Inversion of leaky Lamb wave data by simplex algorithm.* J. Acoust. Soc. Am., Vol. 88, 1990, pp 482-491.

Knopoff, L. *A matrix method for elastic wave problems.* Bull. Seism. Soc. Am, Vol. 54, 1964, pp 431-438.

Kolsky, H. *Stress waves in solids.* Dover Publications, New York, 1963.

Kumar, V. *Attenuation and velocity of waves propagating along a steel-steel interface.* J. Appl. Phys., Vol. 54, 1983, pp 1141-1143.

Kushibiki, J., Ishikawa, T., Chubachi, N. *Cut-off characteristics of leaky Sezawa and pseudo-Sezawa wave modes for thin-film characterisation.* Appl. Phys. Lett. 57 (19), Am. Inst. Phys., Nov 1990, pp 1967-1969.

Lamb, H. *On waves in an elastic plate.* Proc. Roy. Soc., Vol 93 PT Series A, 1917, pp 114-128

Lee, D.A., Corbly, D.M. *Use of interface waves for nondestructive inspection.* IEEE Trans. Sonics and Ultrasonics, Vol. SU-24, No. 3, 1977, pp 206-212.

Love, A.E.H. *Some problems of geodynamics.* Cambridge University Press, London, 1911.

Love, A.E.H. *Mathematical theory of elasticity.* Cambridge University Press, London, 1927.

Lowe, M.J.S., Cawley, P. *The detection of a brittle layer at the bondline in diffusion bonded titanium.* In press, in Review of Progress in Quantitative NDE, 1993.

Mal, A.K., Kundu, T. *Reflection of bounded acoustic beams from a layered solid.* Review of Progress in Quantitative NDE, Vol 6, 1987, pp 109-116.

Mal, A.K., Xu, P.C., Bar-Cohen, Y. *Analysis of leaky Lamb waves in bonded plates.* Int. J. Engng. Sci., Vol 27, 1989, pp 779-791.

Mal, A.K., Xu, P.C., Bar-Cohen, Y. *Leaky Lamb waves for the ultrasonic nondestructive evaluation of adhesive bonds.* J. Eng. Mat. and Tech., Vol 112, ASME, 1990, pp 255-259.

Malvern, L.E. *Introduction to the mechanics of a continuous medium.* Prentice-Hall, New Jersey, 1969.

Margetan, F.J., Thompson, R.B. *Microstructural noise in titanium alloys and its influence on the detectability of hard-alpha inclusions.* Review of Progress in Quantitative NDE, Vol 11, 1992, pp 1717-1724.

Margetan, F.J., Thompson, R.B., Gray, T.A., Rose, J.H. *Experimental studies pertaining to the interaction of ultrasound with metal-metal bonds.* Review of Progress in Quantitative NDE, Vol 9, 1990, pp 1323-1330.

Mason, W.P. *Physical Acoustics and the Properties of Solids*, Van Nostrand, New Jersey, 1958.

NAG Ltd., Wilkinson House, Jordan Hill Road, Oxford.

Nagy, P.B., Adler, L. *Nondestructive evaluation of adhesive joints by guided waves.* J. Appl. Phys., Vol. 66, 1989, pp 4658-4663.

Nagy, P.B., Rypien, D.V., Adler, L. *Dispersive properties of leaky interface waves in adhesive layers.* Review of Progress in Quantitative NDE, Vol 9, 1990, pp 1247-1255.

Nayfeh, A.H., Chimenti, D.E., Adler, L.,Crane, R.L. *Ultrasonic leaky waves in the presence of a thin layer.* J. Appl. Phys., Vol. 52, 1981, pp 4985-4994.

Norris, B. *Liquid interface diffusion (LID) bonding of titanium structures.* In Designing with Titanium, Institute of Metals, 1986, pp 83-86.

Osborne, M.F.M., Hart, S.D. *Transmission, reflection, and guiding of an exponential pulse by a steel plate in water. I. Theory.* J. Acoust. Soc. Am., Vol. 17, 1945, pp 1-18.

Osborne, M.F.M., Hart, S.D. *Transmission, reflection, and guiding of an exponential pulse by a steel plate in water. II. Experiment.* J. Acouust. Soc. Am., Vol. 18, 1946, pp 170-184.

Palmer, D.D, Rehbein, D.H., Smith, J.F., Buck, O. *Nondestructive characterization of the mechanical strength of diffusion bonds. II. Application of a quasi-static spring model.* J. Nondestr. Eval., Vol. 7, 1988, pp 167-174.

Partridge, P.G. *Diffusion bonding of metals.* AGARD, LS 154, 1987, pp 5.1-5.23.

Pialucha, T.P. *The reflection coefficient from interface layers in NDT of adhesive joints.* PhD thesis, University of London, 1992.

Pialucha, T.P., Lowe, M.J.S., Cawley, P. *Validity of different models of interfaces in adhesion and diffusion bonded joints.* In press, in Review of Progress in Quantitative NDE, 1993.

Pialucha, T.P., Guyott, C.C.H., Cawley, P. *Amplitude spectrum method for the measurement of phase velocity.* Ultrasonics, Vol 27, 1989, pp 270-279.

Pilant, W.L. *Complex roots of the Stoneley wave equation.* Bull. Seism. Soc. Am, Vol. 62, No. 1, 1972, pp 285-299.

Pilarski, A. *Ultrasonic evaluation of the adhesion degree in layered joints.* Materials Evaluation, Vol. 43, Am. Soc. Nondestructive Testing, 1985, pp 765-770.

Press, W.H., Flannery, B.P., Teukolsky, S.A., Vetterling, W.T. *Numerical recipes.* Cambridge University Press, Cambridge, 1986.

Press, F., Harkrider, D., Seafeldt, C.A. *A fast convenient program for computation of surface-wave dispersion curves in multilayered media.* Bull. Seism. Soc. Am, Vol. 51, No. 4, 1961, pp 495-502.

Randall, M.J. *Fast programs for layered half-space problems.* Bull. Seism. Soc. Am, Vol. 57, No. 6, 1967, pp 1299-1316.

Rayleigh, Lord. *On waves propagating along the plane surface of an elastic solid.* Proc. London Math. Soc., Vol 17, 1885.

RMI. *Facts about the metallography of titanium.* RMI Company, Niles, Ohio, USA, 1981.

Rokhlin, S.I. *Interface properties characterization by interface and Lamb waves.* Review of Progress in Quantitative NDE, Vol 5, 1986, pp 1301-1308.

Rokhlin, S.I., Hefets, M., Rosen, M. *An elastic interface wave guided by a thin film between two solids.* J. Appl. Phys., Vol. 51, 1980, pp 3579-3582.

Rokhlin, S.I., Hefets, M., Rosen, M. *An ultrasonic interface wave method for predicting the strength of adhesive bonds.* J. Appl. Phys., Vol. 52, 1981, pp 2847-2851.

Rokhlin, S.I., Wang, W., Wang, Y.J. *Ultrasonic evaluation of interphasial properties in adhesive joints.* Review of Progress in Quantitative NDE, Vol 9, 1990, pp 1231-1238.

Rose, J.H. *Ultrasonic characterization of solid-solid bonds from microstructural changes.* Review of Progress in Quantitative NDE, Vol 7, 1988, pp 1311-1317.

Rose, J.H. *Reflection coefficients for defective diffusion bonds.* Review of Progress in Quantitative NDE, Vol 9, 1990, pp 1317-1322.

Rose, J.L., Nayfeh, A., Pilarski, A. S*urface waves for material characterization.* J. Appl. Mechanics, Vol. 57, 1990, pp 7-11.

Schmidt, H., Jensen, F.B. *Efficient numerical solution technique for wave propagation in horizontally stratified environments.* Comp. & Maths. with Appls., Vol. 11, 1985, pp 699-715.

Schmidt, H., Tango, G. *Efficient global matrix approach to the computation of synthetic seismograms.* Geophys. J.R. Astr. Soc., Vol. 84, 1986, pp 331-359.

Scholte, J.G. *The range and existence of Rayleigh and Stoneley waves.* Mon. Not. Roy. Astron. Soc. Geophys. Suppl., Vol. 5, 1947, pp 120-126.

Schwab, F.A., Knopoff, L. *Fast surface wave and free mode computations.* Methods in Computational Physics, Vol II, ed. Bolt, B.A., Academic Press, New York, 1972, pp 87-180.

Stephen, D. *Superplastic forming and diffusion bonding of titanium.* In Designing with Titanium, Institute of Metals, 1986, pp 108-124.

Stoneley, R. *Elastic waves at the surface of separation of two solids.* Proc. Roy. Soc., Vol 106, 1924, pp 416-428.

Thompson, R.B., Margetan, F.J., Rose, J.H., Batra, N.K. *Effects of interstitial oxygen on the ultrasonic properties of titanium alloys*. Review of Progress in Quantitative NDE, Vol 11, 1992, pp 1725-1732.

Thomson, W.T. *Transmission of elastic waves through a stratified solid medium.* J. Appl. Phys., Vol. 21, 1950, pp 89-93.

Timoshenko, S.P., Goodier, J.N. *Theory of elasticity.* McGraw-Hill, Tokyo, 1970.

Tolstoy, I., Usdin, E. *Dispersive properties of stratified elastic and liquid media: a ray theory.* Geophysics, Vol. 18, 1953, pp 844-870.

Viktorov, I.A. *Rayleigh and Lamb waves.* Plenum Press, New York, 1970.

Watson, T.H. *A real frequency, complex wave-number analysis of leaking modes.* Bull. Seism. Soc. Am, Vol. 62, No. 1, 1972, pp 369-541.

Weglein, R.D. *Acoustic micro-metrology.* IEEE Trans. Sonics and Ultrasonics, Vol. SU-32, No. 2, 1985, pp 225-234.

Weglein, R.D. *Titanium diffusion bond evaluation via acoustic microscopy.* Ultrasonics Symposium, IEEE, 1988, pp 1045-1048.

Wolf, J., Ngoc, T.D.K., Kille, R., Mayer, W.G. *Investigation of Lamb waves having a negative group velocity.* J. Acoust. Soc. Am., Vol. 83, 1988, pp 122-126.

Worlton, D.C. *Ultrasonic testing with Lamb waves.* Nondestructive Testing, 1957, pp 218-222.

Xu, P.C., Mal, A.K., Bar-Cohen, Y. *Inversion of leaky Lamb wave data to determine cohesive properties of bonds.* Int. J. Engng. Sci., Vol 28, 1990, pp 331-346.